WASM: Mineral, Energy and Chemical Engineering

Metal Organic Frameworks (MOFs) Technology for Wastewater Remediation

Naser Kazem Al Amery

This thesis is presented for the Degree of

Doctor of Philosophy

of

Curtin University

November 2020

Declaration

To the best of my knowledge and belief, this thesis contains no material previously published by another person or other persons, except where due acknowledgment has been made.

This thesis contains no material that has been accepted for an award of any other degree or diploma in any university.

Acknowledgements

Firstly, I would like to thank Curtin University for giving me the opportunity to study a course in Doctor of Philosophy – Chemical Engineering. I would like to express my sincere gratitude to my supervisors Prof. Shaomin Liu and Shaobin Wang for their continuous support of my PhD study and related research, there patience, motivation and immense knowledge. There guidance helped me at all times during the research for, and writing of, this thesis. I cannot imagine having a better advisor and mentor for my PhD study.

Besides my supervisor, I would like to thank the rest of my thesis committee: Prof. Ha-Ming Ang, Prof. Xia Lou, Assoc. Prof. Nicoleta Maynard and Dr Qin Li, for their insightful comments and encouragement, and also for the hard questions that incentivised me to widen my research to include various perspectives.

My sincere thanks also go to Dr Hussein Rasool Abid, who provided me the opportunity to give me access to the laboratory and research facilities

I thank my fellow laboratory colleagues for the stimulating discussions, the sleepless nights we worked together to meet deadlines and for all the fun we shared during the years of study. Also, I thank technical staff members of the chemical engineering labs. In particular, I am grateful to Roshanak Doroushi and Jason Wright for their help with providing the facilities and chemicals.

I should like to thank the Capstone Editing team who have generously given valuable efforts and advices during the process of copyediting the thesis. The success of the thesis upon their care and competence. Their conscientiousness is much appreciated.

Last but not the least, I would like to thank my family: my parents, wife, daughters (Zahra, Sarah and Hanan), sons (Mustafa, Ali, Hasan and Hussain) and to my brothers and sisters for supporting me spiritually and emotionally throughout the PhD and my life in general.

Abstract

There are alarming predictions that in the next decade, billions of people living in arid regions will face the challenge of insufficient supply of clean water. In addition, many countries, including Australia, are now confronted with water stress as well as the production of huge volumes of polluted industrial wastewater. Water is the essential substance of life. As a result, there is urgency in research into treating wastewater before its discharge into receiving waters. Many techniques have been utilised to remove pollutants from effluents, such as the use of chemical, physical and biological treatments. Among these techniques, adsorption has been identified as the most effective treatment due to its simplicity, durability and feasibility.

The present scholarly study was designed to synthesise single-metal and bimetal zirconium-based metal organic frameworks (Zr-MOFs or UiO-66), which belong to an extensive class of solid-state crystalline materials with high porosity, tuneable metrics, thermal stability, water stability and organic functionality, using a secondary building unit (SBU) method, and investigate the longstanding challenge of designing and constructing novel crystalline materials from molecular building blocks. In addition, the study aimed to investigate MOF characterisation and applications in wastewater treatment to adsorb highly specific pollutants such as basic (methylene blue [MB]) and acidic (methyl orange [MO]) commercial dyes from aqueous solutions, as thousands of tons of synthetic dyestuffs are discharged annually into the environment through wastewater and are classified as harmful to human and other lives.

A series of single metal and bimetal Zr-MOFs samples with various ratios of M/Zr (M= Ca, Ce, Co, or Al), such as UiO-66, UiO-66-10%Ca, UiO-66-30%Ca, UiO-66-45%Ca, UiO-66-20%Ce, UiO-66-NH_4, UiO-66-10%Co, UiO-66-30%Co, UiO-66-10%Al and UiO-66-30%Al, were successfully and solvothermally obtained by direct synthesis, followed by activation processes with methanol with some modifications.

In this study, we further enhanced the performance of UiO-66 for removal of industrial dyes such as methylene blue (MB) and methyl orange (MO) with improving its textural properties through the introduction of second metal like Ca, Ce, Co or Al into the framework or by using ammonium hydroxide as an additive in the synthesis process. Direct synthesis modification was applied to synthesize modified UiO-66 samples

using Zr as the main metal and Ca, Ce, Co or Al as the second one while ammonium hydroxide was used as an additive in the case of UiO-66-NH_4. It is shown that the variation of M/Zr ratio results in significant changes in textural properties of MOFs and dye uptake of adsorption process.

The Zr-based inorganic SBU was engineered to enable the synthesis of Zr-MOFs with a highly porous and large surface area. The combination of the robust bond of Zr-O and the ability of the inner Zr_6-cluster to rearrange reversibly upon removal or addition of μ_3-OH groups, while maintaining a similar connection to carboxylates, create unparalleled stability in Zr-MOFs. The use of most other MOFs in industrial applications are limited because of their frail properties, such as insufficient thermal, chemical and mechanical stability. However, the necessary qualities for industry applications (decomposition only at high temperatures [more than 500°C], chemical resistance and stability at increasing pressures up to 10.000 kg/cm^2) shown by Zr-MOFs make them appropriate for adsorption of commercial synthetic dyes at an industrial scale.

All adsorbents were characterised using various techniques, including Fourier transform infrared spectroscopy (FTIR), X-ray powder diffraction (XRD), N_2 adsorption and thermogravimetric analysis (TGA). Among UiO-66, UiO-66-Ce, UiO-66-45% Ca and UiO-66-NH_4, the best textural properties of modified Zr-MOF were presented by UiO-66-Ce, which has S_{BET}, pore volume and pore size measurements of 911.85 m^2 g^{-1}, 0.91 cm^3 g^{-1} and 4 nm, respectively. On the other hand, the prime properties for Zr-MOF (M) (M= Ca, Co or Al) were exhibited by UiO-66-10%Al, which has S_{BET}, pore volume and pore size measurements of 1145.953 m^2 g^{-1}, 1.34 cm^3 g^{-1} and 2.33 nm, respectively. In addition, the optimum textural properties in bimetal Zr-MOFs were 10% second metal, including UiO-66-10% Al, UiO-66 10% Ca and UiO-66 10% Co.

Batch adsorption processes were conducted to remove dye pollutants, using contact time and initial concentrations varying from 10 to 75 mg L^{-1} and from 5 to 50 mg L^{-1} for Zr-MOF/MO and Zr-MOF/MB systems, respectively. The results showed that higher initial MB concentrations led to increases in adsorption capacity. The same occurred with longer durations in contact time.

A study of adsorption kinetics was conducted by fitting the experimental data to kinetics models such as the pseudo first order, pseudo second order, Elovich and intraparticle diffusion models. The investigation revealed that the pseudo second order model displayed the best fit among the kinetics models, indicating that the adsorption processes of Zr-MOF/MB systems are generally controlled by the chemisorption process. Further, confirmation of the chemisorption mechanism was achieved using the Elovich model to examine the data. However, the pseudo first order equation was found to be a poor fit for MB sorption by the entire range of MOFs examined (Zr-MOF, Zr-MOF-Al and Zr-MOF-Co); in general, the equation can be applied to the first 20 or 30 min of the adsorption process.

The limitations of the pseudo first order, pseudo second order and Elovich kinetic models are that there is a lack of descriptions of their mechanisms and of the rate-controlling step of the adsorption process. Given these limitations, the study used the intraparticle diffusion model to determine that the overall rate of MB sorption on Zr-MOFs was controlled by more than one step. However, the results obtained from the kinetics study proved that Zr-MOFs effectively removed basic dye from aqueous solutions.

The experimental equilibrium data were fitted to the Langmuir and Freundlich isotherms. While the data agreed with the Langmuir equation for Zr-MOF/MO systems, they were also a good fit with the Freundlich equilibrium model for Zr-MOF/MB systems. However, the maximum adsorption capacity based on the Langmuir model of Zr-MOF/MO systems and Zr-MOF/MB systems were 71.5 mg g^{-1} for UiO-66-Ce and 51.02 mg g^{-1} for UiO-66-10% Co.

Further, this study found that the maximum monolayer adsorption capacity of several adsorbents for MO and MB uptake appeared to be that of the maximum adsorption capacity of Zr-MOFs for MO and MB. This finding is comparable with previously reported results. The results presented here especially that of modified Zr-MOFs with a low second metal content which were boosted the adsorption capacity of UiO-66 remarkably, may facilitate and enhance further improvements to UiO-66 for the purpose of synthesising bimetal MOFs in future research and applications. Furthermore, these updated UiO-66 samples can be selected as potential candidates for industrial application for removal dyes and other contaminants from wastewater.

Publication of this thesis

1. *Facile directions for synthesis, modification and activation of MOFs* (Materials Today Chemistry Journal).
2. *Enhancing acidic dye adsorption by updated version of UiO-66* (Applied Materials and Technology Journal).
3. *Removal of methylene blue (MB) by bimetallic-Metal Organic Framework* (Submitted to Applied Materials and Technology Journal).

Contents

List of Figures

List of Tables

Nomenclature

α	Constant in the Elovich equation
β	Exponent in the Elovich equation
AAC	Acetic acid
AB	Ammonia borane
Ag-MOF	Silver-based Metal Organic Framework ($\{Ag_2Cl(5\text{-eatz})\}_n$ (1) and $\{Ag_6(5\text{-eatz})_6.H_2O\}n$)
Al- MIL-53	Aluminium-based metal organic frameworks
Al-MIL-96	Aluminium-based Metal Organic Framework
Al $(NO_3)_3.9H_2O$	Aluminium nitrate nonahydrate
AWTR	Advanced Waste Treatment Research
BDC	1,4-benzene dicarboxylic acid
BenAc	Benzoic acid
BET	Brunauer–Emmett–Teller
BIPY	2,20-Bipyridine
BPDB	1,4-bis(4-pyridyl)-2,3-diaza-1,3-butadiene
BPDC	4,40-biphenyldicarboxylic acid
BPP	1,3-bis(4-pyridyl) propane
Ca-MOF	Calcium-based Metal Organic Framework
Ca $(NO3)_2.4H_2O$	Calcium nitrate tetrahydrate

C_0	Initial liquid-phase concentration (mg/L)
C_i	Initial liquid-phase concentration (mg/L)
C_e	Equilibrium concentration of dye in solution (mg/L)
Cd-MOF	Cadmium-based Metal Organic Framework ([Cd(2,3-pydc) (bpp) (H_2O)].3H_2O)
Cd ($OAc)_2$.4H_2O	Cadmium acetate tetrahydrate
Ce (III)-doped UiO-66	Cerium-doped zirconium-based Metal Organic Framework
Ce-MOF	Cerium-based Metal Organic Framework ([$Ce_2(ADC)_3(H_2O)_6$].2H_2O)
Ce-UiO-66	Cerium and Zirconium bimetallic Metal Organic Framework
CF_3COOH	Trifluoroacetic acid
COD	Chemical oxygen demand
COFs	Covalent organic frameworks
Co (II)$(ACAC)_2$	Cobalt (II) acetylacetonate
Co-MOF	Cobalt-based Metal Organic Framework({(C_5H_5NH) [Co($C_7H_4NO_4$) ($C_7H_3NO_4$)]. ($C_7H_5NO_4$).(H_2O)}n)
Co-MOF	Cobalt-based Metal Organic Framework ($Co_{1.5}$(tib)(dcpna)].6H_2O)
$CoSiF_6$	Elemental composition of cobalt, silicon and fluorine
Co-ZIF-67	Cobalt-based Zeolitic imidazolate framework 8

CPO-27-Ni	MOF-74(Ni) (Nickle-based Metal Organic Framework) (Nickle dihydroxy benzene dicarboxylate)
CR	Anionic dye Congo red
Cr-MIL-100	Chromium-based Metal Organic Framework
MIL-101[Cr]-SO_3H	Modified chromium-based Metal Organic Framework
Cu-MOF	Copper-based Metal Organic Framework (Copper benzene tricarboxylate) ($[Cu_2(B_4S)\ (H_2O)_8]$. $0.5H_2O$).
Cu-MOF-14	Copper-based Metal Organic Framework
Cu-UiO-66	Copper and zirconium Metal Organic Framework
CSD	Cambridge Structural Database
C_t	Concentration of adsorbate solution at time t (mg/L)
DABCO	1,4-diazabicyclo [2.2.2] octane, Bmim-Cl: Butyl-3-methylimidazolium chloride
DEF	N, N-diethylformamide
DMF	N, N-dimethylformamide
DMOF-1-Zn	Zinc-based metal organic frameworks (Zn_2(1,4-BDC)$_2$(DABCO))
DMSO	Dimethyl Sulfoxide
DOT	2,5-dihydroxyterephthalic acid
DSM	Direct synthesis modification

EA	Environment Agency (England and Wales)
EC	European Community
EPA	US Environmental Protection Agency
ETAD	Ecological and Toxicological Association of the Dyes and Organic Pigments Manufacturers
EtOH	Ethanol
Eu-MOF	Europium-based Metal Organic Framework
Eu $(OAc)_3.6H_2O$	Europium (III) acetate hydrate
Fe-MIL-53	Iron-based Metal Organic Framework
Fe-MIL-88B-NH_2	Iron carboxylate Metal Organic Frameworks
Fe-MIL-100	Iron-based metal organic frameworks
Fe-MOF74	Iron-based Metal Organic Framework
FS	Ionic dye fluorescein sodium
FTIR	Fourier transform infrared spectroscopy
H_2ADC	Acetyledicarboxylato dianion
H_2BDC	1,4 Benzene Dicarboxylic acid
$H_2BDC-NH_2$	2, 5-Diaminoterephthalic acid
H_2BDDB	4,40-(buta-1,3-diyne-1,4-diyl) di benzoate
H_2BPDC	Biphenyl-4,40-dicarboxylic acid
H_2BPP	2,6-bis(pyrazol-3-yl) pyridine

H_4BPTC	3,30,5,50-biphenyltetracarboxylic acid
H_4B_4S	Benzene 1,2,4,5-tetrasulfonic acid
H_2BTAC	benzotriazole-5-carboxylic acid
H_3BTB	Benzene tri benzoic acid
H_3BTC	1,3,5 Benzene Tricarboxylic acid
H_2DABCO	1,4-diazabicyclo [2.2.2] octane
H_3DCPNA	5-(30,50-dicarboxylphenyl) nicotinic acid
H_2DHTP	2,5-dihydroxyterephthalic acid
HF	Hydrofluoric acid
Hf-UiO-66	Hafnium and Zirconium based metal organic frameworks
H_3IDC	4,5-imidazoledicarboxylic acid
HKUST	Hong Kong University of Science and Technology
HKUST-1	Copper-based metal organic frameworks
H_2MFDA	9,9-dimethylfluorene-2,7-dicarboxylic acid
H_2OBA	4,4'-Oxybis (benzoic acid)
H_2PAMPA	N, N'-piperazine bis (methylene phosphonic acid)
H_2PyDC	Pyridine-2,3-dicarboxylic acid or 2,6-pyridinedicarboxylicacid
HPZDC	1H-pyrazole-4-carboxylic acid
InOF-1	Indium-based Metal Organic Framework (Indium biphenyl, tetracarboxylate) ($[In_2(OH)_2(BPTC)].6H_2O$)

IPD	Intraparticle diffusion
IRMOF	Isoreticular metal organic framework
IRMOF-3	Isoreticular zinc-based Metal Organic Framework
JUC	Jilin University,China
JUC-32-Y	Metal Organic Framework-confined ammonia borane system
k_1	Pseudo first-order rate constant (min^{-1})
k_2	Pseudo second-order rate constant ($g\ mg^{-1}\ min^{-1}$)
k_F	Freundlich isotherm constant related to the adsorption capacity ([mg/g] $[L/mg]^{1/n}$)
k_L	Langmuir constant related to the energy of adsorption and affinity of binding sites (L/mg)
La-MOF	Lanthanum-based Metal Organic Framework ($[Ln_2(ADC)_3(H_2O)_6].2H_2O$)
LDH	Layered double hydroxide
Ln-MOF	lanthanide-containing metal-organic frameworks
M	Metal
MB	Methylene blue
MFe_{LAG}	Iron-based Metal Organic Framework
Mg-MOF	Magnesium-based Metal Organic Framework ($\{[Mg\ (HIDC)\ (H_2O)_2].1.5H_2O\}_n$)
Mg-MOF-74	Magnesium-based Metal Organic Framework.

MIL	Materials of Institute Lavoisier
MIL-101(Cr	Chromium-based Metal Organic Framework
MIL-53(Cr)	Chromium-based Metal Organic Framework
$MnCl_2.4H_2O$	Manganese (II) chloride tetrahydrate
Mn-MOF	Manganese-based Metal Organic Framework ($Mn_5(btac)_4(\mu 3\text{-}OH)_2(EtOH)_2.DMF.3EtOH.3H_2O$)
MO	Methyl orange
MOA-3	Iron and aluminium bimetallic Metal Organic Framework (0.5Fe-0.5Al-BTC)
MOF	Metal organic framework
MOF-177	Zinc-based Metal Organic Framework
MOF-235	Iron-based Metal Organic Framework (Fe-BDC MOF)
MOF-5	Zinc-based Metal Organic Framework
M-008	Zinc-based Metal Organic Framework ({[Zn(4,4'-bipy)$(OAc)_2$]}n_2)
MTBS	Methyl tributyl ammonium methyl sulfate
n	Freundlich isotherm constant related to adsorption intensity
Ni-CPO-27	Nickle-based Metal Organic Framework
Ni-MOF	Nickle-based Metal Organic Framework (Nickle benzene tricarboxylate)
NH_2-H_2BDC	2-aminoterephthalic acid

NH_2-UiO-66	NH_2-zirconium-based metal organic frameworks
NMP	N-Methyl-2-pyrrolidone
NOTT-400	Scandium-based Metal Organic Framework
n-ZIF-8	Zinc-based zeolitic imidazolate framework-8 (Zinc (2-methylimidazole)$_2$)
OECD	Organisation for Economic Co-operation and Development
PCN	porous coordination network
PCN-415	Titanium and Zirconium bimetallic Metal Organic Framework
PDMS	Polydimethylsiloxane
pH	Potential of hydrogen
PSM	Post-synthesis modification
PYZ-H	Pyrazine
q_e	Equilibrium mass of pollutant adsorbed on sorbent (mg. g^{-1})
q_m	Langmuir maximum loading capacity (mg. g^{-1})
q_t	Mass of pollutant adsorbed at time t (mg. g^{-1})
R%	Percentage removal of adsorbate
R^2	Linear correlation coefficient
R_L	Dimensionless separation factor
SBUs	Secondary building units
Sc $(SO_3CF_3)_3$	Scandium (III) trifluoro methane sulfonate
SEPA	Scottish Environment Protection Agency

SIFSIX-3-Co	Metal Organic Framework built up from connecting M-SiF_6 pillars through N-donor ligands
ST	Cationic dye safranine (red synthetic dye)
STA-12(Cd)	Carboxylate and phosphonate-based Metal Organic Frameworks
t	Contact time (min)
TBAB	Tetrabutylammonium bromide
$TBAPF_6$	Tetrabutylammonium hexafluorophosphate
Tb-MOF	Terbium-based Metal Organic Framework
TEA	Triethylamine
THF	Tetrahydrofuran
TIB	1,3,5-tris(1-imidazolyl)-benzene
Ti-MIL-125	Titanium-based Metal Organic Framework
Ti $(OiPr)_4$	Titanium Isopropoxide
Ti-Zr-MOFs	Titanium and zirconium bimetallic Metal Organic Framework
UiO	University of Oslo (Universitetet i Oslo)
UiO-66	Zirconium-based metal organic framework
UiO-66-10% Al	Aluminium (10%) and zirconium bimetallic Metal Organic Framework
UiO-66-30% Al	Aluminium (30%) and zirconium bimetallic Metal Organic Framework

UiO-66-Ca	Calcium and zirconium bimetallic Metal Organic Framework
UiO-66-10% Ca	Calcium (10%) and zirconium bimetallic Metal Organic Framework
UiO-66-30% Ca	Calcium (30%) and zirconium bimetallic Metal Organic Framework
UiO-66-Ce	Cerium and zirconium bimetallic Metal Organic Framework
UiO-66-10% Co	Cobalt (10%) and zirconium bimetallic Metal Organic Framework
UiO-66-30% Co	Cobalt (30%) and zirconium bimetallic Metal Organic Framework
UiO-66-NH_4	Modified zirconium-based metal organic framework
UiO-66-NH_2	Modified zirconium-based metal organic framework
UiO-66-P	Modified zirconium-based metal organic framework (phosphate composite)
UK	United Kingdom
US	United States
V	Volume of solution (L)
W	Mass of adsorbent (g)
XRD	X-ray diffraction
YH3	Yttrium trihydride

Y-MOF	Yttrium-based Metal Organic Framework (Yttrium tricarboxylate)
ZIF	Zeolitic imidazolate framework
ZIF-8	Zeolitic imidazolate framework 8
Zn-MOF-5	Zinc-based metal organic frameworks (Zinc benzene dicarboxylate) ($Zn_4O(BDC)_3$)
Zn $(OAc)_2.2H_2O$	Zinc acetate dihydrate
Zn $(OAc)_2.xH_2O$	Zinc acetate hydrate
$ZrCl_4$	Zirconium tetrachloride
Zr-HKUST-1(Cu)	Zirconium and copper bimetallic Metal Organic Framework
ZrPCN111	Zirconium-based metal organic frameworks (Zirconium 4,40-(buta-1,3-diyne-1,4-diyl) dibenzoate)
Zr-UiO-67	Zirconium-based metal organic framework
2OH-H2BDC	2,5-di-hydroxy-1,4-benzenedicarboxylic acid
2-MeIm	2-methylimidazole
4,4'-bipy	4,4'-bipyridyl
5-eatzH	(1S)-1-(5-tetrazolyl) ethylamine

Chapter 1

Introduction

1

Introduction

1.1 Motivation

Water pollution is one of the most undesirable environmental issues in the world requiring urgent solutions. Textile manufacturing produces a huge quantity of waste comprising a variety of pollutants, such as acidic or caustic dissolved solids, toxins and dyes that are typically nondegradable by natural biological processes or in wastewater treatment plants. A number of these dye materials are carcinogenic, mutagenic, teratogenic and additionally hazardous to humankind and other life forms. Hence, their elimination from wastewater is environmentally important [1, 2].

Since the Industrial Revolution, human activities have affected the flow and storage of water and therefore, the quality of accessible fresh water [3]. Lately, industrial advances have left their mark on society as well as the environment. For example, dyes are thought to be unsafe organic compounds for the environment [4–6]; however, various refineries and industries such as textile, chemical, plastic and food processing plants [3] have employed dyes to colour their products. As a result, these industries and processes produce massive volumes of wastewater containing organic compounds of strong colour. Further, some researchers have found that about 50% of the dye is wasted in the dyeing process because of the low degree of dye-fibre fixation [3, 7], which creates a major problem for such industries and is a danger to the environment [13, 14].

Chakrabarti et al. stated that about 40,000 dyes and pigments can be tabulated, consisting of over 7000 different chemical structures [15]. In addition, many of these organics are entirely not biodegradable [16]. It is estimated that nearly 10,000 commercial dyes and pigments are utilised by industries and more than 7×10^5 tonnes are produced annually worldwide [17]. It is reported that 10–15% of the dye could be lost in the effluent during the colouring process [8, 9]; however, new studies show that almost 12% of dyestuff is lost during manufacturing and processing operations. The variation in the level of colour fixation on a cloth is reliant on the type of fibre, the shade of the dye and dyeing parameters. Table 1.1 outlines the fixation rates of different dyes [10]; specifically, it shows that approximately 20% of the dye's organic compounds are passed through to industrial wastewaters [11, 12].

Table 1.1: Percentage of non-fixed dye discharged in the effluent as a function of the class of dye [10].

Dyestuff	EPA	OECD	Spain
Acid dyes	10–20	7–20	5–15
Basic dyes	1	2–3	0–2
Direct dyes	30	5–20	5–20
Disperse dyes	5–25	8–20	0–10
Azoic dyes	25	5–10	10–25
Reactive dyes	50–60	20–50	10–35
Metal complexes	10	2–5	5–15
Chrome dyes	—	—	5–10
Vat dyes	25	5–20	5–30
Sulfur dyes	25	30–40	15–40

Cationic basic dyes (e.g., methylene blue [MB]) and anionic acidic dyes (e.g., methyl orange [MO]), which are pollutant representatives in this study, are commercial dyes that are utilised by many industries as colourants for their products [7]. MB is commonly used in large quantities in medical applications, to colour paper, to dye cottons and wools, as coating on paper stocks, etc. While MB is not significantly dangerous, it has some harmful effects. A high level of exposure to MB may increase heart rate, induce vomiting, shock, formation of Heinz bodies, cyanosis, jaundice and potentially tissue necrosis and quadriplegia in individuals [9, 18]. Further, MO—a famous dye—has been widely used in textile, printing, paper, food and pharmaceutical industries as well as research laboratories [19, 20]. This dye is well known for being a carcinogenic organic substance [20].

The textile industry dyeing process involves many steps, including desizing, scouring, bleaching, dyeing, finishing and drying. The first three steps of the colouring process consume large amounts of water that can typically reach 100–170 litres per kilogram of processed cloth, assuming a strong colour, high chemical oxygen demand and a wide range of pH [3].

Environmental legislation in some countries established very strict limitations on the concentration of contaminants that can be discharged as industrial effluent. Therefore,

all such effluent must be treated to meet the environmental standards set by wastewater legislation [21].

In 1974, the international organisation Ecological and Toxicological Association of Dyes and Organic Pigments Manufacturers (ETAD) was formed for the purpose of minimising the environmental impact of, and protecting users and consumers from, the toxicological effects of dye products, as well as informing government and the public in relation to concerns about their use [22]. More than 90% of the 4000 dyes have been examined in an ETAD survey, with maximum toxicity identified to exist in basic and diazo direct dyes [23].

Many developed countries possess national environmental legislation to control dyes and pigment contaminants, and environmental organisations monitor industry compliance with legislated environmental standards and limits in the US (United States), Canada, Australia, United Kingdom (UK) and European Union member states. While some countries have copied either American or European models, such as Thailand, Turkey and Morocco, other countries like Pakistan, India and Malaysia have been recommended that industries comply with the limits placed on the emission of pollutants [10].

Environmental regulation in the UK is established by the Environment Agency for England and Wales, and the Scottish Environment Protection Agency for Scotland [24]. Generally, the enforcement of legislation relating to the removal of dyes in industrial sewage has been more rigorous in developed countries. For instance, it has been UK environmental policy since September 1997 to have zero synthetic chemicals, including dye-containing compounds, released into the marine environment. In the US, the Advanced Waste Treatment Research (AWTR) program aims to identify suitable treatment methods to safely discharge effluent into environment [21, 25, 26]. Countries in the European Community also possess very stringent regulations to ensure that industrial effluent complies with environmental standards in their countries [23].

Several studies have examined the removal of dye from industrial textile wastewaters using biological, physical and chemical treatments [1, 23, 27]. Chemical methods (oxidative processes) include Fenton's reagent [28], ozonation [29], photochemical destruction [30], sodium hypochlorite (NaOCl) destruction [28], cucurbituril destruction [31, 32] and electrochemical destruction [33]. The biological techniques

examined are divided into many methods, such as decolourisation by white-rot fungi [34], microbial cultures [35], adsorption by living/dead microbial biomass [36] and anaerobic textile-dye bioremediation systems [37]. Physical treatment can be classified into membrane filtration [38], ion exchange [28], irradiation [39], electrokinetic coagulation [40] and adsorption using materials like activated carbon [41], peat [42], woodchips [43], fly-ash, coal mixture [44] and metal organic framework (MOF) materials [19, 45, 46].

Legislated environmental standards have pushed industries to utilise many techniques to remove contaminants from effluents, but these treatments are not sufficiently efficient because of restrictions and limitations. Table 1.2 outlines the advantages and disadvantages of the techniques for removing dyestuff. The preferred method is adsorption due to its simplicity, feasibility, removal efficiency and the high-quality effluent by-product resulting from its application [23, 47, 48].

Table 1.2: Advantages and disadvantages of dye removal methods [7, 23].

Methods	Advantages	Disadvantages
Chemical treatments		
Oxidative process	Simplicity of application	H_2O_2 agent needs to activate by some means
H_2O_2+Fe (II) salts (Fenton's reagent)	Fenton's reagent is a suitable chemical means	Sludge generation
Ozonation	Ozone can be applied in its gaseous state and does not increase the volume of wastewater and sludge	Short half-life (20 min)
Photochemical destruction	No sludge is produced, and foul odours are significantly reduced	Formation of byproducts
Sodium hypochlorite (NaOCl) destruction	Initiates and accelerates azo bond cleavage	Release of aromatic amines
Electrochemical destruction	No consumption of chemicals and no sludge build-up	Relatively high flow rates cause a direct decrease in dye removal
Biological treatments		
Decolourisation by white-rot fungi	White-rot fungi can degrade dyes using enzymes	Enzyme production has been shown to be unreliable

Methods	Advantages	Disadvantages
Other microbial cultures (mixed bacteria)	Decolourised in 24–30 h	Under aerobic conditions azo dyes are not readily metabolised
Adsorption by living/dead microbial biomass	Certain dyes have an affinity for binding with microbial species	Not effective for all dyes
Anaerobic textile-dye bioremediation systems	Allows azo and other water-soluble dyes to be decolourised	Anaerobic breakdown yields methane and hydrogen sulfide
Physical treatments		
Adsorption by activated carbon	Effective removal of wide variety of dyes	Very expensive
Membrane filtration	Removes all dye types	Concentrated sludge production
Ion exchange	Regeneration, no adsorbent loss	Not effective for all dyes
Irradiation	Effective oxidation at laboratory scale	Requires a great deal of dissolved O_2
Electrokinetic coagulation	Economically feasible	High levels of sludge production

1.1.1 Materials of the 20th century

- Metals
- Alloys
- Composites
- Zeolites
- Silicon
- Concrete
- Metal oxides
- Layered double hydroxides (LDHs)
- Polymers
- Pharmaceuticals
- Steel.

They are either organic or inorganic materials [49].

1.1.2 Materials of the 21st century

- MOFs
- Covalent organic frameworks (COFs)
- Zeolitic imidazolate frameworks (ZIFs).

They are organic, inorganic and mixed (organic and inorganic) materials [50].

1.1.3 Metal organic framework (MOF)

MOF [45, 51-57], or hybrid inorganic and organic framework [58], is one of the most famous material of the 21st century characterised by ultra-high porosity with architectural, mechanical and chemical stability [49]. During the past decade, interest has grown tremendously in the design, synthesis and characterisation of crystalline materials constructed from molecular building blocks (clusters and extended groups of atoms) linked by covalent bonds.

The most notable materials are MOFs, in which clusters of polyatomic inorganic metal are joined by polytopic linkers [59]. Typically, MOF-5, which consists of OZn_4 cationic inorganic clusters, are linked to benzene dicarboxylate (BDC) anion organic linkers to form a continuous cubic neutral framework of composition $Zn_4O(BDC)_3$ [51]. Although MOFs are referred to as coordination polymers from time to time, they are differentiated by the strong linkages between their molecules (typically metal-oxide molecules), which are the basis for its robust framework [52, 60]. The realisation that MOFs can be designed and synthesised precisely in a rational way from molecular building blocks has led to the emergence of a discipline referred to as 'reticular chemistry' [61].

In the present context, the important point is that the underlying topology of a MOF framework is like that of a net, with vertices as well as edges that correspond to clusters of atoms; thousands of new MOFs and hundreds of previously unreported nets have been described [61].

As a result of the chemical properties of some MOFs, MOFs such as MOF-5 or isoreticular MOFs are sensitive to water in that their structures are progressively

affected by atmospheric moisture [62, 63, 64]. Water stability is an important indication that MOFs can be introduced successfully in water and wastewater treatments.

MOFs have diverse potential applications, particularly applications that exploit their well-known porous quality; therefore, they can be used in applications for gas storage, gas/vapour separation, catalysis, luminescence, drug delivery [65] and as adsorbents to remove pollutants from water and wastewater [19, 46, 66-78].

1.1.4 Dyes

1.1.4.1 Classification of dyes

The two main constituents of dye are chromophores and auxochromes. While chromophores are the components that give the dye its specific colour, auxochromes are the parts of the dye responsible for producing colour. It is the auxochromes that improve the attraction between the dye and fibres [79]. Textile manufacturing processes commonly use dyes such as basic dyes, acid dyes, reactive dyes, direct dyes, azo dyes, mordant dyes, vat dyes, disperse dyes and sulfur dyes [6]. Specifically, the textile industry currently consumes a huge amount of azo derivatives to colour their products [80]. Table 1.3 lists the commercial textile dyes typically consumed in the colouring process.

Table 1.3: Typical dyes used in textile dyeing operations [6].

Dye class	Description
Acid	Water-soluble anionic compounds
Basic	Water soluble, applied in weakly acidic dyebaths, very bright
Direct	Water-soluble anionic compounds that can be applied directly to cellulosic without mordants (or metals like chromium and copper)
Disperse	Not water soluble
Reactive	Water-soluble anionic compounds, largest dye class
Sulfur	Organic compounds containing sulfur or sodium sulfide
Vat	Water insoluble, oldest dyes, chemically complex

Dyes can be classified into cationic, anionic and non-ionic dyes. Cationic dyes are basic dyes while anionic dyes include direct, acid and reactive dyes [40].

1.1.4.1.1 Cationic dyes

Cationic dyes are considered famous in industries that use acrylic, wool, nylon and silk colouring. Relay on substituted aromatic groups, cationic dyes can obtain specific chemical structures different from each other [81]. This group of toxic dyes can affect human health; prolonged or high-level exposure can lead to allergic dermatitis, skin irritation, mutations and cancer [82].

In addition, based on the positive ion or positive charge of their molecules (from zinc chloride or hydrochloride complexes), these types of dyes are also known as basic dyes [83]. These compounds can easily dissolve in water to form a coloured cationic solution, and include diarylcarbenium, triarylcarbenium, anthraquinone, phthalocyanine, polycarbocyclic, methane and azo dyes. Commercial cationic dyes such as crystal violet, MB, basic blue 41 and basic red 46 are widely used in many industries [84-87]. While some of these dyes are expensive, it is possible to find a dye from this group at competitive prices for specific application [7].

1.1.4.1.2 Anionic dyes

Anionic dyes are also famous in industries that use coloured silk, wool, polyamide, modified acrylic and polypropylene fibres [7]. Depending on the substituted aromatic groups, cationic dyes can have chemical structures that differ from each other. This group of toxic dyes can affect human health because they are organic sulfonic acids [88]. Moreover, based on the negative ion or negative charge of their molecules, these dyes are also known as acid dyes [83].

Specifically, these compounds can easily dissolve in water to form a coloured anionic solution, and include azoic, anthraquinone, triphenylmethan and nitro dyes. Commercial anionic dyes such as acid scarlet, acid turquoise blue, reactive brilliant red, acid fuchsine, orange IV, MO, reactive yellow, red reactive 141, brilliant yellow, acid black 26, acid green 25, acid blue and indigo carmine, are widely used in many industries [89-94]. However, some of these dyes have a low level of fixation onto products [7].

1.1.5 Dye remediation

Adsorption is considered the best technique for removing pollutants in wastewater. Its use of low-cost materials, such as activated carbons, zeolites, biological materials, polymer resins and oxides, has generated excitement [95-101]. The origins of use of carbon in the history of human civilisation dates so far back that it cannot be dated. However, research has identified that in ancient times, Indian Hindus and Egyptians were utilising charcoal to purify drinking water [102, 103].

The simplicity, feasibility and reliability of the adsorption method make this procedure the first choice in wastewater treatment [102]. The employment of MOFs in adsorption more recently has attracted tremendous interest in their applications in wastewater treatment. Several studies have used MOFs like UiO-66, ZIF-67, HKUST-1, MIL-101 and MIL-100 to target specific pollutants in wastewater [104-106]. Specifically, a study has attempted adsorptive removal of MO and MB from aqueous solutions using iron terephthalate (MOF-235)[19]. The advantages of MOFs lie in their chemical properties and textural tuneability: an ultra-high surface area, pore size tuneability and their incorporation of different functionalities [106-110].

Hydrogen bond, electrostatic interactions, π-π interactions and hydrophobic interactions are the mechanisms that control the dye and sorbent molecules in the adsorption process. Any successful adsorption process must involve at least one or more of these mechanisms [72, 106, 111-114].

This pioneering study will demonstrate the mechanisms by which modified UiO-66 (single-metal and bimetal) adsorb cationic MB and anionic MO dyes in wastewater. The experiments used different initial concentrations of dye with contact time, and all experiments were conducted using batch adsorption processes to establish adsorbent uptake.

1.2 Scope and objective of the thesis

The scope and core objective of the thesis is to study the adsorptive and removal properties of MOFs as relating to dye pollutants in wastewater, with the view to determining which MOF has the highest capacity for removing dye pollutants. This overarching objective can be broken down into the following objectives:

- Design, modify, synthesise and activate UiO-66 (Zr-MOF)
- Use reticular synthesis (reticulation chemistry) to form crystalline Zr-MOFs, which possess strong bonds between their constituents (organic and inorganic units)
- Synthesise Zr-MOFs (bimetal MOFs) with structures that are amenable to accepting more than one metal in their vertices
- Analyse and assess the structural integrity, as well as thermal and chemical stability, of MOFs
- Study the textural properties of the MOF adsorbents based on N_2 adsorption/desorption isotherms
- Select MB and MO as dye pollutant models to evaluate the capacity of Zr-MOFs to remove dyes from aqueous wastewater solutions.

1.3 Organisation of the thesis

Chapter 1: This chapter presented the materials of the 20th and 21st centuries. In addition, it briefly outlined the environmental impact of dyes and legislation that limits the concentration of pollutants that can be discharged as industrial effluent. Moreover, it presented the variety of methods for removing dyestuff as well as the advantages and disadvantages of these methods. Further, it described MOFs (adsorbents), specifically Zr-MOFs, and their constituents, as well as the dyes (adsorbates), specifically MO and MB, and their classification and remediation. Finally, the scope, objective and organisation of the thesis were presented.

Chapter 2: This chapter includes a comprehensive detailed literature review of MOF, including its design, methods of synthesis, modification and functionalisation procedures, methods of activation, water stability as well as its capacity for removing organic pollutants (including MO and MB) from water.

Chapter 3: This chapter describes a study dedicated to the adsorptive removal of MO from wastewater using Zr-MOFs (UiO-66-Ce, UiO-66-Ca and UiO-66-NH_4). Further, it reports on the comparative outcome of the best MOF for removing dye, through a modification to the synthesis and activation of MOFs. Modifications of UiO-66

involved the addition of Ce, Ca and NH_4 ions in the synthesis procedure. Characterisation techniques were employed to investigate the structural, thermal and chemical stability of the modified UiO-66.

Chapter 4: This chapter outlines the removal of MB as a model pollutant in aqueous solution, which employed enhanced bimetal Zr-MOFs (UiO-66-10%Ca and UiO-66-30%Ca) and their parent single-metal MOF (UiO-66). Moreover, it demonstrates the modification of UiO-66 using an additive containing Ca ions. It also outlines the characterisation of adsorbents (Zr-MOFs) as well as the kinetic and equilibrium studies performed on the adsorption processes.

Chapter 5: This chapter explains the mechanism and equilibrium isotherms for removing dyes (MB) from simulated effluents of textile industries, by MOFs such as UiO-66, UiO-66-10%Al and UiO-66-30%Al. Further, it demonstrates the successful synthesis of these adsorbents with the modifying step of adding Al ions in the procedure to synthesise Zr-MOF, to obtain bimetal MOFs (UiO-66-10%Al and UiO-66-30%Al). It reports on the characterisation of adsorbents using several procedures such as the Fourier transform infrared, X-ray powder diffraction, Brunauer–Emmett–Teller surface area and thermogravimetric analyses.

Chapter 6: This chapter illustrates the successful synthesis of single-metal and bimetal Zr-MOFs (UiO-66-10%Co and UiO-66-30%Co) using a modified synthesis procedure. Moreover, it describes the application of Zr-MOFs to the removal of cationic dye such as MB in a batch adsorption process. It outlines the use of several models in kinetic and equilibrium studies to fit the experimental adsorption data. In addition, the chapter outlines the characterisation of adsorbents using different measurement techniques.

Chapter 7: This chapter provides a summary of the thesis, including the design, synthesis and modification of single-metal and bimetal Zr-MOFs, such as UiO-66, UiO-66-Ce, UiO-66-Ca, UiO-66-NH_4, UiO-66-10%Ca, UiO-66-30%Ca, UiO-66-10%Al, UiO-66-30%Al, UiO-66-10%Co and UiO-66-30%Co. In addition, it summarises the results of studies examining the removal of contaminants, such as MO and MB, from wastewater by MOF adsorbents, the use of different kinetic and equilibrium models to fit the experimental data and the characterisation of the adsorbents using several measurement techniques.

References

1. Ledakowicz, S., M. Solecka, and R. Zylla, *Biodegradation, decolourisation and detoxification of textile wastewater enhanced by advanced oxidation processes.* Journal of Biotechnology, 2001. **89**(2): p. 175-184.
2. Aljeboree, A.M., A.N. Alshirifi, and A.F. Alkaim, *Kinetics and equilibrium study for the adsorption of textile dyes on coconut shell activated carbon.* Arabian Journal of Chemistry, 2017. **10**: p. S3381-S3393.
3. Mohan, N., N. Balasubramanian, and C.A. Basha, *Electrochemical oxidation of textile wastewater and its reuse.* Journal of Hazardous Materials, 2007. **147**(1): p. 644-651.
4. Allen, S. and B. Koumanova, *Decolourisation of water/wastewater using adsorption.* Journal of the University of Chemical Technology and Metallurgy, 2005. **40**(3): p. 175-192.
5. Klimiuk, E., U. Filipkowska, and B. Libecki, *Coagulation of wastewater containing reactive dyes with the use of polyaluminium chloride (PAC).* Polish Journal of Environmental Studies, 1999. **8**: p. 81-88.
6. Demirbas, A., *Agricultural based activated carbons for the removal of dyes from aqueous solutions: A review.* Journal of Hazardous Materials, 2009. **167**(1): p. 1-9.
7. Salleh, M.A.M., et al., *Cationic and anionic dye adsorption by agricultural solid wastes: A comprehensive review.* Desalination, 2011. **280**(1): p. 1-13.
8. Young, L. and J. Yu, *Ligninase-catalysed decolorization of synthetic dyes.* Water Research, 1997. **31**(5): p. 1187-1193.
9. Lian, L., L. Guo, and C. Guo, *Adsorption of Congo red from aqueous solutions onto Ca-bentonite.* Journal of Hazardous Materials, 2009. **161**(1): p. 126-131.
10. Hessel, C., et al., *Guidelines and legislation for dye house effluents.* Journal of Environmental Management, 2007. **83**(2): p. 171-180.
11. Hema, M. and S. Arivoli, *Comparative study on the adsorption kinetics and thermodynamics of dyes onto acid activated low cost carbon.* International Journal of Physical Sciences, 2007. **2**(1): p. 10-17.
12. Essawy, A.A., A.E.-H. Ali, and M.S.A. Abdel-Mottaleb, *Application of novel copolymer-TiO2 membranes for some textile dyes adsorptive removal from aqueous solution and photocatalytic decolorization.* Journal of Hazardous Materials, 2008. **157**(2): p. 547-552.
13. Qamar, M., M. Saquib, and M. Muneer, *Semiconductor-mediated photocatalytic degradation of anazo dye, chrysoidine Y in aqueous suspensions.* Desalination, 2005. **171**(2): p. 185-193.
14. Roxon, J.J. and A.J. Ryan, *Reduction of water-soluble azo dyes by intestinal bacteria.* Food and Cosmetics Toxicology, 1967. **5**: p. 367-369.
15. Chakrabarti, T., P. Subrahmanyam, and B. Sundaresan, *Biodegradation of recalcitrant industrial wastes.* 1988.
16. Pitter, P. and J. Chudoba, *Biodegradability of organic substance in the aquatic environment*. 1990.
17. Garg, V., R. Kumar, and R. Gupta, *Removal of malachite green dye from aqueous solution by adsorption using agro-industry waste: a case study of Prosopis cineraria.* Dyes and Pigments, 2004. **62**(1): p. 1-10.

18. Kumar, K.V., V. Ramamurthi, and S. Sivanesan, *Modeling the mechanism involved during the sorption of methylene blue onto fly ash.* Journal of Colloid and Interface Science, 2005. **284**(1): p. 14-21.
19. Haque, E., J.W. Jun, and S.H. Jhung, *Adsorptive removal of methyl orange and methylene blue from aqueous solution with a metal-organic framework material, iron terephthalate (MOF-235).* Journal of Hazardous Materials, 2011. **185**(1): p. 507-511.
20. Mittal, A., et al., *Studies on the adsorption kinetics and isotherms for the removal and recovery of Methyl Orange from wastewaters using waste materials.* Journal of Hazardous Materials, 2007. **148**(1): p. 229-240.
21. Ho, Y.S. and G. McKay, *A kinetic study of dye sorption by biosorbent waste product pith.* Resources, Conservation and Recycling, 1999. **25**(3): p. 171-193.
22. Anliker, R., *Ecotoxicology of dyestuffs—a joint effort by industry.* Ecotoxicology and Environmental Safety, 1979. **3**(1): p. 59-74.
23. Robinson, T., et al., *Remediation of dyes in textile effluent: a critical review on current treatment technologies with a proposed alternative.* Bioresource Technology, 2001. **77**(3): p. 247-255.
24. Willmott, N., J. Guthrie, and G. Nelson, *The biotechnology approach to colour removal from textile effluent.* Journal of the Society of Dyers and Colourists, 1998. **114**(2): p. 38-41.
25. Morris, J.C. and W.J. Weber, *Preliminary appraisal of advanced waste treatment processes.* 1962.
26. Weber, W.J. and J.C. Morris, *Equilibria and capacities for adsorption on carbon.* Journal of the Sanitary Engineering Division, 1964. **90**(3): p. 79-108.
27. Georgiou, D., et al., *Degradation of azo-reactive dyes by ultraviolet radiation in the presence of hydrogen peroxide.* Dyes and pigments, 2002. **52**(2): p. 69-78.
28. Slokar, Y.M. and A.M. Le Marechal, *Methods of decoloration of textile wastewaters.* Dyes and pigments, 1998. **37**(4): p. 335-356.
29. Lin, S.H. and C.M. Lin, *Treatment of textile waste effluents by ozonation and chemical coagulation.* Water Research, 1993. **27**(12): p. 1743-1748.
30. Peralta-Zamora, P., et al., *Degradation of reactive dyes I. A comparative study of ozonation, enzymatic and photochemical processes.* Chemosphere, 1999. **38**(4): p. 835-852.
31. Freeman, W.A., W.L. Mock, and N.Y. Shih, *Cucurbituril.* Journal of the American Chemical Society, 1981. **103**(24): p. 7367-7368.
32. Karcher, S., A. Kornmüller, and M. Jekel, *Removal of reactive dyes by sorption/complexation with cucurbituril.* Water Science and Technology, 1999. **40**(4): p. 425-433.
33. Pelegrini, R., et al., *Electrochemically assisted photocatalytic degradation of reactive dyes.* Applied Catalysis B: Environmental, 1999. **22**(2): p. 83-90.
34. Barr, D.P. and S.D. Aust, *Mechanisms white rot fungi use to degrade pollutants.* Environmental Science & Technology, 1994. **28**(2): p. 78A-87A.
35. Knapp, J.S. and P.S. Newby, *The microbiological decolorization of an industrial effluent containing a diazo-linked chromophore.* Water Research, 1995. **29**(7): p. 1807-1809.
36. Tsezos, M. and J.P. Bell, *Comparison of the biosorption and desorption of hazardous organic pollutants by live and dead biomass.* Water Research, 1989. **23**(5): p. 561-568.

37. Carliell, C., S. Barclay, and C. Buckley, *Treatment of exhausted reactive dyebath effluent using anaerobic digestion: laboratory and full-scale trials.* Water S. A., 1996. **22**(3): p. 225-233.
38. Xu, Y., et al., *Treatment of textile dye plant effluent by nanofiltration membrane.* Separation Science and Technology, 1999. **34**(13): p. 2501-2519.
39. Hosono, M., et al., *Decoloration and degradation of azo dye in aqueous solution supersaturated with oxygen by irradiation of high-energy electron beams.* Applied Radiation and Isotopes, 1993. **44**(9): p. 1199-1203.
40. Mishra, G. and M. Tripathy, *A critical review of the treatments for decolourization of textile effluent.* Colourage, 1993. **40**: p. 35-35.
41. Nassar, M.M. and M.S. El-Geundi, *Comparative cost of colour removal from textile effluents using natural adsorbents.* Journal of Chemical Technology & Biotechnology, 1991. **50**(2): p. 257-264.
42. Poots, V.J.P., G. McKay, and J.J. Healy, *The removal of acid dye from effluent using natural adsorbents—I peat.* Water Research, 1976. **10**(12): p. 1061-1066.
43. Nigam, P., et al., *Physical removal of textile dyes from effluents and solid-state fermentation of dye-adsorbed agricultural residues.* Bioresource Technology, 2000. **72**(3): p. 219-226.
44. Gupta, G.S., G. Prasad, and V.N. Singh, *Removal of chrome dye from aqueous solutions by mixed adsorbents: Fly ash and coal.* Water Research, 1990. **24**(1): p. 45-50.
45. Kuppler, R.J., et al., *Potential applications of metal-organic frameworks.* Coordination Chemistry Reviews, 2009. **253**(23-24): p. 3042-3066.
46. Haque, E., et al., *Adsorptive removal of methyl orange from aqueous solution with metal-organic frameworks, porous chromium-benzenedicarboxylates.* Journal of Hazardous Materials, 2010. **181**(1): p. 535-542.
47. Choy, K.K.H., G. McKay, and J.F. Porter, *Sorption of acid dyes from effluents using activated carbon.* Resources, Conservation and Recycling, 1999. **27**(1): p. 57-71.
48. Qadeer, R., *Adsorption behavior of ruthenium ions on activated charcoal from nirtic acid medium.* Colloids and Surfaces A: Physicochemical and Engineering Aspects, 2007. **293**(1): p. 217-223.
49. Conference, C.a.B.D.S.a.T.C.S.T. *Keynote Speaker: Dr. Omar Yaghi*. 2015 [cited 2018 10/11/2018]; Available from: https://www.youtube.com/watch?v=m6sRQjKFssk.
50. Nanotecnologia, I.C.d.N.i. *ICN2 Lecture Prof. Omar M. Yaghi: Reticular Chemistry*. 2018 [cited 2018 10/10/2018]; Available from: https://www.youtube.com/watch?v=OS_VI-8sMF0.
51. Li, H., et al., *Design and synthesis of an exceptionally stable and highly porous metal-organic framework.* nature, 1999. **402**(6759): p. 276.
52. Férey, G., *Hybrid porous solids: past, present, future.* Chemical Society Reviews, 2008. **37**(1): p. 191-214.
53. Horike, S., S. Shimomura, and S. Kitagawa, *Soft porous crystals.* Nature chemistry, 2009. **1**(9): p. 695.
54. Moghadam, P.Z., et al., *Development of a Cambridge Structural Database subset: a collection of metal–organic frameworks for past, present, and future.* Chemistry of Materials, 2017. **29**(7): p. 2618-2625.

55. Li, H., et al., *Establishing microporosity in open metal− organic frameworks: gas sorption isotherms for Zn (BDC)(BDC= 1, 4-benzenedicarboxylate).* Journal of the American Chemical Society, 1998. **120**(33): p. 8571-8572.
56. Li, J.R., J. Sculley, and H.C. Zhou, *Metal–Organic Frameworks for Separations.* Chem. Rev., 2012. **112**: p. 869.
57. Llewellyn, P.L., et al., *High Uptakes of CO2 and CH4 in Mesoporous Metal–Organic Frameworks MIL-100 and MIL-101.* Langmuir, 2008. **24**: p. 7245.
58. Biradha, K., A. Ramanan, and J.J. Vittal, *Coordination polymers versus metal− organic frameworks.* Crystal Growth and Design, 2009. **9**(7): p. 2969-2970.
59. Ma, L., C. Abney, and W. Lin, *Enantioselective catalysis with homochiral metal–organic frameworks.* Chemical Society Reviews, 2009. **38**(5): p. 1248-1256.
60. Yaghi, O.M., et al., *Reticular synthesis and the design of new materials.* Nature, 2003. **423**(6941): p. 705.
61. O'Keeffe, M., et al., *The reticular chemistry structure resource (RCSR) database of, and symbols for, crystal nets.* Accounts of chemical research, 2008. **41**(12): p. 1782-1789.
62. Li, H., et al., *Design and synthesis of an exceptionally stable and highly porous metal-organic framework.* Nature, 1999. **402**: p. 276.
63. Ming, Y., N. Kumar, and D.J. Siegel, *Water Adsorption and Insertion in MOF-5.* ACS Omega, 2017. **2**(8): p. 4921-4928.
64. Bellarosa, L., et al., *How ligands improve the hydrothermal stability and affect the adsorption in the IRMOF family.* Physical Chemistry Chemical Physics, 2013. **15**(40): p. 17696-17704.
65. Kuppler, R.J., et al., *Potential applications of metal-organic frameworks.* Coordination Chemistry Reviews, 2009. **253**(23): p. 3042-3066.
66. Khan, N.A., Z. Hasan, and S.H. Jhung, *Adsorptive removal of hazardous materials using metal-organic frameworks (MOFs): A review.* Journal of Hazardous Materials, 2013. **244-245**: p. 444-456.
67. Hasan, Z., J. Jeon, and S.H. Jhung, *Adsorptive removal of naproxen and clofibric acid from water using metal-organic frameworks.* Journal of Hazardous Materials, 2012. **209-210**: p. 151-157.
68. Ke, F., et al., *Thiol-functionalization of metal-organic framework by a facile coordination-based postsynthetic strategy and enhanced removal of Hg2+ from water.* Journal of Hazardous Materials, 2011. **196**: p. 36-43.
69. Huo, S.-H. and X.-P. Yan, *Metal–organic framework MIL-100 (Fe) for the adsorption of malachite green from aqueous solution.* Journal of Materials Chemistry, 2012. **22**(15): p. 7449-7455.
70. Blanco-Brieva, G., et al., *Effectiveness of metal–organic frameworks for removal of refractory organo-sulfur compound present in liquid fuels.* Fuel, 2011. **90**(1): p. 190-197.
71. Chen, Q., et al., *Selective adsorption of cationic dyes by UiO-66-NH2.* Applied Surface Science, 2015. **327**: p. 77-85.
72. Lin, S., et al., *Adsorption behavior of metal–organic frameworks for methylene blue from aqueous solution.* Microporous and Mesoporous Materials, 2014. **193**: p. 27-34.
73. Leng, F., et al., *Adsorption interaction between a metal–organic framework of chromium–benzenedicarboxylates and uranine in aqueous solution.*

Colloids and Surfaces A: Physicochemical and Engineering Aspects, 2014. **441**: p. 164-169.
74. Peralta, D., et al., *Metal–organic framework materials for desulfurization by adsorption.* Energy & Fuels, 2012. **26**(8): p. 4953-4960.
75. Maes, M., et al., *Selective Removal of N-Heterocyclic Aromatic Contaminants from Fuels by Lewis Acidic Metal–Organic Frameworks.* Angewandte Chemie, 2011. **123**(18): p. 4296-4300.
76. Chen, C., et al., *Kinetic and thermodynamic studies on the adsorption of xylenol orange onto MIL-101(Cr).* Chemical Engineering Journal, 2012. **183**: p. 60-67.
77. Fang, Q.-R., et al., *Functional mesoporous metal− organic frameworks for the capture of heavy metal ions and size-selective catalysis.* Inorganic chemistry, 2010. **49**(24): p. 11637-11642.
78. Wang, C., et al., *Superior removal of arsenic from water with zirconium metal-organic framework UiO-66.* Scientific reports, 2015. **5**: p. 16613.
79. Gupta, V.K. and Suhas, *Application of low-cost adsorbents for dye removal – A review.* Journal of Environmental Management, 2009. **90**(8): p. 2313-2342.
80. Forgacs, E., T. Cserháti, and G. Oros, *Removal of synthetic dyes from wastewaters: a review.* Environment International, 2004. **30**(7): p. 953-971.
81. Eren, E. and B. Afsin, *Investigation of a basic dye adsorption from aqueous solution onto raw and pre-treated sepiolite surfaces.* Dyes and Pigments, 2007. **73**(2): p. 162-167.
82. Eren, E., *Investigation of a basic dye removal from aqueous solution onto chemically modified Unye bentonite.* Journal of Hazardous Materials, 2009. **166**(1): p. 88-93.
83. Tyagi, O., M. Yadav, and M. Yadav, *A Textbook of Synthetic Dyes, 67, Anmol-PVT*. 2002, Ltd.
84. Eren, E., et al., *Adsorption of basic dye from aqueous solutions by modified sepiolite: Equilibrium, kinetics and thermodynamics study.* Desalination, 2010. **252**(1): p. 88-96.
85. El Qada, E.N., S.J. Allen, and G.M. Walker, *Adsorption of basic dyes from aqueous solution onto activated carbons.* Chemical Engineering Journal, 2008. **135**(3): p. 174-184.
86. Atar, N. and A. Olgun, *Removal of basic and acid dyes from aqueous solutions by a waste containing boron impurity.* Desalination, 2009. **249**(1): p. 109-115.
87. Deniz, F. and S.D. Saygideger, *Removal of a hazardous azo dye (Basic Red 46) from aqueous solution by princess tree leaf.* Desalination, 2011. **268**(1): p. 6-11.
88. Attia, A.A., W.E. Rashwan, and S.A. Khedr, *Capacity of activated carbon in the removal of acid dyes subsequent to its thermal treatment.* Dyes and Pigments, 2006. **69**(3): p. 128-136.
89. Shen, D., et al., *Adsorption kinetics and isotherm of anionic dyes onto organo-bentonite from single and multisolute systems.* Journal of Hazardous Materials, 2009. **172**(1): p. 99-107.
90. Qin, Q., J. Ma, and K. Liu, *Adsorption of anionic dyes on ammonium-functionalized MCM-41.* Journal of Hazardous Materials, 2009. **162**(1): p. 133-139.
91. El Boujaady, H., et al., *Removal of a textile dye by adsorption on synthetic calcium phosphates.* Desalination, 2011. **275**(1): p. 10-16.

92. Leechart, P., W. Nakbanpote, and P. Thiravetyan, *Application of 'waste' wood-shaving bottom ash for adsorption of azo reactive dye.* Journal of Environmental Management, 2009. **90**(2): p. 912-920.
93. Bingol, D., N. Tekin, and M. Alkan, *Brilliant Yellow dye adsorption onto sepiolite using a full factorial design.* Applied Clay Science, 2010. **50**(3): p. 315-321.
94. Mahmoodi, N.M., et al., *Adsorption of textile dyes on Pine Cone from colored wastewater: Kinetic, equilibrium and thermodynamic studies.* Desalination, 2011. **268**(1): p. 117-125.
95. Benjamin, M.M., et al., *Sorption and filtration of metals using iron-oxide-coated sand.* Water Research, 1996. **30**(11): p. 2609-2620.
96. Dambies, L., T. Vincent, and E. Guibal, *Treatment of arsenic-containing solutions using chitosan derivatives: uptake mechanism and sorption performances.* Water Research, 2002. **36**(15): p. 3699-3710.
97. Aworn, A., P. Thiravetyan, and W. Nakbanpote, *Preparation of CO2 activated carbon from corncob for monoethylene glycol adsorption.* Colloids and Surfaces A: Physicochemical and Engineering Aspects, 2009. **333**(1): p. 19-25.
98. Namasivayam, C. and D. Kavitha, *Removal of Congo Red from water by adsorption onto activated carbon prepared from coir pith, an agricultural solid waste.* Dyes and Pigments, 2002. **54**(1): p. 47-58.
99. Monser, L. and N. Adhoum, *Modified activated carbon for the removal of copper, zinc, chromium and cyanide from wastewater.* Separation and Purification Technology, 2002. **26**(2): p. 137-146.
100. Wang, S. and Y. Peng, *Natural zeolites as effective adsorbents in water and wastewater treatment.* Chemical Engineering Journal, 2010. **156**(1): p. 11-24.
101. Hui, K.S., C.Y.H. Chao, and S.C. Kot, *Removal of mixed heavy metal ions in wastewater by zeolite 4A and residual products from recycled coal fly ash.* Journal of Hazardous Materials, 2005. **127**(1): p. 89-101.
102. Mohan, D. and C.U. Pittman, *Arsenic removal from water/wastewater using adsorbents—A critical review.* Journal of Hazardous Materials, 2007. **142**(1): p. 1-53.
103. Cheremisinoff, P.N. and F. Ellerbusch, *Carbon adsorption handbook*. 1978: Ann Arbor Science Publishers.
104. Lin, K.-Y.A., Y.-T. Liu, and S.-Y. Chen, *Adsorption of fluoride to UiO-66-NH2 in water: Stability, kinetic, isotherm and thermodynamic studies.* Journal of Colloid and Interface Science, 2016. **461**: p. 79-87.
105. Azhar, M.R., et al., *Adsorptive removal of antibiotic sulfonamide by UiO-66 and ZIF-67 for wastewater treatment.* Journal of Colloid and Interface Science, 2017. **500**: p. 88-95.
106. Azhar, M.R., et al., *One-pot synthesis of binary metal organic frameworks (HKUST-1 and UiO-66) for enhanced adsorptive removal of water contaminants.* Journal of Colloid and Interface Science, 2017. **490**: p. 685-694.
107. Zhou, Q., et al., *One-step synthesis of amino-functionalized attapulgite clay nanoparticles adsorbent by hydrothermal carbonization of chitosan for removal of methylene blue from wastewater.* Colloids and Surfaces A: Physicochemical and Engineering Aspects, 2015. **470**: p. 248-257.

108. Abid, H.R., H.M. Ang, and S. Wang, *Effects of ammonium hydroxide on the structure and gas adsorption of nanosized Zr-MOFs (UiO-66).* Nanoscale, 2012. **4**(10): p. 3089-3094.
109. Jiang, J., et al., *Superacidity in sulfated metal–organic framework-808.* Journal of the American Chemical Society, 2014. **136**(37): p. 12844-12847.
110. Zhang, Y.-B., et al., *Introduction of functionality, selection of topology, and enhancement of gas adsorption in multivariate metal–organic framework-177.* Journal of the American Chemical Society, 2015. **137**(7): p. 2641-2650.
111. Wang, S., et al., *Synergistic and competitive adsorption of organic dyes on multiwalled carbon nanotubes.* Chemical Engineering Journal, 2012. **197**: p. 34-40.
112. Zhang, Q., et al., *A porous metal–organic framework with–COOH groups for highly efficient pollutant removal.* Chemical Communications, 2014. **50**(92): p. 14455-14458.
113. Park, E.Y., et al., *Adsorptive removal of bisphenol-A from water with a metal-organic framework, a porous chromium-benzenedicarboxylate.* Journal of nanoscience and nanotechnology, 2013. **13**(4): p. 2789-2794.
114. Qin, F.-X., et al., *Adsorptive removal of bisphenol A from aqueous solution using metal-organic frameworks.* Desalination and Water Treatment, 2015. **54**(1): p. 93-102.

Chapter 2

Literature review

2

Chapter 2: Literature review

2.1 Introduction

Globally, water pollution problems have dramatically increased because of a fast-growing world population accompanied by insufficient investment in public water supply and treatment projects [1]. Water quality issues are a major challenge for humanity in the 21st century.

Chemical water pollutants can be divided into two categories. The first is natural macropollutants, which typically occur at the milligram per litre level and includes nutrients such as nitrogen and phosphorous, as well as natural organic constituents [2-5]. The second is pollutants produced by the manufacturing industry, which is the largest source of pollutants discharged into water. This sector involves a wide variety of production; therefore, pollutants from each type of production are characterised by their specificity.

Moreover, chemical and petrochemical industries, pulp and paper mills, electroplating industries [6], mining industry [7] and textile industries [8] are considered the main sources of water pollution. Dyes with considerable colouring capacity are widely employed in the textile, pharmaceutical, food, cosmetic, plastic, photographic and paper industries. Therefore, manufacture and use of synthetic dyes to dye fabric have become a huge industry today [9]. Dyes can adhere to compatible surfaces in solution by forming covalent bonds or complexes with salts or metals, by physical adsorption or by mechanical retention.

Dyes are classified according to their application and chemical structure, and are composed of a group of atoms known as chromophores, which are responsible for the colour of the dye [10]. New ecolabels for textile products and tighter restrictions on wastewater discharge are forcing textile wet processors to remove chemicals from their wastewater. This challenge has prompted intensive research in new and advanced treatment technologies [11].

As a result of their physical (colour) and chemical (toxicity) properties, dyes in wastewaters are a danger to the environment. Diversity and intensity of colours lead to potential problems when the effluent is discharged into water streams [12]. Further, many dyes such as Alizarin S, Crocein Orange G, methyl red, Congo Red, methylene

blue (MB)[13], reactive dyes (reactive red RB, reactive black B, Remazol blue)[14] and methyl orange (MO)[15] are toxic and may cause genetic alterations in humans. As their origins are synthetic, these dyes are not recognised in the natural environment and their toxicity is not easily degraded. While sewage treatment plants deal with different kinds of manufactured waste, their technology is unable to degrade the toxic components of many dyes. Therefore, the search for technology to remove or degrade dyes is of primary importance.

Dyes can be classified anionic (acid, direct and reactive dyes), cationic (basic dyes) and non-ionic (disperse dyes)[16]. MB is a dye widely used in different industries. Its colour is light blue to dark blue because of the thiazine group [17]. Although it is not highly hazardous, MB can have various harmful effects. On inhalation, it can give rise to short periods of rapid or difficult breathing; ingestion through the mouth produces a burning sensation and may cause nausea, vomiting, diarrhea and gastritis. A high dose leads to abdominal and chest pain, severe headache, profuse sweating, mental confusion, painful micturition and methaemoglobinemia [12]. As shown in Figure 2.1, MB is a cationic dye that can be adsorbed easily by electrostatic forces on negatively charged surfaces [18].

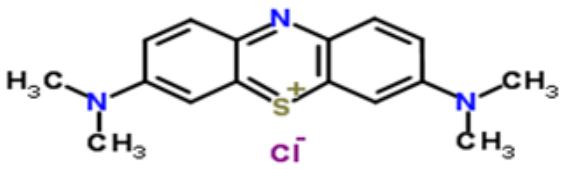

Figure 2.1: The structure of methylene blue.

There is another important dye, MO, which is characterised by a deep orange colour. MO belongs to the group of azo dyes, which are the most common and widely used dyes because they are multipurpose and can be prepared by a facile synthesis process.

This second dye is chosen for investigation because its molecular structure is very different from the first one, as shown in Figure 2.2 [19, 20]. Upon ingestion, MO is metabolised into aromatic amines by intestinal microorganisms or reductive enzymes in the liver, potentially causing cancer [21]. Therefore, the removal of MO before its discharge into the environment is necessary and important.

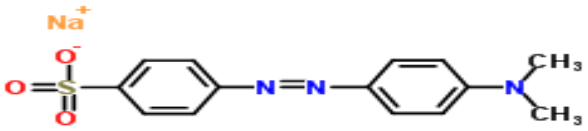

Figure 2.2: The structure of methyl orange.

MB and MO are typical dyes in that they cannot be removed by conventional treatments such as biotreatment; therefore, the removal of such dyes from wastewater has attracted much research interest. Many methods have been tested to remove and degrade these types of dyes, including chemical coagulation, membrane filtration, chemical oxidation, ion exchange and adsorption.

2.2 Discolouration techniques

The discharge of dyes directly into valuable water resources must be avoided. Otherwise, numerous advanced treatment processes must be used. Initially, the treatment of dye wastewater was based on physical processes such as precipitation and equalisation to maintain pH, total dissolved solids and total suspended solids in the discharged water [22]. Later, secondary treatment units such as filtration for biodegradation were used. Nowadays, the activated sludge process is used to remove dyes from wastewater.

Normally, methods of treating industrial wastewater involve the following steps [23]: first, pretreatment (including equalisation and neutralisation) of industrial wastewater effluent before discharging into municipal sewerage systems; then, primary treatment of wastewater is undertaken; next, a secondary treatment (biological treatment) is undertaken. Finally, physical–chemical treatments (tertiary treatment), such as membrane separations, chemical oxidation, ion exchange and/or stripping and adsorption, are undertaken. In practice, biological treatment is the most commonly used process to remove dyes from wastewater.

A large number of bacterial species have been employed to decolour and mineralise various dyes. Biological treatment is relatively inexpensive, and the final products of a biological reaction are not toxic. The reaction can be aerobic (in the presence of oxygen), anaerobic (without oxygen) or combined aerobic–anaerobic [24]. However, some dyes cannot be removed by biological methods. Therefore, physical and chemical methods should be used as advanced treatments.

As the chemical coagulation process relies on the gravity precipitation of suspended particles, chemical flocculants are necessary to increase the efficiency of dye precipitation. However, this process should include a sedimentation basin and clarifiers as essential elements for precipitation [25]. Although chemical coagulation generates a large amount of sludge, it is the most practised treatment for removal of some dyes and is still conducted in many countries. However, its sedimentation process is not always reliable because the coagulation mechanism used to decolourise wastewater is still not understood [26]. Accordingly, industrial dyes can be removed from aqueous solutions by a precipitation process that uses small amounts of ionic liquids as a flocculent. For instance, six dyes can be removed by a precipitation process using solid potassium hexafluorophosphate [27].

Filtration technology is an integral component of drinking water and wastewater treatment applications; it includes microfiltration, ultrafiltration, nanofiltration and reverse osmosis [25]. Dyes are successfully removed from wastewater by ultrafiltration and nanofiltration, while microfiltration is not ideal for wastewater treatment due to its large pore size. In addition, dye molecules may block membrane pores in nanofiltration or ultrafiltration technology, adding costs and shortening membrane life, which makes their application limited in terms of treating dyes in

wastewater [22, 28]. In contrast, reverse osmosis filtration uses pressure to force water through a membrane that is impervious to most pollutants. Reverse osmosis is an operative decolouring and desalting method for a diverse range of dye wastes to produce pure H_2O [29, 30].

Oxidation treatment is a method for clarifying wastewater by using oxidising agents such as chlorine, hydrogen peroxide, ozone or potassium permanganate. Oxidation methods are usually used in decolourisation processes to completely or partially degrade the dyes. As effective oxidation of dyes can reduce complex molecules to CO_2 and H_2O, pH and catalysts are considered major factors in oxidation processes [22]. Commercial dyes are designed to resist photodegradation, so the selection of optimal photocatalytic conditions to decolourise dyes requires considerable expertise. Because of significant commercial and environmental interest, the efficacy with which a large number of catalysts and irradiation conditions decolourise various synthetic dyes has been established [31].

The ion exchange technique is a versatile and effective tool for treating aqueous hazardous waste, including dyes. ion exchange process during the wastewater remediation of dye is the key to decrease the effect of hazardous load to a form of reusable materials by converting them to lesser toxic substances. In addition, ion exchange process has substantial role in the separating and concentrating of contaminants. Since ion exchange resins due to their selectivity and high capacity can be considered as a favourable adsorbent for colour pollutants in textile industry [32, 33].

Adsorption is defined as either partitioning of chemical species between the bulk phase and interface, or accumulation of substances near the interface. The driving force for the adsorption process is surface affinity towards adsorbates. According to the binding energy, adsorption can be sorted into two types: chemisorption and physisorption. Physisorption takes place by van der Waals force, hydrogen bonding and electrostatic force, while chemisorption causes the interaction of adsorbents with adsorbates through strong bonds, such as ionic, covalent and coordinate bonds [34]. This process effectively removes chemical pollutants from wastewater using a porous substance that has a high surface area and high surface affinity towards adsorbates [35]. As it is preferable to recover an adsorbate and regenerate an adsorbent in industrial

applications, the use of physisorption processes to treat wastewater is widespread. Adsorption is a top-of-the-range treatment procedure for removing dissolved organic pollutants like dyes from industrial waste water [36]. Adsorbents, such as zeolites [37-39], activated alumina [40-42] and activated carbon [43-45], have lower costs and are commonly used to remove different types of dyes [35].

Recently, MOFs have captured scientific attention due to their attractive specifications such as large surface area, high pore volume, tuneable pore size, innumerable functionalities and facile modification. Several MOFs with sufficient water stability were used to remove dyes from wastewater and found to be highly efficient at dye removal. As such, a review of their synthesis, activation methods and applications in removing dyes from wastewater is vital.

2.3 Metal organic frameworks

2.3.1 Introduction

Different terminologies, such as coordination polymers, metal organic frameworks and hybrid inorganic and organic framework materials, have been used to describe the non-molecular or extended solid-state structures containing metal ions and organic spacer ligands. However, solid-state chemists tend to prefer the term 'MOF' [46].

MOFs are made by linking inorganic units (metal nodes, metal clusters or metal ions) and organic units (organic linker) using strong bonds. The flexibility with which the structural geometry, size and functionality can be varied has led to reported syntheses and studies of more than 20,000 different MOFs in the past decade [47].

The aromatic organic acid should have ditopic or polytopic carboxyl groups that, when linked to metal-containing units, yield architecturally robust crystalline MOF structures with typical porosity in up to 90% of the MOF crystal volume. The structures and functions of MOFs are often tailored by designing the organic linkers to be of specific length, geometry and functional group. The surface areas of MOFs typically range from 1000 to 10,000 m^2/g: above the values of traditional porous materials such as activated carbons and zeolites [48].

As mentioned above, the synthesis of MOFs requires two essential precursors, the first being metal salt and the second multidentate organic linker. Organic linkers and metal

nodes can govern some MOF properties for selective applications [49]. All cation elements in the periodic table have been used as inorganic nodes to build MOFs. The most reliable metals for synthesising MOFs are Ag^{+1}, Zn^{+2}, Mn^{+2}, Mg^{+2}, Co^{+2}, Zr^{+4}, Ti^{+4}, Hf^{+4}, Rf^{+4}, Cu^{+2}, Al^{+3}, Fe^{+3}, Cr^{+3} and V^{+3}.

Several organic linkers of different lengths have been employed in MOF synthesis, such as 1,4-benzenedicarboxylic acid, 1,3,5-benzenetricarboxylic acid, biphenyl-4,4′-dicarboxylic acid, 4,4′,4″-s-triazine-2,4,6-triyl-tribenzoic acid, 1,3,5-tris(4-carboxyphenyl) benzene, 2,6-naphthalenedicarboxylic acid and others with their derivatives. As examples, Figure 2.3 provides a structural description of zinc terephthalate MOF (MOF-5), zirconium terephthalate MOF (UiO-66)[50], copper trimesate MOF (HKUST-1)[51] and aluminium terephthalate MOF (MIL-53)[52]. The inorganic building of each element has been demonstrated to differ because of the variety in valency and denticity of the organic linkers.

MOFs have been extensively used in different applications based on the specific properties of their linkers and metal clusters. Further, some of these materials have been known to undergo structural transformation upon removal of solvent molecules in the activation process. Therefore, it was thought that the volume of the unit cells might contract after discarding the solvent molecules from the structure because of strong π-π stacking interactions between the aromatic rings of the organic linkers [53, 54].

Some studies have found that MOFs such as MIL-53 (Al, Cr and Fe) exhibit dynamic characteristics: its pores can change in size from narrow to large and vice versa upon dehydration and hydration, respectively. This characteristic may be determined by the nature of the guest molecule (guest–guest interactions), the type of metal and organic linker (host–guest interactions) and the applied pressure [55-57].

MOFs have been synthesised, activated and modified via different methods and used in various applications, such as gas storage and separation, catalysis, sensing applications, drug deliveries and recently, in water treatment.

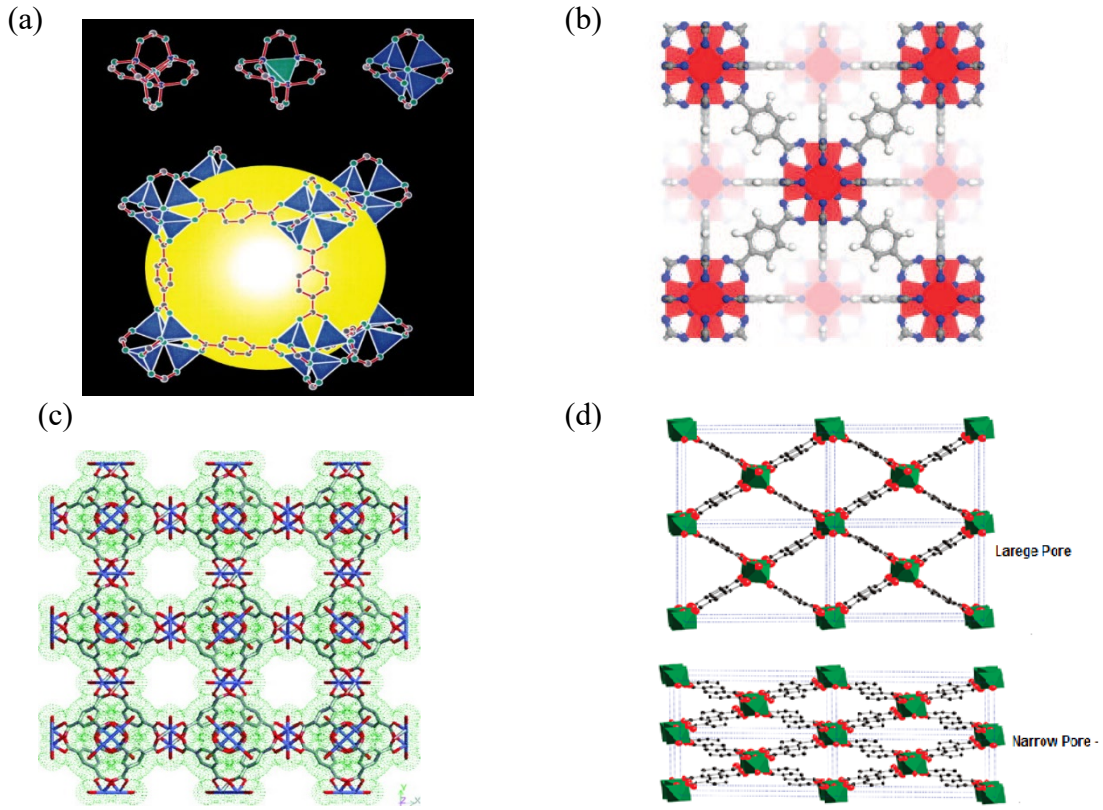

Figure 2.3: Structural description of various kinds of MOFs. (a) Top, the Zn_4 (O) O_{12-6} cluster. Bottom, one of the cavities in the $Zn_4(O)(BDC)_3$ framework (MOF-5)[58]. (b) Zr-MOF with 1,4-benzene-dicarboxylate (BDC) as linker, UiO-66 [50]. (c) The cubic cell of Cu-MOF (HKUST-1)[51]. (d) Large pore and narrow pore structures of the MIL-53(Al)[52].

2.3.2 Reticular chemistry

The origin of reticular chemistry comes from the Latin word 'reticulum', which means having the form of a net or appearing netlike [59]. The secondary building unit (SBU) method can be considered pivotal to the discovery of permanently porous MOFs and to laying the foundations of a new field of chemistry called 'reticular chemistry' [60]. Thus, reticular chemistry is chemistry of binding molecular building blocks (molecules and clusters) to create strong bonds and obtain crystalline extended structures [61]. Figure 2.4 shows some examples of the materials created using basic reticular chemistry.

2.3.2.1 Inspiration for synthesis of MOFs

The motivation for synthesising MOFs comes from coordination networks materials which have single-metal nodes in their vertices. These vertices consist of a single-

metal ion node bonded weakly with a neutral organic donor linker. An example is the Cu-N (pyridine, nitrile)-type bond (e.g., adiponitrile = $NC(CH_2)_4CN$ [see Figures 2.5 and 2.6])[62-64].

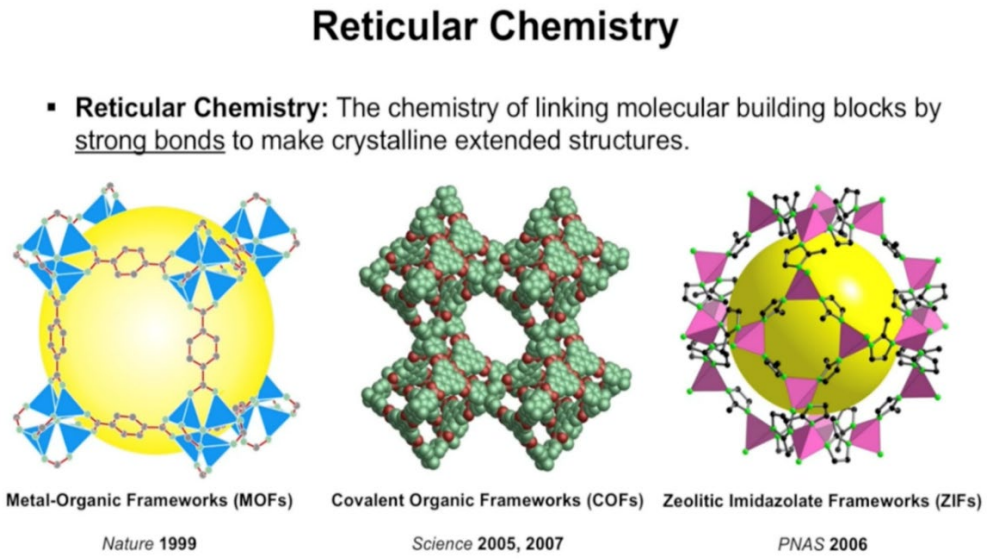

Figure 2.4: Examples of crystalline extended materials [62].

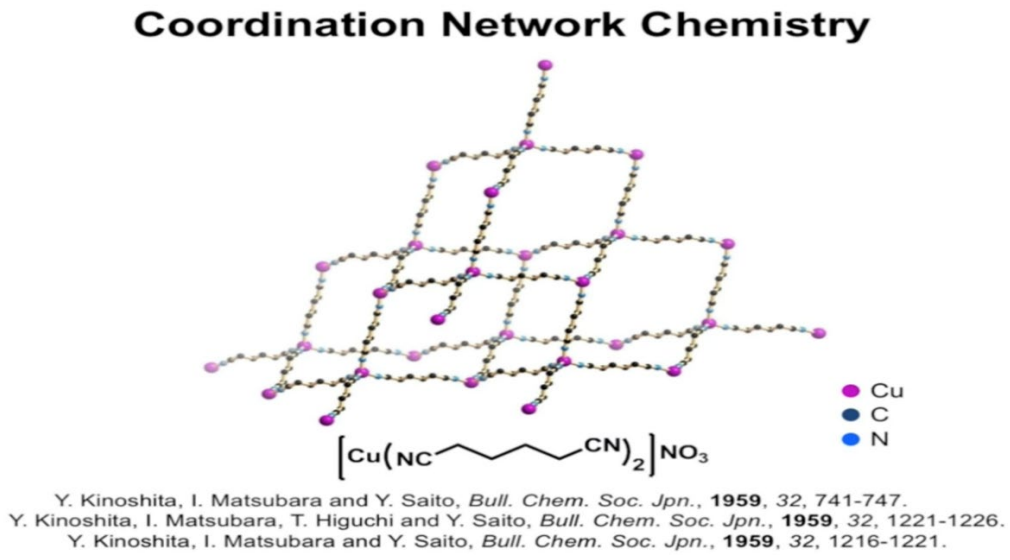

Figure 2.5: Example of the first coordination network [63, 65].

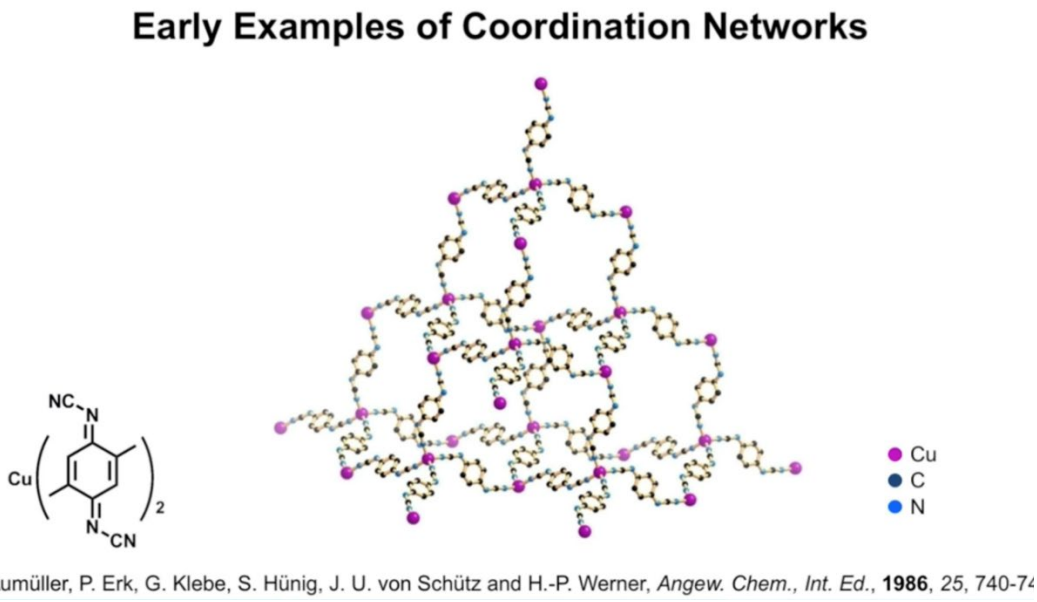

Figure 2.6: Example of an early coordination network [62, 66].

During the end of the 1980s and 1990s, a large number of research papers reported the use of metal ions and neutral donor linkers to synthesise coordination networks materials. These materials proved to have a handful of structure types whose number is limited by the coordination geometries that can be understood using single-metal nodes [64, 67-69]. Based on the weak chemical bonds between the vertices (see Figures 2.7–2.9) and the linker (see Figures 2.10–2.16), coordination networks are non-porous, chemically unstable, undesignable and collapse when the solvents are removed or the ions exchange in the pores.

Such characteristics inspired scientists and researchers to strengthen the chemical bonds between the vertex and the linker (i.e., chelation of metal ions with a charged organic linker) and make MOFs with strong chemical bonds, such as C-C, C-H, C-O and M-O bonds [50, 70-72]. SBUs were created so that these structures of SBUs could serve as rigid, directional and stable building units in the design of robust crystalline materials with predictable structures and properties (see Figures 2.7 and 2.8)[62, 65]. Specifically, this feature of SBU led to the creation of MOFs with ultra-high porosity and structural complexity.

This body of research has led to a unique chemistry framework of architectural, mechanical and chemical stability in MOFs [59, 62, 73]. Despite carrying out reactions involving ligand, linker, metal exchange and metalation reactions, as well as precisely

controlled formation of ordered vacancies, MOFs are able to maintain their structure, crystallinity and porosity. These characteristics of the MOFs, derived from SBUs, make them useful in many applications, such as gas and vapour adsorption, separation processes, removal of contaminants from wastewater and SBU-mediated catalysis [59].

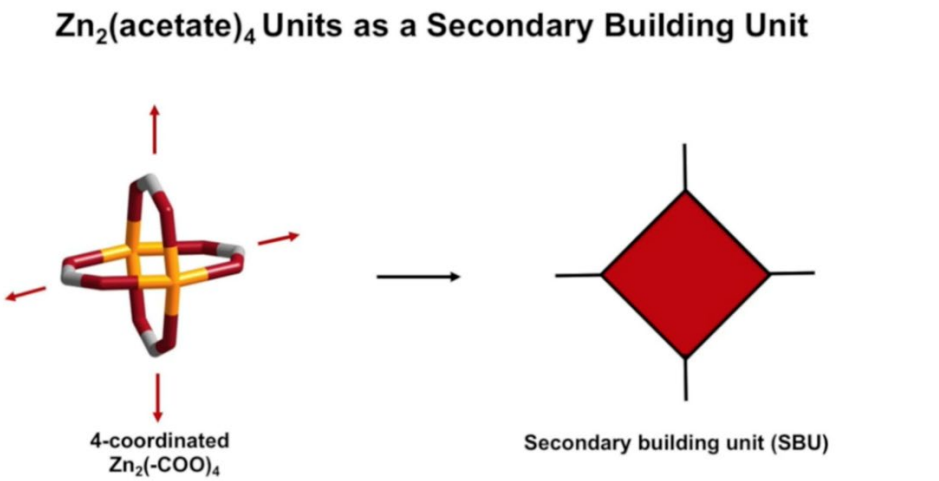

Figure 2.7: Secondary Building Unit (SBU)[62, 65].

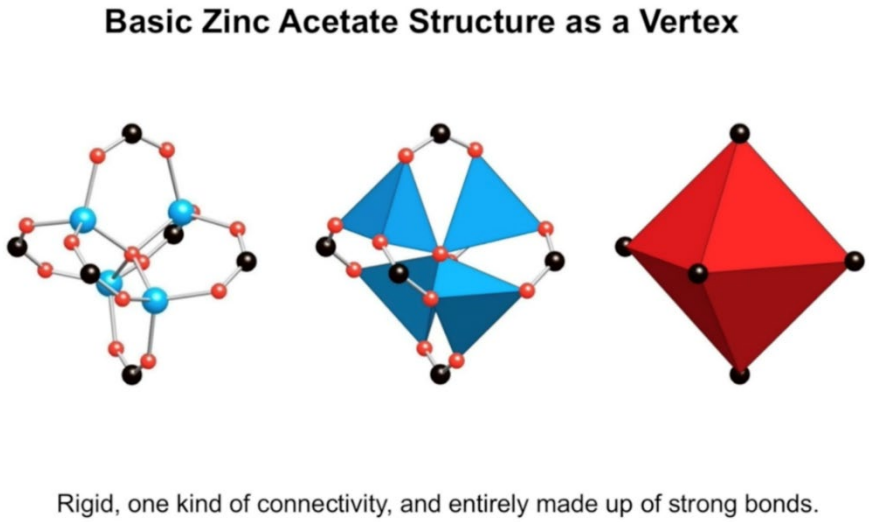

Figure 2.8: Basic zinc acetate structure as a vertex vertex [62].

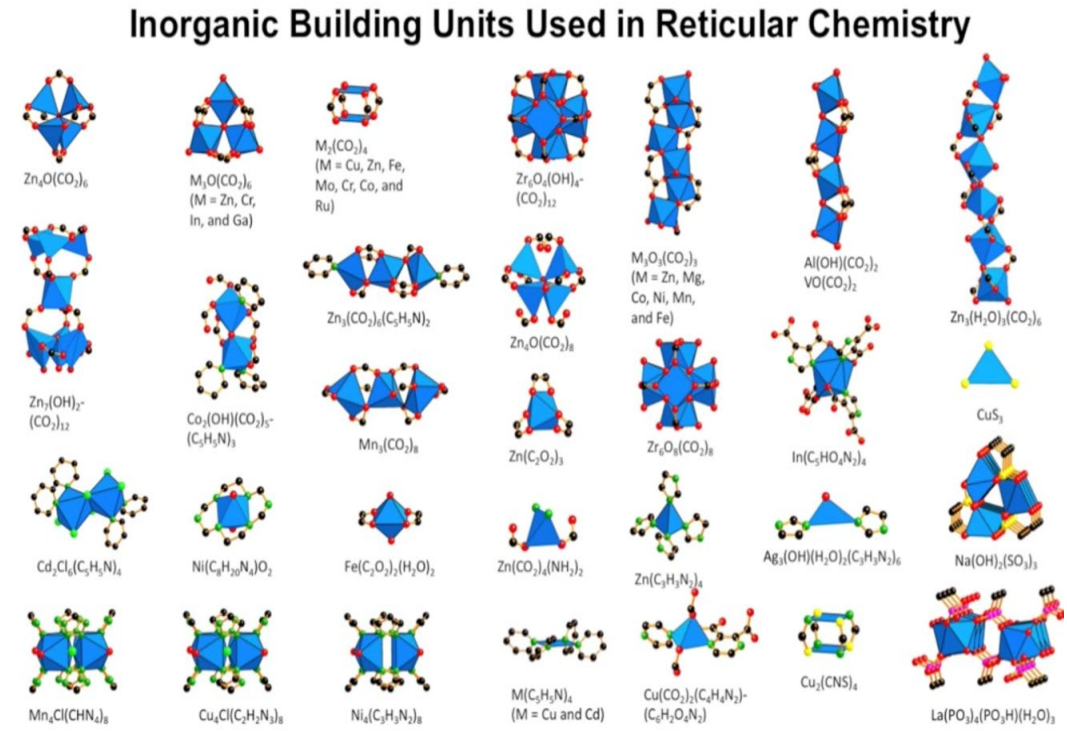

Figure 2.9: Inorganic secondary building units (SBUs) used in reticular chemistry [65].

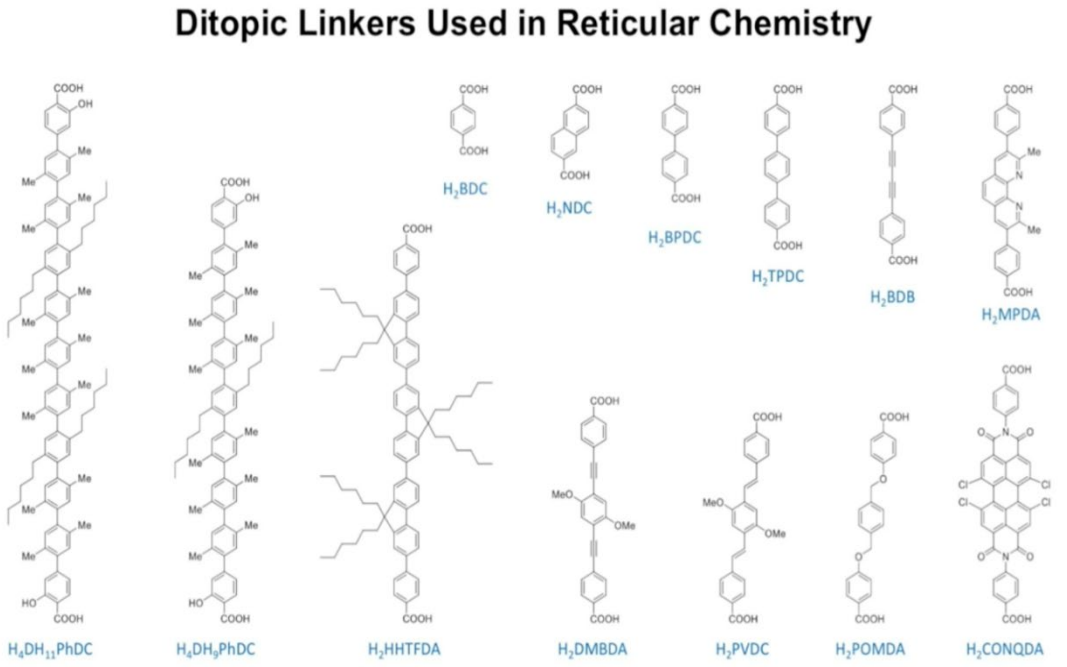

Figure 2.10: Ditopic linkers used in reticular chemistry [62, 65].

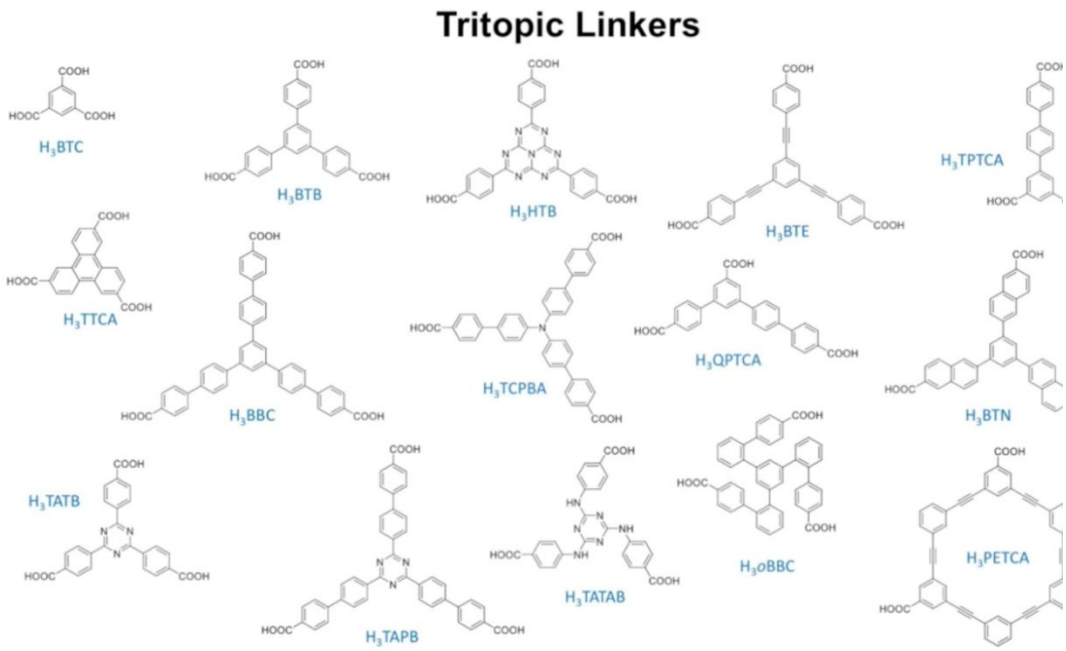

Figure 2.11: Tritopic linkers used in reticular chemistry [62, 65].

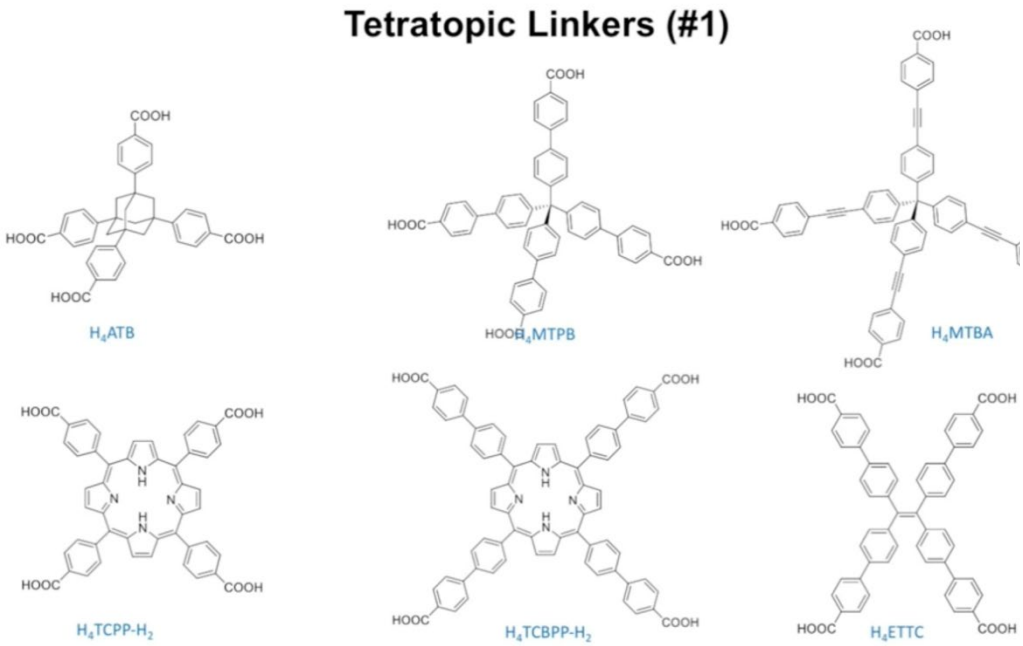

Figure 2.12: Tetratopic linkers used in reticular chemistry [62, 65].

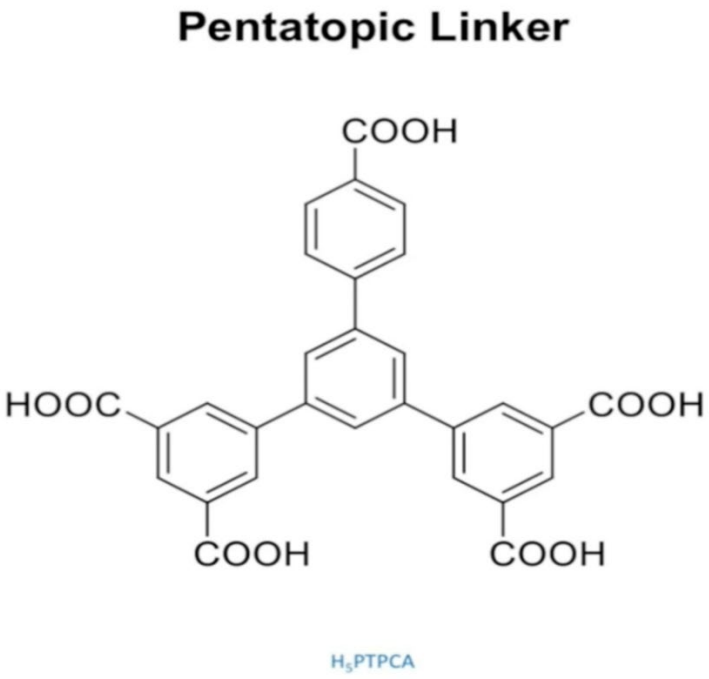

Figure 2.13: Pentatopic linkers used in reticular chemistry [62, 65].

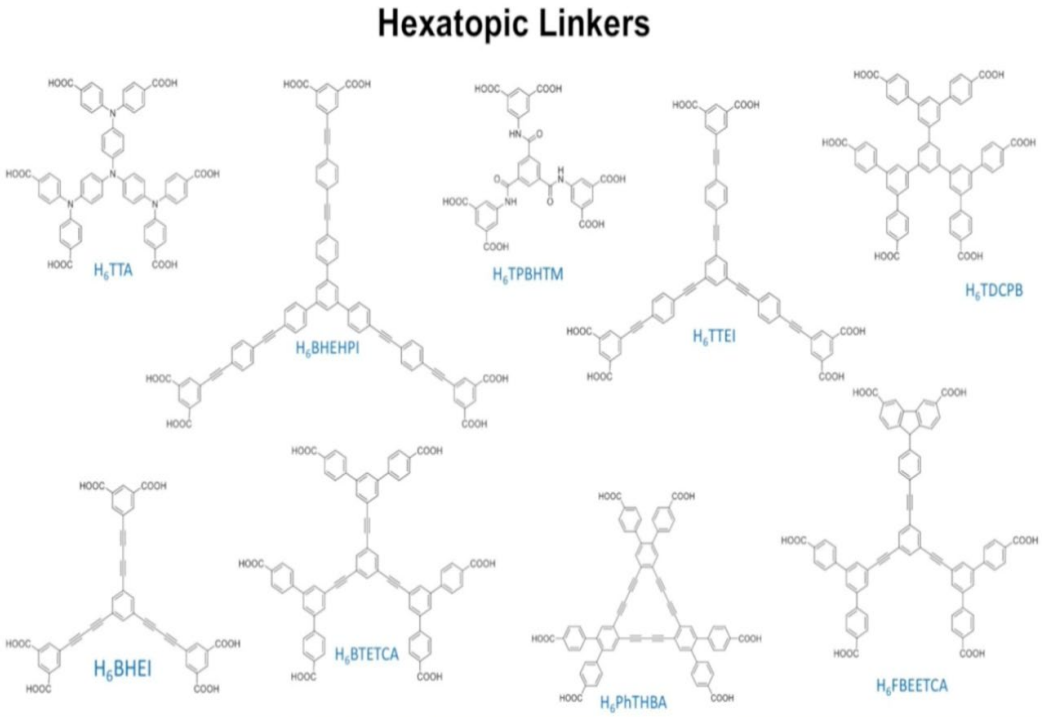

Figure 2.14: Hexatopic linkers used in reticular chemistry [62, 65].

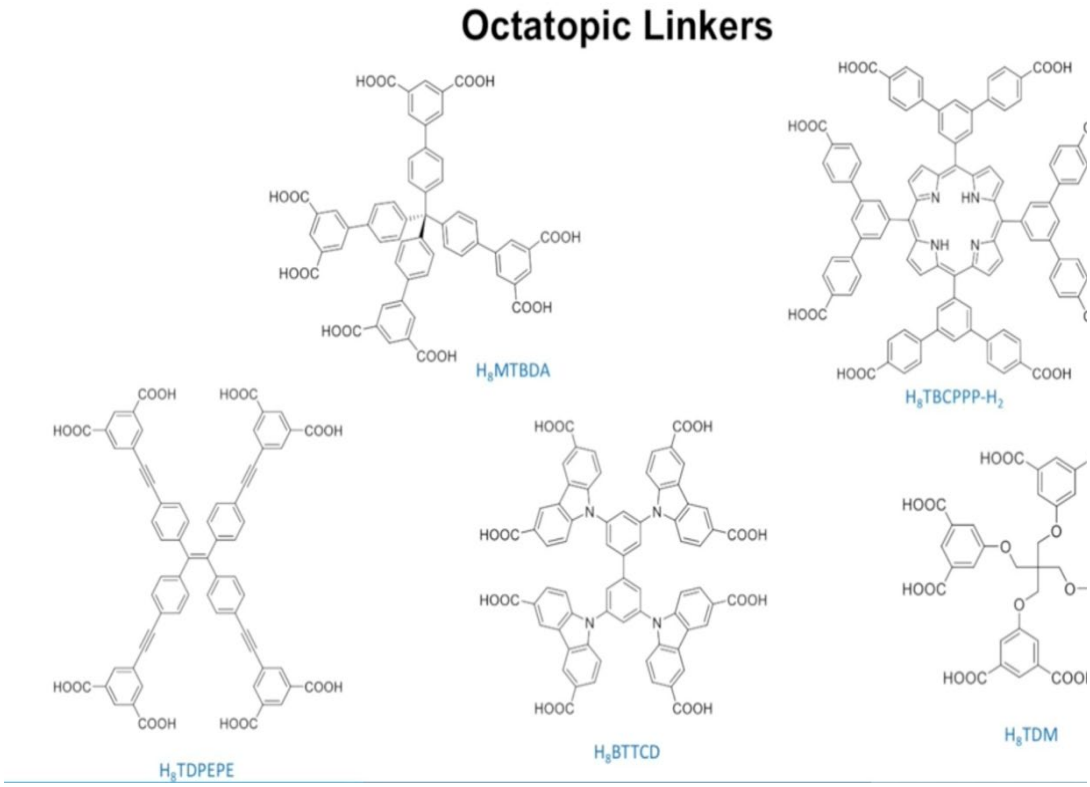

Figure 2.15: Octatopic linkers used in reticular chemistry [62, 65].

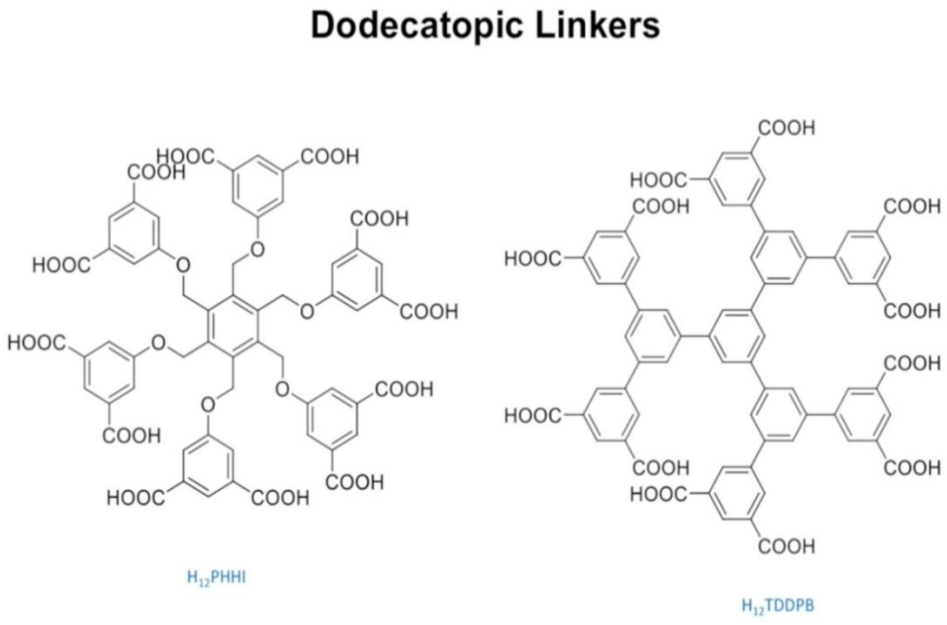

Figure 2.16: Dodecatopic linkers used in reticular chemistry [62, 65].

2.3.2.2 The SBU approach

The key aspect of the SBU method is that it achieved what was considered unattainable at the time: the use of molecular chemistry laws (organic and inorganic) to obtain extended solid-state structures. This innovation has made the SBU an important element in the design and development of MOFs. It has also widened the field of possibilities for controlling constituents of materials at the molecular level, to make 'materials on demand' such as zero-dimensional (0D), one-dimensional (1D), two-dimensional (2D) and three-dimensional (3D) crystalline porous extended materials [74-79].

Using SBUs in the first half of 1998, Hailian and co-workers reported the synthesis of the first new material, called 'MOF-2' ($Zn_2[BDC]_2[H_2O]_2$). MOF-2 is a binuclear paddle wheel of zinc clusters ($Zn_2[–COO]_4[H_2O]_2$) aided at the vertex (SBU) to form 2D porous layers by reticulation of Zn^{2+} ions with a charged organic linker called 1,4-benzene dicarboxylate ($BDC^{2–}$)[80].

Using the same SBU approach to synthesise MOFs, other researchers have used the tetranuclear (basic zinc acetate cluster [$Zn_4O(\text{-}COO)_6$]) as SBU and reported the formation of 3D MOFs (called 'MOF-5'). The reticular chemistry of the SBUs utilises BDC linkers to generate MOF-5 ($Zn_4O[BDC]_3$), which has the key features of exceptional architectural stability, porosity and an ultra-high surface area [81]. The design and formulation of MOF-5 and other 3D MOFs, like HKUST-1 and $Cu_3(BTC)_2(H2O)_3$ (BTC = benzene-1,3,5-tricarboxylate)[82], employ the SBU approach inspired by the pioneering MOF-2 study [59].

As at 7 June 2018, the Cambridge Crystallographic Data Centre has identified in its Cambridge Structural Database (CSD) 84,185 MOF structures [83], as well as numerous published articles on the synthesis, structure and applications of MOFs every year (see Figure 2.17). Interest, growth and advances in MOF chemistry, inspired by the SBU approach, have given rise to significant and numerous expansions in the range of Brunauer–Emmett–Teller (BET) surface area (see Figure 2.18) and of MOFs that have been synthesised, studied and used in applications [59].

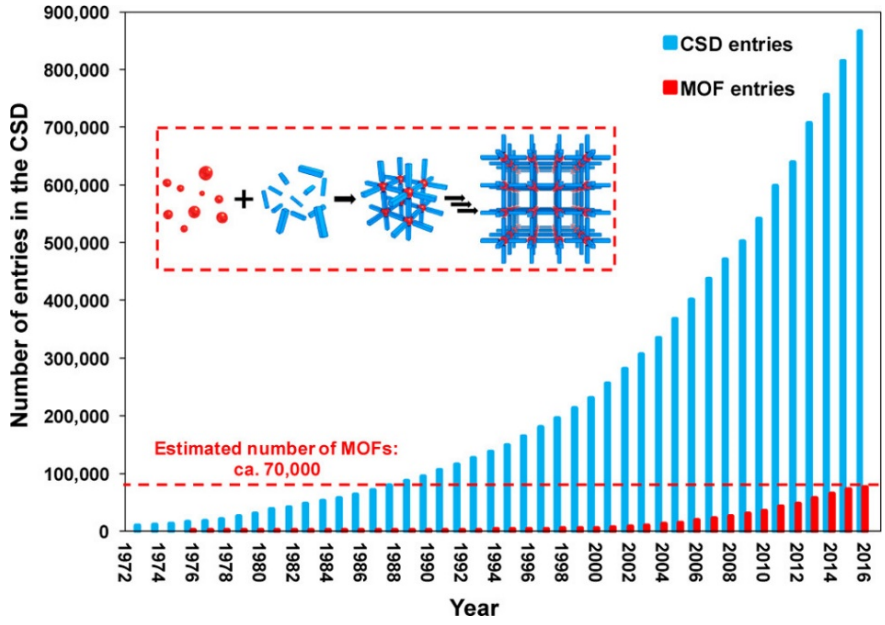

Figure 2.17: Growth of the CSD and MOF entries since 1972. The inset shows the MOF self-assembly process from building blocks: metals (red spheres) and organic ligands (blue struts)[83].

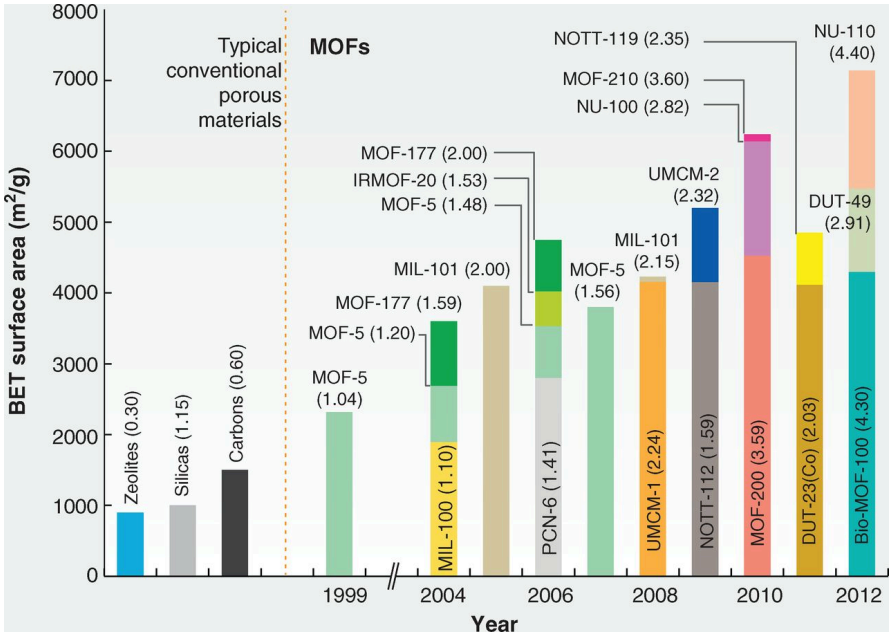

Figure 2.18: Progress in the synthesis of MOFs with ultra-high porosity. BET surface areas of MOFs and typical conventional materials were estimated from gas adsorption measurements [84].

2.3.3 MOF design

Although innovative synthesis to create novel materials is more art than science, the most crucial component of its technology is that new substances are created serendipitously.

Until the end of twentieth century, when the SBU approach was discovered, scientists used methods referred to as 'mix and wait', 'shake and bake' or 'heat and beat'. These methods worked well to synthesise essential solid-state materials, and researchers will continue to use these methods to obtain interesting compounds to benefit industries and communities [60].

However, nowadays technological revolution and high demand worldwide for materials in different industrial applications have developed MOF chemistry to the stage of designing crystalline extended materials for a specific function and composition, structure, functionality, porosity, metrics for a metal organic structure and dynamics with high reliability [85, 86]. Advances in MOF chemistry have enabled the production of materials with highly specific and cooperative applications [74, 75, 87].

The belief in the lack of association between the structure of the starting materials and resultant materials was the reason for the lack of predictability in the structures of new solid-state materials, such as coordination networks and other extended solids that were synthesised using traditional methods. Based on MOF chemistry in the SBU approach, the designed material can be made reliably by governing the reaction conditions under which a certain SBU targets a predetermined geometry, topology and structural connectivity of both building units [88]. The design of MOFs requires precise knowledge about the chemistry of the metal ion that will be utilised to form a specific SBU, because small differences in the conditions of synthesis can lead to the formation of different types of SBU. Moreover, the structure of the organic linker during the synthesis process must remain unchanged so that the constituents of the linker will not affect the formation of the intended SBU [89].

The process of reticular synthesis is key to designing MOFs with predetermined topologies. Appropriate building units are selected to build the targeted net. Edge-transitive nets or default topology can be formed by any assumed set of building units (vertices and linkers).

Figure 2.19 shows a reticular table that provides the edge-transitive nets for any given combination of building units and their augmented form (which are commonly produced in reticular synthesis); possible non edge-transitive nets are also indicated by the empty boxes. According to the reticular table, a suitable selection of shape and size of building units enables scientists to fabricate any structure for a specific application.

From a topological point of view, a reticular synthesis of MOFs that uses similar building units with the same geometry and connectivity, but differ in size, can result in what is called 'isoreticular frameworks. Therefore, although the structures of building units may be similar in topology, their different metrics may be employed to create materials having different applications (see Figure 2.20)[70, 84].

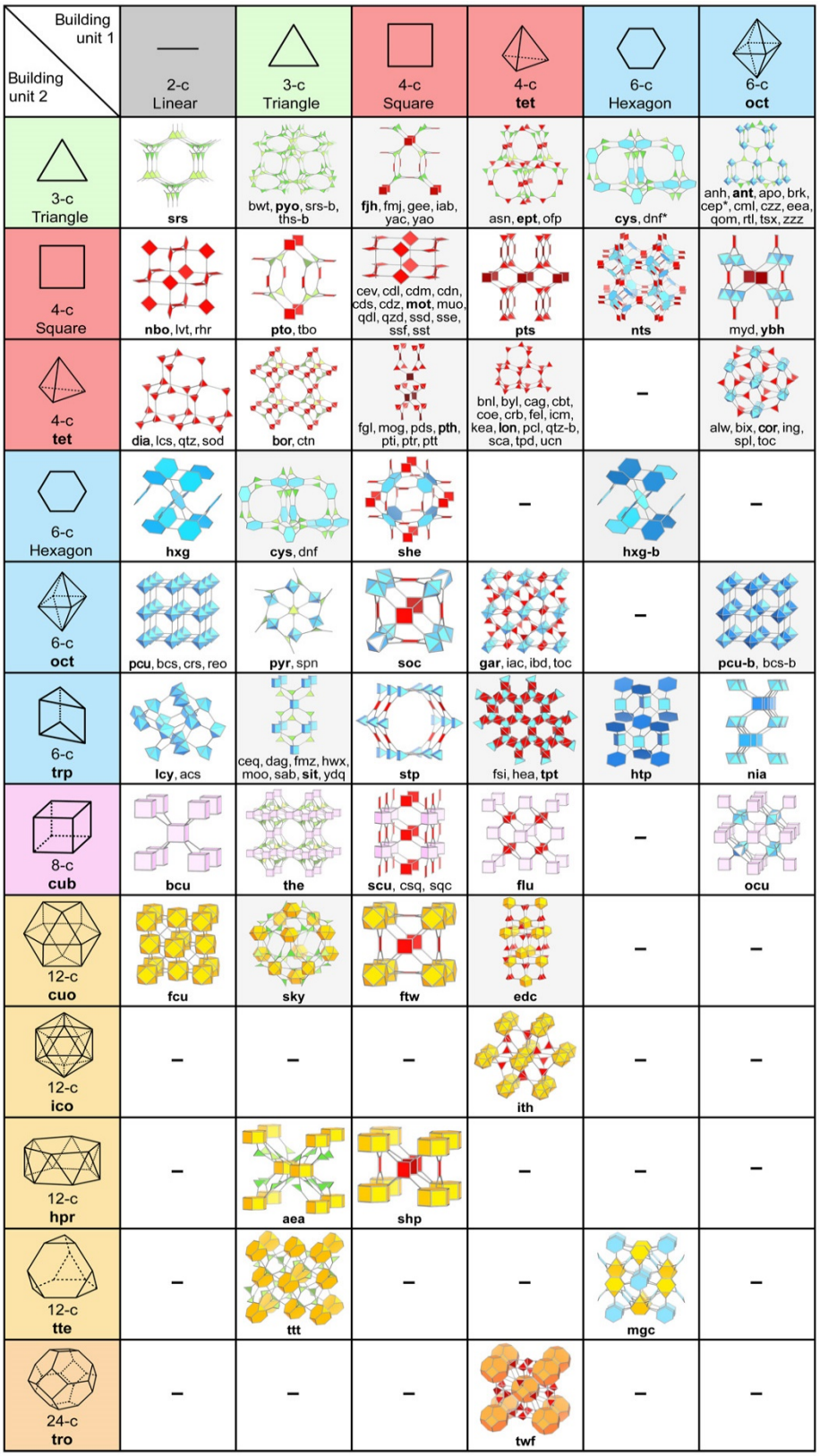

Figure 2.19: The reticular table. A table of possible bipartite nets representing binary frameworks made by reticular chemistry. All topologies are shown as their corresponding augmented net [59, 62].

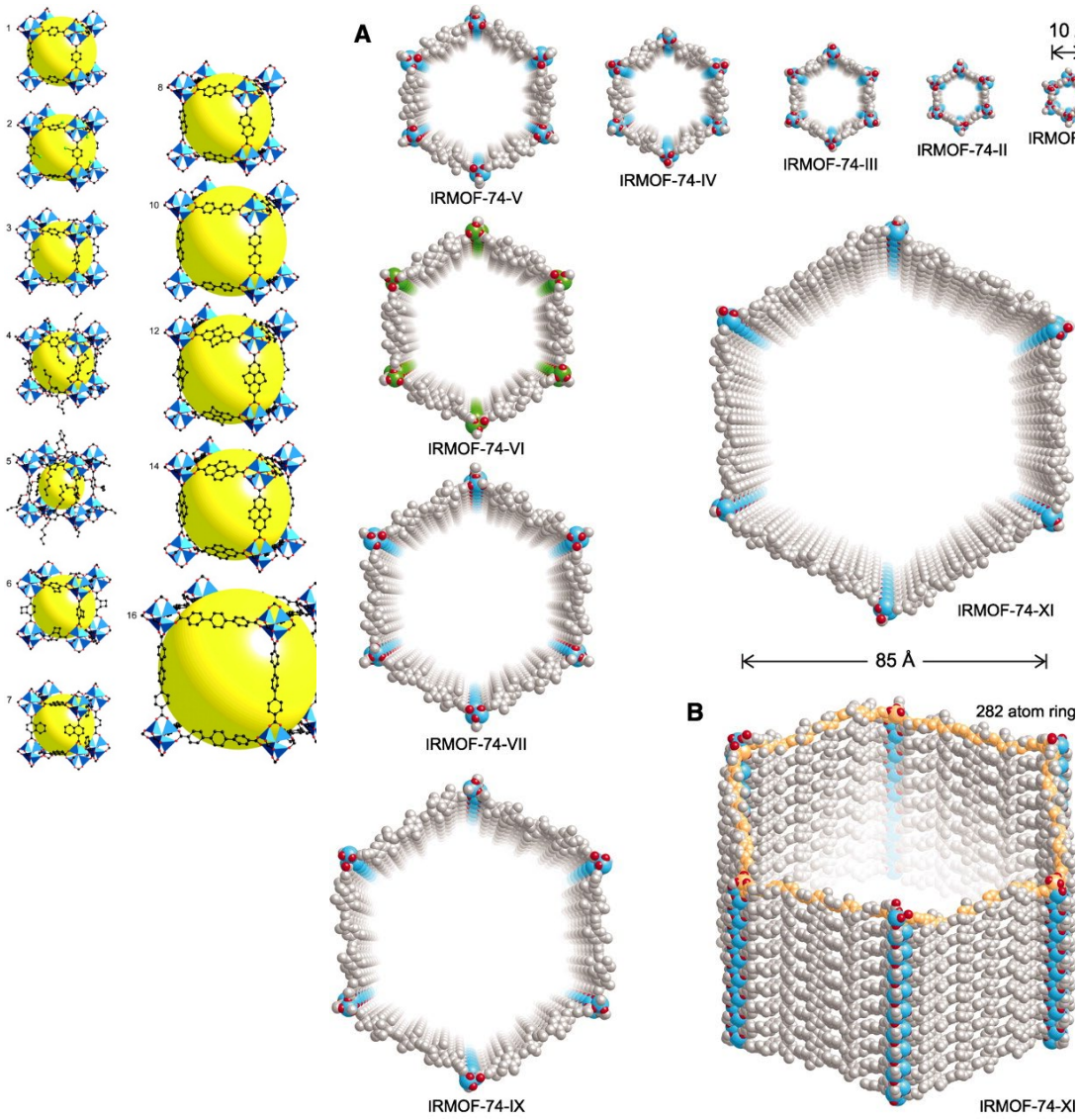

Figure 2.20: Isoreticular structures of isoreticular metal organic framework (IRMOF-n) (n = 1 through 7, 8, 10, 12, 14 and 16), labelled respectively [70]. (A) Perspective views of a single one-dimensional channel shown for each member of an IRMOF series. Perspective side view of the hexagonal channel, showing the ring of 282 atoms (highlighted in gold) that define the pore aperture of the largest member of the series, IRMOF-74-XI [90].

2.3.4 Synthesis methods

Metal organic frameworks (MOFs) have been synthesised by two main chemical approach (Liquid phase synthesis and Solid phase synthesis) as well as new technique so called Ionothermal synthesis which also considered as liquid phase synthesis.

2.3.4.1 Liquid-phase synthesis

Three constituents must be available in the synthesis procedure: the first is a metal salt, the second is a suitable organic linker and the third is a solvent. Most MOFs are synthesised in liquid-phase syntheses, where the metal salt and organic ligand are mixed together with the selective solvent inside a suitable container or the metal salt and organic ligand are dissolved separately in the solvent and then mixed in a single pot [91]. Solute–solvent interactions include hydrogen boding, ion–dipole, dipole–dipole, dipole-induced dipole, solvophobic, and dispersion or London interactions.

Generally, the effects of the solvents depend on several factors: solubility, reactivity, stability, donor number, dielectric constant, polarity and boiling point temperature [92, 93]. Consequently, solvents or co-solvents play a primary role in the topological control of the structure of porous materials [94]. Solvent aside, the results of this method are controlled by several factors: concentration of reagents, heating temperature and heating duration, pH of the solution and the nature of the precursors. These factors affect the morphologies, crystal sizes, topologies and phase purity of the produced material [95]. There are many reliable methods for liquid-phase synthesis of MOFs; these are described below.

2.3.4.1.1 Slow evaporation method

The slow evaporation method is the oldest conventional method for growing crystals and has been used recently to synthesise MOFs in a very simple procedure, as shown in Figure 2.21. It generally does not require external energy.

Although this method is chosen occasionally because it is a low-temperature process, its major drawback is that it consumes too much time compared with other methods [91]. However, if an increased yield has priority over high crystal quality, the reaction times can be significantly reduced by increasing the concentration of precursors and using agitation [96]. Consequently, the product formed under these conditions may or may not be identical to those achieved by other methods used to produce highly crystalline materials [97].

In the slow evaporation method, a solution of the initial materials is concentrated by slow evaporation of the solvent at constant low temperature. Sometimes the process contains co-solvents, which can increase the solubility of the reagents and accelerate

the process through quicker evaporation of low–boiling point solvents [91]. Table 2.1 demonstrates some MOFs which are prepared by slow evaporation synthesis method.

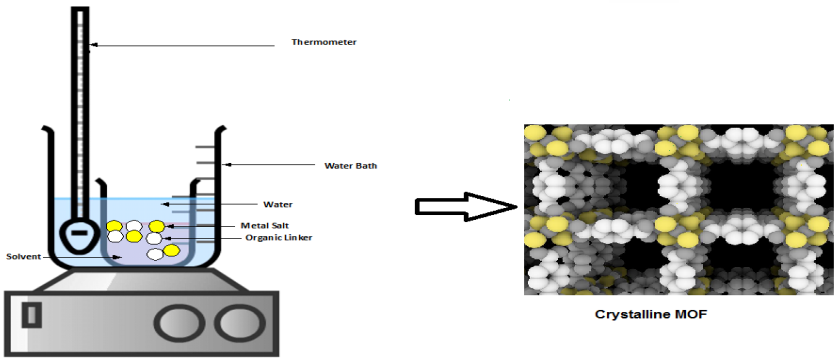

Figure 2.21: Slow evaporation method for synthesis of MOFs.

2.3.4.1.2 Hydrothermal or solvothermal method

The hydrothermal and solvothermal method are widely used in the synthesis of advanced porous materials, such as zeolites, metal oxides and MOFs. The term 'hydrothermal' means any homogeneous or heterogeneous chemical reaction in the presence of water at above room temperatures and at a pressure greater than 1 atm; whereas the term 'solvothermal' indicates the chemical reaction occurs in the presence of an organic solvent [98] (see Figure 2.22).

This method should be carried out in closed vessels, such as a glass vial or acid digestion vessel [91]. Glass vials are mostly used for reactions at temperatures lower than 373 K. Acid digestion vessels are usually used for reactions at higher temperatures. The pressure inside the vessel is directly related to its volumetric capacity and the volume occupied by the solvents. In fact, to control the autogenous pressure, the volume occupied by the organic solvent should be less than 75% of the total capacity of the vessel, while that occupied by aqueous solvents should be less than 30% of the total volume. The solvent is carefully selected based on its chemistry [99]. The solvents are either protic—hydrogen donors with high dielectric constant and polarity, such as water, ethanol, methanol or acetic acid—or aprotic solvents such as dimethyl sulfoxide, N, N-dimethylformamide, dimethylformamide, acetonitrile or acetone. Aprotic solvents cannot take part in hydrogen bonding and they have intermediate dielectric constant and polarity [100]. Table 2.1 show some MOFs which are prepared by hydrothermal or solvothermal techniques.

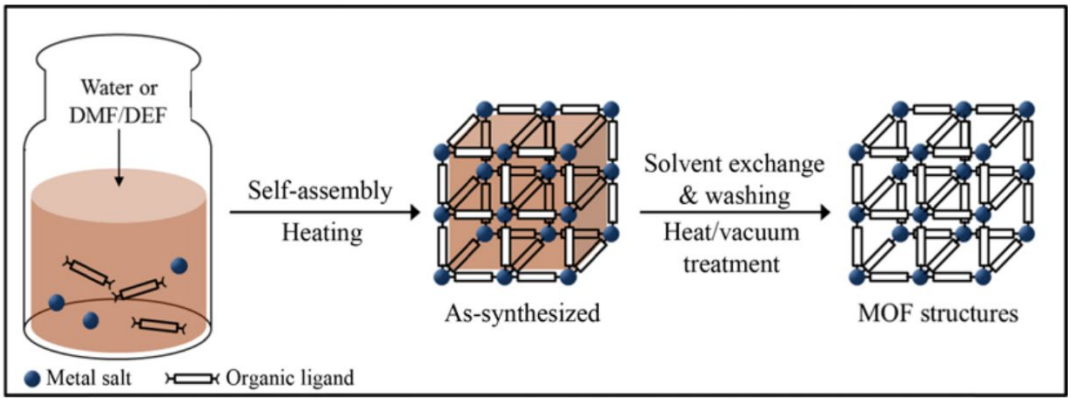

Figure 2.22: Hydrothermal/Solvothermal synthesis of MOFs [101].

2.3.4.1.3 Electrochemical method

The electrochemical method is a promising and environmentally friendly technique for fabricating MOFs, because its conditions for synthesis are mild, the crystal growth occurs relatively quickly, the method can be easily scaled up [102] and there is possibility of controlling the reaction conditions directly during the synthesis process. The concept relies on an electrochemical method to raise the pH and subsequent deprotonation of the linker. As a result of anodic dissolution, the nucleation of MOF crystals starts near the electrode surface with the consequent formation of a thin MOF layer [103].

In narrative detail, the electrochemical method uses an electrode to generate the metal ions by immersing the electrode in a solution of the linker and an electrolyte material. After applying a set voltage, metal ions are produced around the surface of the electrode and then directly react with the deprotonated linkers in the solution to form the MOF molecules near the electrode surface. The quality of the product by this method depends on several parameters, including the applied voltage, specific current, the gap between the electrodes, duration of synthesis, type of solvent, chemistry of the linker and electrolyte concentrations [104].

Electrochemical synthesis allows more control over the reactant concentration during synthesis over the course of time, since it is performed without building pressure. Therefore, not only can the metal be added at different rates by controlling the anodic oxidation, but the linker can also be continuously added to the solution. In addition, it

should be possible to carefully control the oxidation state of the metal simply by adjusting the voltage to the electrode [105].

An electrochemical synthesis method was proposed to avoid the major disadvantages that beset conventional methods, such as large amounts of waste, the risks and costs associated with anions such as nitrates and chlorides, and oxidation and corrosion hazards [106]. Functionalised isoreticular metal organic framework (IRMOF-3) was successfully prepared by an electrochemical method using a zinc plate as the anode, a copper plate as cathode while the co-solvents dimethylformamide (DMF) and ethanol were used to dissolve the organic linker and the electrolyte (tetrabutylammonium bromide)[107], as shown in Figure 2.23. Table 2.1 illustrate some MOFs which are prepared by electrochemical approach.

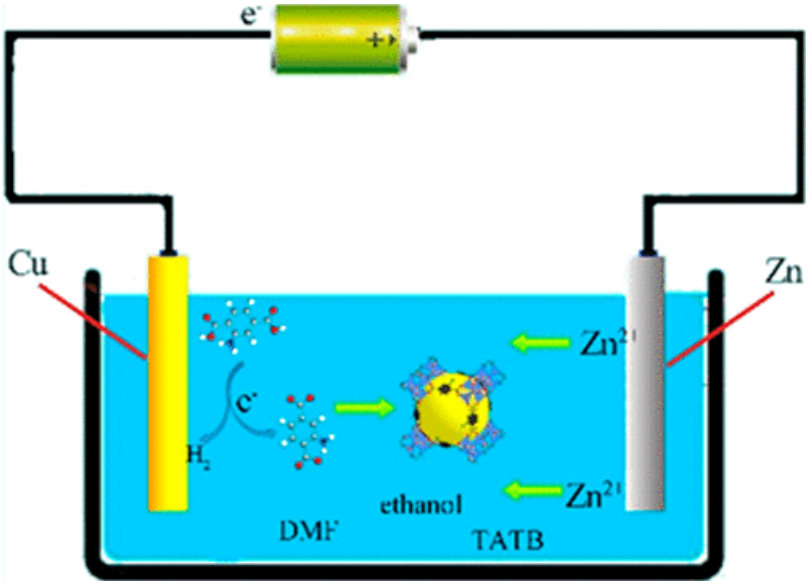

Figure 2.23: Electrochemical synthesis of IRMOF-3 [107].

2.3.4.1.4 Sonochemical method

The sonochemical method usually uses the energy of ultrasound (in the range 20 kHz to 1000 kHz) to accelerate the reaction between metal centres and organic ligands in the solvent [108].

This ultrasound-assisted method for synthesising MOFs is recent technology, rapid, economic and environmentally friendly. Its main advantage is that in requiring unusual reaction conditions, such as high pressure and temperature, the reaction time is short [109].Specifically, ultrasound causes chemical or physical changes via a solution of

precursors. The acoustic cavitation process involves the formation, growth and prompt collapse of microbubbles in a solution of precursors as a result of pressure fluctuations that occur in the applied sound field [110], which create local hot spots of high temperature and pressure of short duration [111]. The extreme conditions can promote chemical reactions by immediate formation of a superfluous crystallisation nuclei. The characterisation of the product is affected by the duration of ultrasonication, temperature and applied ultrasound power [112].

As shown in Figure 2.24, sonochemical methods can generate homogeneous nucleation centres, with considerable reductions in crystallisation time compared with conventional hydrothermal methods [91, 101]. Table 2.1 demonstrate some MOFs which are prepared by sonochemical synthesis.

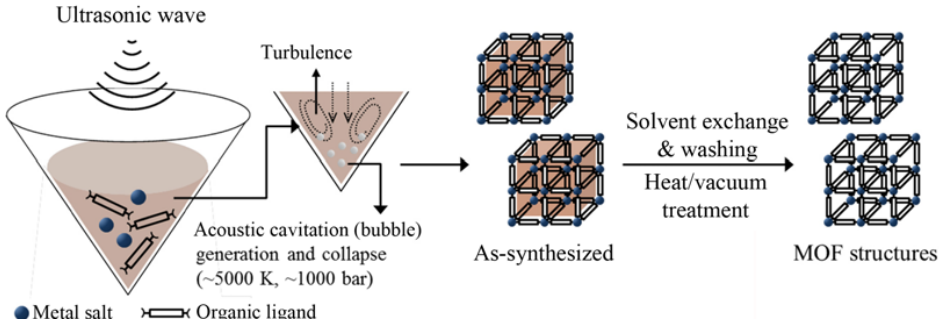

Figure 2.24: Synthesis MOFs by sonochemical method [101].

2.3.4.1.5 Microwave method

The microwave-assisted method is a very fast method for synthesising MOFs; microwave irradiation provides energy for the growth of MOFs over a short period. It was originally used to yield nanosized metal oxides because it was fast, clean and economic [113]. The benefits of this method include high productivity, phase selectivity, small particle size and control over morphology [114, 115].

The principle of microwave-assisted synthesis is to build up the interaction of electromagnetic waves with mobile electric charges in the solution (polar solvent, metal ions, deprotonated organic ligand). Crystalline powders are formed very quickly,

within a minute, from an identical starting mixture under microwave irradiation at temperatures between 423 K and 493 K [115]. However, concentrated reagent solutions are not preferred because it may lead to the production of metal oxides [116].

There are many disadvantages to the microwave method. A high reaction temperature can result through rapid microwave heating in a sealed vessel. In addition, solvents with lower boiling points can be used under pressure (in closed-vessel conditions) and heated at temperatures considerably higher than their boiling points [117].

As shown in Figure 2.25, highly crystalline UiO-67 was created by microwave-assisted synthesis at a lower temperature and over a shorter period than that achieved by conventional solvothermal synthesis. Microwave heating resulted in a product with textural properties, morphology and affinity for adsorption similar to that achieved by solvothermal synthesis [118]. Table 2.1 show some MOFs which are prepared by microwave method.

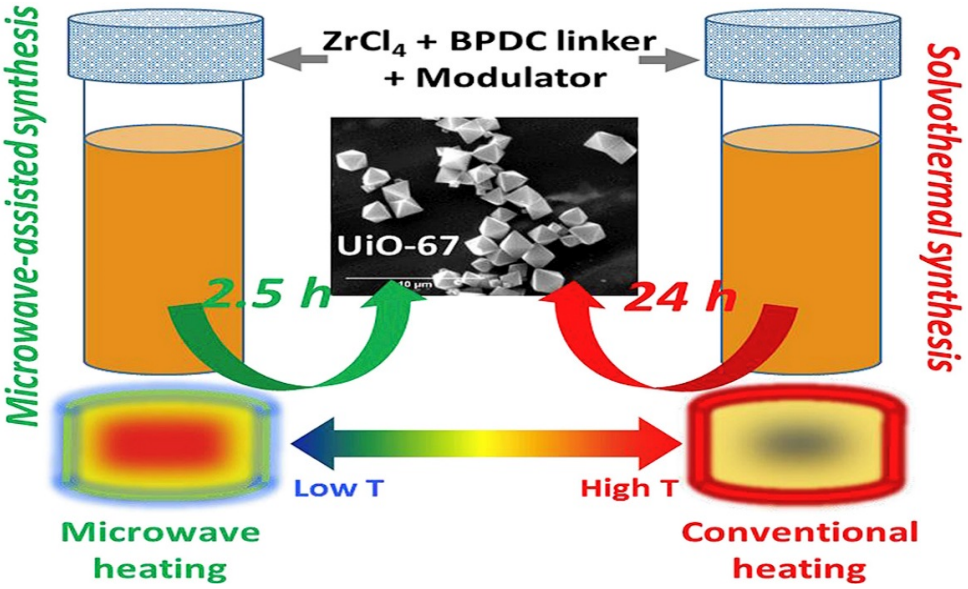

Figure 2.25: Synthesis of UiO-67 by microwave heating compared with conventional heating [118].

2.3.4.1.6 Spray drying method

The spray-drying process starts with atomisation of a solution of precursors into a spray of microdroplets, using a two-fluid nozzle. This step is accomplished by

simultaneously injecting the solution at a certain flow rate with compressed air, or with nitrogen gas at another flow rate. The droplet of a precursor is suspended by a gas stream heated to a certain temperature, which evaporates the solvent and persuades the precursors to diffuse radially to the surface. Then, the concentration of the precursor increases continuously until the required concentration on the surface is reached, when the nanosized MOF crystals start to grow and accumulate on the surface [119], as shown in Figure 2.26.

The spray-drying method has been modified to be a continuous process to allow the collection of dry MOFs in the form of microspherical superstructures. Further, the used solvent can be recovered easily; therefore, this process is cost and waste efficient [120]. Table 2.1 illustrate some MOFs which are prepared by spray drying synthesis.

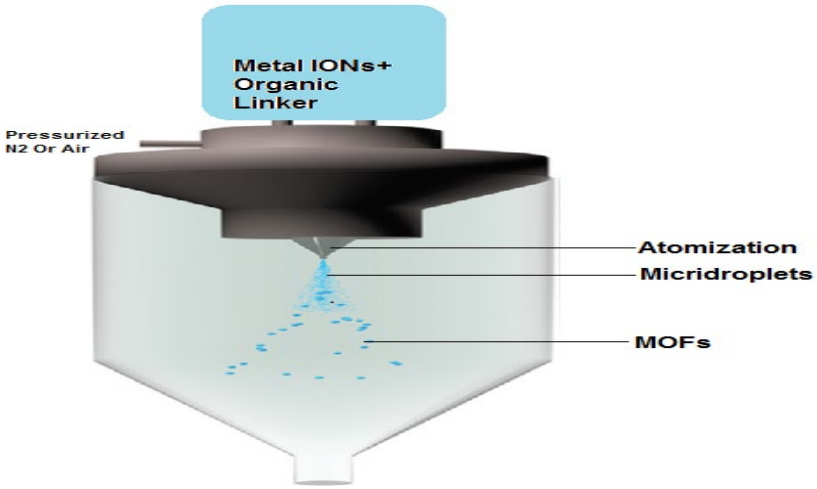

Figure 2.26: Synthesis of MOFs by spray flow method.

2.3.4.1.7 Flow chemistry method

The flow chemistry method is an ultra-fast continuous process for synthesising MOFs with tuneable characteristics, depending on the temperature, residence time and slug volume [121].

Specifically, this method consists of four major parts: a syringe system, a microtubular reactor, a temperature-controlled oil bath and a glass vial to collect the product, as described in Figure 2.27. The syringe system includes three syringes: the first to supply the silicon oil solution to prevent plugging of the reactor and aggregation of the

particles, the second to inject the metal solution and the third to inject the organic ligand solution [122]. The product can precipitate to the bottom of the vial, underneath a layer that is related to the solvents and another layer related to the silicon oil.

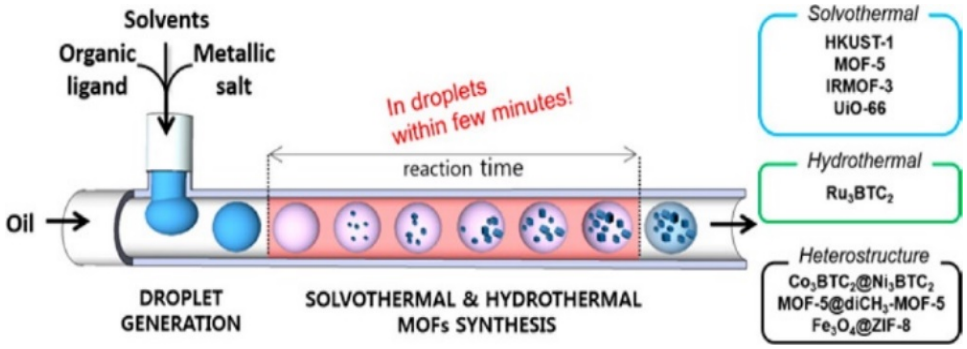

Figure 2.27: Flow chemistry method for preparing MOFs.

Another wet synthesis method, solid-state synthesis, is used to synthesise and control the growth of different MOF nanocrystals on various mesoporous substrates. This method permits the rational construction of hierarchical hybrid porous systems for given applications, while overcoming the limitations of current solvothermal methods. The integration of MOFs with mesoporous materials would benefit from mass-transfer kinetics of mesoporosity, avoid the limitation of diffusion in bulk particles, impart sphericity to MOF particles and protect MOF structures from physical forces that could cause attrition of bulk particles in fluidised processes [123]. Table 2.1 show some MOFs which are prepared by flow chemistry method.

2.3.4.2 Solid-phase synthesis

Grinding solid reagents under solvent-free or low-solvent conditions is emerging as a general synthetic technique that is an alternative to conventional solvent-intensive methods, because it is quicker and easier [124]. Solid-state synthesis has difficulties with obtaining single crystals and therefore, with determining product structure—otherwise quite easy in solution-phase synthesis [91]. Mechanosynthesis is a well-known technique in metallurgy and mineral processing, but within the last few decades it has expanded rapidly into many areas of chemistry such as catalysis, inorganic chemistry and pharmaceutical synthesis.

The use of mechanochemical methods to construct MOFs has significantly improved the synthesis of porous MOFs [125]. Practical demand for mechanosynthesis has

increased because this method can be used to synthesise some MOFs that are challenging to synthesise by conventional wet synthesis methods, due to the slightly low solubility of reactants [126].

Further, there are three diverse mechanochemical methods of synthesising MOFs. First, the solvent-free grinding technique is the simplest and uses hydrated metal salts. Water is released after grinding. Second, the liquid-assisted grinding technique is faster and more flexible, as it utilises a little catalytic amount in the liquid phase to accelerate the mobility of the reagents, their partial dissolution or even eutectic formation [127, 128]. Third, the ion- and liquid-assisted grinding technique, utilises a catalytic liquid with drops of salt additives to increase the rate of MOF production. This last technique produces unpredictable structure-directing effects by the insertion of salt ions in the porous MOF. Figure 2.28 shows the mechanochemical synthesis via the solvent-free grinding method, using a ball mill grinder.

By using these three techniques, many versatile MOFs have been synthesised [129]. Most reports of mechanochemical synthesis employ mills with small balls in a weight of less than one gram to achieve reactions between the metal salts and organic linkers to produce sufficient amounts of MOF with high surface area [130, 131]. Table 2.1 demonstrate some MOFs which are prepared by mechanochemical synthesis.

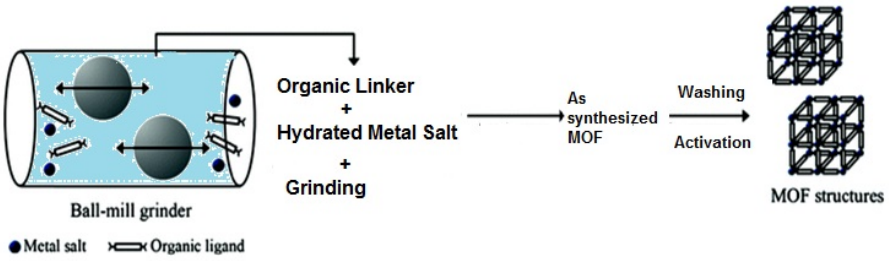

.

Figure 2.28: Laboratory preparation of MOFs by mechanochemical synthesis.

Although hydrothermal and solvothermal methods are time consuming, they are the most commonly used technique by researchers in this field to synthesise MOFs.

2.3.5 Modification and functionalisation

There are two strategies for modifying MOFs: modifying during synthesis and modifying post synthesis.

2.3.5.1 Direct synthesis modification (DSM)

The name of this method suggests it is possible to enhance the textural characteristics and active functionalities of parent MOFs in the same pot of synthesis by adding additives or other chemicals.

An advantage MOFs possess over other porous materials is the ability to readily change the nature of their pores through functionalisation. With respect to dicarboxylate-based MOFs, dicarboxylic acids that contain additional functionalities can in some cases be employed directly in the synthesis to yield isoreticular MOFs [70, 132], which may exhibit lower pore volume and smaller pore size [133].

In comparison with other porous materials, MOFs are reliable in having diverse functional groups. The facile modification of MOFs is considered key to the successful application of these hybrid materials. MOFs have two types of chemical components (metal and linker) that enable the insertion of new active functional groups [134]. Functionality plays a significant role in MOF chemistry, since their potential capacity for a wide range of applications depends heavily on the possibility of integrating various chemical functionalities into MOFs [135, 136]. Functionalised MOFs can exhibit interesting physical and chemical properties, including accelerated adsorption kinetics and catalysis [137].

DSM is a very helpful method for obtaining new selective functional groups in MOFs if they originally possess a functional group on the surface of their pores. For example, UiO-66 was modified using functionalised terephthalic acid in the same synthesis procedure to obtain different functional groups, such as NH_2, NO_2, Cl_2 and Br_2, on the surface of pores while maintaining the same topology [138-140], as shown in Figure 2.29.

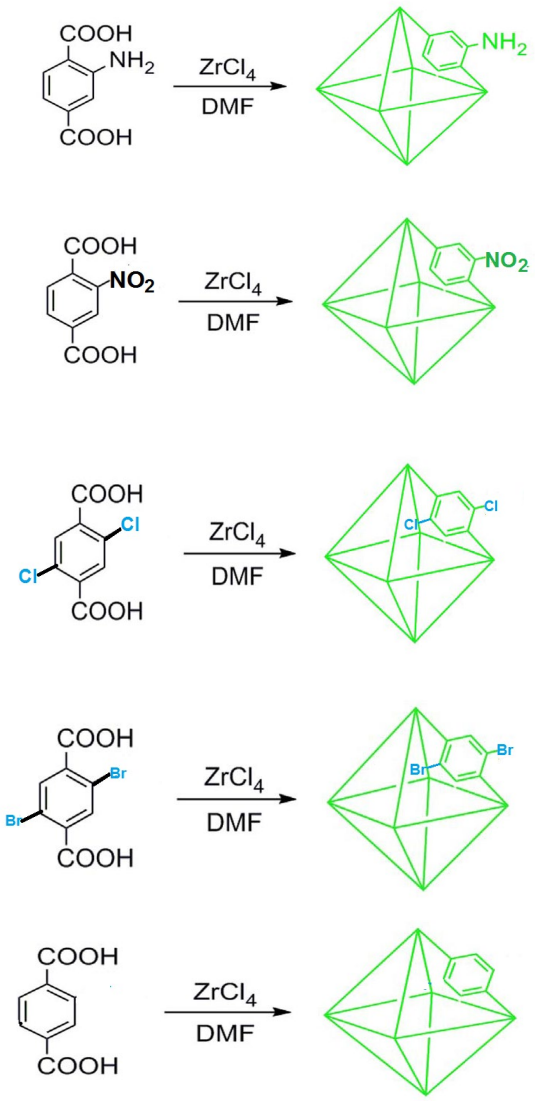

Figure 2.29: Modification of UiO-66 using functionalised terephthalic acid in the same synthesis procedure to obtain different functional groups. (a) NH_2-UiO-66, (b) NO_2-UiO-66, (c) Cl_2-UiO-66, (d) Br_2-UiO-66, (e) UiO-66.

However, in some cases it is necessary to adapt the synthesis procedure to optimise the conditions for each substituted organic linker, because of differences in solubility or chemical reactivity. This is demonstrated by the synthesis of 2OH-UiO-66—which succeeded not by following the same procedure as that for UiO-66 but by adopting the co-solvent synthesis method [141].

The synthesis of isostructural MOFs with different linkers is, therefore, not straightforward. By introducing substituents on the aromatic linker, certain control

over the electronic density of the metal nodes, derived from the electron's influence through withdrawing or donating substituents, can be gained [142].

Moreover, DSM can be achieved by adding a trace of specified chemicals (as additives) into the original mixture during synthesis. For instance, ammonium hydroxide was used as an additive in the direct synthesis of UiO-66 to improve its textural properties and reduce crystal size [143], while acetic acid was used in the similar way to enlarge the crystal size of UiO-66 [144].

Further, using co-solvents instead of a single solvent in DSM has enabled novel and fascinating modifications to pore size, pore volume [145, 146] and morphology of crystalline MOFs [147]. Additional research has found that when a series of uniform crystals with different MIL-96 morphologies were synthesised, using water as the main solvent mixed with different ratios of secondary solvents (e.g., DMF, toluene or THF), the modified MIL-96 exhibited excellent stability in neutral to acidic aqueous conditions.

In addition, the DSM method has been used to enhance the activity and functionality of MOFs by installing other linkers or other metals in parent MOFs. Although it is known that the crystallisation process may not be succussed to accommodate different molecules in the same lattice units, MOFs exhibit contrasting behaviour because the organic ligands are not closely packed within the lattice. Consequently, modification is made possible with the use of various linkers or metals to construct mixed-component MOFs [105].

Based on the properties of organic linkers, there are three strategies for synthesising mixed-linker MOFs. The first strategy uses linkers with identical geometries. Whereas, preparation of MOFs includes more than one identical linkers have been adapted after confirming the successful synthesis of different isoreticular MOFs with the same topology [148, 149], a series of metal–organic polynuclear clusters with small multidentate ligands were designed, which were further extended by the secondary ligands to construct multifunctional mixed-linker MOF materials [150, 151], as shown in Figure 2.30. Integrating multiple ligands with identical linking chemistry is an efficient route to multivariate MOFs with increasing complexity and functionality. It is possible to obtain distinct functionalities in a single phase; while the distribution of functional groups is not ordered, the backbone of the structure is ordered [87].

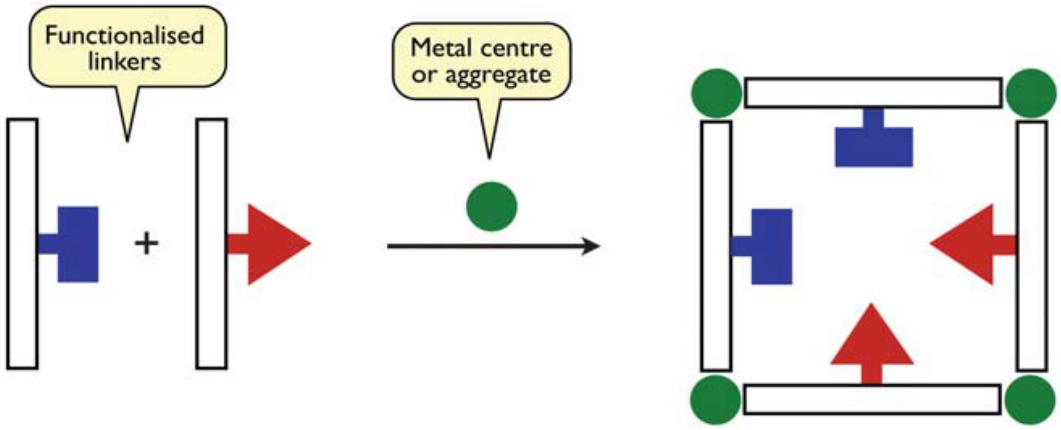

Figure 2.30: Preparation of mixed-linker MOF using linkers of identical geometry [152].

The second strategy for synthesising mixed-linker MOFs employs linkers with different geometries. When two or more organic ligands of divergent size, shape and coordination attraction are used, specific coordination of the different organic ligands with metals is made. This strategy provides opportunities to functionalise parent MOFs and enhance pore size with topologies of lower symmetry. Additionally, this strategy may lead to synthesis of new materials with different topologies [153, 154].

The third strategy uses a second linker as a crowning agent, because it should have reduced the number of functional groups. The relative rates of bond creation and exchange determine the role of the truncated monomer in the crystallisation. If growth is quicker than exchange, a shortened monomer is incorporated throughout the whole network, which raises around these defect positions. If exchange is quicker relative to framework growth, the shortened monomer will preferentially exist in the faces of the growing crystal, and supply a means to control the crystal's size, shape and surface functionality [155].

DSM is the best method for synthesising mixed-linker MOFs, especially the first strategy outlined above. \Many metal–organic polynuclear nodes with small polydentate organic linker are premeditated, which are further extended by secondary linkers to build multifunctional mixed-linker MOF materials [154].

There are several advantages in introducing auxiliary organic ligands in MOF, such as the addition of different active functional groups, the emergence of selective textural properties and the production of defect-tolerant MOFs. In addition, the introduction of

auxiliary organic ligands in MOFs may lead to the production of new multifunctional porous materials [154].

The preparation of mixed-metal MOFs by the single-pot synthesis method (DSM) is very difficult [156] because inserting new auxiliary metal nodes into the structure of MOFs leads to fragile frameworks with unpredictable topologies and functional groups. However, classical MOFs have high surface areas, exceptional pore volumes and high thermal stability; therefore, they can be considered the best candidates for modifying mixed-metal MOFs by the DSM method, as described in Figure 2.31.

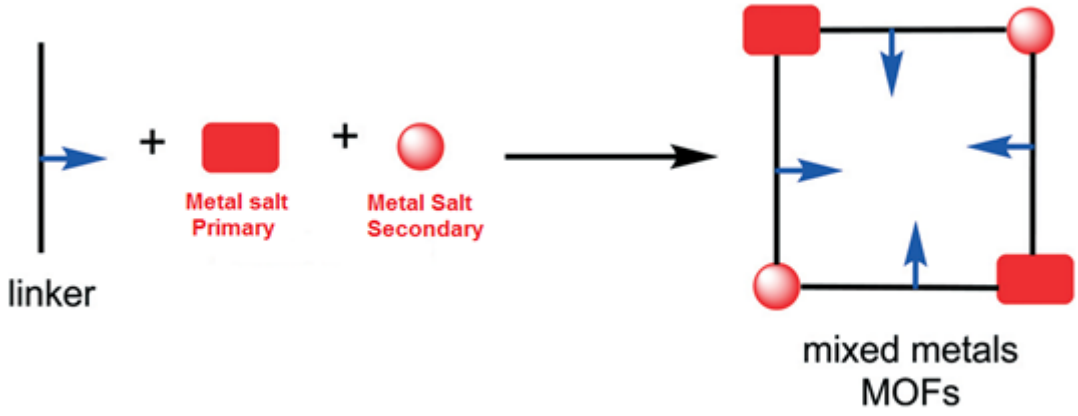

Figure 2.31: Preparation of mixed-metal MOFs by the direct synthesis method.

The efficiency with which the main metal is replaced by the auxiliary metal depends on several conditions, such as coulombic charge, ionic radii and coordination geometry; therefore, both metals should be highly similar in ionic radii and coordination geometry. Otherwise, a large size difference can lead to lattice disorder [157] or produce an independent solid phase without participating in the main backbone structure [158]. Conversely, in some cases of relative low size difference, preparation of mixed-metal MOF succeeds and enhances the porosity of the parent MOF. In addition, the availability of unsaturated metal sites on the parent MOF can enhance the incorporation of the second metal in the mixed-metal MOF. While some mixed-metal MOFs have been successfully synthesised, BET surface areas have decreased with increasing incorporation ratios of a second metal [159]. In contrast, some mixed-metal MOFs have been successfully produced without observed changes to the BET surface area [160].

According to the principle of establishing interfaces to separate two solid phases, the possibility of developing new materials has arisen because significant changes to engineering properties can be obtained if the interfacial structure is distorted [161]. Consequently, properties different to those of discrete phases can be gained, opening up another approach that uses DSM to synthesise core–shell MOFs. The chemical contrast between the centre and surface is obvious in the resulting MOFs. In other words, a MOF can be built epitaxially on the surface of a different crystalline material to create heterogeneous materials in which the shell and core of each crystal are not the same [152], as shown in Figures 2.15 and 2.16.

The DSM method to produce core–shell MOFs involves the following. First, two MOFs are prepared. Second, the crystalline powder of each MOF is centrifuged. Third, the supernatant of the MOF is added (1) to the crystalline material of the MOF, (2) and vice versa. Finally, the mixture is transferred into a separate autoclave that is tightly sealed and heated at a mild temperature to produce core–shell MOFs (MOFa and MOFb; Figure 2.32). This method can produce multilinker core–shell MOFs, as shown in Figure 2.32, and bimetallic core–shell MOFs, as shown in Figure 2.33. This method is closer to post-synthesis than DSM because the nucleus of the crystalline MOF should be synthesised first, followed by MOF's surrounding shell.

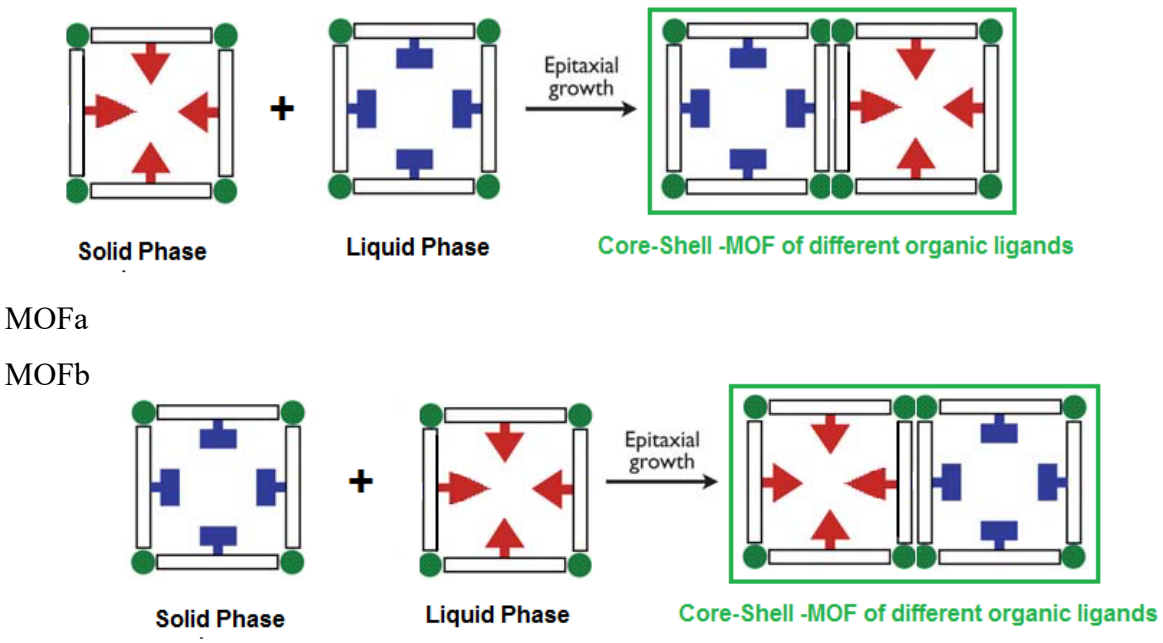

Figure 2.32: Preparation of core–shell MOFs (MOFa+MOFb) of different linkers.

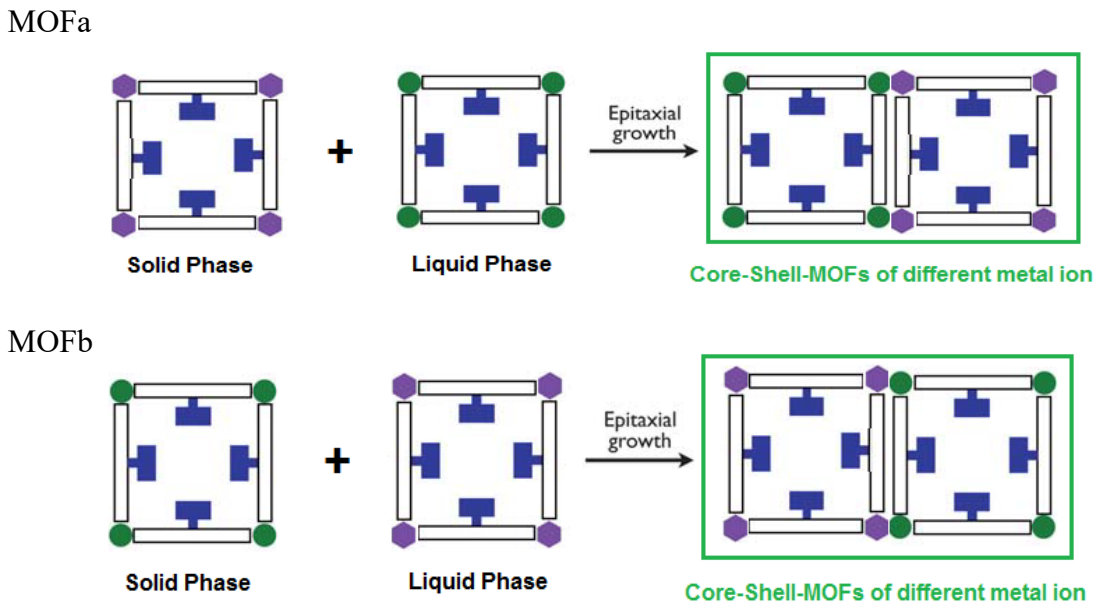

Figure 2.33: preparation of core–shell MOFs (MOFa+ MOFb) of different metal.

2.3.5.2 Post-synthesis modification (PSM)

PSM is used to modify materials that have already been synthesised. The modification aims to insert a functional group to improve their textural properties or enhance their particular application without significant change to the lattice structure [135], as described in Figure 2.34.

The simplest PSM is the activation process via solvent exchange to remove the coordinated solvent, which may be coordinated with a metal centre during the synthesis process [162]. As mentioned previously, inserting an active group by using functionalised organic linkers may lead to further complications in the synthesis procedure or prevent the construction of MOF, because under hydrothermal conditions the presence of functional groups may cause problematic solubility or may coordinate with the metal centre [134]. However, simple functional groups have been prepared successfully; consequently, as a result of high porosity, large pore volume and pore size in MOFs, the insertion of other functional groups in MOFs for specific applications has been achieved by the post-synthesis method [163, 164].

Figure 2.34: Inserting functional group in MOF by the post-synthesis method.

To be exchangeable in PSM, the functional group should be compatible with the original functional group. There are many scenarios in which PSM is applicable. First, it is preferable to use an inert functional group on the organic linker in the main synthesis procedure to maintain structural integrity and to ensure the pores are fully open. Following this, introducing an active functional group instead of an inert group can facilitate PSM. Second, some MOFs such as MIL-53 and UiO-66 have a bridging OH group; therefore, PSM can be used to exchange the hydroxyl group for other functional groups to enable special application [163]. Third, it is directly functionalised by displacing the hydrogen atom from the BDC linker under tough conditions, and by inserting an active functional group with a covalent bond [164]. Fourth, PSM can succeed by coordinating the new metal in the main skeleton to produce bimetal MOFs (mixed MOFs or M-MOFs), as shown in Figure 2.35.

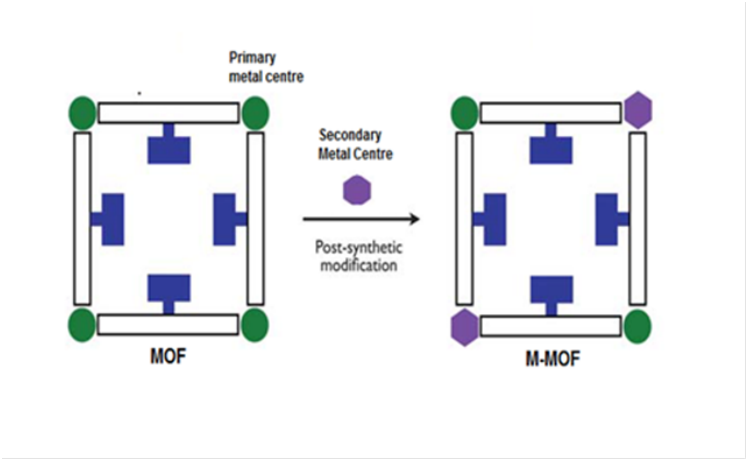

Figure 2.35: Synthesis of mixed MOF (M-MOF) by the post-synthesis method.

The synthesis of M-MOFs in PSM happens at a much slower rate than in DSM; therefore, PSM can be achieved by adjusting the percentage of ion exchanged and

checking the results of elemental analysis of the metal solution and final product [151]. Specifically, the single metal should be prepared first with high crystallinity and then activated to remove all non-reacted precursors. The metal exchange procedure is undertaken by soaking crystalline MOFs in the second metal solution for several days or by treating the activated crystalline MOF solvothermally in a solution of the selective second metal [151, 156]. The replacement of a metal ion at the location of another occurs partially or completely. Therefore, through mixed metals PSM can produce new MOFs if the second metal can exchange with all metal sites of the main metal [157, 165].

However, the process of completely replacing the metal ion faces significant kinetic obstacles because of ultra-micropores, steric hindrance and captivity in unusual coordination geometries. Hence, the partial exchange of metals dominates the PSM process to produce mixed-metal MOFs. Similar to DSM, metal exchanges in PSM occur between metals that are similar in ionic radius and coordination geometries [157, 166].

Mixed-linker MOFs have been synthesised by PSM according to first scenario (i.e., using an inert functional group on the organic linker in the main synthesis, followed by an active functional group in the PSM). Therefore, prior to PSM, it is preferable for MOFs to have 2-amino-1, 4-benzenedicarboxylate (BDC-NH2) or other linkers with potential for diverse organic transformation [152]. During PSM, the partial reaction of the active functional group can be attributed to the increasing steric burden inside the pores as a result of the high degree of functionalisation [151].

To resolve the challenges in the single-pot synthesis and post-synthesis methods, multistep synthetic methods—derived from retrosynthetic analysis—to synthesise MOFs have been recently proposed. This technique uses kinetic analysis of the targeted MOFs into their synthons (metal precursors and organic ligands). The synthons are consequently gathered into the intended MOF structure stage by stage under kinetic control, using recognised post-synthetic modification strategies to eventually form the planned multicomponent MOFs. By this method, the synthesis of very crystalline MOFs, included bimetal and multilinker MOFs, becomes possible [156].

2.3.6 Activation methods

As-synthesised MOFs are mostly blocked by solvents and unreacted precursors that may fill the pores, undesirable guests must be discarded in a process called the activation process. The removal of solvent molecules, especially when they have high boiling points or high surface tension, may lead to collapse of the framework due to high surface tensions and capillary forces that are imposed on the structure by the liquid to gas transformation of the trapped solvent molecules. Consequently, significant capillary forces, and hence surface tension, can be created during activation and cause frameworks to fully or partially collapse [95].

Activation processes are affected by factors such as the chemistry of guest molecules, pore size and functionality of the MOF surface. In many instances, the experimentally observed surface areas and pore volumes are significantly lower than those predicted in simulations based on single-crystal structures, and incomplete activation is often invoked to explain observed data [167]. Known activation methods are described below.

2.3.6.1 Evacuation process

The evacuation process is used when the porous materials have very low thermal stability and the guest materials are connected to the structure by van der Waals forces or hydrogen bonding. Generally, the samples are first filtered under vacuum and then washed by a suitable solvent to remove the guest molecules from the external surface, so that they can be forced to migrate out of the pores when placed in a vacuum, while maintaining structural integrity.

2.3.6.2 Heating process and inert gas

The activation method of the heating process and inert gas uses the heating process to evaporate the solvent and sublimate the residual precursors from the pores. Prior to undertaking this method, it is preferable that the decomposition temperature of a MOF is identified from a thermogravimetric analysis (TGA) profile. Then, the MOF can be heated at a temperature less than half the decomposition temperature. This method can perfectly remove small guest molecules (such as methanol and ethanol) from MOFs. While it is recommended to use inert gas to homogenise the powder during the heating

process, it may lead to partial damage of the structure. Also, some residual reactants may remain inside the pores.

2.3.6.3 Heating and evacuation process

The heating and evacuation process require three conditions. First, the MOF powder must be dried at low temperature to remove moisture. Second, heating should occur at a selected temperature based on the MOF's TGA profile. Third, evacuation should occur at very low pressure during the heating process.

However, ensuring that these conditions are met does not guarantee the integrity of the structure, because the structures may partially collapse. Therefore, the rate of evacuation needs to be gradually increased during the heating process.

2.3.6.4 Solvent exchange and evacuation

In the solvent exchange and evacuation method, the as-synthesised crystals are firstly washed by a synthesis solvent to remove unreacted precursors, then with a suitable solvent such as chloroform or methanol to remove the guest molecules (synthesis solvent) from the surface. To remove residuals and guest molecules from the pores, the material should then be immersed in the solvent for several hours or days. During this time, the soaking solution is replaced with fresh solvent at regular intervals. After the solvent exchange process is complete, the sample is filtered, air-dried and placed under vacuum at room temperature for a specified period [168]. As the soaking may be time consuming, the washed samples can be solvothermally treated by the solvent at a mild temperature over several hours, then filtered, dried and evacuated at room temperature.

2.3.6.5 Solvent exchange followed by evacuation and heating

The method of solvent exchange followed by evacuation and heating includes two techniques: a) soaking the synthesised MOFs and b) treating the dried synthesised MOFs solvothermally.

The first technique, soaking the synthesised MOFs in a suitable solvent [58], the solvent should have lower molecular weight, lower donor constant, lower surface tension and lower boiling point [95]. Further, the specified weight of the MOF should be firstly washed very well by the same solvent used in the synthesis, then dried at

room temperature under vacuum or in an oven at 373 K. The dried sample should then be soaked in the selective solvent for a specified period; it is preferable that the solvent is changed at least twice during the soaking period. Finally, the sample should be dried again and then heated under vacuum at a suitable temperature [143].

The second technique involves solvothermal treatment of the dried synthesised MOF by a suitable solvent at a suitable temperature [169]. The selective solvent for the exchange process should be highly polar, consist of hydrogen bond acceptors and is not a hydrogen bond donor [170]. Specifically, a specified weight of the solvent should be washed and dried very well, then immersed in the selective exchangeable solvent and mixed very well. After that, the suspension should be transferred to a Teflon-lined autoclave which should be tightly closed and sealed. Next, the autoclave should be placed in a preheating oven at a temperature less than the temperature used in the synthesis for a specified period. Finally, the product should be filtered, dried and then heated under vacuum at a suitable temperature [171].

2.3.6.6 CO_2 supercritical CO_2 drying

In the supercritical CO_2 drying method, the as-synthesised crystals are soaked in ethanol for 3d to exchange all guest solvents with ethanol. Again, the soaking solution is replaced with new ethanol every 24h. The ethanol-exchanged samples are then soaked in liquid CO_2 in a supercritical dryer for more than 6h, with the chamber purged with fresh liquid CO_2 every hour. During this period, the temperature in the dryer is maintained between –5°C to +5°C. The temperature is then increased to 40°C (i.e., above the critical point of CO_2 [31°C]) and maintained for 30 min. Finally, the supercritical CO_2 in the drying chamber is slowly released over a period of 18h [172].

2.3.6.7 Benzene freeze-drying

Benzene freeze-drying is based on the principle of solvent exchange activation and CO_2 supercritical CO_2 drying [173]. The high boiling points of solvents, which may be incorporated in the MOFs, can be exchanged with that of a solvent (such as benzene) that can then be removed by freeze-drying. The frozen solvent molecules can be removed from the MOFs by solid–gas transition under vacuum at temperatures below its freezing point. Bypassing the liquid phase eliminates the negative effect of surface tension that induces the mesopore to collapse, and thereby enhances the permanent porosity of MOFs [167, 174].

2.3.6.8 Photothermal activation

Photothermal activation is a one-step method that depends on the photo-irradiation of MOFs, which causes them to heat up [175]. This effect is called the 'photothermal effect'.

Ideally, one could exploit the conversion of light into heat to selectively increase the local temperature of a given MOF and its surroundings, while minimising heat diffusion and energy loss. The effect of photothermal interaction on MOFs is stimulated by their direct irradiation with a ultraviolet–visible lamp. After irradiation, the localised light-to-heat conversion in the MOF structures leads to the rapid removal of guest molecules and thus reduces the activation time considerably [176]. The MOF must be a photothermally active material for this activation method to succeed [175].

While the CO_2 supercritical CO_2 drying and benzene freeze-drying are more efficient activation methods in terms of achieving MOF porosity, the literature reveals that the most popular activation method is solvent exchange accompanied by heating at mild temperature.

In regard to the activation process for mixed-metal or mixed-linker MOFs, the solvent exchange method is not always recommended because MOFs need to be carefully activated. Further, this method might lead to the replacement of auxiliary linkers or auxiliary metals by solvent molecules. However, the solvent exchange of coordinated metal or linker enhances the structural defects and textural properties in the main skeleton [157, 177]. To maintain the content of the second component in the final product, as-synthesised MOFs should be activated by a heating treatment accompanied by evacuation at a mild temperature (lower than the boiling point of the solvent used in the synthesis).

2.4 Water stability of MOFs

Water stability is an essential indication that the MOF can be used in a water treatment. As a result of their chemical properties, some MOFs are sensitive to water content and their structures are gradually affected by moisture in the atmosphere. Examples of such MOFs include MOF-5 [58, 178] or its isoreticular form [179].

The water stability of MOFs can be easily checked by PXRD. If after exposure to moisture, an XRD pattern is identical to that of the same material in the absence of moisture, it is a good indication of MOF stability in water or in wet environment.

However, measurement of the BET surface area is also essential to check whether porous materials such as MOFs are waterproof. While some materials have been reported as having the same XRD patterns in humid and dry atmospheres, their BET surface areas had significantly decreased in dry conditions [180]. Chemically, water molecules with high polarity are likely to attack a hydrophilic target in MOF structures; therefore, the coordination bonds between the metal clusters and organic linkers are targeted first. Consequently, the organic ligand might be displaced [181] or the structure might be partially or totally destroyed [182].

MOFs with water stability must have high hydrothermal resistance to prevent water molecules interloping into their structure; otherwise, they may loss crystallinity and whole porosity. Thus, MOF structures with great stability normally have strong coordination bonds (thermodynamic stability) or significant steric hindrance (kinetic stability) to prevent the detrimental hydrolysis reactions that break metal–ligand bonds [183].

Various approaches have focused on MOF-5 and its isoreticular forms to improve their hydrothermal stability. Principally, there are several ways to synthesise MOFs with high stability in water.

(1) The first method is to use high-valence metal ions. High-valence metal ions with high charge density build stronger coordination bonds with organic ligands. This phenomenon has been extensively detected by MOF material scientists and researchers and justified by the hard/soft acid/base view.

Moreover, high-valence metal clusters with a higher coordination number typically produce a strong firm structure, making the metal–metal bonds less liable to water molecules [50, 184]. Therefore, with the most frequently used carboxylate-type linkers, high-valence metal ions (including Al^{3+}, Fe^{3+}, Cr^{3+} and Zr^{4+}) have been used to synthesise MOFs that are hydrothermally stable. For instance, the famous Al-based MIL-96 [147], Fe-based MIL-100 [185] and Cr-based MIL-101 [186] exhibit high water stability. Interestingly, M^{IV}-MOFs, which include metal clusters of Ti, Zr or Hf, exhibit superior chemical and water stability under acidic and some basic conditions

because they are high-valence metal cations with high charge density; consequently, they require more organic linkers to balance their charges to form stronger MOFs [49, 141, 187].

The stability of MOFs can also be affected by the operating environment; therefore, MOFs constructed from metal ions of high-valence number with carboxylate-based linkers exhibit significant stability in an acidic environment and very weak stability in a basic environment [188]. In acid, metal ions and proton (H_3O^{+1}) compete to interact with the organic linker. However, metals of high valence are more dominant than protons in building strong coordination bonds with terephthalates, while OH^{-1} in basic environments has a strong affinity towards metal ions of high-valence number, thus replacing organic ligands [49, 189].

(2) The second method uses nitrogen-donor ligands. Employing the azolate organic ligand (such as imidazolates, pyrazolates, triazolates and tetrazolates) has produced MOFs with water stability. When softer nitrogen-containing ligands interact with softer divalent metal ions, a framework of high-water stability can be synthesised. An instance of such a framework is the zeolitic imidazolate framework (ZIF), which uses Zn^{2+} or Co^{2+} with imidazolate ligands to build a multiplicity of stable structures similar in topology to zeolite [71, 190, 191].

(3)The third method functionalises pore surfaces by their hydrophobic functional groups [192]. This method primarily involves the functionalisation of the BDC linker in the MOF-5 framework, with one or more hydrophobic functionalities during in situ MOF synthesis, by direct synthesis or post synthesis [193]. Therefore, the Zn−O bond can be shielded by combining numerous hydrophobic functional groups on the BDC ligand.

Modified MOFs have unpredictable surface areas, pore sizes and pore volumes. Generally, incorporating a polar functional group such as NO_2, NH_3, Br, Cl or OH on the dicarboxylate organic linkers reduces the water stability of the resulting MOF relative to the parent MOF, because the polar functional groups facilitate hydrolysis of the Zn−O bond. However, using hydrophobic functional groups such as methyl groups or polydimethylsiloxane (PDMS) on the terephthalate ligand can produce stronger MOFs with higher water duty, because water molecules are hydrophilic and do not

have any affinity towards hydrophobic functional groups. Consequently, the Zn−O bond is protected from attack by water molecules [194, 195].

(4) The fourth method of ensuring water stability is to coat the surface of MOFs with hydrophobic materials. For example, MOF-5, HKUST-1 and ZnBT were coated with PDMS (a hydrophobic silicone) to successfully enhance their water stabilities [196]. This method also maintains the MOF's BET surface area and textural properties [197, 198].

(5) The fifth method is to insert second-phase hydrophobic nanoparticles inside the MOFs, as demonstrated by the insertion of multiwalled carbon nanotubes in MOF-5 using the single-pot synthesis procedure. The resultant MOF had a higher surface area and hydrothermal stability than the virgin MOF-5, although their topologies were the same [199].

(6) Mixed-metal MOFs may exhibit higher water stability than single-metal MOFs; for instance, the water resistance of MOF-5(Zn^{2+}) was enormously increased by the partial exchange of Zn^{2+} with Ni^{2+} in Ni-MOF-5(Zn^{2+})[200]. However, mixed-metal Ti-Zr-MOFs such as PCN-415 demonstrated excellent stability in acidic aqueous solutions, similar to that of UiO-66 [201]. The most promising MOF proven to have practical applications in the water environment is Zr-MOF, which has showed hydrophobic behaviour. It could have a high concentration of defects because of missing organic ligands and can become more hydrophilic while maintaining stability [189, 202].

2.5 Removal of organic pollutants in water by MOFs

The removal of organic pollutants in industrial wastewater has become an important issue for numerous researchers and scientists. Adsorption techniques have been widely used for this purpose, with different adsorbents such as activated carbon [203], metal oxides [204] and zeolites [205]. Recently, researchers have used water-stable MOFs as successful adsorbents to removal chemicals from water, such as dyes [206], phenolic compounds [207], monoethylene glycol [141] and pharmaceutical wastes [208].

Dyes are the most effective pollutants in the public water supply system; therefore, their removal was undertaken by many researchers using MOFs as adsorbents. Haque

et al. (2010) claimed that MIL-101(Cr) and MIL-53(Cr) were used as adsorbents to remove harmful anionic dyes such as MO from water. Their results showed that the adsorption capacities of MIL-101(Cr) were higher than those of MIL-53(Cr) because of the former's large pore size: Adsorption capacity increased with the pore size of the porous material. They suggested that the adsorption mechanism for dye using MOFs partly depended on the electrostatic interaction between the anionic MO and cationic adsorbent [209].

Mahmood et al. (2015) reported the synthesis of bimetallic metal–organic gels such as MOA-3 (0.5Fe-0.5Al-BTC) by conventional solvothermal synthesis. The surface area, pore size and pore volume of these gels were improved, evident by the increased pore volume in MOFs with growing heterogeneity in their structure.

As the specific density of accessible sites was enhanced, the adsorption rate was increased. MOA-3 (0.5Fe-0.5Al-BTC) demonstrated maximum uptake of dyes over a short period at neutral pH. The open metal sites, textural properties, the phenomenon of structural breathing and electrostatic interaction between the MOFs and dyes were found to be major influential factors in the adsorption process [210].

Haque et al. (2011) claimed that an Fe-BDC MOF (MOF-235) was used to clarify the aqueous solution of anionic and cationic dyes, including MO and MB. The removal efficiencies of these dyes by MOF-235 were much higher than by conventional adsorbents such as activated carbon, although the specific surface area of this MOF could not be determined by nitrogen at 77 K. The investigators concluded that some MOFs can be attractive adsorbents of some harmful chemicals, like dyes in wastewater. The adsorption mechanism was attributed to the presence of electrostatic interactions between the dye and the adsorbent. Specifically, this MOF can have positive (framework) and negative charges (charge-balancing anion), respectively; therefore, it can capture anionic and cationic dyes.

In addition, they found that the adsorption capacities for MO and MB changed with pH, due to the increasing number of OH^{-1} ions on the surface of the adsorbent with increasing pH condition. However, another suggested mechanism is the π–π interactions between the benzene rings of the dye and MOF [211]. Hasan et al. (2015) discussed the removal of various hazardous materials from wastewater and diagnosed

that the adsorption mechanism between pollutants and MOFs involve hydrophobic interactions, electrostatic enhancement and π–π interactions [212].

Shuang et al. (2014) claimed that Cu-MOF (HKUST-1) was effectively used to remove MB from wastewater. HKUST-1 has a large BET surface area and a large pore volume; these boosted the adsorption uptake of MB in a neutral environment through electrostatic attraction. Indeed, although it was supposed that the adsorption of MB as a cationic dye might increase in a basic environment, when the pH was greater than 7, the adsorption uptake of MB dropped. Likewise, when the surface of pores of the Cu-MOF was positively charged, in an acidic environment the adsorption capacity fell because of repulsion between similar charges.

However, in aqueous solutions with pH > 7 (adjusted by dropwise additions of NaOH), the adsorbed amounts of MB reduced. This was thought to be due to the chemical reaction between the MB and NaOH molecules to produce NaCl (aq) and MB-$S^{+}OH$ (aq). The presence of NaCl might have decreased the adsorption of MB-$S^{+}OH$ (aq)[213].

Electrostatic interactions aside, other adsorption mechanisms, such as π–π interactions and hydrogen bonds between the organic ligands of HKUST-1 and the benzene rings of the MB dye, cannot be excluded [214]. Zhao et al. (2017) reported that two Cr-MOFs (MIL-101[Cr] and MIL-101[Cr]-SO_3H) were successfully prepared and used to remove and separate the ionic dye fluorescein sodium (FS) and the cationic dye safranine (red synthetic dye) (ST) from wastewater. Interestingly, MIL-101(Cr) could adsorb the FS dye but had difficultly adsorbing the ST dye, and MIL-101(Cr)-SO_3H displayed the reverse phenomenon. Importantly, high adsorption capacity with high selectivity of the two MOFs was also attributed to the solution mixture of both dyes. Zhao et al. claimed that an investigation into the underlying mechanisms has found that the performance of this adsorbent was caused by negatively charging the surface of MIL-101(Cr)-SO_3H and attributed to the existence of $-SO_3H$ functional groups. Further, their investigation of FS adsorption mechanisms in MOFs, using MIL-101(Cr), found that it was occurring via electrostatic interaction and ion exchange. They also suggested that both the -OH site in the ligand and the open metal site may play prominent roles in the adsorption of anionic dye (FS). In MIL-101(Cr)-SO_3H

[215], the functional groups of $-SO_3$ and the ionisation process of $-SO_3H$ groups in aqueous solution were the adsorption sites for cationic dye ST [216].

Jiang et al. (2016) described that ZIF-8 was prepared by hydrothermal synthesis and tested as an adsorbent to eliminate harmful anionic dye Congo red (CR) from water. The removal efficiency was very high and the adsorption capacity of the dye by ZIF-8 was ultra-high. The adsorption mechanism mainly depended on the electrostatic interactions between the anionic dye of negative charge and ZIF-8 of positive charge. In addition, π–π interactions between the benzene rings of ZIF-8 and those of the dye could have contributed to the adsorption process [217].

Enugu et al. (2018) reported that cationic nickel-based MOF-1 and -2 exhibited potential adsorption ability to remove neutral (methyl red [MR]), anionic (Congo red [CR]) and cationic dye (rhodamine [ChB]). Relatively, Ni-MOFs' removal of anionic dyes was more efficient (97.30% and 98.65% for CR) than that of neutral dyes (48.16% and 44.88% for MR), while the lowest removal efficiency was found for cationic dyes (28.69% and 17.41% for ChB). Their study showed that the cationic Ni-MOFs displayed reasonable adsorption capacity for cationic dyes, attributed to the electrostatic interactions between the positive imidazolium moieties in the Ni-MOFs and the negative moiety of the cationic dyes [218].

Li et al. (2017) found that Zr–MOF (PCN-222) exhibits exceptional adsorption capacities for some charged dyes, independently and together in aqueous solution, because this MOF has a large pore and a specific surface area. Moreover, PCN-222 was found to not only remove MB and MO from a single-dye solution or a mixture, but also to do so in only 60 minutes. The investigators claimed that the large pore size of PCN-222 facilitates rapid adsorption and enables the co-adsorption of large-sized MB–MO aggregates possible. They proposed that a push-pull mechanism is dominant in dual adsorption by this MOF; that is, it is possible that MO pushes MB dimerisation and the MB dimer pulls MO together to be adsorb by PCN-222, and vice versa. Therefore, cationic MB's dimerisation can be promoted in the presence of anionic MO, by self-association through π–π stacking interactions between the aromatic rings [219].

Zhang et al. (2017) claimed that UiO-66 exhibited high adsorption capacity for acid orange 7. This can be attributed to the presence of open active metal sites which significantly increases adsorption by magnifying the strength of the interaction with

the dye molecules. Furthermore, improved π delocalisation and appropriate pore size of UiO-66 lead to the highest level of host-guest interactions [220].

Moldavia et al. (2018) claimed that the results indicated that while the structure of UiO-66 was mostly retained, its adsorption capacity for dyes was slightly reduced after long-term water ageing. They reported that the adsorption capacity of UiO-66 for MO was greater than that for MB, particularly in acidic and neutral conditions, because of its higher electrostatic attraction and the π-π stacking interactions of aromatic rings [221].

In addition, Embay et al. (2018) found that UiO-66 had excellent adsorbent capacity for anionic dyes as compared to cationic dyes. The adsorption mechanism for the sulfonated anionic dyes in neutral condition was explained as the interaction of the sulfonate group in anionic dyes with the hydroxide bridges in UiO-66 via hydrogen bonds [222].

Chen et al. (2015) used UiO-66 and UiO-66-NH_2 to remove cationic and anionic dyes and reported that the highest adsorption uptake of cationic dyes was seen in UiO-66-NH_2 while anionic dye molecules were eliminated by UiO-66. Generally, they found that the external surface area, pore volume and zeta potential were the most influential factors in the adsorption process; therefore, the adsorption capacity of cations by UiO-66-NH_2 was higher because of the MOF's higher external surface area, pore volume and zeta potential [223]. Yang (2017) used PSM to produce a nanoscale UiO-66-phosphate composite (UiO-66-P), a negatively charged MOF with exceptional adsorption capacity for cationic dyes. However, anionic dyes were not adsorbed by UiO-66-P because of its high electronegative charge, which can cause high electrostatic repulsion [224].

Qi et al. (2017) claimed that the modulation of UiO-66, by adding acetic acid or hydrochloric acid in the solution of precursors, can promote selectivity for anionic dyes over cationic dyes. The adsorption of mixed dyes indicated that the acetic acid–promoted UiO-66 had exceptional selective adsorption for anionic dyes. Accordingly, hydrogen ions in the synthesis of acid-promoted UiO-66 played a crucial role in dye selective adsorption [225].

Yang et al. (2018) reported that the synthesis and characterisation of Ce (III)-doped UiO-66 nanocrystals indicated that these crystals had the potential to efficiently

remove organic dyes, such as MB, MO, CR and acid chrome blue K from aqueous solutions. They found that Ce(III)-doping increased the number of adsorption sites and promoted π–π interactions between the adsorbent and the adsorbate, thus improving the adsorption capacity for cationic and anionic dyes and overriding the effect of electrostatic interactions [226].

Azhar et al. (2017) stated that the adsorption capacities of HKUST-1 are higher than UiO-66 and commercial activated carbon. They also found that the adsorption capacities for cationic dyes were enhanced in Cu-UiO-66(Or) and Zr-HKUST-1(Cu), although the former had the higher capacity. In addition, they claimed that the adsorption of dyes is usually dependent on electrostatic interactions, π-π interactions, hydrogen bonding and hydrophobic interactions between the adsorbents and dyes [227].

It appears that the dominant mechanism in adsorption of dyes by MOFs depends on the characteristics of the MOF, including its vacant metal sites, the chemistry of its organic ligands (polarity of functional groups and length of benzene chain), as well as the type of valent charge of the dye, the nature of benzene rings and the structural groups of the dye molecule. Zr-MOFs have demonstrated adsorbent ability to remove dyes from aqueous solutions while maintaining their own structures. Mixed-metal MOFs have been successfully used to remove dyes from wastewater, but studies of these MOFs have been very limited.

Table 2.1: MOFs with different precursors and solvents prepared by different approaches (liquid phase, solid phase).

Method	MOFs	Precursors	Solvents	Reference
Slow evaporation	HKUST-1	Cu (NO_3)2.3H2O, H_3BTC	DMSO	[228]
	MOF-177	Zn $(OAc)_2.2H_2O$, H_3BTB	DEF	[229]
	Ni-MOF	Ni $(NO_3)_2.6H_2O$, H_3BTC	NaOH, H_2O, CH_3CN	[230]
	Cd-MOF	Cd $(NO_3)_2.4H_2O$, H_2BPP, H_2PyDC	H_2O, EtOH, NaOH	[231]
	La-MOF	La $(NO_3)_3$-xH_2O, H_2ADC	H_2O	[232]
	Ce-MOF	Ce $(NO_3)_3$-3H_2O, H_2ADC	H_2O	[232]
	Co-MOF	$CoCl_2.6H_2O$, H_2PyDC	H_2O, C_5H_5N	[233]

Method	MOFs	Precursors	Solvents	Reference
Hydrothermal/Solvothermal	M-008	Zn $(OAc)_2.xH_2O$, 4,40-bipy	MeOH, H_2O	[234]
	Ag-MOF	AgCl, 5-EATZH	MeOH, $NH_3.H_2O$	[235]
	Cu-MOF	$Cu_2(OH)_2(CO_3)$, H_4B_4S	H_2O	[236]
	Cu-HKUST-1	Cu $(NO_3)_2.3H_2O$, H_3BTC	H_2O, EtOH	[237]
	Zn-MOF-5	Zn $(NO_3)_2.4H_2O$, H_2BDC	DEF	[238]
	Zr-PCN-111	$ZrCl_4$, H_2BDDB	DMF, CF_3COOH	[239]
	Co-MOF	Co $(NO_3)_2.6H_2O$, H_3DCPNA	DMF, DXN, H_2O	[240]
	Mn-MOF	Mn $(CH_3COO)_2.4H_2O$, H_2BTAC	DMF, EtOH	[241]
	Ti-MIL-125	$Ti(OiPr)_4$, H_2BDC	DMF, MeOH	[242]
	Y-JUC-32	Y $(NO_3)_3.6H2O$, H_3BTC	AB, MeOH	[243]
	Al-MIL-96	Al $(NO_3)_3.9H_2O$, H_3BTC	H_2O	[244]
	Eu-MOF	Eu $(NO_3)_3.6H_2O$, H_2MFDA	CH_3CH_2OH, DMF, H_2O	[245]
	Ni-CPO-27	Ni $(CH_3CO_2)_2.x\ H_2O$, H_4DHTP	HF, H_2O	[246]
	Fe-MOF74	$FeCl_2.4H_2O$, 2OH-H_2BDC	DMF, C_3H8O, H_2O	[247]
	Mn-MOF	$MnCl_2.4H_2O$, H_3BTC	DMF, $C_2H_6O_2$, TEA	[248]
	Eu-MOF	Eu $(NO_3)_3.6H_2O$, H_3BTC	H_2O, DMF	[249]
	Ca-MOF	Ca $(NO_3)_2.4H_2O$, H_4AZBZ-TC	DMF	[250]
	Mg-MOF-74	Mg $(CH_3COO)_2.4H_2O$, 2OH-H_2BDC	DMF, H_2O, EtOH	[251]
	Zn-MOF-5	Zn $(NO_3)_2.6H_2O$, H_2BDC	DMF	[252]
	Zr-UiO-66	$ZrCl_4$, H_2BDC	DMF, EtOH, CH_3CO_2H, TBAB	[253]
Electrochemical	Cu-KHUST-1	Cu- electrode, H_3BTC	EtOH, MTBS	[254]
	Fe-MIL-100	Fe electrode, BTC	MeOH, MTBS	[255]
	Al-MIL-53	Al electrode, BDC	DMF, H_2O, KCl	[254]
	Zn-DMOF-1	Zn electrode, BDC, DABCO	DMF, $LiClO_4$	[256]
	Zn-MOF-5	Zn $(NO_3)_2.6H_2O$, H_2BDC	Bmim-Cl, DMF	[257]
	Ti-MIL-100	TiCl4, H_2BDC	DMF, EtOH, $TBAPF_6$	[258]
	Cu-MOF	Cu-electrode, H_3BTC	H_2O, EtOH, MTBS	[259]
	Ni-MOF	Ni-electrode, H_3BTC	H_2O, EtOH, TBATFB	[260]

Method	MOFs	Precursors	Solvents	Reference
Sonochemical	NH2-UiO-66	Zr-electrode, NH_2-H_2BDC	CH_3CO_2H, DMF, TABA	[261]
	Cu-HKUST-1	$C_4H_6CuO_4.xH_2O$, H_2BDC	DMF, EtOH, H_2O	[262]
	Zn-MOF-5	(Zn $(NO_3)_2.6H_2O$, H_2BDC	NMP	[263]
	Fe-MIL-53	$FeCl_3$,$6H_2O$, H_2BDC	DMF	[264]
	Ce-UiO-66	$(NH_4)_2Ce$ $(NO_3)_6$, H_2BDC	H_2O, DMF	[265]
	Mg-MOF	Mg $(NO_3)_2.6H_2O$, H_3BDC, KOH	H_2O	[266]
	Ni-MOF	Ni $(NO_3)_2.6H_2O$, H_3BTC	DMF, EtOH	[267]
	Al-MIL-53	$FeCl_3.6H_2O$, H_2BDC	DMF	[268]
	Cd-MOF	Cd $(OAc)_2.4H_2O$, BPDB, H_2OBA	DMF	[269]
	Ln-MOFs	Eu $(OAc)_3.6H_2O$, H_2BDC	DMF	[270]
	Tb-MOF	Tb $(NO_3)_3.6H_2O$, H_3BTC	DMF, EtOH, H_2O	[271]
Microwave	Cr-MIL-100	Cr $(NO_3)_3$. XH_2O, H_3BTC	H_2O, HF	[272]
	Fe-MIL-100	$FeCl_3.6H_2O$, NH_2-H_2BDC	EtOH, DMF, HCl, H_2O	[273]
	Zn-MOF-5	Zn $(NO_3)_2.4H_2O$, H_2BDC	NMP	[274]
	Cu-HKUST-1	Cu $(NO_3)_2.3H_2O$, H_3BTC	H_2O, EtOH	[275]
	Mg-MOF	Mg $(NO_3)_2.6H_2O$, DOT	DMF, EtOH, H_2O	[276]
	Ni-MOF	Ni $(NO_3)_2.6H_2O$, H_4DHTP	DMF, MeOH, H_2O	[277]
	Co-MOF	Co $(ACAC)_2$, H_2BPDC	DMF, $CHCl_3$	[278]
	Hf-UiO-66	$HfCl_4$, H_2BDC	DMF, CH_3COOH	[279]
	Zr-UiO-67	$ZrCl_4$, BPDC	DMF, BenAc or HCl	[280]
Spray drying	Cu-HKUST-1	Cu $(NO_3)_2.2.5H_2O$, H_3BTC	DMF, EtOH, H_2O	[281]
	Fe-MIL-88A	$FeCl_3.6H_2O$, $C_4H_4O_4$	H_2O, NaOH	[281]
	Zr-UiO-66	$ZrOCl_2.8H_2O$, H_2BDC-NH_2	H_2O, AAC	[282]
	Ni-MOF	Ni $(CH_3COO)_2.4H_2O$, HPZDC	DMF, H_2O	[283]
	Co-SIFSIX-3	$CoSiF_6$, HPYZ	MeOH	[284]
	Fe-MIL100	Fe $(NO_3)_3.9H_2O$, H_3BTC	DMF	[283]

Method	MOFs	Precursors	Solvents	Reference
Flow chemistry	Zn-ZIF-8	Zn $(CH_3CO_2)_2$. XH_2O, 2-MeIm	H_2O	[285]
	Zn-IRMOF-3	Zn (CH_3CO_2)2. XH_2O, DHBDC	DMF	[281]
	Mg-MOF-74	Mg $(NO_3)_2.6H_2O$, DHBDC	DMF, EtOH, H_2O	[281]
	Co-ZIF-67	Co $(OAc)_2.4H_2O$, 2-MeIm	H_2O	[286]
	Cu-HKUST-1	Cu $(NO_3)_2.2.5H_2O$, H_3BTC	DMF, EtOH	[287]
	Al-MIL-53	Al $(NO_3)_3.9H_2O$, H_2BDC	H_2O	[288]
	Zn-MOF-5	Zn $(NO_3)_2.6H_2O$, H_2BDC	DMF	[289]
	Zr-UiO-66	$ZrCl_4$, H_2BDC	DMF	[290]
	Ni-MOF-74	Ni $(CH_3COO)_2.4H_2O$, 2OH-H_2BDC	H_2O, DMF	[291]
	Cd-STA-12	Cd $(AcO)_2.2H_2O$, H_2PAMPA	H_2O, KOH	[290]
	Ce-MOF	Ce $(NH_4)_2(NO_3)_6$, H_2BDC	DMF	[292]
	Fe-MIL-88B-NH2	$FeCl_3.6H_2O$, NH_2-H_2BDC	H_2O, DMF	[293]
	Ni-CPO-27-Ni	Ni $(CH_3COO)_2.4H_2O$, 2OH-H_2BDC	H_2O	[294]
Ionothermal	Co-MOF	Co $(NO_3)_2.6H_2O$, H_2BDC	1-Ethyl-3-methylimidazolium chloride	[295]
	Zn-MOF	Zn $(NO_3)_2.6H_2O$, H_3BTC	1-Ethyl-3-methylimidazolium bromide	[296]
	Mn-MOF	Mn (OAc)2, H3BTC	propyl -3-methylimidazolium-iodine	[297]
	Cd-MOF	Cd $(NO_3)_2.4H_2O$, H_2BDC	1-butyl-3-methylimidazolium bromide	[298]
	Zn-MOF	Zn $(NO_3)_2.6H_2O$, H_2BDC	1-butyl-3-methylimidazolium bromide	[299]
	Zn-MOF	Zn $(NO_3)_2.6H_2O$, H_2BDC	1-Amyl-3-methylimidazolium Iodine	[299]
	Mg-MOF	Mg $(NO_3)_2.6H_2O$, H_2OBA	1-butyl-2,3-dimethylimidazolium-Bromide	[300]
	In-MOF	In $(NO_3)_3$,6 H_2O, H_2DABCO	1-Ethyl-3-methylimidazolium ethylsulfate	[301]
	Cu-MOF	Cu $(NO_3)_2.3H_2O$, H_2BPP	1-butyl-3-methylimidozolium-tetrafluoroborate	[302]

Method	MOFs	Precursors	Solvents	Reference
Mechanochemical	Ni-MOF	Ni $(OAc)_2.4H_2O$, H_3TMA	1-butyl 3-methylimidazolium-bromide	[303]
	Eu-MOF	$EuCl_3$. $6H_2O$, H_2BDC	1-ethyl-3-methylimidazolium bromide	[304]
	Cu-MOF-14	Cu $(CH_3COO)_2.H_2O$, H_3BTC	Nil	[305]
	Zn-MOF-74	ZnO, 2OH-H_2BDC	H_2O	[306]
	Cd-MOF	Cd $(CH_3COO)_2.2H_2O$, H3BTC	Nil	[307]
	Zr-UiO-66	$Zr_6O_4(OH)_4(MC)_{12}$, H_2BDC	H2O	[308]
	Ni-MOF	Ni $(OAc)_2.4H_2O$, H_3BTC	MeOH, EtOH, DMF	[309]
	In-OF-1	In $(OAc)_3.6H_2O$, H_4BPTC	H_2O, DMF, CH_3CN	[310]
	Y-MOF	YH_3, H_3BTC	Nil	[311]
	Fe-MOF	Fe $(NO_3)_3.9H_2O$, H_3BTC	TMAOH	[312]
	Cr-MIL-101	Cr $(NO_3)_3.9H_2O$, H_2BDC	Nil	[313]

2.6 Summary

Water pollution problems have dramatically increased throughout the world because of unanticipated economic growth, manufacturing expansions and urbanisation due to a fast-growing world population accompanied by insufficient investment in basic water supply and treatment projects. Due to their physical (colour) and chemical (toxicity) properties, dyes in wastewaters are a major danger to the environment. Their diversity and intensity of colours lead to potential troubles when they are discharged into water streams.

Further, many dyes such as Alizarin S, Crocein Orange G, methyl red, Congo red, MB, reactive dyes (reactive red RB, reactive black B, Reason Blue) and MO are toxic and may cause genetic alterations in human and other beings. In addition, as they are synthetic in origin, these dyes are not recognised in the natural environment and do not degrade easily. Discharging dyes directly into valuable water resources must be stopped; otherwise, numerous new treatment processes are required and must be built and used.

Physical and chemical methods should be employed in advanced treatments to maintain standard concentrations of chemicals in wastewater. The adsorption process is very effective for removing chemical pollutants (adsorbates) from wastewater by using adsorbents having a high surface area and surface affinity towards adsorbates. In industrial applications, it is preferable to recover adsorbates and regenerate adsorbents; therefore, the use of physisorption processes to treat water is widespread. Adsorbents such as zeolites, activated alumina and activated carbon, made from affordable sources, are commonly used in different applications.

Recently, MOFs have attracted much research attention because of their delightful and picturesque specifications such large surface area, pore volume, tuneable pore size, innumerable functionalities and capacity for facile modifications. The impetus for synthesising MOFs originated in studies of coordination networks, which have single-metal nodes in their vertices. These vertices consist of a single-metal ion node bonded weakly with a neutral organic donor linker such as Cu-N (pyridine, nitrile)-type bond. As a result of the weak chemical bonds between the vertices and linkers, coordination networks are non-porous, chemically unstable, undesignable and collapse with the removal of solvents or with the exchange of ions in the pores.

These characteristics of coordination networks motivated scientist and researchers to strengthen the chemical bonds between the vertex and the linker (via reticular chemistry) to make MOFs that consist entirely strong chemical bonds such as C-C, C-H, C-O and M-O [50, 70-72]. They did so by creating SBUs, which are rigid, directional and stable building units that enable the design of robust crystalline materials with predictable structures and properties.

Specifically, the features of SBU have enhanced the design and synthesis of MOFs with ultra-high porosity and structural complexity. Several MOFs with sufficient water stability have been examined for the removal of dyes from wastewater and demonstrated very high removal efficiency.

The design, synthesis and characteristics of MOFs were briefly and carefully reviewed in this chapter. MOFs can be synthesised in two ways. The first is a liquid-phase synthesis, which includes slow evaporation, or hydrothermal/solvothermal, electrochemical, sonochemical, spray-drying, microwave, and flow chemistry

methods. The second is solid-phase synthesis, represented by mechanochemical methods.

The review has identified that the solvothermal/hydrothermal method is the most popular method among researchers. As-synthesised MOFs are mostly blocked by solvents and unreacted precursors in this method; this blockage fills the pores and therefore, undesirable guests must be discarded by a process called the activation process.

There are several activation methods, including evacuation, heating, heating and vacuum, solvent exchange and evacuation, solvent exchange accompanied by evacuation and heating, CO_2 supercritical CO_2 drying, benzene freeze-drying and photothermal activations. The activation method used most to date is activation by solvent exchange with evacuation.

Water stability is an essential sign that an MOF can succeed in a water treatment application. A water-stable MOF must have sufficient hydrothermal resistance to prevent water molecules from interloping into the MOF structure to avoiding loss of structural integrity and whole porosity. Thus, MOF structures with great stability normally possess strong coordination bonds (thermodynamic stability) or significant steric hindrance (kinetic stability) to prevent the detrimental hydrolysis reactions that break metal–ligand bonds. Moreover, high-valence metal clusters with higher coordination number typically produce firm structures and make the metal-linked bonds less vulnerable to water molecules. Therefore, using carboxylate-type linkers, high-valence metal ions, including Al^{+3}, Fe^{3+}, Cr^{3+} and Zr^{4+}, have been used to synthesise hydrothermally stable MOFs. In addition, incorporating a polar functional group such as NO_2, NH_3, Br, Cl or OH on the dicarboxylate organic linker reduces water stability of the resulting MOF compared to the parent MOF, because these polar functional groups facilitate hydrolysis of the M−O bond (such as the Zn–O bond). However, using hydrophilic functional groups such as methyl groups or polydimethylsiloxane on the terephthalate ligand can produce stronger MOFs with higher water stability, because water molecules are hydrophilic and have no affinity towards hydrophobic.

Waterproof MOFs have been scientifically investigated for its capacity to remove dyes from aqueous solution. The findings in the literature are that the dominant mechanism

responsible for MOFs' adsorption of dyes relies on the characteristics of MOFs—including their vacant metal sites, chemistry of organic ligands (polarity of functional groups and length of benzene chain)—as well as dye characteristics, such as the type of valent charge, the nature of benzene rings and the structural groups within a dye molecule. Zr-MOFs have exhibited significant ability to remove dyes from aqueous solution while maintaining their own structures. Mixed-metal MOFs have also been successfully used to remove dyes from wastewater, although studies on these MOFs have been very limited.

References

1. Wu, C., et al., *Water pollution and human health in China.* Environmental Health Perspectives, 1999. **107**(4): p. 251-256.
2. Schwarzenbach, R.P., et al., *Global Water Pollution and Human Health.* Annual Review of Environment and Resources, 2010. **35**(1): p. 109-136.
3. Gruber, N. and J.N. Galloway, *An Earth-system perspective of the global nitrogen cycle.* Nature, 2008. **451**: p. 293.
4. Filippelli, G.M., *The global phosphorus cycle: past, present, and future.* Elements, 2008. **4**(2): p. 89-95.
5. Jorgenson, A.K., *Political-Economic Integration, Industrial Pollution and Human Health:A Panel Study of Less-Developed Countries, 1980—2000.* International Sociology, 2009. **24**(1): p. 115-143.
6. Vysokomornaya, O.V., E.Y. Kurilenko, and A.A. Shcherbinina. *Major contaminants in industrial and domestic wastewater*. in *MATEC Web of Conferences*. 2015. EDP Sciences.
7. Kempe, J., *Review of water pollution problems and control strategies in the South African mining industry.* Water Science and Technology, 1983. **15**(2): p. 27-58.
8. Vandevivere, P.C., R. Bianchi, and W. Verstraete, *Treatment and reuse of wastewater from the textile wet-processing industry: Review of emerging technologies.* Journal of Chemical Technology & Biotechnology: International Research in Process, Environmental AND Clean Technology, 1998. **72**(4): p. 289-302.
9. Kant, R., *Textile dyeing industry an environmental hazard.* Natural Science, 2012. **Vol.04No.01**: p. 5.
10. Chequer, F.M.D., et al., *Textile dyes: dyeing process and environmental impact*, in *Eco-friendly textile dyeing and finishing*. 2013, InTech.
11. C., V.P., B. Roberto, and V. Willy, *Review: Treatment and reuse of wastewater from the textile wet-processing industry: Review of emerging technologies.* Journal of Chemical Technology & Biotechnology, 1998. **72**(4): p. 289-302.
12. Ghosh, D. and K.G. Bhattacharyya, *Adsorption of methylene blue on kaolinite.* Applied Clay Science, 2002. **20**(6): p. 295-300.
13. Lachheb, H., et al., *Photocatalytic degradation of various types of dyes (Alizarin S, Crocein Orange G, Methyl Red, Congo Red, Methylene Blue) in water by UV-irradiated titania.* Applied Catalysis B: Environmental, 2002. **39**(1): p. 75-90.
14. Gül, Ü.D., *Treatment of dyeing wastewater including reactive dyes (Reactive Red RB, Reactive Black B, Remazol Blue) and Methylene Blue by fungal biomass.* Water SA, 2013. **39**: p. 593-598.
15. DI, Ç., *Decolorization of methylene blue and methyl orange with Ag doped TiO2 under UV-A and UV-visible conditions: process optimization by response surface method and toxicity evaluation.* 2016.
16. Mishra, G. and M. Tripathy, *A critical review of the treatments for decolourization of textile effluent.* Colourage, 1993. **40**(10): p. 35-38.
17. Banat, F., et al., *Photodegradation of methylene blue dye by the UV/H2O2 and UV/acetone oxidation processes.* Desalination, 2005. **181**(1): p. 225-232.

18. Chen, Z., et al., *Adsorption of cationic dye (methylene blue) from aqueous solution using poly(cyclotriphosphazene-co-4,4'-sulfonyldiphenol) nanospheres.* Applied Surface Science, 2014. **289**: p. 495-501.
19. Grabowski, L., et al., *Breakdown of methylene blue and methyl orange by pulsed corona discharge.* Plasma Sources Science and Technology, 2007. **16**(2): p. 226.
20. Byun, K.-T. and H.-Y. Kwak, *Degradation of methylene blue under multibubble sonoluminescence condition.* Journal of Photochemistry and Photobiology A: Chemistry, 2005. **175**(1): p. 45-50.
21. Chung, K.-T., S.E. Stevens, and C.E. Cerniglia, *The Reduction of Azo Dyes by the Intestinal Microflora.* Critical Reviews in Microbiology, 1992. **18**(3): p. 175-190.
22. Gupta, V.K. and Suhas, *Application of low-cost adsorbents for dye removal – A review.* Journal of Environmental Management, 2009. **90**(8): p. 2313-2342.
23. Perry, R., D. Green, and J. Maloney, *Perry's Chemical Engineers' Handbook, McGraw-Hill, New York, 1997.*
24. Van der Zee, F.P. and S. Villaverde, *Combined anaerobic–aerobic treatment of azo dyes—a short review of bioreactor studies.* Water research, 2005. **39**(8): p. 1425-1440.
25. Cheremisinoff, N.P., *Handbook of water and wastewater treatment technologies*. 2001: Butterworth-Heinemann.
26. Janezcko, M. and S. Gaydardzhiev. *Removal of dyes from textile wastewater by chemical coagulation*. in *XXIII International Mineral Processing Congress, 3-8 September 2006, Istanbul*. 2006. Promedadvertising Agency.
27. Ali, M., et al., *Efficient precipitation of dyes from dilute aqueous solutions of ionic liquids.* Analytical sciences, 2006. **22**(8): p. 1051-1053.
28. Cooper, P., *Removing colour from dyehouse waste waters — a critical review of technology available.* Journal of the Society of Dyers and Colourists, 1993. **109**(3): p. 97-100.
29. Marcucci, M., et al., *Treatment and reuse of textile effluents based on new ultrafiltration and other membrane technologies.* Desalination, 2001. **138**(1-3): p. 75-82.
30. Al-Bastaki, N., *Removal of methyl orange dye and Na2SO4 salt from synthetic waste water using reverse osmosis.* Chemical Engineering and Processing: Process Intensification, 2004. **43**(12): p. 1561-1567.
31. Forgacs, E., T. Cserháti, and G. Oros, *Removal of synthetic dyes from wastewaters: a review.* Environment International, 2004. **30**(7): p. 953-971.
32. Karcher, S., A. Kornmüller, and M. Jekel, *Anion exchange resins for removal of reactive dyes from textile wastewaters.* Water Research, 2002. **36**(19): p. 4717-4724.
33. Suteu, D., D. Bilba, and S. Coseri, *Macroporous polymeric ion exchangers as adsorbents for the removal of cationic dye basic blue 9 from aqueous solutions.* Journal of Applied Polymer Science, 2014. **131**(1).
34. Bajpai, A. and M. Rajpoot, *Adsorption techniques-a review.* 1999.
35. Yagub, M.T., et al., *Dye and its removal from aqueous solution by adsorption: A review.* Advances in Colloid and Interface Science, 2014. **209**: p. 172-184.
36. Vital RK, S.K., Shaik KB, *Dye Removal by Adsorption: A Review* Journal of Bioremediation & Biodegradation, 2016. **7**(6).

37. Wang, S. and Y. Peng, *Natural zeolites as effective adsorbents in water and wastewater treatment.* Chemical Engineering Journal, 2010. **156**(1): p. 11-24.
38. Wang, S., H. Li, and L. Xu, *Application of zeolite MCM-22 for basic dye removal from wastewater.* Journal of colloid and interface science, 2006. **295**(1): p. 71-78.
39. Karadag, D., et al., *Basic and reactive dye removal using natural and modified zeolites.* Journal of Chemical & Engineering Data, 2007. **52**(6): p. 2436-2441.
40. Kannan, C., T. Sundaram, and T. Palvannan, *Environmentally stable adsorbent of tetrahedral silica and non-tetrahedral alumina for removal and recovery of malachite green dye from aqueous solution.* Journal of hazardous materials, 2008. **157**(1): p. 137-145.
41. Gupta, V.K., S. Agarwal, and T.A. Saleh, *Synthesis and characterization of alumina-coated carbon nanotubes and their application for lead removal.* Journal of hazardous materials, 2011. **185**(1): p. 17-23.
42. Kim, Y., et al., *Arsenic removal using mesoporous alumina prepared via a templating method.* Environmental science & technology, 2004. **38**(3): p. 924-931.
43. Kadirvelu, K., et al., *Utilization of various agricultural wastes for activated carbon preparation and application for the removal of dyes and metal ions from aqueous solutions.* Bioresource technology, 2003. **87**(1): p. 129-132.
44. Malik, P., *Dye removal from wastewater using activated carbon developed from sawdust: adsorption equilibrium and kinetics.* Journal of Hazardous Materials, 2004. **113**(1-3): p. 81-88.
45. Hameed, B., A.M. Din, and A. Ahmad, *Adsorption of methylene blue onto bamboo-based activated carbon: kinetics and equilibrium studies.* Journal of hazardous materials, 2007. **141**(3): p. 819-825.
46. Biradha, K., A. Ramanan, and J.J. Vittal, *Coordination Polymers Versus Metal−Organic Frameworks.* Crystal Growth & Design, 2009. **9**(7): p. 2969-2970.
47. Furukawa, H., et al., *The Chemistry and Applications of Metal-Organic Frameworks.* Science, 2013. **341**(6149).
48. Li, M., et al., *Topological Analysis of Metal–Organic Frameworks with Polytopic Linkers and/or Multiple Building Units and the Minimal Transitivity Principle.* Chemical Reviews, 2014. **114**(2): p. 1343-1370.
49. Yuan, S., et al., *Stable Metal–Organic Frameworks with Group 4 Metals: Current Status and Trends.* ACS Central Science, 2018. **4**(4): p. 440-450.
50. Cavka, J.H., et al., *A new zirconium inorganic building brick forming metal organic frameworks with exceptional stability.* Journal of the American Chemical Society, 2008. **130**(42): p. 13850-13851.
51. Chui, S.S.-Y., et al., *A Chemically Functionalizable Nanoporous Material [Cu3(TMA)2(H2O)3]n.* Science, 1999. **283**(5405): p. 1148-1150.
52. Boutin, A., et al., *The Behavior of Flexible MIL-53(Al) upon CH4 and CO2 Adsorption.* The Journal of Physical Chemistry C, 2010. **114**(50): p. 22237-22244.
53. Alhamami, M., H. Doan, and C.H. Cheng, *A Review on Breathing Behaviors of Metal-Organic-Frameworks (MOFs) for Gas Adsorption.* Materials, 2014. **7**(4): p. 3198.
54. Zeng, M.-H., X.-L. Feng, and X.-M. Chen, *Crystal-to-crystal transformations of a microporous metal–organic laminated framework triggered by guest*

exchange, dehydration and readsorption. Dalton Transactions, 2004(15): p. 2217-2223.
55. Loiseau, T., et al., *A Rationale for the Large Breathing of the Porous Aluminum Terephthalate (MIL-53) Upon Hydration.* Chemistry – A European Journal, 2004. **10**(6): p. 1373-1382.
56. Millange, F., et al., *Effect of the nature of the metal on the breathing steps in MOFs with dynamic frameworks.* Chemical Communications, 2008(39): p. 4732-4734.
57. Férey, G. and C. Serre, *Large breathing effects in three-dimensional porous hybrid matter: facts, analyses, rules and consequences.* Chemical Society Reviews, 2009. **38**(5): p. 1380-1399.
58. Li, H., et al., *Design and synthesis of an exceptionally stable and highly porous metal-organic framework.* Nature, 1999. **402**: p. 276.
59. Kalmutzki, M.J., N. Hanikel, and O.M. Yaghi, *Secondary building units as the turning point in the development of the reticular chemistry of MOFs.* Science advances, 2018. **4**(10): p. eaat9180.
60. Yaghi, O.M., et al., *Reticular synthesis and the design of new materials.* Nature, 2003. **423**(6941): p. 705.
61. Tranchemontagne, D.J., et al., *Reticular chemistry of metal–organic polyhedra.* Angewandte Chemie International Edition, 2008. **47**(28): p. 5136-5147.
62. Nanotecnologia, I.C.d.N.i. *ICN2 Lecture Prof. Omar M. Yaghi: Reticular Chemistry*. 2018 [cited 2018 10/10/2018]; Available from: https://www.youtube.com/watch?v=OS_VI-8sMF0.
63. Kinoshita, Y., I. Matsubara, and Y. Saito, *The crystal structure of bis (succinonitrilo) copper (I) nitrate.* Bulletin of the Chemical Society of Japan, 1959. **32**(7): p. 741-747.
64. Abrahams, B., et al., *Assembly of porphyrin building blocks into network structures with large channels.* Nature, 1994. **369**(6483): p. 727.
65. Conference, C.a.B.D.S.a.T.C.S.T. *Keynote Speaker: Dr. Omar Yaghi*. 2015 [cited 2018 10/11/2018]; Available from: https://www.youtube.com/watch?v=m6sRQjKFssk.
66. Aumüller, A., et al., *A radical anion salt of 2, 5-dimethyl-N, N′-dicyanoquinonediimine with extremely high electrical conductivity.* Angewandte Chemie International Edition in English, 1986. **25**(8): p. 740-741.
67. Hoskins, B. and R. Robson, *Design and construction of a new class of scaffolding-like materials comprising infinite polymeric frameworks of 3D-linked molecular rods. A reappraisal of the zinc cyanide and cadmium cyanide structures and the synthesis and structure of the diamond-related frameworks [N (CH3) 4][CuIZnII (CN) 4] and CuI [4, 4', 4'', 4'''-tetracyanotetraphenylmethane] BF4. xC6H5NO2.* Journal of the American Chemical Society, 1990. **112**(4): p. 1546-1554.
68. Yaghi, O. and H. Li, *Hydrothermal synthesis of a metal-organic framework containing large rectangular channels.* Journal of the American Chemical Society, 1995. **117**(41): p. 10401-10402.
69. Subramanian, S. and M.J. Zaworotko, *Porous solids by design:[Zn (4, 4'-bpy) 2 (SiF6)] n· xDMF, a single framework octahedral coordination polymer with large square channels.* Angewandte Chemie International Edition in English, 1995. **34**(19): p. 2127-2129.

70. Eddaoudi, M., et al., *Systematic design of pore size and functionality in isoreticular MOFs and their application in methane storage.* Science, 2002. **295**(5554): p. 469-472.
71. Park, K.S., et al., *Exceptional chemical and thermal stability of zeolitic imidazolate frameworks.* Proceedings of the National Academy of Sciences, 2006. **103**(27): p. 10186-10191.
72. Kandiah, M., et al., *Synthesis and stability of tagged UiO-66 Zr-MOFs.* Chemistry of Materials, 2010. **22**(24): p. 6632-6640.
73. Yaghi, O.M., *ICN2 Lecture Prof. Omar M. Yaghi: Reticular Chemistry*. 2018.
74. Stein, A., S.W. Keller, and T.E. Mallouk, *Turning down the heat: design and mechanism in solid-state synthesis.* Science, 1993. **259**(5101): p. 1558-1564.
75. Yaghi, O., M. O'Keeffe, and M. Kanatzidis, *Design of solids from molecular building blocks: golden opportunities for solid state chemistry.* Journal of Solid State Chemistry, 2000. **152**(1): p. 1-2.
76. Biradha, K., Y. Hongo, and M. Fujita, *Open square-grid coordination polymers of the dimensions 20× 20 Å: remarkably stable and crystalline solids even after guest removal.* Angewandte Chemie International Edition, 2000. **39**(21): p. 3843-3845.
77. Eddaoudi, M., et al., *Porous metal− organic polyhedra: 25 Å cuboctahedron constructed from 12 Cu2 (CO2) 4 paddle-wheel building blocks.* Journal of the American Chemical Society, 2001. **123**(18): p. 4368-4369.
78. Moulton, B., et al., *Nanoballs: nanoscale faceted polyhedra with large windows and cavities.* Chemical Communications, 2001(9): p. 863-864.
79. Eddaoudi, M., et al., *Cu2 [o-Br-C6H3 (CO2) 2] 2 (H2O) 2⊙(DMF) 8 (H2O) 2: A Framework Deliberately Designed To Have the NbO Structure Type.* Journal of the American Chemical Society, 2002. **124**(3): p. 376-377.
80. Li, H., et al., *Establishing microporosity in open metal− organic frameworks: gas sorption isotherms for Zn (BDC)(BDC= 1, 4-benzenedicarboxylate).* Journal of the American Chemical Society, 1998. **120**(33): p. 8571-8572.
81. Li, H., et al., *Design and synthesis of an exceptionally stable and highly porous metal-organic framework.* nature, 1999. **402**(6759): p. 276.
82. Chui, S.S.-Y., et al., *A chemically functionalizable nanoporous material [Cu3 (TMA) 2 (H2O) 3] n.* Science, 1999. **283**(5405): p. 1148-1150.
83. Moghadam, P.Z., et al., *Development of a Cambridge Structural Database subset: a collection of metal–organic frameworks for past, present, and future.* Chemistry of Materials, 2017. **29**(7): p. 2618-2625.
84. Furukawa, H., et al., *The chemistry and applications of metal-organic frameworks.* Science, 2013. **341**(6149): p. 1230444.
85. Li, Q., et al., *Docking in metal-organic frameworks.* Science, 2009. **325**(5942): p. 855-859.
86. Deng, H., et al., *Robust dynamics.* Nature chemistry, 2010. **2**(6): p. 439.
87. Deng, H., et al., *Multiple Functional Groups of Varying Ratios in Metal-Organic Frameworks.* Science, 2010. **327**(5967): p. 846-850.
88. Eddaoudi, M., et al., *Modular chemistry: secondary building units as a basis for the design of highly porous and robust metal− organic carboxylate frameworks.* Accounts of Chemical Research, 2001. **34**(4): p. 319-330.
89. Kalmutzki, M.J., N. Hanikel, and O.M. Yaghi, *Secondary building units as the turning point in the development of the reticular chemistry of MOFs.* Science Advances, 2018. **4**(10).

90. Deng, H., et al., *Large-pore apertures in a series of metal-organic frameworks.* science, 2012. **336**(6084): p. 1018-1023.
91. Dey, C., et al., *Crystalline metal-organic frameworks (MOFs): synthesis, structure and function.* Acta Crystallographica Section B: Structural Science, Crystal Engineering and Materials, 2014. **70**(1): p. 3-10.
92. Persson, I., *Solvation and complex formation in strongly solvating solvents.* Pure and applied chemistry, 1986. **58**(8): p. 1153-1161.
93. El Seoud, O.A., *Understanding solvation.* Pure and Applied Chemistry, 2009. **81**(4): p. 697-707.
94. Yang, X. and A.E. Clark, *Preferential Solvation of Metastable Phases Relevant to Topological Control Within the Synthesis of Metal–Organic Frameworks.* Inorganic Chemistry, 2014. **53**(17): p. 8930-8940.
95. Howarth, A.J., et al., *Best practices for the synthesis, activation, and characterization of metal–organic frameworks.* Chemistry of Materials, 2016. **29**(1): p. 26-39.
96. Rowsell, J.L. and O.M. Yaghi, *Metal–organic frameworks: a new class of porous materials.* Microporous and Mesoporous Materials, 2004. **73**(1-2): p. 3-14.
97. Hafizovic, J., et al., *The Inconsistency in Adsorption Properties and Powder XRD Data of MOF-5 Is Rationalized by Framework Interpenetration and the Presence of Organic and Inorganic Species in the Nanocavities.* Journal of the American Chemical Society, 2007. **129**(12): p. 3612-3620.
98. Yoshimura, M. and K. Byrappa, *Hydrothermal processing of materials: past, present and future.* Journal of Materials Science, 2008. **43**(7): p. 2085-2103.
99. Abid, H.R., *Capture of carbon dioxide in metal organic frameworks*. 2012, Curtin University.
100. Parker, A.J., *The effects of solvation on the properties of anions in dipolar aprotic solvents.* Quarterly Reviews, Chemical Society, 1962. **16**(2): p. 163-187.
101. Lee, Y.-R., J. Kim, and W.-S. Ahn, *Synthesis of metal-organic frameworks: A mini review.* Korean Journal of Chemical Engineering, 2013. **30**(9): p. 1667-1680.
102. Pirzadeh, K., et al., *Electrochemical synthesis, characterization and application of a microstructure Cu3(BTC)2 metal organic framework for CO2 and CH4 separation.* Korean Journal of Chemical Engineering, 2018. **35**(4): p. 974-983.
103. Al-Kutubi, H., et al., *Electrosynthesis of Metal–Organic Frameworks: Challenges and Opportunities.* ChemElectroChem, 2015. **2**(4): p. 462-474.
104. Al-Kutubi, H., et al., *Electrosynthesis of metal–organic frameworks: challenges and opportunities.* ChemElectroChem, 2015. **2**(4): p. 462-474.
105. Martinez Joaristi, A., et al., *Electrochemical Synthesis of Some Archetypical Zn2+, Cu2+, and Al3+ Metal Organic Frameworks.* Crystal Growth & Design, 2012. **12**(7): p. 3489-3498.
106. Van de Voorde, B., et al., *Mechanical properties of electrochemically synthesised metal–organic framework thin films.* Journal of Materials Chemistry C, 2013. **1**(46): p. 7716-7724.
107. Wei, J.-Z., et al., *Rapid and Large-Scale Synthesis of IRMOF-3 by Electrochemistry Method with Enhanced Fluorescence Detection Performance for TNP.* Inorganic Chemistry, 2018. **57**(7): p. 3818-3824.

108. Chatel, G. and J.C. Colmenares, *Sonochemistry: from Basic Principles to Innovative Applications.* Topics in Current Chemistry, 2017. **375**(1): p. 8.
109. Vinoth, V., et al., *Sonochemical synthesis of silver nanoparticles anchored reduced graphene oxide nanosheets for selective and sensitive detection of glutathione.* Ultrasonics Sonochemistry, 2017. **39**: p. 363-373.
110. Safarifard, V. and A. Morsali, *Applications of ultrasound to the synthesis of nanoscale metal–organic coordination polymers.* Coordination Chemistry Reviews, 2015. **292**: p. 1-14.
111. Leong, T., M. Ashokkumar, and S. Kentish, *THE FUNDAMENTALS OF POWER ULTRASOUND - A REVIEW.* 2011. **39**(ACOUSTICS AUSTRALIA): p. 54 - 63.
112. Sargazi, G., et al., *A systematic study on the use of ultrasound energy for the synthesis of nickel–metal organic framework compounds.* Ultrasonics Sonochemistry, 2015. **27**: p. 395-402.
113. Lagashetty, A., et al., *Microwave-assisted route for synthesis of nanosized metal oxides.* Science and Technology of Advanced Materials, 2007. **8**(6): p. 484-493.
114. Horcajada, P., et al., *Porous metal–organic-framework nanoscale carriers as a potential platform for drug delivery and imaging.* Nature Materials, 2009. **9**: p. 172.
115. Jhung, S.H., et al., *Microwave Synthesis of Hybrid Inorganic–Organic Porous Materials: Phase-Selective and Rapid Crystallization.* Chemistry – A European Journal, 2006. **12**(30): p. 7899-7905.
116. Isaeva, V.I. and L.M. Kustov, *Microwave activation as an alternative production of metal-organic frameworks.* Russian Chemical Bulletin, 2016. **65**(9): p. 2103-2114.
117. Das, B.C., D. Bhowmik, and S. Chaudhuri, *Microwave System.* The Pharma Innovation, 2012. **1**(6, Part A): p. 1.
118. Vakili, R., et al., *Microwave-assisted synthesis of zirconium-based metal organic frameworks (MOFs): Optimization and gas adsorption.* Microporous and Mesoporous Materials, 2018. **260**: p. 45-53.
119. Carné-Sánchez, A., et al., *A spray-drying strategy for synthesis of nanoscale metal–organic frameworks and their assembly into hollow superstructures.* Nature Chemistry, 2013. **5**: p. 203.
120. Garzón-Tovar, L., et al., *A spray-drying continuous-flow method for simultaneous synthesis and shaping of microspherical high nuclearity MOF beads.* Reaction Chemistry & Engineering, 2016. **1**(5): p. 533-539.
121. Gimeno-Fabra, M., et al., *Instant MOFs: continuous synthesis of metal–organic frameworks by rapid solvent mixing.* Chemical Communications, 2012. **48**(86): p. 10642-10644.
122. Paseta, L., et al., *Accelerating the Controlled Synthesis of Metal–Organic Frameworks by a Microfluidic Approach: A Nanoliter Continuous Reactor.* ACS Applied Materials & Interfaces, 2013. **5**(19): p. 9405-9410.
123. Luz, I., M. Soukri, and M. Lail, *Confining Metal–Organic Framework Nanocrystals within Mesoporous Materials: A General Approach via "Solid-State" Synthesis.* Chemistry of Materials, 2017. **29**(22): p. 9628-9638.
124. Crawford, D., et al., *Synthesis by extrusion: continuous, large-scale preparation of MOFs using little or no solvent.* Chemical Science, 2015. **6**(3): p. 1645-1649.

125. Friščić, T., *New opportunities for materials synthesis using mechanochemistry.* Journal of Materials Chemistry, 2010. **20**(36): p. 7599-7605.
126. Friščić, T., et al., *Clean and efficient synthesis using mechanochemistry: coordination polymers, metal-organic frameworks and metallodrugs.* Croatica Chemica Acta, 2012. **85**(3): p. 367-378.
127. Michalchuk, A.A.L., I.A. Tumanov, and E.V. Boldyreva, *Complexities of mechanochemistry: elucidation of processes occurring in mechanical activators via implementation of a simple organic system.* CrystEngComm, 2013. **15**(32): p. 6403-6412.
128. Mottillo, C. and T. Friščić, *Advances in Solid-State Transformations of Coordination Bonds: From the Ball Mill to the Aging Chamber.* Molecules, 2017. **22**(1): p. 144.
129. Rubio-Martinez, M., et al., *New synthetic routes towards MOF production at scale.* Chemical Society Reviews, 2017. **46**(11): p. 3453-3480.
130. Baláž, P., et al., *Hallmarks of mechanochemistry: from nanoparticles to technology.* Chemical Society Reviews, 2013. **42**(18): p. 7571-7637.
131. Klimakow, M., et al., *Mechanochemical Synthesis of Metal−Organic Frameworks: A Fast and Facile Approach toward Quantitative Yields and High Specific Surface Areas.* Chemistry of Materials, 2010. **22**(18): p. 5216-5221.
132. Keenan, L.L., et al., *Secondary amine-functionalised metal–organic frameworks: direct syntheses versus tandem post-synthetic modifications.* CrystEngComm, 2016. **18**(30): p. 5710-5717.
133. Morris, W., et al., *Framework mobility in the metal–organic framework crystal IRMOF-3: Evidence for aromatic ring and amine rotation.* Journal of Molecular Structure, 2011. **1004**(1): p. 94-101.
134. Cohen, S.M., *Postsynthetic Methods for the Functionalization of Metal–Organic Frameworks.* Chemical Reviews, 2012. **112**(2): p. 970-1000.
135. Yujia, S. and Z. Hong-Cai, *Recent progress in the synthesis of metal–organic frameworks.* Science and Technology of Advanced Materials, 2015. **16**(5): p. 054202.
136. Sun, Y. and H.-C. Zhou, *Recent progress in the synthesis of metal–organic frameworks.* Science and technology of advanced materials, 2015. **16**(5): p. 054202.
137. Jambovane, S.R., et al., *Continuous, One-pot Synthesis and Post-Synthetic Modification of NanoMOFs Using Droplet Nanoreactors.* Scientific Reports, 2016. **6**: p. 36657.
138. Garibay, S.J. and S.M. Cohen, *Isoreticular synthesis and modification of frameworks with the UiO-66 topology.* Chemical Communications, 2010. **46**(41): p. 7700-7702.
139. Biswas, S. and P. Van Der Voort, *A General Strategy for the Synthesis of Functionalised UiO-66 Frameworks: Characterisation, Stability and CO2 Adsorption Properties.* European Journal of Inorganic Chemistry, 2013. **2013**(12): p. 2154-2160.
140. Abid, H.R., et al., *Amino-functionalized Zr-MOF nanoparticles for adsorption of CO2 and CH4.* International Journal of Smart and Nano Materials, 2013. **4**(1): p. 72-82.

141. Zaboon, S., et al., *Removal of monoethylene glycol from wastewater by using Zr-metal organic frameworks.* Journal of Colloid and Interface Science, 2018. **523**: p. 75-85.
142. Stock, N. and S. Biswas, *Synthesis of Metal-Organic Frameworks (MOFs): Routes to Various MOF Topologies, Morphologies, and Composites.* Chemical Reviews, 2012. **112**(2): p. 933-969.
143. Abid, H.R., H.M. Ang, and S. Wang, *Effects of ammonium hydroxide on the structure and gas adsorption of nanosized Zr-MOFs (UiO-66).* Nanoscale, 2012. **4**(10): p. 3089-3094.
144. Schaate, A., et al., *Modulated Synthesis of Zr-Based Metal–Organic Frameworks: From Nano to Single Crystals.* Chemistry – A European Journal, 2011. **17**(24): p. 6643-6651.
145. Seetharaj, R., et al., *Dependence of solvents, pH, molar ratio and temperature in tuning metal organic framework architecture.* Arabian Journal of Chemistry, 2016.
146. Abid, H.R., et al., *Enhanced CO2 Adsorption and Selectivity of CO2/N2 on Amino-MIL-53(Al) Synthesized by Polar Co-solvents.* Energy & Fuels, 2018. **32**(4): p. 4502-4510.
147. Azhar, M.R., et al., *Cascade applications of robust MIL-96 metal organic frameworks in environmental remediation: Proof of concept.* Chemical Engineering Journal, 2018. **341**: p. 262-271.
148. Rada, Z.H., et al., *Effects of -NO2 and -NH2 functional groups in mixed-linker Zr-based MOFs on gas adsorption of CO2 and CH4.* Progress in Natural Science: Materials International, 2018. **28**(2): p. 160-167.
149. Kong, X., et al., *Mapping of Functional Groups in Metal-Organic Frameworks.* Science, 2013. **341**(6148): p. 882-885.
150. Reimer, N., et al., *Three Series of Sulfo-Functionalized Mixed-Linker CAU-10 Analogues: Sorption Properties, Proton Conductivity, and Catalytic Activity.* Chemistry – A European Journal, 2015. **21**(35): p. 12517-12524.
151. Dhakshinamoorthy, A., A.M. Asiri, and H. Garcia, *Mixed-metal or mixed-linker metal organic frameworks as heterogeneous catalysts.* Catalysis Science & Technology, 2016. **6**(14): p. 5238-5261.
152. Burrows, A.D., *Mixed-component metal–organic frameworks (MC-MOFs): enhancing functionality through solid solution formation and surface modifications.* CrystEngComm, 2011. **13**(11): p. 3623-3642.
153. Koh, K., A.G. Wong-Foy, and A.J. Matzger, *A Crystalline Mesoporous Coordination Copolymer with High Microporosity.* Angewandte Chemie International Edition, 2008. **47**(4): p. 677-680.
154. Qin, J.-S., et al., *Mixed-linker strategy for the construction of multifunctional metal–organic frameworks.* Journal of Materials Chemistry A, 2017. **5**(9): p. 4280-4291.
155. Bunck, D.N. and W.R. Dichtel, *Mixed Linker Strategies for Organic Framework Functionalization.* Chemistry – A European Journal, 2013. **19**(3): p. 818-827.
156. Yuan, S., et al., *Retrosynthesis of multi-component metal−organic frameworks.* Nature Communications, 2018. **9**(1): p. 808.
157. Yang, X. and Q. Xu, *Bimetallic Metal–Organic Frameworks for Gas Storage and Separation.* Crystal Growth & Design, 2017. **17**(4): p. 1450-1455.

158. Wang, L.J., et al., *Synthesis and Characterization of Metal–Organic Framework-74 Containing 2, 4, 6, 8, and 10 Different Metals.* Inorganic Chemistry, 2014. **53**(12): p. 5881-5883.
159. Wang, T., et al., *Enhanced adsorption of dibenzothiophene with zinc/copper-based metal–organic frameworks.* Journal of Materials Chemistry A, 2015. **3**(42): p. 21044-21050.
160. Schejn, A., et al., *Cu2+-doped zeolitic imidazolate frameworks (ZIF-8): efficient and stable catalysts for cycloadditions and condensation reactions.* Catalysis Science & Technology, 2015. **5**(3): p. 1829-1839.
161. Xie, L., et al., *Mixed-Valence Iron(II, III) Trimesates with Open Frameworks Modulated by Solvents.* Inorganic Chemistry, 2007. **46**(19): p. 7782-7788.
162. An, J. and N.L. Rosi, *Tuning MOF CO2 Adsorption Properties via Cation Exchange.* Journal of the American Chemical Society, 2010. **132**(16): p. 5578-5579.
163. Lin, Y., C. Kong, and L. Chen, *Amine-functionalized metal–organic frameworks: structure, synthesis and applications.* RSC Advances, 2016. **6**(39): p. 32598-32614.
164. Bernt, S., et al., *Direct covalent post-synthetic chemical modification of Cr-MIL-101 using nitrating acid.* Chemical Communications, 2011. **47**(10): p. 2838-2840.
165. Pal, T.K., et al., *Significant Gas Adsorption and Catalytic Performance by a Robust CuII–MOF Derived through Single-Crystal to Single-Crystal Transmetalation of a Thermally Less-Stable ZnII–MOF.* Chemistry – A European Journal, 2015. **21**(52): p. 19064-19070.
166. Kozachuk, O., et al., *A Solid-Solution Approach to Mixed-Metal Metal–Organic Frameworks – Detailed Characterization of Local Structures, Defects and Breathing Behaviour of Al/V Frameworks (Eur. J. Inorg. Chem. 26/2013).* European Journal of Inorganic Chemistry, 2013. **2013**(26).
167. Mondloch, J.E., et al., *Activation of metal–organic framework materials.* CrystEngComm, 2013. **15**(45): p. 9258-9264.
168. Bae, Y.-S., et al., *Strategies for characterization of large-pore metal-organic frameworks by combined experimental and computational methods.* Chemistry of Materials, 2009. **21**(20): p. 4768-4777.
169. Ahnfeldt, T., et al., *Synthesis and Modification of a Functionalized 3D Open-Framework Structure with MIL-53 Topology.* Inorganic Chemistry, 2009. **48**(7): p. 3057-3064.
170. Easteal, A.J. and L.A. Woolf, *Solute–solvent interaction effects on tracer diffusion coefficients.* Journal of the Chemical Society, Faraday Transactions 1: Physical Chemistry in Condensed Phases, 1984. **80**(5): p. 1287-1295.
171. Abid, H.R., et al., *Synthesis, characterization, and CO2 adsorption of three metal-organic frameworks (MOFs).* Polyhedron, 2016. **120**: p. 103-111.
172. Nelson, A.P., et al., *Supercritical Processing as a Route to High Internal Surface Areas and Permanent Microporosity in Metal−Organic Framework Materials.* Journal of the American Chemical Society, 2009. **131**(2): p. 458-460.
173. Ma, L., et al., *Freeze Drying Significantly Increases Permanent Porosity and Hydrogen Uptake in 4,4-Connected Metal–Organic Frameworks.* Angewandte Chemie International Edition, 2009. **48**(52): p. 9905-9908.

174. Lohe, M.R., M. Rose, and S. Kaskel, *Metal–organic framework (MOF) aerogels with high micro- and macroporosity.* Chemical Communications, 2009(40): p. 6056-6058.
175. Espín, J., et al., *The photothermal effect in MOFs: covalent post-synthetic modification of MOFs mediated by UV-Vis light under solvent-free conditions.* Chemical Communications, 2018. **54**(33): p. 4184-4187.
176. Espín, J., et al., *Photothermal Activation of Metal–Organic Frameworks Using a UV–Vis Light Source.* ACS Applied Materials & Interfaces, 2018. **10**(11): p. 9555-9562.
177. Lee, S.J., et al., *Multicomponent Metal–Organic Frameworks as Defect-Tolerant Materials.* Chemistry of Materials, 2016. **28**(1): p. 368-375.
178. Ming, Y., N. Kumar, and D.J. Siegel, *Water Adsorption and Insertion in MOF-5.* ACS Omega, 2017. **2**(8): p. 4921-4928.
179. Bellarosa, L., et al., *How ligands improve the hydrothermal stability and affect the adsorption in the IRMOF family.* Physical Chemistry Chemical Physics, 2013. **15**(40): p. 17696-17704.
180. Schoenecker, P.M., et al., *Effect of Water Adsorption on Retention of Structure and Surface Area of Metal–Organic Frameworks.* Industrial & Engineering Chemistry Research, 2012. **51**(18): p. 6513-6519.
181. Tan, K., et al., *Water interactions in metal organic frameworks.* CrystEngComm, 2015. **17**(2): p. 247-260.
182. Tan, K., et al., *Stability and hydrolyzation of metal organic frameworks with paddle-wheel SBUs upon hydration.* Chemistry of Materials, 2012. **24**(16): p. 3153-3167.
183. Wang, C., et al., *Applications of water stable metal–organic frameworks.* Chemical Society Reviews, 2016. **45**(18): p. 5107-5134.
184. Qadir, N.u., S.A.M. Said, and H.M. Bahaidarah, *Structural stability of metal organic frameworks in aqueous media – Controlling factors and methods to improve hydrostability and hydrothermal cyclic stability.* Microporous and Mesoporous Materials, 2015. **201**: p. 61-90.
185. Chen, Y.-R., et al., *Investigation of the Water Adsorption Properties and Structural Stability of MIL-100(Fe) with Different Anions.* Langmuir, 2018. **34**(14): p. 4180-4187.
186. Zang, Y., et al., *Highly stable chromium(III) terephthalate metal organic framework (MIL-101) encapsulated 12-tungstophosphoric heteropolyacid as a water-tolerant solid catalyst for hydrolysis and esterification.* Reaction Kinetics, Mechanisms and Catalysis, 2013. **109**(1): p. 77-89.
187. Abid, H.R., et al., *Nanosize Zr-metal organic framework (UiO-66) for hydrogen and carbon dioxide storage.* Chemical Engineering Journal, 2012. **187**: p. 415-420.
188. Wang, K., et al., *Pyrazolate-Based Porphyrinic Metal–Organic Framework with Extraordinary Base-Resistance.* Journal of the American Chemical Society, 2016. **138**(3): p. 914-919.
189. Ghosh, P., Y.J. Colón, and R.Q. Snurr, *Water adsorption in UiO-66: the importance of defects.* Chemical Communications, 2014. **50**(77): p. 11329-11331.
190. Banerjee, R., et al., *High-Throughput Synthesis of Zeolitic Imidazolate Frameworks and Application to CO₂ Capture.* Science, 2008. **319**(5865): p. 939-943.

191. He, M., et al., *Facile synthesis of zeolitic imidazolate framework-8 from a concentrated aqueous solution.* Microporous and Mesoporous Materials, 2014. **184**: p. 55-60.
192. Bosch, M., M. Zhang, and H.-C. Zhou, *Increasing the Stability of Metal-Organic Frameworks.* Advances in Chemistry, 2014. **2014**: p. 8.
193. Yang, J., et al., *Methyl modified MOF-5: a water stable hydrogen storage material.* Chemical Communications, 2011. **47**(18): p. 5244-5246.
194. Nguyen, J.G. and S.M. Cohen, *Moisture-Resistant and Superhydrophobic Metal−Organic Frameworks Obtained via Postsynthetic Modification.* Journal of the American Chemical Society, 2010. **132**(13): p. 4560-4561.
195. Jasuja, H., Y.-g. Huang, and K.S. Walton, *Adjusting the Stability of Metal–Organic Frameworks under Humid Conditions by Ligand Functionalization.* Langmuir, 2012. **28**(49): p. 16874-16880.
196. Yuan, J., et al., *Superwetting nanowire membranes for selective absorption.* Nature Nanotechnology, 2008. **3**: p. 332.
197. Yang, S.J. and C.R. Park, *Preparation of Highly Moisture-Resistant Black-Colored Metal Organic Frameworks.* Advanced Materials, 2012. **24**(29): p. 4010-4013.
198. Zhang, W., et al., *A facile and general coating approach to moisture/water-resistant metal–organic frameworks with intact porosity.* Journal of the American Chemical Society, 2014. **136**(49): p. 16978-16981.
199. Yang, S.J., et al., *Preparation and Enhanced Hydrostability and Hydrogen Storage Capacity of CNT@MOF-5 Hybrid Composite.* Chemistry of Materials, 2009. **21**(9): p. 1893-1897.
200. Li, H., et al., *Enhanced Hydrostability in Ni-Doped MOF-5.* Inorganic Chemistry, 2012. **51**(17): p. 9200-9207.
201. Feng, D., et al., *Zirconium-Metalloporphyrin PCN-222: Mesoporous Metal–Organic Frameworks with Ultrahigh Stability as Biomimetic Catalysts.* Angewandte Chemie International Edition, 2012. **51**(41): p. 10307-10310.
202. Furukawa, H., et al., *Water adsorption in porous metal–organic frameworks and related materials.* Journal of the American Chemical Society, 2014. **136**(11): p. 4369-4381.
203. Malik, P.K., *Dye removal from wastewater using activated carbon developed from sawdust: adsorption equilibrium and kinetics.* Journal of Hazardous Materials, 2004. **113**(1): p. 81-88.
204. Wawrzkiewicz, M., et al., *Adsorptive removal of acid, reactive and direct dyes from aqueous solutions and wastewater using mixed silica–alumina oxide.* Powder Technology, 2015. **278**: p. 306-315.
205. Wang, C., et al., *Adsorption of Dye from Wastewater by Zeolites Synthesized from Fly Ash: Kinetic and Equilibrium Studies.* Chinese Journal of Chemical Engineering, 2009. **17**(3): p. 513-521.
206. Mohammadi, A.A., et al., *Metal-organic framework Uio-66 for adsorption of methylene blue dye from aqueous solutions.* International Journal of Environmental Science and Technology, 2017. **14**(9): p. 1959-1968.
207. Lv, G., et al., *Selectivity adsorptive mechanism of different nitrophenols on UiO-66 and UiO-66-NH2 in aqueous solution.* Journal of Chemical & Engineering Data, 2016. **61**(11): p. 3868-3876.
208. Azhar, M.R., et al., *Adsorptive removal of antibiotic sulfonamide by UiO-66 and ZIF-67 for wastewater treatment.* Journal of colloid and interface science, 2017. **500**: p. 88-95.

209. Haque, E., et al., *Adsorptive removal of methyl orange from aqueous solution with metal-organic frameworks, porous chromium-benzenedicarboxylates.* Journal of Hazardous Materials, 2010. **181**(1): p. 535-542.
210. Mahmood, A., et al., *Hierarchical heteroaggregation of binary metal-organic gels with tunable porosity and mixed valence metal sites for removal of dyes in water.* Scientific reports, 2015. **5**: p. 10556.
211. Haque, E., J.W. Jun, and S.H. Jhung, *Adsorptive removal of methyl orange and methylene blue from aqueous solution with a metal-organic framework material, iron terephthalate (MOF-235).* Journal of Hazardous Materials, 2011. **185**(1): p. 507-511.
212. Hasan, Z. and S.H. Jhung, *Removal of hazardous organics from water using metal-organic frameworks (MOFs): plausible mechanisms for selective adsorptions.* Journal of Hazardous Materials, 2015. **283**: p. 329-339.
213. Hameed, B.H. and A.A. Ahmad, *Batch adsorption of methylene blue from aqueous solution by garlic peel, an agricultural waste biomass.* Journal of Hazardous Materials, 2009. **164**(2): p. 870-875.
214. Lin, S., et al., *Adsorption behavior of metal–organic frameworks for methylene blue from aqueous solution.* Microporous and Mesoporous Materials, 2014. **193**: p. 27-34.
215. Akiyama, G., et al., *Cellulose Hydrolysis by a New Porous Coordination Polymer Decorated with Sulfonic Acid Functional Groups.* Advanced Materials, 2011. **23**(29): p. 3294-3297.
216. Zhao, X., et al., *Reversing the Dye Adsorption and Separation Performance of Metal–Organic Frameworks via Introduction of −SO3H Groups.* Industrial & Engineering Chemistry Research, 2017. **56**(15): p. 4496-4501.
217. Jiang, C., et al., *Efficient adsorptive removal of Congo red from aqueous solution by synthesized zeolitic imidazolate framework-8.* Chemical Speciation & Bioavailability, 2016. **28**(1-4): p. 199-208.
218. Ezugwu, C.I., et al., *Cationic nickel metal-organic frameworks for adsorption of negatively charged dye molecules.* Data in Brief, 2018. **18**: p. 1952-1961.
219. Li, H., et al., *Enhanced adsorptive removal of anionic and cationic dyes from single or mixed dye solutions using MOF PCN-222.* RSC Advances, 2017. **7**(27): p. 16273-16281.
220. Zhang, K.-D., et al., *Adsorption Behavior of High Stable Zr-Based MOFs for the Removal of Acid Organic Dye from Water.* Materials, 2017. **10**(2).
221. Molavi, H., et al., *Selective dye adsorption by highly water stable metal-organic framework: Long term stability analysis in aqueous media.* Applied Surface Science, 2018. **445**: p. 424-436.
222. Embaby, M.S., et al., *The adsorptive properties of UiO-66 towards organic dyes: A record adsorption capacity for the anionic dye Alizarin Red S.* Chinese Journal of Chemical Engineering, 2018. **26**(4): p. 731-739.
223. Chen, Q., et al., *Selective adsorption of cationic dyes by UiO-66-NH2.* Applied Surface Science, 2015. **327**: p. 77-85.
224. Yang, J.-M., *A facile approach to fabricate an immobilized-phosphate zirconium-based metal-organic framework composite (UiO-66-P) and its activity in the adsorption and separation of organic dyes.* Journal of Colloid and Interface Science, 2017. **505**: p. 178-185.
225. Qiu, J., et al., *Acid-promoted synthesis of UiO-66 for highly selective adsorption of anionic dyes: Adsorption performance and mechanisms.* Journal of Colloid and Interface Science, 2017. **499**: p. 151-158.

226. Yang, J.-M., et al., *Adsorptive removal of organic dyes from aqueous solution by a Zr-based metal–organic framework: effects of Ce(iii) doping.* Dalton Transactions, 2018. **47**(11): p. 3913-3920.
227. Azhar, M.R., et al., *One-pot synthesis of binary metal organic frameworks (HKUST-1 and UiO-66) for enhanced adsorptive removal of water contaminants.* Journal of Colloid and Interface Science, 2017. **490**: p. 685-694.
228. Ameloot, R., et al., *Direct patterning of oriented metal–organic framework crystals via control over crystallization kinetics in clear precursor solutions.* Advanced materials, 2010. **22**(24): p. 2685-2688.
229. Tranchemontagne, D.J., J.R. Hunt, and O.M. Yaghi, *Room temperature synthesis of metal-organic frameworks: MOF-5, MOF-74, MOF-177, MOF-199, and IRMOF-0.* Tetrahedron, 2008. **64**(36): p. 8553-8557.
230. Zou, R.-Q., et al., *Rational assembly of a 3D metal–organic framework for gas adsorption with predesigned cubic building blocks and 1D open channels.* Chemical communications, 2005(28): p. 3526-3528.
231. Wang, G.-H., et al., *Metal–organic frameworks based on the pyridine-2, 3-dicarboxylate and a flexible bispyridyl ligand: syntheses, structures, and photoluminescence.* CrystEngComm, 2009. **11**(2): p. 292-297.
232. Michaelides, A. and S. Skoulika, *Reactive microporous rare-earth coordination polymers that exhibit single-crystal-to-single-crystal dehydration and rehydration.* Crystal growth & design, 2005. **5**(2): p. 529-533.
233. Murinzi, T., E. Hosten, and G. Watkins, *Synthesis and characterization of a cobalt-2, 6-pyridinedicarboxylate MOF with potential application in electrochemical sensing.* Polyhedron, 2017. **137**: p. 188-196.
234. Alfonso-Herrera, L.A., et al., *M-008: A stable and reusable metalorganic framework with high crystallinity applied in the photocatalytic hydrogen evolution and the degradation of methyl orange.* Journal of Photochemistry and Photobiology A: Chemistry, 2020. **389**: p. 112240.
235. Liu, J., F. Wang, and J. Zhang, *Synthesis, structure and luminescent of Ag based homochiral metal tetrazolate coordination polymers.* Inorganic Chemistry Communications, 2018. **89**: p. 41-45.
236. Muesmann, T.W., et al., *Synthesis of 1, 2, 4, 5-Benzenetetrasulfonic Acid (H4B4S) and its Implementation as a Linker for Building Metal-Organic Frameworks on the Example of [Cu2 (B4S)(H2O) 8]· 0.5 H2O.* Zeitschrift für anorganische und allgemeine Chemie, 2010. **636**(7): p. 1307-1312.
237. Schlesinger, M., et al., *Evaluation of synthetic methods for microporous metal–organic frameworks exemplified by the competitive formation of [Cu2 (btc) 3 (H2O) 3] and [Cu2 (btc)(OH)(H2O)].* Microporous and Mesoporous Materials, 2010. **132**(1-2): p. 121-127.
238. Hausdorf, S., et al., *Gaseous species as reaction tracers in the solvothermal synthesis of the zinc oxide terephthalate MOF-5.* The Journal of Physical Chemistry A, 2007. **111**(20): p. 4259-4266.
239. Stewart, L., et al., *A zirconium metal–organic framework with an exceptionally high volumetric surface area.* Dalton Transactions, 2017. **46**(41): p. 14270-14276.
240. Meng, Q., et al., *A porous cobalt (II) metal–organic framework with highly efficient electrocatalytic activity for the oxygen evolution reaction.* Polymers, 2017. **9**(12): p. 676.

241. Han, Z.-B., et al., *Mn (II)-based porous metal–organic framework showing metamagnetic properties and high hydrogen adsorption at low pressure.* Inorganic Chemistry, 2012. **51**(1): p. 674-679.
242. Dan-Hardi, M., et al., *A new photoactive crystalline highly porous titanium (IV) dicarboxylate.* Journal of the American Chemical Society, 2009. **131**(31): p. 10857-10859.
243. Li, Z., et al., *Ammonia borane confined by a metal− organic framework for chemical hydrogen storage: enhancing kinetics and eliminating ammonia.* Journal of the American Chemical Society, 2010. **132**(5): p. 1490-1491.
244. Loiseau, T., et al., *MIL-96, a porous aluminum trimesate 3D structure constructed from a hexagonal network of 18-membered rings and μ 3-oxo-centered trinuclear units.* Journal of the American Chemical Society, 2006. **128**(31): p. 10223-10230.
245. Zhou, X.-H., et al., *A flexible Eu (III)-based metal–organic framework: turn-off luminescent sensor for the detection of Fe (III) and picric acid.* Dalton Transactions, 2013. **42**(34): p. 12403-12409.
246. Dietzel, P.D., et al., *Hydrogen adsorption in a nickel based coordination polymer with open metal sites in the cylindrical cavities of the desolvated framework.* Chemical Communications, 2006(9): p. 959-961.
247. Bhattacharjee, S., et al., *Solvothermal synthesis of Fe-MOF-74 and its catalytic properties in phenol hydroxylation.* Journal of nanoscience and nanotechnology, 2010. **10**(1): p. 135-141.
248. Xue, M., et al., *Solvothermal synthesis, structure and magnetism of two novel 3D metal-organic frameworks based on infinite helical Mn–O–C rod-shaped building units.* Journal of molecular structure, 2006. **796**(1-3): p. 165-171.
249. Xu, B., et al., *Solvothermal synthesis of luminescent Eu (BTC)(H 2 O) DMF hierarchical architectures.* CrystEngComm, 2012. **14**(8): p. 2914-2919.
250. Miller, S.R., et al., *A rare example of a porous Ca-MOF for the controlled release of biologically active NO.* Chemical Communications, 2013. **49**(71): p. 7773-7775.
251. Campbell, J. and B. Tokay, *Controlling the size and shape of Mg-MOF-74 crystals to optimise film synthesis on alumina substrates.* Microporous and Mesoporous Materials, 2017. **251**: p. 190-199.
252. Yang, H., et al., *Electrochemical synthesis of flower shaped morphology MOFs in an ionic liquid system and their electrocatalytic application to the hydrogen evolution reaction.* RSC Advances, 2014. **4**(30): p. 15720-15726.
253. Zhang, T., et al., *Rapid synthesis of UiO-66 by means of electrochemical cathode method with electrochemical detection of 2, 4, 6-TCP.* Inorganic Chemistry Communications, 2020. **111**: p. 107671.
254. Martinez Joaristi, A., et al., *Electrochemical Synthesis of Some Archetypical Zn2+, Cu2+, and Al3+ Metal Organic Frameworks.* Crystal Growth & Design, 2012. **12**(7): p. 3489-3498.
255. Campagnol, N., et al., *High pressure, high temperature electrochemical synthesis of metal–organic frameworks: films of MIL-100 (Fe) and HKUST-1 in different morphologies.* Journal of Materials Chemistry A, 2013. **1**(19): p. 5827-5830.
256. Khazalpour, S., et al., *Electrochemical synthesis of pillared layer mixed ligand metal–organic framework: DMOF-1–Zn.* RSC Advances, 2015. **5**(46): p. 36547-36551.

257. Yang, H.-m., et al., *In situ electrochemical synthesis of MOF-5 and its application in improving photocatalytic activity of BiOBr.* Transactions of Nonferrous Metals Society of China, 2015. **25**(12): p. 3987-3994.
258. Antonio, A.M., J. Rosenthal, and E.D. Bloch, *Electrochemically Mediated Syntheses of Titanium (III)-Based Metal–Organic Frameworks.* Journal of the American Chemical Society, 2019. **141**(29): p. 11383-11387.
259. Ameloot, R., et al., *Patterned growth of metal-organic framework coatings by electrochemical synthesis.* Chemistry of Materials, 2009. **21**(13): p. 2580-2582.
260. Jabarian, S. and A. Ghaffarinejad, *Electrochemical Synthesis of NiBTC Metal Organic Framework Thin Layer on Nickel Foam: An Efficient Electrocatalyst for the Hydrogen Evolution Reaction.* Journal of Inorganic and Organometallic Polymers and Materials, 2019. **29**(5): p. 1565-1574.
261. Wei, J.-Z., et al., *Rapid and low-cost electrochemical synthesis of UiO-66-NH2 with enhanced fluorescence detection performance.* Inorganic chemistry, 2019. **58**(10): p. 6742-6747.
262. Li, Z.-Q., et al., *Ultrasonic synthesis of the microporous metal–organic framework Cu3 (BTC) 2 at ambient temperature and pressure: an efficient and environmentally friendly method.* Materials Letters, 2009. **63**(1): p. 78-80.
263. Son, W.-J., et al., *Sonochemical synthesis of MOF-5.* Chemical Communications, 2008(47): p. 6336-6338.
264. Haque, E., et al., *Synthesis of a metal–organic framework material, iron terephthalate, by ultrasound, microwave, and conventional electric heating: a kinetic study.* Chemistry–A European Journal, 2010. **16**(3): p. 1046-1052.
265. Stawowy, M., et al., *The impact of synthesis method on the properties and CO2 sorption capacity of UiO-66 (Ce).* Catalysts, 2019. **9**(4): p. 309.
266. Tahmasian, A., A. Morsali, and S.W. Joo, *Sonochemical syntheses of a one-dimensional Mg (II) metal-organic framework: a new precursor for preparation of MgO one-dimensional nanostructure.* Journal of Nanomaterials, 2013. **2013**.
267. Israr, F., et al., *High yield synthesis of Ni-BTC metal–organic framework with ultrasonic irradiation: role of polar aprotic DMF solvent.* Ultrasonics sonochemistry, 2016. **31**: p. 93-101.
268. Gordon, J., H. Kazemian, and S. Rohani, *Rapid and efficient crystallization of MIL-53 (Fe) by ultrasound and microwave irradiation.* Microporous and mesoporous materials, 2012. **162**: p. 36-43.
269. Masoomi, M.Y. and A. Morsali, *Sonochemical synthesis of nanoplates of two Cd (II) based metal–organic frameworks and their applications as precursors for preparation of nano-materials.* Ultrasonics sonochemistry, 2016. **28**: p. 240-249.
270. Tao, C.-a., et al., *Sonochemical synthesis of photoluminescent nanoscale Eu (III)-containing metal-organic frameworks.* Materials Science, 2015. **21**(4): p. 554-558.
271. Xiao, J.-D., et al., *Rapid synthesis of nanoscale terbium-based metal–organic frameworks by a combined ultrasound-vapour phase diffusion method for highly selective sensing of picric acid.* Journal of Materials Chemistry A, 2013. **1**(31): p. 8745-8752.

272. Jhung, S.-H., J.-H. Lee, and J.-S. Chang, *Microwave synthesis of a nanoporous hybrid material, chromium trimesate.* Bulletin of the Korean Chemical Society, 2005. **26**(6): p. 880-881.
273. Arenas-Vivo, A., D. Avila, and P. Horcajada, *Phase-Selective Microwave Assisted Synthesis of Iron (III) Aminoterephthalate MOFs.* Materials, 2020. **13**(6): p. 1469.
.274 Choi, J.-S., et al., *Metal–organic framework MOF-5 prepared by microwave heating: Factors to be considered.* Microporous and Mesoporous Materials, 2008. **116**(1-3): p. 727-731.
275. Seo, Y.-K., et al., *Microwave synthesis of hybrid inorganic–organic materials including porous Cu3 (BTC) 2 from Cu (II)-trimesate mixture.* Microporous and Mesoporous Materials, 2009. **119**(1-3): p. 331-337.
276. Wu, X., et al., *Microwave synthesis and characterization of MOF-74 (M= Ni, Mg) for gas separation.* Microporous and mesoporous materials, 2013. **180**: p. 114-122.
277. Chen, C., et al., *Microwave-assisted rapid synthesis of well-shaped MOF-74 (Ni) for CO2 efficient capture.* Inorganic chemistry, 2019. **58**(4): p. 2717-2728.
278. Skoda, D., et al., *Microwave-assisted synthesis of platelet-like cobalt metal-organic framework, its transformation to porous layered cobalt-carbon nanocomposite discs and their utilization as anode materials in sodium-ion batteries.* Journal of Energy Storage, 2020. **27**: p. 101113.
279. Dang, Y.T., et al., *Microwave-assisted synthesis of nano Hf-and Zr-based metal-organic frameworks for enhancement of curcumin adsorption.* Microporous and Mesoporous Materials, 2020. **298**: p. 110064.
280. Vakili, R., et al., *Microwave-assisted synthesis of zirconium-based metal organic frameworks (MOFs): Optimization and gas adsorption.* Microporous and Mesoporous Materials, 2018. **260**: p. 45-53.
281. Carné-Sánchez, A., et al., *A spray-drying strategy for synthesis of nanoscale metal–organic frameworks and their assembly into hollow superstructures.* Nature Chemistry, 2013. **5**(3): p. 203-211.
282. Avci-Camur, C., et al., *Aqueous production of spherical Zr-MOF beads via continuous-flow spray-drying.* Green chemistry, 2018. **20**(4): p. 873-878.
283. Garzón-Tovar, L., et al., *A spray-drying continuous-flow method for simultaneous synthesis and shaping of microspherical high nuclearity MOF beads.* Reaction Chemistry & Engineering, 2016. **1**(5): p. 533-539.
284. Guillerm, V., et al., *Continuous One-Step Synthesis of Porous M-XF 6-Based Metal-Organic and Hydrogen-Bonded Frameworks.* 2017.
285. Tanaka, S. and R. Miyashita, *Aqueous-System-Enabled Spray-Drying Technique for the Synthesis of Hollow Polycrystalline ZIF-8 MOF Particles.* ACS omega, 2017. **2**(10): p. 6437-6445.
286. Chaemchuen, S., et al., *Spray drying of zeolitic imidazolate frameworks: investigation of crystal formation and properties.* CrystEngComm, 2018. **20**(25): p. 3601-3608.
287. Gimeno-Fabra, M., et al., *Instant MOFs: continuous synthesis of metal–organic frameworks by rapid solvent mixing.* Chemical Communications, 2012. **48**(86): p. 10642-10644.
288. Bayliss, P.A., et al., *Synthesis of metal–organic frameworks by continuous flow.* Green Chemistry, 2014. **16**(8): p. 3796-3802.

289. Faustini, M., et al., *Microfluidic approach toward continuous and ultrafast synthesis of metal–organic framework crystals and hetero structures in confined microdroplets.* Journal of the American Chemical Society, 2013. **135**(39): p. 14619-14626.
290. Waitschat, S., M.T. Wharmby, and N. Stock, *Flow-synthesis of carboxylate and phosphonate based metal–organic frameworks under non-solvothermal reaction conditions.* Dalton Transactions, 2015. **44**(24): p. 11235-11240.
291. Albuquerque, G.H., et al., *Gas–liquid segmented flow microwave-assisted synthesis of MOF-74 (Ni) under moderate pressures.* CrystEngComm, 2015. **17**(29): p. 5502-5510.
292. d'Arras, L., et al., *Fast and continuous processing of a new sub-micronic lanthanide-based metal–organic framework.* New Journal of Chemistry, 2014. **38**(4): p. 1477-1483.
293. Paseta, L., et al., *Accelerating the controlled synthesis of metal–organic frameworks by a microfluidic approach: a nanoliter continuous reactor.* ACS applied materials & interfaces, 2013. **5**(19): p. 9405-9410.
294. Didriksen, T., A.I. Spjelkavik, and R. Blom, *Continuous synthesis of the metal—organic framework CPO-27-Ni from aqueous solutions.* Journal of Flow Chemistry, 2017.
295. Zhang, Z.-H., L. Xu, and H. Jiao, *Ionothermal synthesis, structures, properties of cobalt-1, 4-benzenedicarboxylate metal–organic frameworks.* Journal of Solid State Chemistry, 2016. **238**: p. 217-222.
296. Xu, L., E.-Y. Choi, and Y.-U. Kwon, *Ionothermal synthesis of a 3D Zn–BTC metal-organic framework with distorted tetranuclear [Zn4 (μ4-O)] subunits.* Inorganic Chemistry Communications, 2008. **11**(10): p. 1190-1193.
297. Xu, L., et al., *Novel Mn (II)-Based Metal–Organic Frameworks Isolated in Ionic Liquids.* Crystal growth & design, 2013. **13**(3): p. 1260-1266.
298. Liao, J.-H. and W.-C. Huang, *Ionic liquid as reaction medium for the synthesis and crystallization of a metal-organic framework:(BMIM) 2 [Cd3 (BDC) 3Br2](BMIM= 1-butyl-3-methylimidazolium, BDC= 1, 4-benzenedicarboxylate).* Inorganic Chemistry Communications, 2006. **9**(12): p. 1227-1231.
299. Zhang, Z.-H., et al., *Combination effect of ionic liquid components on the structure and properties in 1, 4-benzenedicarboxylate based zinc metal–organic frameworks.* Dalton Transactions, 2015. **44**(41): p. 17980-17989.
300. Wu, Z.-F., et al., *Ionothermal synthesis of a metal-organic framework constructed by magnesium (II) and 4, 4'-oxybis (benzoic acid) ligand.* Inorganic Chemistry Communications, 2012. **24**: p. 166-169.
301. Zhang, J., S. Chen, and X. Bu, *Multiple Functions of Ionic Liquids in the Synthesis of Three-Dimensional Low-Connectivity Homochiral and Achiral Frameworks.* Angewandte Chemie, 2008. **120**(29): p. 5514-5517.
302. Jin, K., et al., *[Cu (i)(bpp)] BF 4: the first extended coordination network prepared solvothermally in an ionic liquid solvent.* Chemical communications, 2002(23): p. 2872-2873.
303. Lin, Z., A.M. Slawin, and R.E. Morris, *Chiral induction in the ionothermal synthesis of a 3-D coordination polymer.* Journal of the American Chemical Society, 2007. **129**(16): p. 4880-4881.
304. Cao, H.-Y., et al., *Ionothermal syntheses, crystal structures and luminescence of three three-dimensional lanthanide-1, 4-benzenedicarboxylate frameworks.* Inorganica Chimica Acta, 2014. **414**: p. 226-233.

305. Klimakow, M., et al., *Mechanochemical synthesis of metal− organic frameworks: a fast and facile approach toward quantitative yields and high specific surface areas.* Chemistry of Materials, 2010. **22**(18): p. 5216-5221.
306. Julien, P.A., et al., *In situ monitoring and mechanism of the mechanochemical formation of a microporous MOF-74 framework.* Journal of the American Chemical Society, 2016. **138**(9): p. 2929-2932.
307. Guo, Z., et al., *Air-Flow Impacting Synthesis of Metal Organic Frameworks: A Continuous, Highly Efficient, Large-Scale Mechanochemical Synthetic Method.* ACS Sustainable Chemistry & Engineering, 2020. **8**(10): p. 4037-4043.
308. Huang, Y.-H., et al., *Green and rapid synthesis of zirconium metal–organic frameworks via mechanochemistry: UiO-66 analog nanocrystals obtained in one hundred seconds.* Chemical Communications, 2017. **53**(43): p. 5818-5821.
309. Zhang, R., et al., *Ultrafast synthesis of Ni-MOF in one minute by ball milling.* Nanomaterials, 2018. **8**(12): p. 1067.
310. Chen, Y., et al., *Highly efficient mechanochemical synthesis of an indium based metal-organic framework with excellent water stability.* Chemical Engineering Science, 2017. **158**: p. 539-544.
311. Singh, N.K., M. Hardi, and V.P. Balema, *Mechanochemical synthesis of an yttrium based metal–organic framework.* Chemical Communications, 2013. **49**(10): p. 972-974.
312. Pilloni, M., et al., *Liquid-assisted mechanochemical synthesis of an iron carboxylate Metal Organic Framework and its evaluation in diesel fuel desulfurization.* Microporous and Mesoporous Materials, 2015. **213**: p. 14-21.
313. Leng, K., et al., *Rapid synthesis of metal–organic frameworks MIL-101 (Cr) without the addition of solvent and hydrofluoric acid.* Crystal Growth & Design, 2016. **16**(3): p. 1168-1171.

Chapter 3

Adsorptive study of removing harmful dye (methyl orange) by NH_4 modified Zr-MOF, Ce-modified Zr-MOF and Ca-modified Zr-MOF

3

Chapter 3: Adsorptive study of removing harmful dye (methyl orange) by NH_4 modified Zr-MOF, Ce-modified Zr-MOF and Ca-modified Zr-MOF

3.1 Abstract

In this study, three improved versions of UiO-66 were successfully synthesised. UiO-66-NH_4, UiO-66-Ca and UiO-66-Ce were characterised to confirm their structural integrity, the stability of the functional groups on the surface and their thermal stability. Activated samples were used to remove harmful anionic dye (methyl orange [MO]) from wastewater. A batch adsorption process was employed to investigate the relative efficiency with which these metal organic frameworks (MOFs) removed MO from aqueous solution. Based on the results, UiO-66-Ce exhibited the highest uptake of 71.5 mg/g, while the adsorption capacity of UiO-66-NH_4 and UiO-66-Ca were 62.5 mg/g and 50.25 mg/g, respectively. Langmuir and Freundlich isotherms were employed to simulate the experimental data. In addition, pseudo first-order and pseudo second-order equations were used to describe the adsorption mechanism. The results presented here may facilitate and enhance further improvements in UiO-66 MOF and more generally, in the synthesis of bimetal MOFs in future research.

3.2 Introduction

Lately, significant volumes of coloured wastewater are created by a wide variety of industries, including textile, leather, paper, printing, dyestuff and plastic industries [1]. Based on the high impacts of colour on the quality of water, the removal of dyestuff from polluted water is becoming a very important issue [1]. In addition, the high visibility of dye means that even a small amount of it is undesirable. Moreover, many dyes are toxic and even carcinogenic [1-3].

Given its stability in light and oxidation reactions, nondegradable synthetic dyes are one of many challenges for environmentalists [3]. Physical, chemical and biological methods have been applied to the remediation of dyes in aqueous solution [1, 3, 4]. Among the range of proposed methods, one of the most feasible is adsorptive removal due to its high efficiency, economics, simplicity of design and its operation [3, 4].

Methyl orange (MO) is classified as a common acidic (anionic) dye used widely in many industries, including textile, printing, paper, food, pharmaceutical industries, as well as in wood, silk and research laboratories [2, 4, 5]. The toxicity of MO has drawn research interest to the removal of this synthetic [2-4]. According to the above explanation, MO was chosen for examination in the present study because it is a typical acidic dye. To remove such a cationic dye, many solid materials have been tested as adsorbents to decolour contaminated wastewater, such as activated carbon [6-14], graphene oxide [15], layered double hydroxide (LDH)[16], waste materials (industrial by-products)[2, 17-23], zeolite [24], waste materials (raw agricultural by-products)[25-37], natural inorganic materials [38-45], natural organic materials [46-50].

Metal organic frameworks (MOFs) (hybrid materials) are a class of extended structure crystalline solid porous materials that have been used widely in many applications [51-58]. They can be constructed from inorganic vertices containing metal and organic linkers with tuneable pore size, at meso-, micro- and ultra-microporous [59-62] scales by altering the connectivity [51-53, 63]. The characteristics of MOFs, including its structural and functional tunability, have led to explosive growth in research in recent decades [64]. Due to their exceptional properties, MOFs have been used in a wide range of applications, including gas and vapour storage, molecular separations, chemical catalysis, chemical sensing, ion exchange, drug deliveries (18-20) and hazardous materials [54-57, 62, 65-75].

Recently in the realm of advanced porous materials, the role of MOFs as adsorbents in adsorptive separations or purifications has attracted much interest [76-79]. MOFs are extensively used in different research fields because of their versatile characteristics [80-82]. They are strong contenders in the search for adsorptive removers of MO form aqueous solutions: for example, the use of MIL-101 MOF has been reported successful in the field of wastewater research [83].

The present study seeks to address a research gap in the literature on the use of MOFs to remove MO in wastewater. It shows the use of modified single and bimetal Zr-MOFs that are water and structurally stable, porous and extended solid material to remediate MO-polluted wastewater. Examination of adsorption of anionic dye (MO) into three kinds of MOFs-named UiO-66-Ce, UiO-66-Ca and UiO-66-NH_4 reveals the

adsorption properties of these MOFs, and the opportunities for their use as sorbents to remove cationic (acidic) dye from wastewater.

3.3 Materials and methods

3.3.1 Synthesis and activation

All chemicals were supplied by Sigma-Aldrich (Australia) without further purifications.

UiO-66-Ce was synthesised under autogenous pressure. An exact amount of terephthalic acid (0.3771 g, 2.27 mmol; Sigma-Aldrich, 98%) was mixed with 31.387 mL of DMF (Sigma-Aldrich, 99%). The mixture was next stirred for 10 min until a clear solution was formed. Following this, $ZrCl_4$ (0.529 g, 2.27 mmol; Sigma-Aldrich, 99%) was added into the solution and stirred for 5 min. $CeN_3O_9.6H_2O$ (0.1971 g; Sigma-Aldrich, 99%) was then added to the reactants and stirred for 15 min. The reactant mixture was loaded into a Teflon-lined autoclave, sealed and placed in a preheated electric oven (120 °C) for 24 h. The white powder of UiO-66-Ce was collected by centrifugation and washed with DMF at least three times. The product was then dried and immersed in absolute methanol (100%; Sigma-Aldrich) for 5 d, then filtered, dried and heated under vacuum at 473 K overnight before being applied as adsorbent.

UiO-66-Ca was synthesised by mixing $ZrCl_4$ (1.5 g, 6.44 mmol) with terephthalic acid (1.3 g, 7.82 mmol) in 70 mL of DMF; after 30 min, $Ca(NO_3)$ (0.675 g, 2.86 mmol), $2.4H_2O$ (99%; Sigma-Aldrich) then 5 mL of deionised water was added into the mixture. Eventually, the mixture was transferred to a Teflon-lined autoclave, where it is tightly sealed and moved into a preheating oven at 405 K. The product was then filtered, dried and immersed in absolute methanol (100%; Sigma-Aldrich) for 5 d, then filtered, dried and heated under vacuum at 473 K overnight before use as adsorbent.

UiO-66-NH_4 was synthesised solvothermally, according to the reported single-solvent method [84]. A solution of 32 mL of DMF was divided equally into two batches. In the first batch, 2.27 mmol of terephthalic acid was added and mixed for 15 min, then NH_4OH (0.4 mL, 2 M) was added dropwise to this mixture. In the second batch, 2.27 mmol of $ZrCl_4$ was mixed into the solvent for approximately 30 min.

Following the above, both batch solutions were mixed for approximately 20 min. Finally, the resulting solution was placed inside a 45 mL polytetrafluoroethylene-lined stainless-steel vessel (Parr Instrument Company) and placed in an oven at 393 K for 24 h. After cooling to room temperature, vacuum filtration was used to separate the white gel-like material, which were dried in an oven at 353 K for 24 h. For activation of the modified UIO-66, a solvent exchange method using chloroform was performed by mixing 100 mg of the sample material in 50 mL of chloroform for 30 min, then soaked for 5 d. The product was subsequently filtered by vacuum filtration and dried in the oven at 373 K for 2h. The final product was heated under vacuum at 473K for 2d.

3.3.2 Characterisation

Thermal stability of UiO-66-Ce, UiO66-Ca and UiO66-NH_4 were assessed by a thermogravimetric analysis (TGA) instrument (Thermogravimetric Analyzer/DSC1 STARe system; Mettler-Toledo, Ohio, US). The samples were loaded into a pan and heated to 1173K at a rate of 5K/min. The air gas flow rate was maintained at 10 mL/min.

FTIR spectra (Spectrum 100 FT-IR spectrometer, PerkinElmer, Waltham, USA) were obtained to check the stability of the functional groups on the organic ligands. The spectra were scanned from 600 to 4000 cm^{-1} with a resolution of 4 cm^{-1} using an attenuated total reflectance technique.

X-ray powder diffraction patterns were obtained with an X-ray diffractometer (D8 Advance, Bruker AXS) using Cu Kα radiation ($\lambda = 1.5406$ Å) with accelerating voltage and current of 40 kV and 40 mA, respectively.

N_2 adsorption/desorption (Autosorb-1, Quantachrome Instruments) was used to determine N_2 isotherms as well as the pore size and surface area of MOFs. The samples were evacuated at 473 K for 24 h prior to adsorption measurements under high vacuum. They were then used to determine the surface area, pore size and pore volume.

3.3.3 Adsorption process

An aqueous stock solution of MO (1000 ppm) was prepared by dissolving MO ($C_{14}H_{14}N_3NaO_3S$, molecular weight 327.3 g.mol^{-1}; Sigma-Aldrich) in deionised water. Aqueous solutions with different concentrations of MO (5–100 ppm) were prepared by successive dilution of the stock solution with water. MO concentrations were determined using an absorbance of 464 for the solutions after obtaining the ultraviolet (UV) spectra of the solution with a spectrophotometer (UV spectrophotometer). The calibration curve was obtained from the spectra of the standard solutions (5–100 ppm).

Prior to adsorption, the adsorbents were dried overnight under vacuum at 373 K. Several glass containers were cleaned, dried and filled to 20 mL with MO of different concentrations, ranging from 10 to 75 ppm. Subsequently, the exact amount of the adsorbent (20 mg) was put in each container.

The dye solutions containing the adsorbents were mixed well by a magnetic stirrer and maintained for 5 min to 24h at 298K. The samples for analysis were collected by syringe filter at different sampling intervals. A UV spectrometer was used to determine the dye concentration in the supernatant.

Dye uptake by Zr-MOF at any time and equilibrium time may be expressed below by Equations 3.1 and 3.2, respectively, and percentage removal of MO is calculated using Equation 3.3 [85] as follows.

$$q_t = (C_0 - C_t)\frac{V}{m} \tag{3.1}$$

$$q_e = (C_0 - C_e)\frac{V}{m} \tag{3.2}$$

$$R\% = \frac{(C_0 - C_t)}{C_0} X100, \tag{3.3}$$

Where:

q_t: the amount of MB adsorbed per unit weight of MOF at any time t (mg/g)

q_e: the amount of MB adsorbed per unit weight of MOF at equilibrium (mg/g)

C_0: initial concentration of the MB solution at time zero (mg/L)

C_t: concentration of MB solution at time t (mg/L)

C_e: concentration of MB solution at equilibrium (mg/L)

V: volume of MB solution in the adsorption batch process (L)

R%: percentage removal of MB

m: Zr-MOF mass used in the adsorption batch process (g).

The adsorption mechanism and rate of diffusion were fitted to two kinetic models, including pseudo first-order and pseudo second-order models [86-89]. Moreover, the sorption of MO by Zr-MOFs was investigated using the Langmuir and Freundlich adsorption isotherm [86-88, 90].

3.4 Results and discussion

3.4.1 Characterisation

Figure 3.1(a) shows the PXRD pattern for the UiO-66 samples before and after use with water, which demonstrates that the structures are the same as those in previously reported studies [84, 91].Furthermore, Figure 3.1(a) compares the XRD pattern of UiO-66-Ca, UiO-66-Ce and UiO-66-NH_4 with that of UiO-66 before and after use in water. The results demonstrate that the integrity of the structure was maintained and excellent water stability in all samples, which indicates that the synthesis and activation procedures succeeded reliably without suspected impurities of a metal oxide inside the pores. The strong crystalline nature of the synthesized MOFs (UiO-66, UiO-66-Ca, UiO-66-Ce and UiO-66-NH_4) is evidently demonstrated from XRD patterns.

In addition, FTIR spectra of the samples in this study are shown in Figure 3.1(b): all functional groups seen on the surface of UiO-66 in previous studies [92] were observed and maintained on the surface of UiO-66-Ca, UiO-66-Ce and UiO-NH_4. Formation of UiO-66 was confirmed by the peak at 1550–1630 cm−1, which refers to coordinated carboxylates with metal centres. However, the stretching variation band of CO bond in free carboxylic acid throughout the region (1640–1670 cm^{-1}) mostly disappeared in all samples; this is positive indication of a successful activation procedure to remove non-reacted carboxylic acid and free solvent from the pores.

Further, the thermal stability (TGA) of these samples was investigated, as demonstrated in Figure 3.1(c). All MOFs samples have three-stage profiles which represent weight loss of the material. The first stage weight loss of TGA graphs is attributed to evaporation of moisture and uncoordinated DMF occurring around 393K

for different samples. While the second stage of the graph occurs at about 570K indicating samples' weight loss is referred to breakdown of uncoordinated BDC and coordinated solvent molecules. On the other hand, the third stage of weight loss occurs at 750K is ascribed to devastation of coordinated BDC and porous structure of parent and modified MOFs. The samples have the same thermal stability as that reported in previous studies [84, 93], and remain stable up to approximately 750K. Therefore the additives which was used to improve Zr-MOF cannot affect the thermal stability of the enhanced materials.

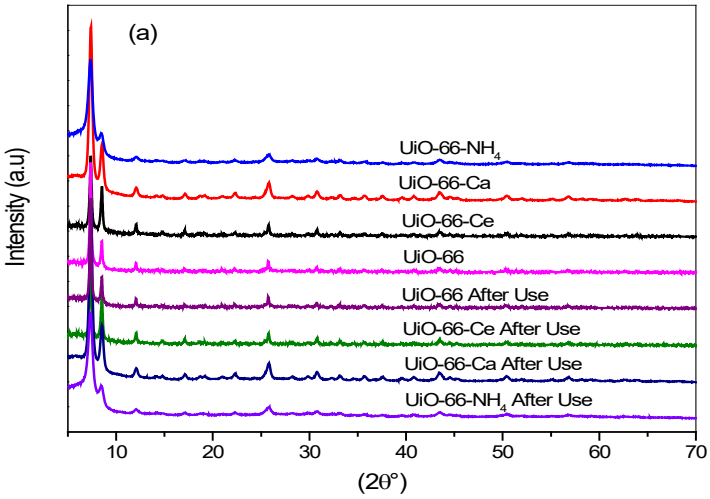

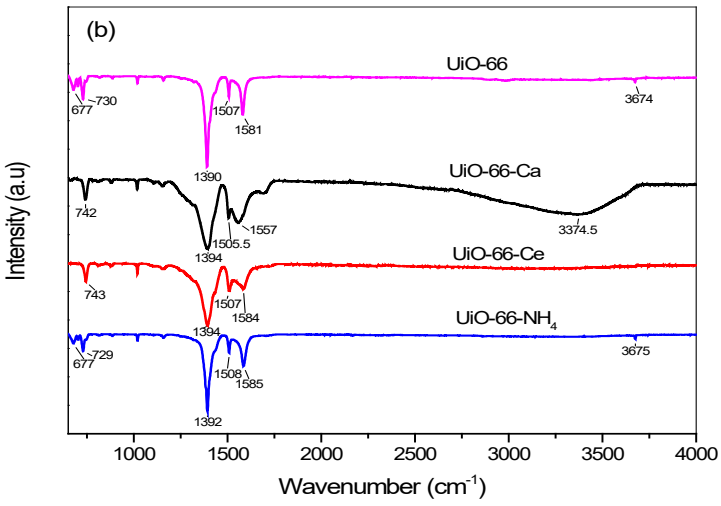

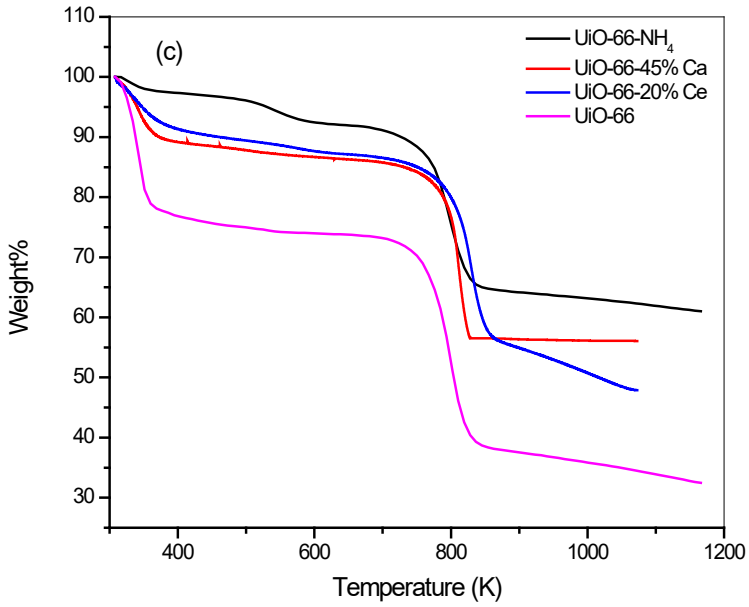

Figure 3.1: Metal organic framework characterisation. (a) PXRD patterns, (b) FTIR spectra and (c) TGA profiles for UiO-66, UiO-66-Ca. and UiO-66-Ce samples UiO-66-NH_4 samples.

Figure 3.2 (c) shows the N_2 adsorption/desorption isotherm on the UiO-66 samples, which confirm their porosity. These samples appear to have pores in the long range extending from micropores to macropores. Primary micropore fillings were achieved at low relative pressures up to 0.01, as shown in Figure 3.2.(c) Larger micropores were filled in the long range of relative pressure up to 0.9, as represented by the relatively horizontal line. However, hysteresis of desorption isotherm over adsorption isotherm is indicated by the presence of neck-bottle mesopores. In addition, rapid increases in the adsorption rate at higher pressures, close to 0.999, can be evidence of the presence of macropores.

Figure 3.2 (h) shows N_2 adsorption-desorption isotherm from which surface area was found using the multipoint BET method. On the other hand, external surface area was computed with the t-plot method. Furthermore, the total pore volume was calculated at P/P0 equal to 0.99. In addition, the pore size distribution was carried out using a micro porous method for the average pore size. Figure 3.2.(a and b) demonstrate mesopore and micropore distribution of pristine and modified UiO-66. In addition,

Table 3.1 displays the textural properties of the UIO-66 samples. Specific surface area (S_{BET}) was reduced following the incorporation of the trace content of a second metal in the UiO-66 structure. It was 1064 and 911.85 $m^2. g^{-1}$ in UiO-66-Ca and UiO-66-Ce, respectively. The S_{BET} of UiO-66-NH_4 was approximately the same as that published for UiO-66: 1226 $m^2. g^{-1}$. The pore volume and pore size were enhanced in all the samples; the largest pore volume and pore size were found for UiO-66-NH_4, which was 1.65 cc. g^{-1} and 5.4 nm, respectively. In UiO-66-Ca and UiO-66-Ce, these values were 1.32 cc. g^{-1} and 4.95 nm, 0.9098 cc. g^{-1} and 3.99 nm, respectively. Consequently, the external surface area of UiO-66-NH_4, UiO-66-Ca and UiO-66-Ce was 331, 292.50 and 224.45 $m^2. g^{-1}$, respectively.

Table 3.1: Textural properties of Parent and Modified Zr-MOF samples.

Material:	**BET surface area (m^2 g^{-1})**	**Average pore volume (cm^3g^{-1})**	**Average pore size (nm)**
UiO-66	1585.5	0.82	1.04
UiO-66-Ca	1064	1.32	4.95
UiO-66-Ce	911.85	0.9098	3.99
UiO-66-NH_4	1226	1.65	5.4

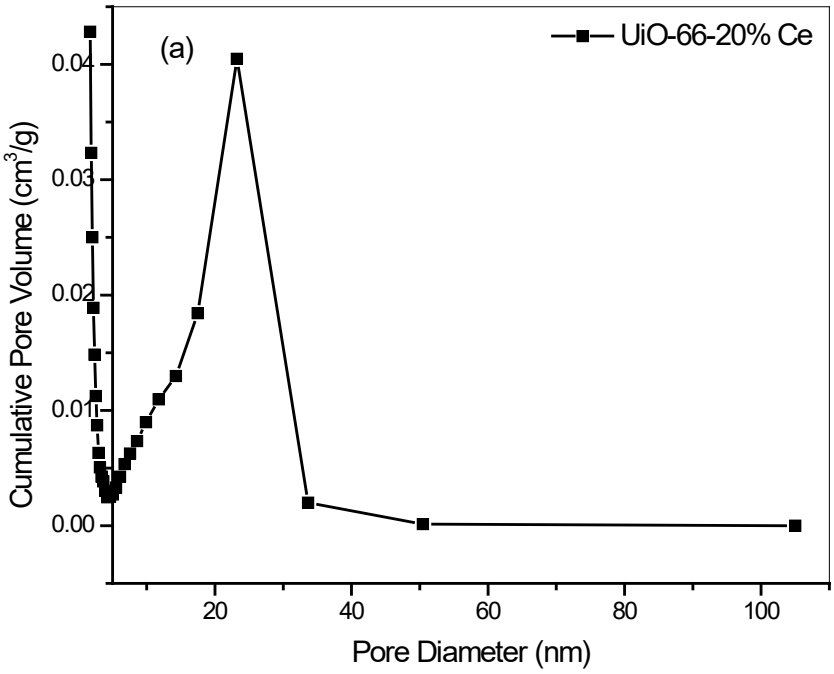

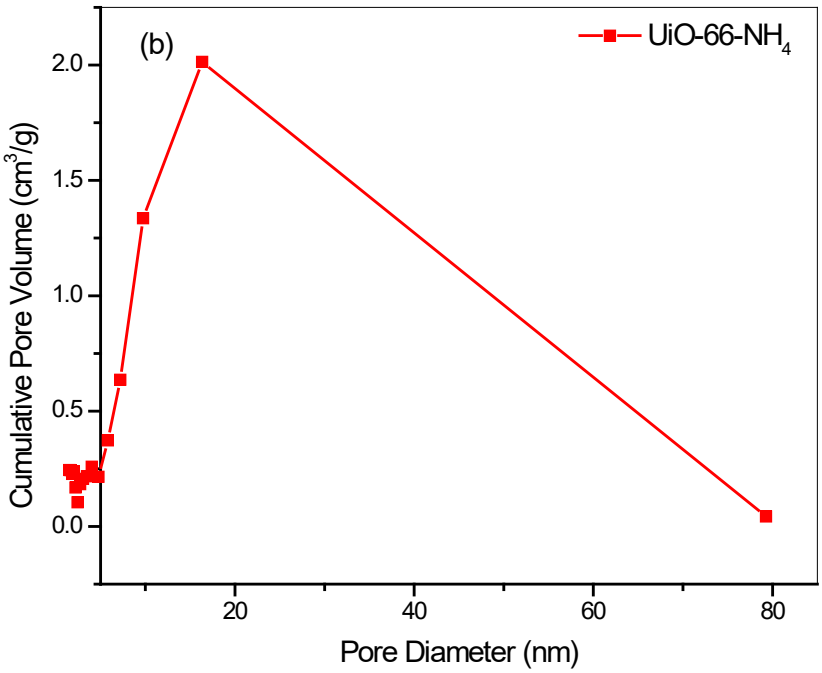
(b)
UiO-66-NH4
Cumulative Pore Volume (cm3/g)
Pore Diameter (nm)
0.0
0.5
1.0
1.5
2.0
20
40
60
80

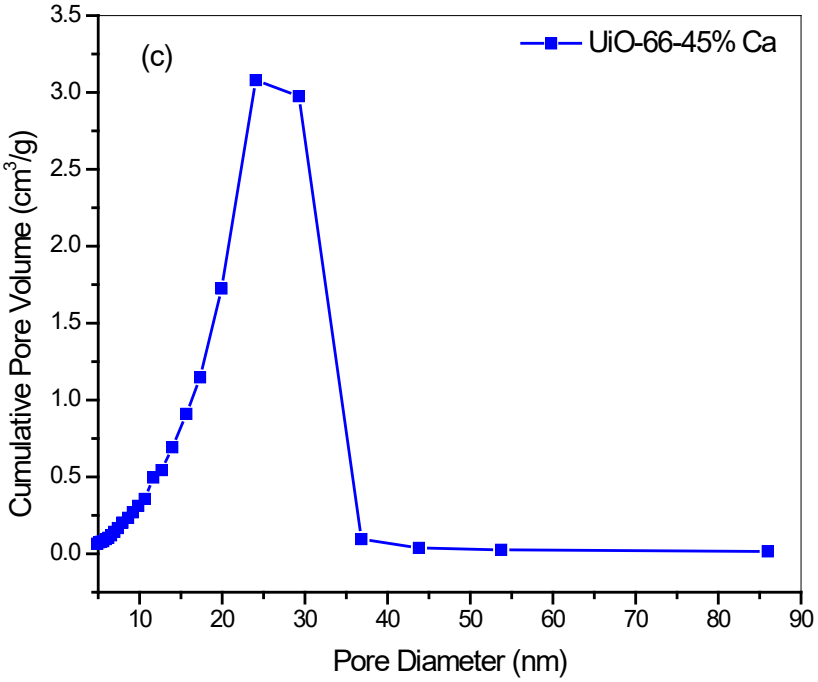
(c)
UiO-66-45% Ca
Cumulative Pore Volume (cm3/g)
Pore Diameter (nm)
0.0
0.5
1.0
1.5
2.0
2.5
3.0
3.5
10
20
30
40
50
60
70
80
90

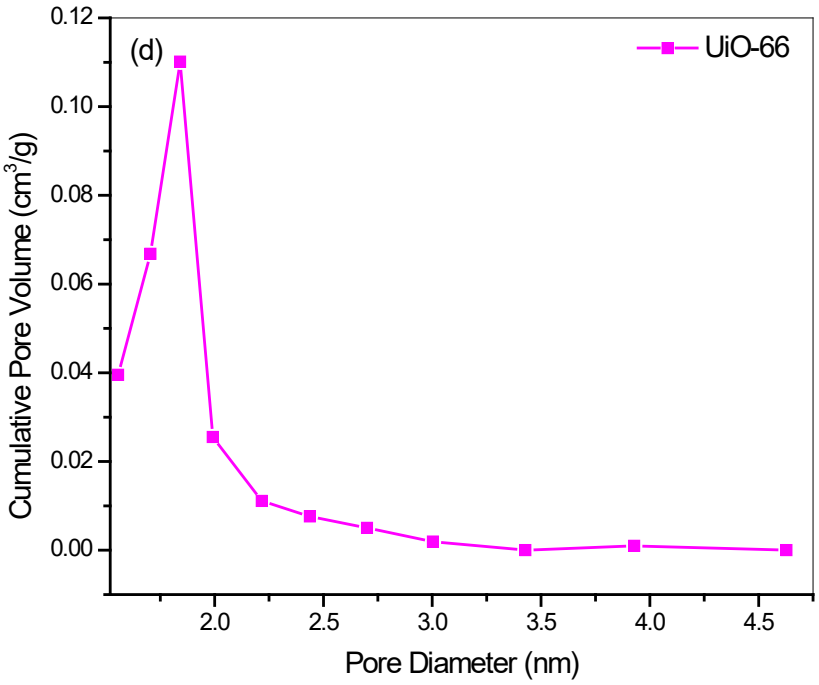
(d)
UiO-66
Cumulative Pore Volume (cm3/g)
0.12
0.10
0.08
0.06
0.04
0.02
0.00
2.0
2.5
3.0
3.5
4.0
4.5
Pore Diameter (nm)

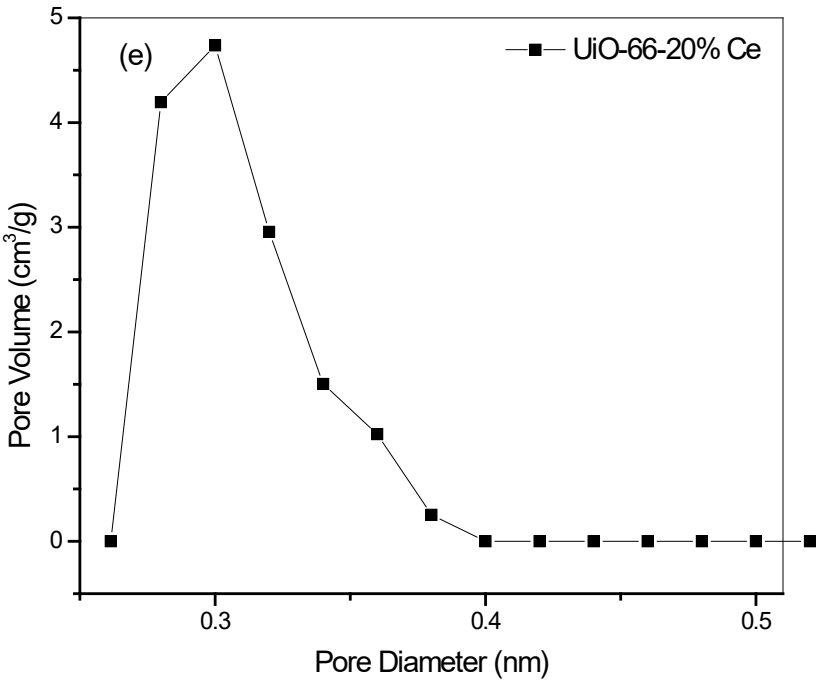
(e)
UiO-66-20% Ce
Pore Volume (cm3/g)
5
4
3
2
1
0
0.3
0.4
0.5
Pore Diameter (nm)

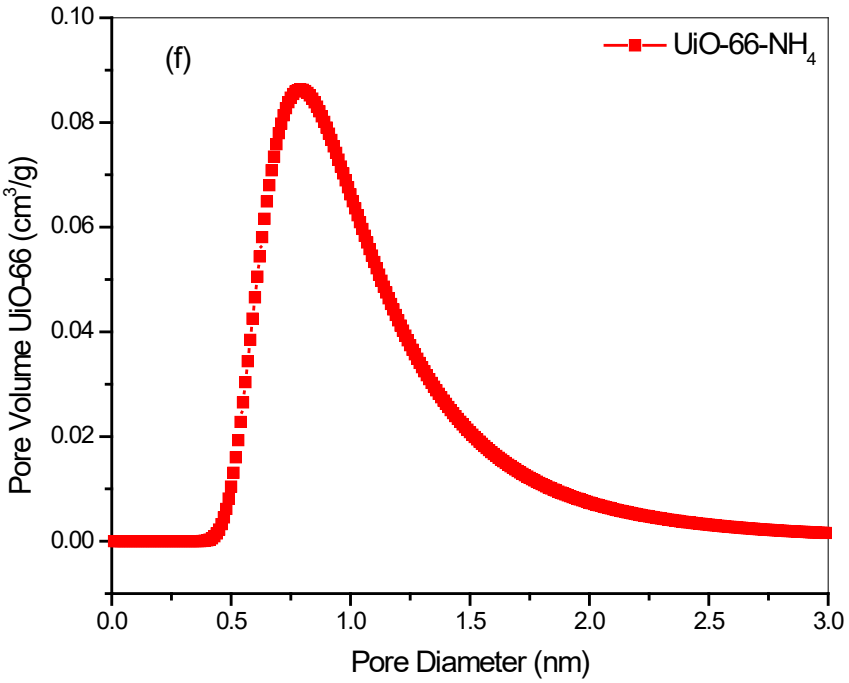
(f)
UiO-66-NH4
Pore Volume UiO-66 (cm3/g)
0.10
0.08
0.06
0.04
0.02
0.00
0.0
0.5
1.0
1.5
2.0
2.5
3.0
Pore Diameter (nm)

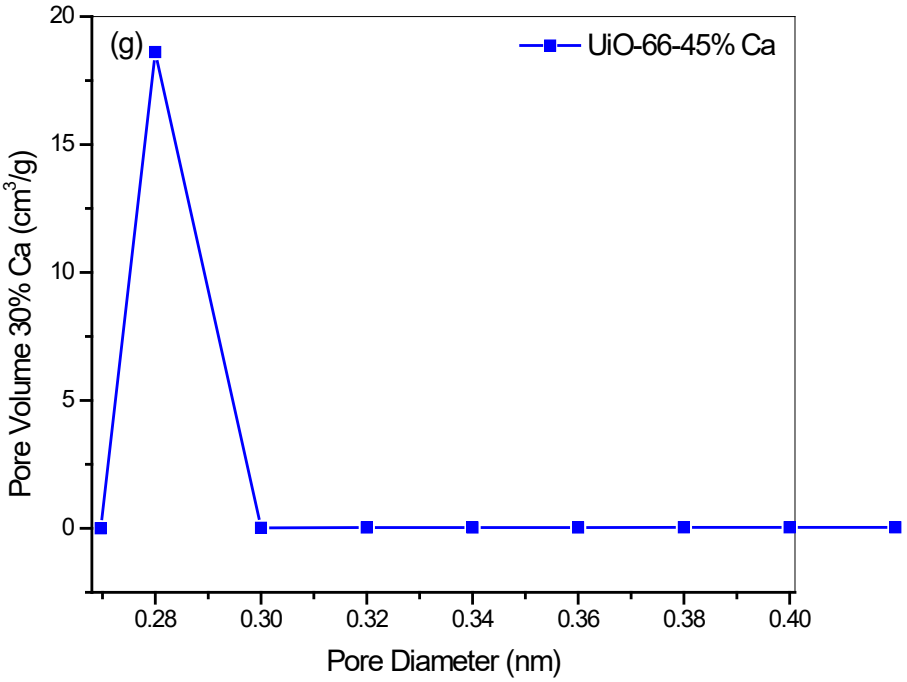
(g)
UiO-66-45% Ca
Pore Volume 30% Ca (cm3/g)
20
15
10
5
0
0.28
0.30
0.32
0.34
0.36
0.38
0.40
Pore Diameter (nm)

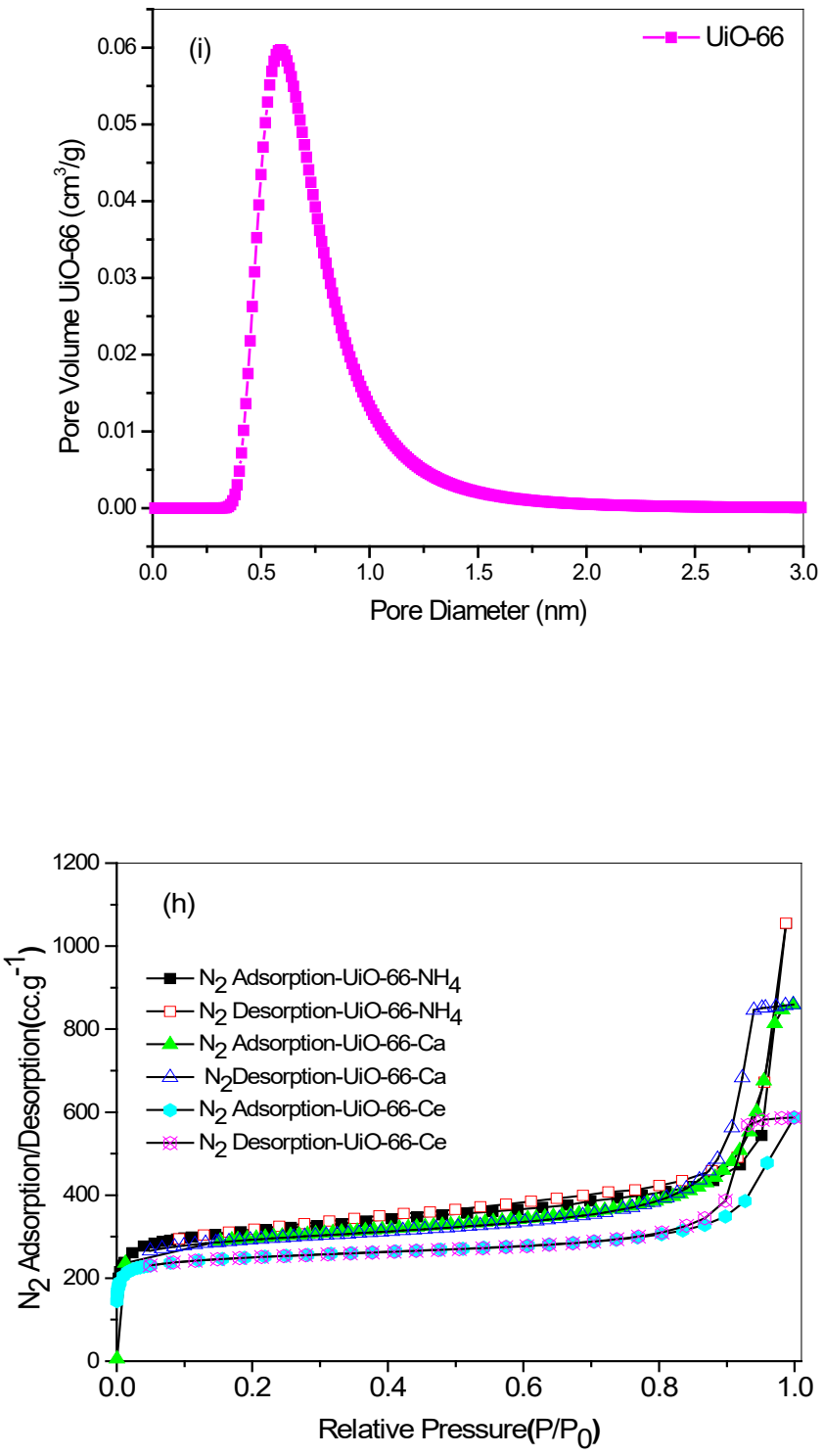

Figure 3.2: Mesopore (a, b, c and d) and micropore (e, f, g and i) distribution and N_2 adsorption/desorption (h) of UiO-66-Ca, UiO-66-Ce and UiO-66-NH_4 samples.

3.5 Adsorption kinetics

3.5.1 Pseudo first-order and pseudo second-order models

Kinetics adsorption studies are crucial because they reliably indicate one criterion of adsorbent efficiency, the rate of adsorption, and they provide a clear picture of the adsorption mechanism. The linear relationship of pseudo first-order model can be expressed as [94]:

$$l\,n(q_e - q_t) = l\,n(q_e) - k_1 t. \tag{3.4}$$

The linear form of the pseudo second-order model is given as [87]:

$$\frac{t}{q_t} = \frac{1}{k_2 \quad q_e^2} + \frac{1}{q_e} t\,, \tag{3.5}$$

Where:

q_e: amount adsorbed at equilibrium (mg. g^{-1})

q_t: amount adsorbed at time t (mg. g^{-1})

t: adsorption time (min)

k_1: first-order kinetic constant (min^{-1})

k_2: second-order kinetic constant (g/mg min).

Given the above, a $\ln(q_e - q_t)$ versus t plot can lead to a straight line whose slope and intercept indicate the value of k_1 and q_e, respectively [95-97]. In addition, t/q_t versus t can be plotted to give a linear relationship whose slope and intercept provides q_e and k_2, respectively [98-100].

To precisely compare the adsorption kinetics, changes in adsorbed amount over time were treated with pseudo first-order and pseudo second-order kinetic models [86-88, 101-103]. Tables 3.2 and 3.3 show the obtained parameter of rate constant studies of various initial concentrations of MO, by fitting the experimental data to the pseudo first-order and second-order equations. The obtained correlation coefficients (R^2) of the pseudo first- and second-order adsorption models revealed that the R^2 values of the pseudo second-order model were higher (greater than 0.99) compared with those of the pseudo first-order model, and its calculated equilibrium adsorption capacity ($q_{e,cal}$) was consistent with the q_e determined from the plot based on experimental data.

Higher R^2 values of the second-order model and identical values of q_e for both theoretical and experimental data led to the fact that the pseudo second-order adsorption mechanism is predominant for Zr-MOF adsorption of dye. Therefore, the overall rate of MO uptake in Zr-MOF processes appear to be controlled by the chemisorption process [104], including valence forces contributing to the sharing or exchange of electrons [89, 105]. The major reason causing the significant difference in adsorption among different MOFs is due to large pore size and better pore structure as well as chemical properties of adsorbent. Adsorption capacity increased with the pore size of the porous material. They suggested that the adsorption mechanism for dye using MOFs partly depended on the electrostatic interaction between the anionic MO and cationic adsorbent.

However, previous studies have reported the same phenomenon for the adsorptive removal of methylene blue (MB) by activated carbon developed from Ficus carica bast [89], the adsorption kinetics of MB and MO by raw date pits and its activated carbon [106], the adsorptive removal of MO by tin oxide nanoparticles loaded on activated carbon and activated carbon prepared from Pistacia atlantica wood [107].

It is also notable that in general the rate constant of the pseudo second-order model (k_2) decreases with increases in the initial MO concentration in all MO/Zr-MOF adsorption systems, except for the initial concentration of 30 mgL^{-1}. It appears from Table 3.3 that the rate constant (k_2) increased in adsorbents when the initial concentration was set at 30 mgL^{-1}, while it decreased at lower and higher concentrations; this can indicate an abundance of negative MO charge, which increases with increases in the initial concentration. Hence, the mobility of MO molecules may be affected by its initial concentration: their mobility first increases as the concentration is increased up to the overcharge limit, then decreases when the initial concentration is further increased beyond the overcharge limit.

Contact time is a very important factor in the efficiency of the sorption process. As shown in Figure 3.3 (a, b, c, d, e and f), the MO uptake occurs during contact times that range from 0.0 to 300 min, with initial MO concentrations of 10, 17.5, 30 and 75 mgL^{-1}. Figure 3.3 illustrates the effect of contact time on MO adsorption by Zr-MOFs. The adsorbed quantity of MO by UiO-66-Ce was higher than those by UiO-66-NH_4 or UiO-66-4Ca. It also shows that the amount of adsorbed MO increased

slightly with increases in initial concentration and contact time, verifying the positive correlation between amount of dye adsorbed and dye concentration levels and contact time. Specifically, most of the MO uptake by Zr-MOFs occurred in the first 30 min, indicating that in the beginning of the adsorption process, an increase in contact time led to substantial occupation of the adsorbents' surfaces by MO molecules with accompanying decrease in MO concentrations in contaminated solutions.

The accessibility of many active sites on the surfaces of Zr-MOF enhances mass transfer of MO to Zr-MOF surfaces, giving rise to rapid adsorption in the starting period of the contact time. Further, with increasing contact time, the upload of MO onto Zr-MOF slows as the number of available adsorptive sites decreases, until an equilibrium reflecting the saturation state of adsorbents is attained. For all MO/Zr-MOF systems, such an equilibrium was determined to have been reached at approximately 50 min as a result of the occupation of active sites by adsorbates as well as the repulsive force between the molecules of adsorbed MO and MO in the bulk solution.

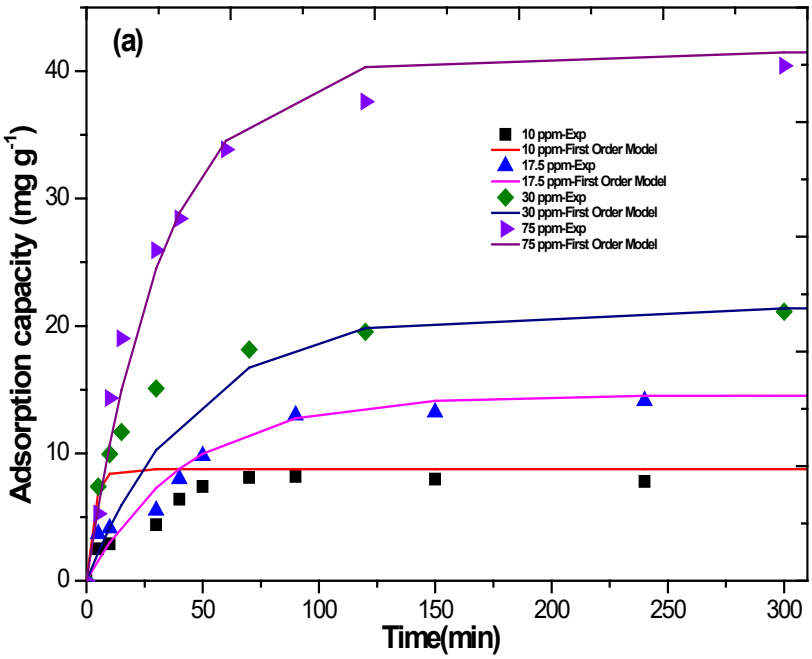

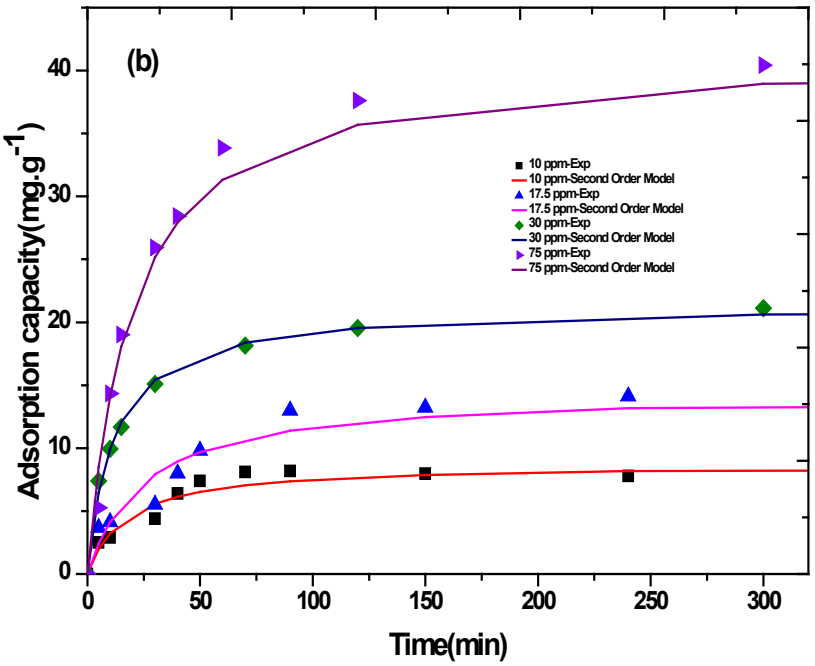
(b)
Adsorption capacity(mg.g-1)
Time(min)
10 ppm-Exp
10 ppm-Second Order Model
17.5 ppm-Exp
17.5 ppm-Second Order Model
30 ppm-Exp
30 ppm-Second Order Model
75 ppm-Exp
75 ppm-Second Order Model

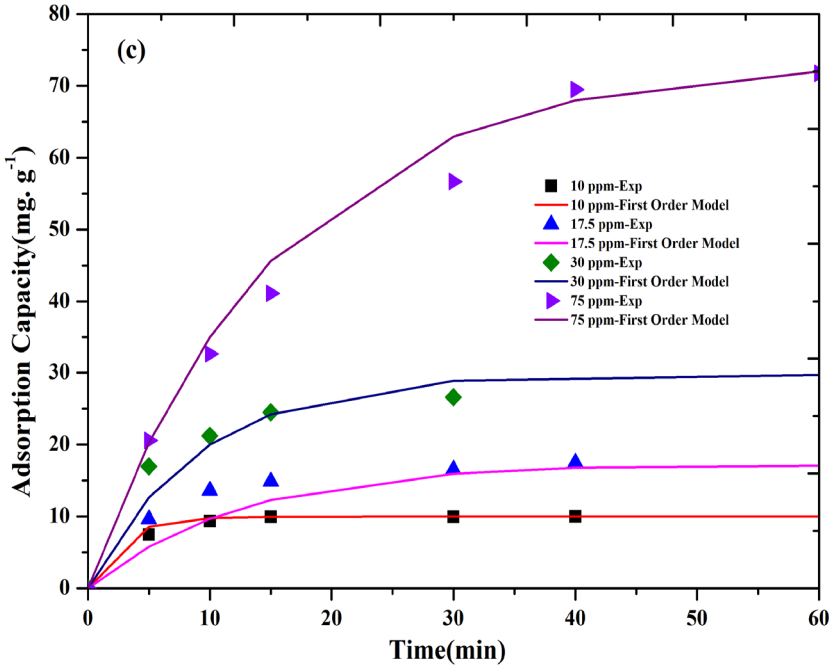
(c)
Adsorption Capacity(mg. g-1)
Time(min)
10 ppm-Exp
10 ppm-First Order Model
17.5 ppm-Exp
17.5 ppm-First Order Model
30 ppm-Exp
30 ppm-First Order Model
75 ppm-Exp
75 ppm-First Order Model

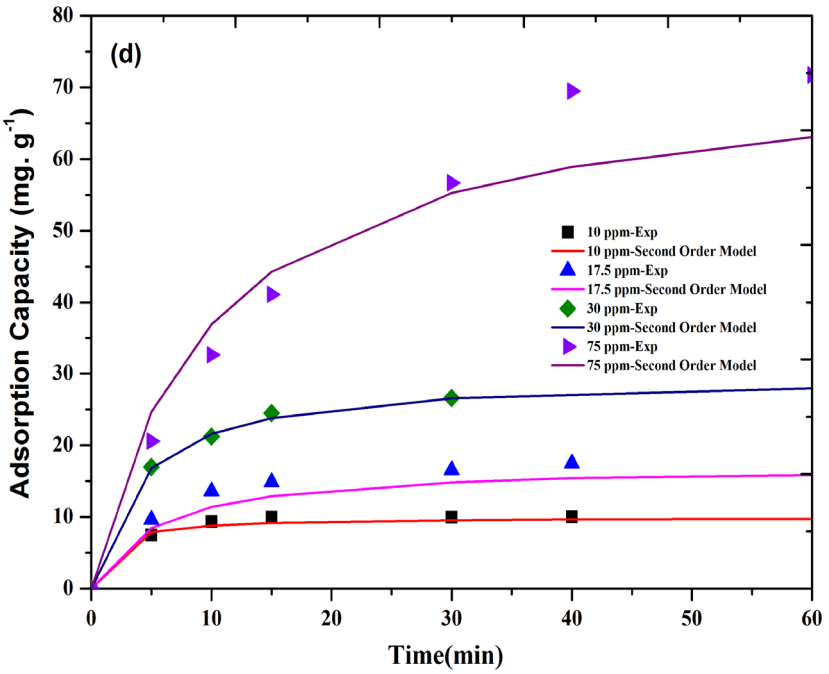
(d)
Adsorption Capacity (mg. g-1)
Time(min)
10 ppm-Exp
10 ppm-Second Order Model
17.5 ppm-Exp
17.5 ppm-Second Order Model
30 ppm-Exp
30 ppm-Second Order Model
75 ppm-Exp
75 ppm-Second Order Model

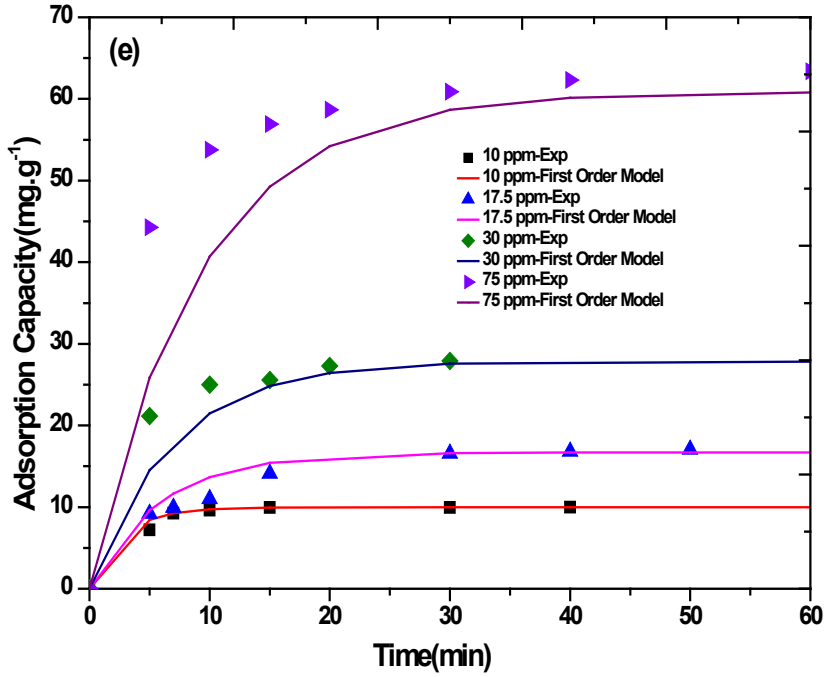
(e)
Adsorption Capacity(mg.g-1)
Time(min)
10 ppm-Exp
10 ppm-First Order Model
17.5 ppm-Exp
17.5 ppm-First Order Model
30 ppm-Exp
30 ppm-First Order Model
75 ppm-Exp
75 ppm-First Order Model

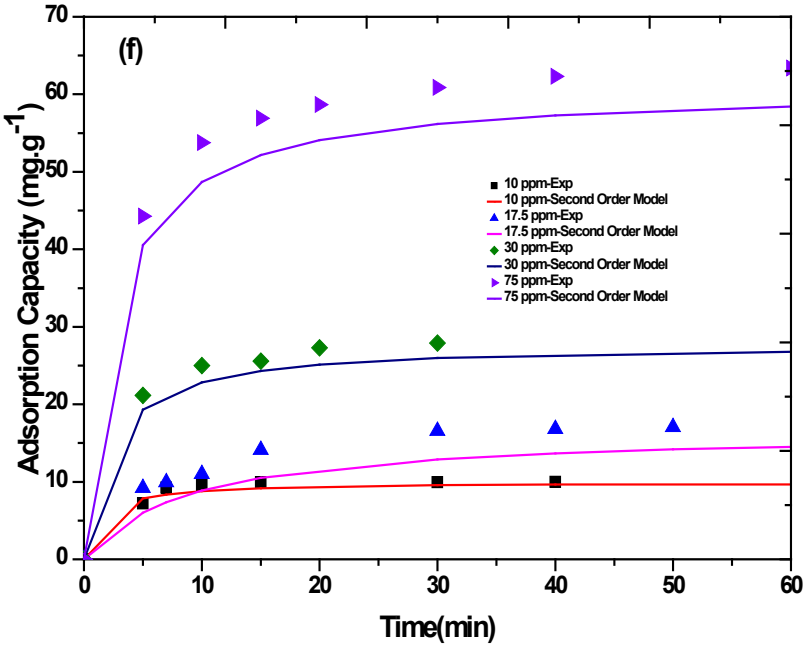

Figure 3.3: Fitting of experimental data by first-order and second-order kinetic models of MO adsorption onto UiO-66-Ca (a, b), UiO-66-Ce (c, d) and UiO-66- NH_4 (e, f).

Table 3.2: Calculated kinetics constant (k_1) and correlation coefficient (R^2) for C_i = 10, 17.5, 30 and 75 ppm.

Adsorbent	Adsorbate	Pseudo first-order kinetics constant k_1 (min^{-1})							
		10 ppm		17.5 ppm		30 ppm		75 ppm	
		k_1	R^2	k_1	R^2	k_1	R^2	k_1	R^2
UiO-66-NH_4	MO	0.3701	0.9767	0.1713	0.9743	0.1472	0.9322	0.1105	0.9755
UiO-66-Ce	MO	0.3854	0.9487	0.0807	0.9728	0.1098	0.9703	0.0647	0.9657
UiO-66-Ca	MO	0.3170	0.9614	0.0231	0.9525	0.0217	0.9711	0.0298	0.9031

Table 3.3: Calculated kinetics constant (k_2) and correlation coefficient (R^2) for C_i = 10, 17.5, 30 and 75 ppm.

Adsorbent	Adsorbate	Pseudo second-order kinetics constant k_2 (g/[mg.min])							
		10 ppm		17.5 ppm		30 ppm		75 ppm	
		k_2	R^2	k_2	R^2	k_2	R^2	k_2	R^2
UiO-66-NH_4	MO	0.0726	0.9962	0.0067	0.9917	0.0161	0.9994	0.0065	0.9999
UiO-66-Ce	MO	0.0756	0.9989	0.0107	0.9992	0.0085	0.9992	0.0013	0.9981
UiO-66-Ca	MO	0.0067	0.9996	0.0027	0.9993	0.0040	0.9999	0.0012	0.9999

3.6 Equilibrium study

Concentration measurements of solid/solute for contact time equal to saturation or equilibrium state are important to determining the isotherm data which in turn, are very important to the design of the adsorbent. Many isotherms were established to describe sorption equilibrium isotherms. Two equilibrium relationships were employed to fit the equilibrium data, including Langmuir [108] and Freundlich [109] isotherms.

3.6.1 Freundlich isotherm

Heterogeneous systems can be described by the empirical equation referred to as Freundlich isotherm [109], which may be expressed as follows.

$$q_e = k_F C_e^{1/n} \tag{3.6}$$

Equation 3.6 can be linearized by applying to both sides of the model and simplifying to the below:

$$\ln(q_e) = \ln(k_F) + \frac{1}{n}\ln(C_e), \tag{3.7}$$

Where:

k_F: the calculated Freundlich equilibrium constant (mg/g $[L/mg]^{1/n}$) as an indicator of the adsorption capacity

n: a measure of the deviation from linearity of adsorption (g/L).

The favourability of the adsorption system can be tested by determining the reciprocal of the magnitude of the exponent n value. When the value of n is greater than one, it can be concluded that the adsorption process is favourable. From the straight-line plot of $\ln(q_e)$ versus $\ln(C_e)$, the values of n and k_F can be simply found from the slope and intercept, respectively. The values of these parameters were obtained for UiO-66-NH_4, UiO-66-Ce and UiO-66-Ca, as well as their correlation coefficients (R^2), as listed in Table 3.4.

3.6.2 Langmuir isotherm

Langmuir model [108] is one of the most important equilibrium isotherms that have been used for long time examining adsorption processes with success. The

assumption of such isotherm presumes that the adsorption can be happened at specific homogeneous adsorptive sites of the adsorbent and the forces of attraction between adsorbate and adsorbent are depend on the distance from the adsorption surface. More specifically, these electrostatic forces decrease rapidly with the distance between the sorbate and the sorbent surface. In addition, all active adsorptive sites have the same energy as well as the adsorbent has homogeneous structure [110].

It is clear from the result of this study that pristine and modified Zr-MOFs were used to remove pollutants from aqueous solution of anionic and cationic dyes, including MO and MB. The removal efficiencies of these dyes by parent and modified Zr-MOFs were much better than by conventional adsorbents such as activated carbon. It can be concluded Zr-MOFs can be attractive adsorbents of some harmful chemicals, like dyes in wastewater. The adsorption mechanism was attributed to the presence of electrostatic interactions between the dye and the adsorbent. Specifically, those MOFs can have positive (framework) and negative charges (charge-balancing anion), respectively; therefore, it can capture anionic and cationic dyes.

The nonlinear form of Langmuir equation can be expressed as follow:

$$q_e = \frac{q_m k_L C_e}{(1 + k_L C_e)} \tag{3.8}$$

Whereas the linear form of Langmuir model may be written as below:

$$\frac{C_e}{q_e} = \frac{1}{q_m} C_e + \frac{1}{k_L q_m}, \tag{3.9}$$

Where:

q_m: Langmuir maximum loading capacity (mg/g)

k_L: Langmuir constant related to the energy of adsorption and affinity of binding sites (L/mg)

C_e: the equilibrium concentration of dye in solution (mg/L)

q_e: amount of dye adsorbed at equilibrium per unit mass of sorbent (mg/g).

For obtaining the parameters of equilibrium like q_m and k_L from the experimental data, C_e/q_e against C_e can be plotted yielding linear relationship with slop ($1/q_m$) and

intercept ($1/k_Lq_m$). The values of these parameters were found for UiO-66-NH_4, UiO-66-Ce, and UiO-66-Ca including correlation coefficients (R^2) and listed in Table 3.4. Furthermore, based on linear regression coefficients (R^2), the best agreement to experimental equilibrium data was Langmuir model verifying that the monolayer adsorption occurs on Zr-MOFs surfaces with homogeneous distribution of active sites. The maximum adsorption capacity (q_m) of the UiO-66-Ce, UiO-66-NH_4 and UiO-66-Ca were 71.5, 62.50 and 50.25 mg g^{-1}, respectively. The simulated adsorption behaviour appeared that UiO-66-Ce is the adsorbent for removal the MO from wastewater with maximum adsorption capacity of 71.5 mg. g^{-1}. UiO-66-Ce exposed good affinity for MO adsorption with excellent performance because of its superior characteristics, having the large pore volume and pore size in its nanosized particles which leads to enhance the adsorption capacity of UiO-66-Ce. Figure 3.4 displays fitted experimental data by Langmuir and Freundlich isotherms. It is observed that MO adsorption onto UiO-66-Ce and UiO-66-NH_4 fitted well with the Langmuir model, while its adsorption onto UiO-66-Ca fitted well with both isotherms. Similar results have been reported in other studies: the efficient adsorption of MB by polydopamine microspheres [111], removal of MB from aqueous solutions by kaolin [85], adsorption of MB onto bamboo-based activated carbon [112] and adsorptive removal of MO from aqueous solutions with iron terephthalate (MOF-235)[113]. Other reported equilibrium results were compared with the results in this study and listed in Table 3.5, showing relatively strong performance by Zr-MOFs. UiO-66-Ce and UiO-66-NH_4 here have better performance than MIL due to improving in pore structure and size, chemical properties and coordination with enriched open metal sites. In addition, the affinity of MO to modified MOFs is greater than MIL.

The expression of essential characteristics of the Langmuir isotherm is very important indication for the favourability of adsorption process which may be written based on a dimensionless constant separation factor (R_L) as follows:

$$R_L = \frac{1}{(1 + k_L C_0)}, \tag{3.10}$$

Where:

C_0: the initial concentration of adsorbate (mg/L),

k_L: (L/mg) is Langmuir constant.

Type of the isotherm can be predicted from the R_L value indicating the favourability of the process of adsorption. It may be equal to zero, one, greater than one, or between greater than zero to less than one proofing that the adsorption process is either irreversible, linear, unfavourable, or favourable, respectively. According to experimental data, all values of R_L are between $0 < R_L < 1$ confirming that all the adsorption systems of MO/Zr-MOFs are favourable.

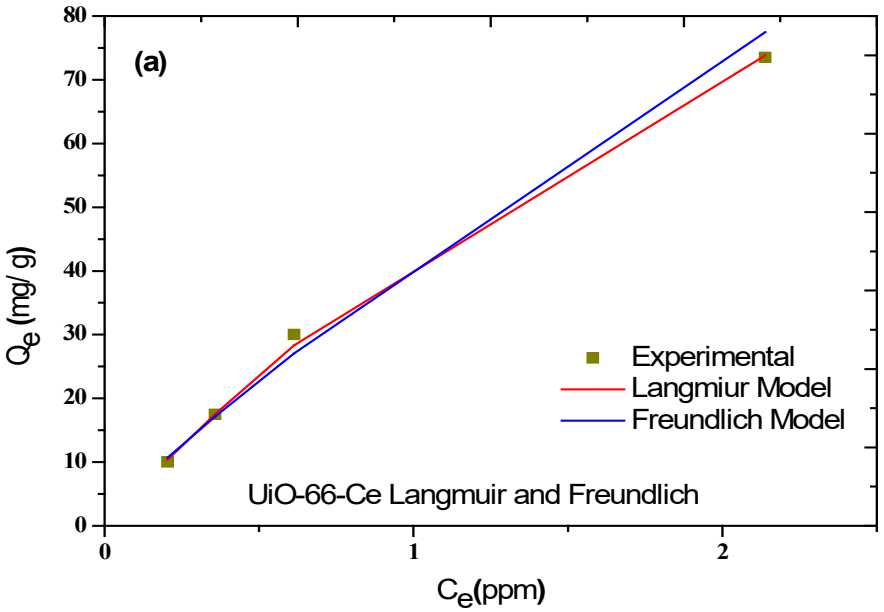

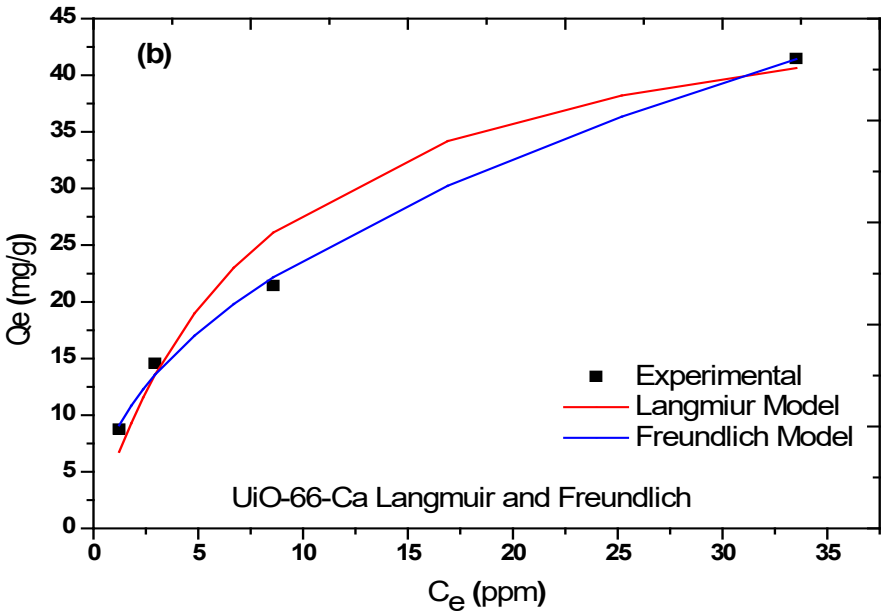

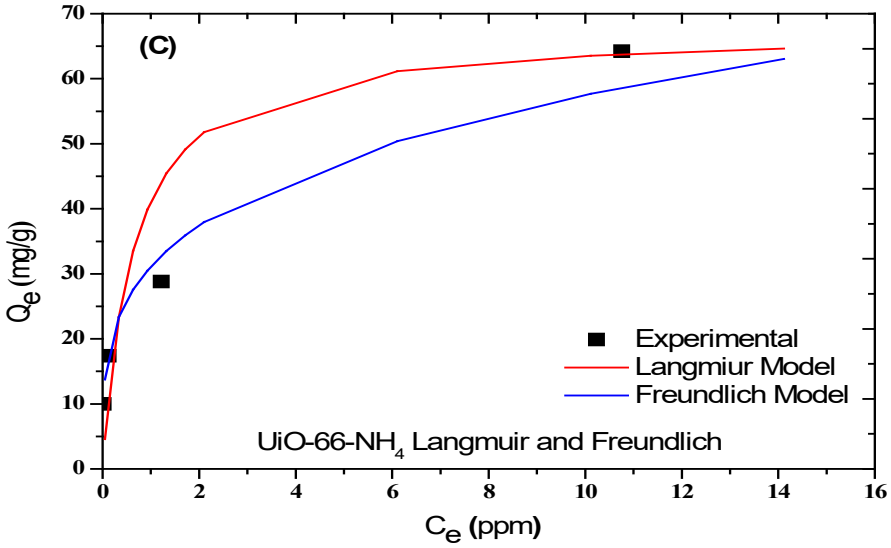

Figure 3.4: Adsorption equilibrium isotherms of MO adsorption onto (a) UiO-66-Ce, (b) UiO-66-Ca and (c) UiO-66-NH_4.

Table 3.4: Calculated equilibrium constants (k_L, k_F, q_m, n and correlation coefficient (R^2) for MO adsorption onto UiO-66-NH_4, UiO-66-C_e and UiO-66-Ca, for C_i = 10, 17.5, 30 and 75 ppm.

Adsorbent	Adsorption isotherm model	Parameters	Values	R^2
UiO-66-NH_4	Langmuir	q_m (mg/g)	62.56	0.963
		K_L (L/mg)	1.56	
	Freundlich	K_F ([mg/g] [L/mg]$^{1/n}$)	31.13	0.928
		n (g/L)	3.75	
UiO-66-Ce	Langmuir	q_m (mg/g)	71.50	0.964
		K_L (L/mg)	0.256	
	Freundlich	K_F ([mg/g] [L/mg]$^{1/n}$)	40.8	0.991
		n (g/L)	1.18	
UiO-66-Ca	Langmuir	q_m (mg/g)	50.25	0.993
		K_L (L/mg)	0.126	
	Freundlich	K_F ([mg/g] [L/mg]$^{1/n}$)	8.284	0.992
		n (g/L)	2.1824	

Table 3.5: Comparison of monolayer equilibrium capacity for MO onto different sorbents.

Adsorbent	Condition	q_m (mg/g)	Reference
UiO-66-Ce	Normal	71.50	This study
UiO-66-NH_4	Normal	62.5	This study
UiO-66-Ca	Normal	50.25	This study
Hypercrosslinked polymeric adsorbent	Normal	70.9	[114]
Metal organic framework (MIL-53)	Normal	57.9	[115]
Multiwalled carbon nanotubes	Normal	52.86	[106]
Chitosan	Normal	34.83	[37]
Modified montmorillonite	Normal	24.00	[116]
Banana peel	Normal	21	[117]
Orange peel	Normal	20.5	[118]
Modified ultra-fine coal powder	Normal	18.52	[119]
Graphene oxide	Normal	16.83	[15]
Chitosan/kaolin/γ-Fe_2O_3	Normal	14.2	[120]
Bottom ash	Normal	13.35	[5]
De-oiled soya	Normal	13.46	[5]
Activated carbon	Normal	11.2	[115]
Activated alumina	Normal	9.8	[121]
Diaminoethanesporopollenin biopolymer	Normal	4.7	[122]
Bottom ash	Normal	3.62	[2]

3.7 Conclusion

Three adsorbents (UiO-66, UiO-66-Ca and UiO-66-NH_4) were used to remove acidic dye (MO). They were synthesised using different methods with trace additives of a secondary chemical. The textural properties were improved and enhanced for water treatment applications. The characterisation of single and bimetal Zr-MOFs reveals that they have water and thermal stability, a robust structure, suitable textural properties and functional groups. The experimental data was fitted for kinetic adsorption and adsorption equilibrium: adsorption by MO/Zr-MOF systems depends on the initial concentration of dye, with improved uptake by MOFs with increased initial concentrations of MO. The highest correlation coefficient obtained among all MO adsorption by Zr-MOFs systems confirms pseudo second-order kinetics and indicates that the overall rate of MO uptake by Zr-MOF appears to be controlled by the chemisorption process, including valence forces through sharing or exchange of electrons.

However, all MO/Zr-MOF systems obeyed the Langmuir isotherm model, verifying that the adsorption of dye molecules by adsorbents are monolayered and occurs on a

homogeneous adsorbent structure with adsorptive sites of identical energy. Moreover, UiO-66-Ce was the most efficient adsorbent to remove MO, exhibiting the highest adsorption capacity equal to 71.5 mg g^{-1}. These Bimetal UiO-66 are potential candidates for industrial applications to remove other contaminants from wastewater.

References

1. Crini, G., *Non-conventional low-cost adsorbents for dye removal: A review.* Bioresource Technology, 2006. **97**(9): p. 1061-1085.
2. Mittal, A., et al., *Studies on the adsorption kinetics and isotherms for the removal and recovery of Methyl Orange from wastewaters using waste materials.* Journal of Hazardous Materials, 2007. **148**(1): p. 229-240.
3. Chen, S., et al., *Equilibrium and kinetic studies of methyl orange and methyl violet adsorption on activated carbon derived from Phragmites australis.* Desalination, 2010. **252**(1): p. 149-156.
4. Rafatullah, M., et al., *Adsorption of methylene blue on low-cost adsorbents: A review.* Journal of Hazardous Materials, 2010. **177**(1): p. 70-80.
5. Mittal, A., et al., *Studies on the adsorption kinetics and isotherms for the removal and recovery of Methyl Orange from wastewaters using waste materials.* Journal of Hazardous Materials, 2007. **148**(1-2): p. 229-240.
6. Singh, K.P., et al., *Color removal from wastewater using low-cost activated carbon derived from agricultural waste material.* Industrial & Engineering Chemistry Research, 2003. **42**(9): p. 1965-1976.
7. Luo, X. and L. Zhang, *High effective adsorption of organic dyes on magnetic cellulose beads entrapping activated carbon.* Journal of Hazardous Materials, 2009. **171**(1): p. 340-347.
8. Bello, O.S. and M.A. Ahmad, *Coconut (Cocos nucifera) shell based activated carbon for the removal of malachite green dye from aqueous solutions.* Separation Science and Technology, 2012. **47**(6): p. 903-912.
9. Ozer, C., et al., *Removal of methylene blue from aqueous solutions using phosphoric acid activated carbon produced from hazelnut husks.* Toxicological & Environmental Chemistry, 2012. **94**(7): p. 1283-1293.
10. Royer, B., et al., *Applications of Brazilian pine-fruit shell in natural and carbonized forms as adsorbents to removal of methylene blue from aqueous solutions—Kinetic and equilibrium study.* Journal of Hazardous Materials, 2009. **164**(2-3): p. 1213-1222.
11. Yang, J. and K. Qiu, *Preparation of activated carbons from walnut shells via vacuum chemical activation and their application for methylene blue removal.* Chemical Engineering Journal, 2010. **165**(1): p. 209-217.
12. Tan, I., A. Ahmad, and B. Hameed, *Adsorption of basic dye using activated carbon prepared from oil palm shell: batch and fixed bed studies.* Desalination, 2008. **225**(1-3): p. 13-28.
13. Malarvizhi, R. and Y.-S. Ho, *The influence of pH and the structure of the dye molecules on adsorption isotherm modeling using activated carbon.* Desalination, 2010. **264**(1-2): p. 97-101.
14. Lorenc-Grabowska, E. and G. Gryglewicz, *Adsorption characteristics of Congo Red on coal-based mesoporous activated carbon.* Dyes and pigments, 2007. **74**(1): p. 34-40.

15. Robati, D., et al., *Removal of hazardous dyes-BR 12 and methyl orange using graphene oxide as an adsorbent from aqueous phase.* Chemical Engineering Journal, 2016. **284**: p. 687-697.

16. Zaghouane-Boudiaf, H., M. Boutahala, and L. Arab, *Removal of methyl orange from aqueous solution by uncalcined and calcined MgNiAl layered double hydroxides (LDHs).* Chemical Engineering Journal, 2012. **187**: p. 142-149.

17. Santos, S.C., V.J. Vilar, and R.A. Boaventura, *Waste metal hydroxide sludge as adsorbent for a reactive dye.* Journal of Hazardous Materials, 2008. **153**(3): p. 999-1008.

18. Golder, A., A. Samanta, and S. Ray, *Anionic reactive dye removal from aqueous solution using a new adsorbent—Sludge generated in removal of heavy metal by electrocoagulation.* Chemical Engineering Journal, 2006. **122**(1-2): p. 107-115.

19. Gulnaz, O., et al., *Sorption of basic dyes from aqueous solution by activated sludge.* Journal of Hazardous Materials, 2004. **108**(3): p. 183-188.

20. Otero, M., et al., *Kinetic and equilibrium modelling of the methylene blue removal from solution by adsorbent materials produced from sewage sludges.* Biochemical Engineering Journal, 2003. **15**(1): p. 59-68.

21. Wang, S., Q. Ma, and Z. Zhu, *Characteristics of coal fly ash and adsorption application.* Fuel, 2008. **87**(15-16): p. 3469-3473.

22. Kumar, K.V., V. Ramamurthi, and S. Sivanesan, *Modeling the mechanism involved during the sorption of methylene blue onto fly ash.* Journal of colloid and interface science, 2005. **284**(1): p. 14-21.

23. Gupta, V., et al., *Removal of rhodamine B, fast green, and methylene blue from wastewater using red mud, an aluminum industry waste.* Industrial & engineering chemistry research, 2004. **43**(7): p. 1740-1747.

24. Huang, M., et al., *Photocatalytic discolorization of methyl orange solution by Pt modified TiO2 loaded on natural zeolite.* Dyes and Pigments, 2008. **77**(2): p. 327-334.

25. Ho, Y.-S., T.-H. Chiang, and Y.-M. Hsueh, *Removal of basic dye from aqueous solution using tree fern as a biosorbent.* Process Biochemistry, 2005. **40**(1): p. 119-124.

26. Özacar, M. and İ.A. Şengil, *Adsorption of metal complex dyes from aqueous solutions by pine sawdust.* Bioresource technology, 2005. **96**(7): p. 791-795.

27. Ho, Y.-S. and G. McKay, *Sorption of dyes and copper ions onto biosorbents.* Process Biochemistry, 2003. **38**(7): p. 1047-1061.

28. Kyzas, G.Z., N.K. Lazaridis, and A.C. Mitropoulos, *Removal of dyes from aqueous solutions with untreated coffee residues as potential low-cost adsorbents: Equilibrium, reuse and thermodynamic approach.* Chemical engineering journal, 2012. **189**: p. 148-159.

29. Han, X., X. Niu, and X. Ma, *Adsorption characteristics of methylene blue on poplar leaf in batch mode: Equilibrium, kinetics and thermodynamics.* Korean Journal of Chemical Engineering, 2012. **29**(4): p. 494-502.

30. Feng, Y., et al., *Methylene blue adsorption onto swede rape straw (Brassica napus L.) modified by tartaric acid: equilibrium, kinetic and adsorption mechanisms.* Bioresource technology, 2012. **125**: p. 138-144.

31. Saeed, A., M. Sharif, and M. Iqbal, *Application potential of grapefruit peel as dye sorbent: kinetics, equilibrium and mechanism of crystal violet adsorption.* Journal of hazardous materials, 2010. **179**(1-3): p. 564-572.

32. Wang, X.S., et al., *Comparison of basic dye crystal violet removal from aqueous solution by low-cost biosorbents.* Separation Science and Technology, 2008. **43**(14): p. 3712-3731.

33. Han, R., et al., *Biosorption of methylene blue from aqueous solution by fallen phoenix tree's leaves.* Journal of Hazardous Materials, 2007. **141**(1): p. 156-162.

34. Pavan, F.A., et al., *Methylene blue biosorption from aqueous solutions by yellow passion fruit waste.* Journal of hazardous materials, 2008. **150**(3): p. 703-712.

35. Deniz, F. and S.D. Saygideger, *Removal of a hazardous azo dye (Basic Red 46) from aqueous solution by princess tree leaf.* Desalination, 2011. **268**(1-3): p. 6-11.

36. Wong, Y.C., et al., *Adsorption of acid dyes on chitosan—equilibrium isotherm analyses.* Process Biochemistry, 2004. **39**(6): p. 695-704.

37. Saha, T.K., et al., *Adsorption of methyl orange onto chitosan from aqueous solution.* Journal of water resource and protection, 2010. **2**(10): p. 898.

38. Auta, M. and B. Hameed, *Modified mesoporous clay adsorbent for adsorption isotherm and kinetics of methylene blue.* Chemical Engineering Journal, 2012. **198**: p. 219-227.

39. Wibulswas, R., *Batch and fixed bed sorption of methylene blue on precursor and QACs modified montmorillonite.* Separation and Purification Technology, 2004. **39**(1): p. 3-12.

40. Ho, Y.S. and C.C. Chiang, *Sorption Studies of Acid Dye by Mixed Sorbents.* Adsorption, 2001. **7**(2): p. 139-147.

41. Vimonses, V., et al., *Kinetic study and equilibrium isotherm analysis of Congo Red adsorption by clay materials.* Chemical Engineering Journal, 2009. **148**(2): p. 354-364.

42. Hong, S., et al., *Adsorption thermodynamics of Methylene Blue onto bentonite.* Journal of Hazardous Materials, 2009. **167**(1): p. 630-633.

43. Hajjaji, M., A. Alami, and A.E. Bouadili, *Removal of methylene blue from aqueous solution by fibrous clay minerals.* Journal of Hazardous Materials, 2006. **135**(1): p. 188-192.

44. Chakrabarti, S. and B.K. Dutta, *On the adsorption and diffusion of Methylene Blue in glass fibers.* Journal of Colloid and Interface Science, 2005. **286**(2): p. 807-811.

45. Phan, T.N.T., M. Bacquet, and M. Morcellet, *Synthesis and Characterization of Silica Gels Functionalized with Monochlorotriazinyl β-Cyclodextrin and their Sorption Capacities towards Organic Compounds.* Journal of inclusion phenomena and macrocyclic chemistry, 2000. **38**(1): p. 345-359.

46. Aksu, Z. and S. Tezer, *Biosorption of reactive dyes on the green alga Chlorella vulgaris.* Process Biochemistry, 2005. **40**(3): p. 1347-1361.

47. Marungrueng, K. and P. Pavasant, *High performance biosorbent (Caulerpa lentillifera) for basic dye removal.* Bioresource Technology, 2007. **98**(8): p. 1567-1572.

48. Maurya, N.S., et al., *Biosorption of dyes using dead macro fungi: Effect of dye structure, ionic strength and pH.* Bioresource Technology, 2006. **97**(3): p. 512-521.

49. Waranusantigul, P., et al., *Kinetics of basic dye (methylene blue) biosorption by giant duckweed (Spirodela polyrrhiza).* Environmental Pollution, 2003. **125**(3): p. 385-392.

50. Fu, Y. and T. Viraraghavan, *Removal of Congo Red from an aqueous solution by fungus Aspergillus niger.* Advances in Environmental Research, 2002. **7**(1): p. 239-247.

51. Férey, G., *Hybrid porous solids: past, present, future.* Chemical Society Reviews, 2008. **37**(1): p. 191-214.

52. Kitagawa, S., R. Kitaura, and S.i. Noro, *Functional porous coordination polymers.* Angewandte Chemie International Edition, 2004. **43**(18): p. 2334-2375.

53. Yaghi, O.M., et al., *Reticular synthesis and the design of new materials.* Nature, 2003. **423**(6941): p. 705-714.

54. Murray, L.J., M. Dincă, and J.R. Long, *Hydrogen storage in metal–organic frameworks.* Chemical Society Reviews, 2009. **38**(5): p. 1294-1314.

55. Farrusseng, D., S. Aguado, and C. Pinel, *Metal–organic frameworks: opportunities for catalysis.* Angewandte Chemie International Edition, 2009. **48**(41): p. 7502-7513.

56. Lee, J., et al., *Metal–organic framework materials as catalysts.* Chemical Society Reviews, 2009. **38**(5): p. 1450-1459.

57. Li, J.-R., R.J. Kuppler, and H.-C. Zhou, *Selective gas adsorption and separation in metal–organic frameworks.* Chemical Society Reviews, 2009. **38**(5): p. 1477-1504.

58. Horcajada, P., et al., *Flexible porous metal-organic frameworks for a controlled drug delivery.* Journal of the American Chemical Society, 2008. **130**(21): p. 6774-6780.

59. Abrahams, B.F., et al., *Assembly of porphyrin building blocks into network structures with large channels.* Nature, 1994. **369**: p. 727.

60. Zhou, H.-C., J.R. Long, and O.M. Yaghi, *Introduction to Metal–Organic Frameworks.* Chemical Reviews, 2012. **112**(2): p. 673-674.

61. Horike, S., S. Shimomura, and S. Kitagawa, *Soft porous crystals.* Nature Chemistry, 2009. **1**: p. 695.

62. Farha, O.K. and J.T. Hupp, *Rational Design, Synthesis, Purification, and Activation of Metal−Organic Framework Materials.* Accounts of Chemical Research, 2010. **43**(8): p. 1166-1175.

63. Furukawa, H., et al., *The Chemistry and Applications of Metal-Organic Frameworks.* Science, 2013. **341**(6149): p. 1230444.

64. Kitagawa, S., *Metal–organic frameworks (MOFs).* Chemical Society Reviews, 2014. **43**(16): p. 5415-5418.

65. Allendorf, M., et al., *Luminescent metal–organic frameworks.* Chemical Society Reviews, 2009. **38**(5): p. 1330-1352.

66. Min, K.S. and M.P. Suh, *Silver(I)−Polynitrile Network Solids for Anion Exchange: Anion-Induced Transformation of Supramolecular Structure in the Crystalline State.* Journal of the American Chemical Society, 2000. **122**(29): p. 6834-6840.

67. Llewellyn, P.L., et al., *High Uptakes of CO2 and CH4 in Mesoporous Metal □ Organic Frameworks MIL-100 and MIL-101.* Langmuir, 2008. **24**(14): p. 7245-7250.

68. Cychosz, K.A., A.G. Wong-Foy, and A.J. Matzger, *Liquid phase adsorption by microporous coordination polymers: removal of organosulfur compounds.* Journal of the American Chemical Society, 2008. **130**(22): p. 6938-6939.

69. Hamon, L., et al., *Comparative study of hydrogen sulfide adsorption in the MIL-53 (Al, Cr, Fe), MIL-47 (V), MIL-100 (Cr), and MIL-101 (Cr) metal− organic frameworks at room temperature.* Journal of the American Chemical Society, 2009. **131**(25): p. 8775-8777.

70. Cui, Y., et al., *Luminescent Functional Metal–Organic Frameworks.* Chemical Reviews, 2012. **112**(2): p. 1126-1162.

71. Bae, Y.-S., et al., *Carborane-based metal–organic frameworks as highly selective sorbents for CO 2 over methane.* Chemical Communications, 2008(35): p. 4135-4137.

72. Bae, Y.-S., et al., *Enhancement of CO 2/N 2 selectivity in a metal-organic framework by cavity modification.* Journal of Materials Chemistry, 2009. **19**(15): p. 2131-2134.

73. Ma, L., C. Abney, and W. Lin, *Enantioselective catalysis with homochiral metal–organic frameworks.* Chemical Society Reviews, 2009. **38**(5): p. 1248-1256.

74. An, J., S.J. Geib, and N.L. Rosi, *Cation-Triggered Drug Release from a Porous Zinc−Adeninate Metal−Organic Framework.* Journal of the American Chemical Society, 2009. **131**(24): p. 8376-8377.

75. Horcajada, P., et al., *Metal–organic frameworks as efficient materials for drug delivery.* Angewandte chemie, 2006. **118**(36): p. 6120-6124.

76. Vinu, A. and K. Ariga, *New ideas for mesoporous materials.* Advanced Porous Materials, 2013. **1**(1): p. 63-71.

77. Zhou, Z. and M. Hartmann, *Progress in enzyme immobilization in ordered mesoporous materials and related applications.* Chemical Society Reviews, 2013. **42**(9): p. 3894-3912.

78. Ariga, K., et al., *Materials nanoarchitectonics for environmental remediation and sensing.* Journal of Materials Chemistry, 2012. **22**(6): p. 2369-2377.

79. Li, J.-R., J. Sculley, and H.-C. Zhou, *Metal–organic frameworks for separations.* Chemical reviews, 2011. **112**(2): p. 869-932.

80. Ahmed, I. and S.H. Jhung, *Composites of metal–organic frameworks: preparation and application in adsorption.* Materials today, 2014. **17**(3): p. 136-146.

81. Khan, N.A., Z. Hasan, and S.H. Jhung, *Adsorption and removal of sulfur or nitrogen-containing compounds with metal-organic frameworks (MOFs).* Advanced Porous Materials, 2013. **1**(1): p. 91-102.

82. Khan, N.A., Z. Hasan, and S.H. Jhung, *Adsorptive removal of hazardous materials using metal-organic frameworks (MOFs): a review.* Journal of hazardous materials, 2013. **244**: p. 444-456.

83. Haque, E., et al., *Adsorptive removal of methyl orange from aqueous solution with metal-organic frameworks, porous chromium-benzenedicarboxylates.* Journal of hazardous materials, 2010. **181**(1-3): p. 535-542.

84. Abid, H.R., H.M. Ang, and S. Wang, *Effects of ammonium hydroxide on the structure and gas adsorption of nanosized Zr-MOFs (UiO-66).* Nanoscale, 2012. **4**(10): p. 3089-3094.

85. Mouni, L., et al., *Removal of Methylene Blue from aqueous solutions by adsorption on Kaolin: Kinetic and equilibrium studies.* Applied Clay Science, 2018. **153**: p. 38-45.

86. Hameed, B. and A. Rahman, *Removal of phenol from aqueous solutions by adsorption onto activated carbon prepared from biomass material.* Journal of Hazardous Materials, 2008. **160**(2): p. 576-581.

87. Ho, Y.-S. and G. McKay, *Pseudo-second order model for sorption processes.* Process biochemistry, 1999. **34**(5): p. 451-465.

88. Wang, S., H. Li, and L. Xu, *Application of zeolite MCM-22 for basic dye removal from wastewater.* Journal of colloid and interface science, 2006. **295**(1): p. 71-78.

89. Pathania, D., S. Sharma, and P. Singh, *Removal of methylene blue by adsorption onto activated carbon developed from Ficus carica bast.* Arabian Journal of Chemistry, 2017. **10**: p. S1445-S1451.

90. Lin, S.-H. and R.-S. Juang, *Adsorption of phenol and its derivatives from water using synthetic resins and low-cost natural adsorbents: a review.* Journal of environmental management, 2009. **90**(3): p. 1336-1349.

91. Zaboon, S., et al., *Removal of monoethylene glycol from wastewater by using Zr-metal organic frameworks.* Journal of Colloid and Interface Science, 2018. **523**: p. 75-85.

92. Abid, H.R., et al., *Nanosize Zr-metal organic framework (UiO-66) for hydrogen and carbon dioxide storage.* Chemical Engineering Journal, 2012. **187**: p. 415-420.

93. Abid, H.R., et al., *Adsorption of CH4 and CO2 on Zr-metal organic frameworks.* Journal of colloid and interface science, 2012. **366**(1): p. 120-124.

94. Lagergren, S., *About the theory of so-called adsorption of soluble substances.* Sven. Vetenskapsakad. Handingarl, 1898. **24**: p. 1-39.

95. Wu, Z., et al., *Adsorptive removal of methylene blue by rhamnolipid-functionalized graphene oxide from wastewater.* Water Research, 2014. **67**: p. 330-344.

96. Gupta, N., A.K. Kushwaha, and M.C. Chattopadhyaya, *Application of potato (Solanum tuberosum) plant wastes for the removal of methylene blue and malachite green dye from aqueous solution.* Arabian Journal of Chemistry, 2016. **9**: p. S707-S716.

97. Chen, L., et al., *High performance agar/graphene oxide composite aerogel for methylene blue removal.* Carbohydrate Polymers, 2017. **155**: p. 345-353.

98. Fan, S., et al., *Removal of methylene blue from aqueous solution by sewage sludge-derived biochar: Adsorption kinetics, equilibrium, thermodynamics and mechanism.* Journal of Environmental Chemical Engineering, 2017. **5**(1): p. 601-611.

99. Kumar, A. and H.M. Jena, *Removal of methylene blue and phenol onto prepared activated carbon from Fox nutshell by chemical activation in batch and fixed-bed column.* Journal of Cleaner Production, 2016. **137**: p. 1246-1259.

100. Albadarin, A.B., et al., *Activated lignin-chitosan extruded blends for efficient adsorption of methylene blue.* Chemical Engineering Journal, 2017. **307**: p. 264-272.

101. Asfaram, A., et al., *Rapid removal of Auramine-O and Methylene blue by ZnS:Cu nanoparticles loaded on activated carbon: A response surface methodology approach.* Journal of the Taiwan Institute of Chemical Engineers, 2015. **53**: p. 80-91.

102. Roosta, M., et al., *Optimization of the ultrasonic assisted removal of methylene blue by gold nanoparticles loaded on activated carbon using*

experimental design methodology. Ultrasonics Sonochemistry, 2014. **21**(1): p. 242-252.

103. Auta, M. and B.H. Hameed, *Chitosan–clay composite as highly effective and low-cost adsorbent for batch and fixed-bed adsorption of methylene blue.* Chemical Engineering Journal, 2014. **237**: p. 352-361.

104. Ho, Y. and G. McKay, *The sorption of lead (II) ions on peat.* Water research, 1999. **33**(2): p. 578-584.

105. Bhattacharyya, K.G. and A. Sharma, *Kinetics and thermodynamics of methylene blue adsorption on neem (Azadirachta indica) leaf powder.* Dyes and pigments, 2005. **65**(1): p. 51-59.

106. Mahmoudi, K., et al., *Kinetics and equilibrium studies on removal of methylene blue and methyl orange by adsorption onto activated carbon prepared from date pits-A comparative study.* Korean Journal of Chemical Engineering, 2015. **32**(2): p. 274-283.

107. Ghaedi, M., et al., *Application of least squares support vector regression and linear multiple regression for modeling removal of methyl orange onto tin oxide nanoparticles loaded on activated carbon and activated carbon prepared from Pistacia atlantica wood.* Journal of Colloid and Interface Science, 2016. **461**: p. 425-434.

108. Langmuir, I., *The constitution and fundamental properties of solids and liquids. II. Liquids.* Journal of the American Chemical Society, 1917. **39**(9): p. 1848-1906.

109. Freundlich, H., *Über die adsorption in lösungen.* Zeitschrift für physikalische Chemie, 1907. **57**(1): p. 385-470.

110. Hameed, B.H., D.K. Mahmoud, and A.L. Ahmad, *Sorption of basic dye from aqueous solution by pomelo (Citrus grandis) peel in a batch system.* Colloids and Surfaces A: Physicochemical and Engineering Aspects, 2008. **316**(1): p. 78-84.

111. Fu, J., et al., *Adsorption of methylene blue by a high-efficiency adsorbent (polydopamine microspheres): Kinetics, isotherm, thermodynamics and mechanism analysis.* Chemical Engineering Journal, 2015. **259**: p. 53-61.

112. Hameed, B.H., A.T.M. Din, and A.L. Ahmad, *Adsorption of methylene blue onto bamboo-based activated carbon: Kinetics and equilibrium studies.* Journal of Hazardous Materials, 2007. **141**(3): p. 819-825.

113. Haque, E., J.W. Jun, and S.H. Jhung, *Adsorptive removal of methyl orange and methylene blue from aqueous solution with a metal-organic framework material, iron terephthalate (MOF-235).* Journal of Hazardous Materials, 2011. **185**(1): p. 507-511.

114. Huang, J.-H., et al., *Adsorption of Rhodamine B and methyl orange on a hypercrosslinked polymeric adsorbent in aqueous solution.* Colloids and Surfaces A: Physicochemical and Engineering Aspects, 2008. **330**(1): p. 55-61.

115. Haque, E., et al., *Adsorptive removal of methyl orange from aqueous solution with metal-organic frameworks, porous chromium-benzenedicarboxylates.* Journal of Hazardous Materials, 2010. **181**(1): p. 535-542.

116. Chen, D., et al., *Characterization of anion–cationic surfactants modified montmorillonite and its application for the removal of methyl orange.* Chemical Engineering Journal, 2011. **171**(3): p. 1150-1158.

117. Annadurai, G., R.-S. Juang, and D.-J. Lee, *Use of cellulose-based wastes for adsorption of dyes from aqueous solutions.* Journal of hazardous materials, 2002. **92**(3): p. 263-274.

118. Gurusamy, A., *L. Duu-Jong (2002). Use of cellulose-based wastes for adsorption of dyes from aqueous solutions.* J. Hazard. Mater. B. **92**: p. 263-274.

119. Zhuannian, L., et al., *Adsorption behavior of methyl orange onto modified ultrafine coal powder.* Chinese Journal of Chemical Engineering, 2009. **17**(6): p. 942-948.

120. Zhu, H.-Y., R. Jiang, and L. Xiao, *Adsorption of an anionic azo dye by chitosan/kaolin/γ-Fe2O3 composites.* Applied Clay Science, 2010. **48**(3): p. 522-526.

121. Iida, Y., et al., *Sonochemically enhanced adsorption and degradation of methyl orange with activated aluminas.* Ultrasonics, 2004. **42**(1-9): p. 635-639.

122. Küçükosmanoğlu, M., O. Gezici, and A. Ayar, *The adsorption behaviors of Methylene Blue and Methyl Orange in a diaminoethane sporopollenin-mediated column system.* Separation and Purification Technology, 2006. **52**(2): p. 280-287.

Chapter 4

Bimetal Ca-modified Zr-MOFs to enhance methylene blue removal in wastewater

4

Chapter 4: Bimetal Ca-modified Zr-MOFs to enhance methylene blue removal in wastewater

4.1 Abstract

In this study, parent Zr-MOF and two improved versions of UiO-66 metal organic frameworks (MOFs) were synthesised successfully: UiO-66, UiO-66-10%Ca and UiO-66-30%Ca. The syntheses aimed to remove the harmful pollutant, a cationic dye (methylene blue (MB)) from wastewater. Competition between the abovementioned MOFs was done to know which one most favourable. Adsorption techniques, along with safe laboratory rule, were investigated to identify the optimal concentration of solute on adsorbent. Based on the results, UiO-66-10%Ca exhibited the highest adsorption capacity with maximum Langmuir capacity of 50.25 mg g^{-1}, with UiO-66-30%Ca and UiO-66 displaying lower loading. Langmuir and Freundlich models were employed to describe isotherms. A kinetics study was achieved by fitting pseudo first-order and pseudo second-order equations. In addition, an intraparticle diffusion model was utilised. The results presented here may facilitate the further enhancement of UiO-66 MOFs and advance the synthesis of bimetal MOFs in future research to be applied in the field of wastewater treatment.

4.2 Introduction

Dyes exist where there is civilisation. They are used to colour products, and are employed in various industries, such as the food, paper, carpet, rubber, plastic, cosmetic, acrylic, wool, nylon, silk and textile industry [1-3].

Cationic methylene blue (tetramethylthionine chloride [MB])[4] is a basic thiazine dye (Figure 4.1)[5]. It is broadly utilised to colour textile, print calico and cotton, dye leather and as a general dye and tannin. These processes involve oxidation−reduction, and to dye leather, a purified zinc-free form is used. It is also used as antiseptic and for other medicinal purposes [6, 7]. As a basic dye, MB is not strongly hazardous, but may cause some harmful effects on humans and aquatic lives. It is also resistant to biological degradation)[8]. Acute exposure to MB can cause increased heart rate, vomiting, shock, cyanosis, jaundice, quadriplegia, Heinz body formation and tissue necrosis in humans [7, 9, 10].

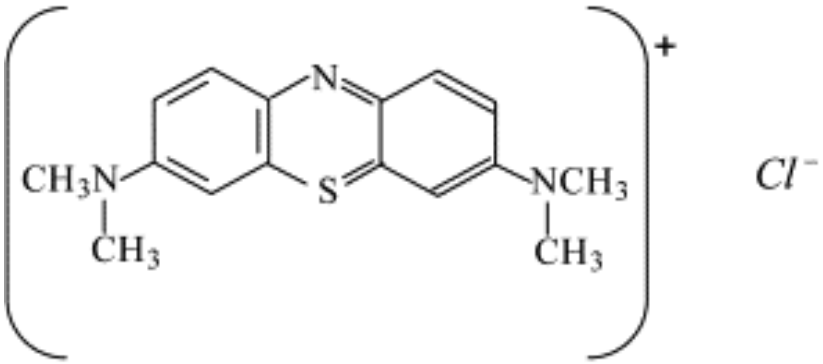

Figure 4.1: Chemical structure of MB [1].

Water is a precious resource for all living creatures on earth. A significant environmental challenge is the removal of dye pollutants from fabric and textile wastewater. Runoffs from colouring firms and associated industrial processes are renowned for being extremely coloured. More than 100,000 dyes are used in commercial manufacturing processes to produce over 7×10^5 metric tonnes per year. It is calculated that some dyestuffs (5–10%) are discharged in industrial waste throughout production processes [1, 11-13]. However, in the textile dyeing process the percentage of dye that ends up in the effluent can reach 50% as a result of weak dye-fibre fixation [7, 14]. The use of dyes to colour products consumes significant volumes of water; consequently, a substantial amount of coloured wastewater can be generated [15]. Coloured sewer water runoffs from the abovementioned industries into natural watercourses have increased wastewater toxicity, chemical oxygen demand of effluent and reduced light penetration, which has had devastating results on photosynthetic phenomena [13]. Aesthetically, the presence of dyes in surface and underground waters is not safe, pleasant or welcomed. Consequently, some governments have attempted to prevent the discharge of wastewater into natural streams without appropriate screening and treating [16].

Many approaches to dye removal have been proposed to treat the industrial wastewater [6, 17]. The techniques are classified into three main types: physical, chemical and biological treatments. These techniques employ aerobic and anaerobic microbial degradation, coagulation and chemical oxidation, membrane separation process, electrochemical processes, filtration, softening and reverse osmosis. However,

limitations exist in all abovementioned methods and none were effective in removing dyes from runoffs [18].

Its low cost, easy availability, simplicity of design, high efficiency, ease of operation, biodegradability and ability to treat dyes in more concentrated forms, make the adsorption technique the simplest process for dye removal [10, 19]. While activated carbon is presently believed to be the most operative adsorbent, its high cost means its production and regeneration remain uneconomical [20, 21]. The use of biological and chemical precipitation to remove colour is efficient and economic where dye concentrations are relatively high [9]. The advantages and disadvantages of various methods of dye removal from wastewaters are chronically occured [22]. Of the variety of physicochemical systems investigated, adsorption is considered the most effective technique [7, 23].

The limitations of using activated carbons have led researchers to seek low-priced dye sorbents, such as coal, fly-ash, silica gel, wool waste, agricultural waste, wood waste, and clay materials [10, 24]. Researchers have successfully demonstrated the removal of MB from aqueous solutions using low-cost materials, such as rice husk [9], Indian rosewood sawdust [22], neem leaf powder [2], pumice powder [24], pyrophyllite [25], perlite [26], jute processing waste [27], eggshells [28] and fly-ash [29].

In recent years, research and development in the field of design and synthesis of MOFs has led to a rapid growth in practical and conceptual developments [30-35]. An extensive class of crystalline materials has become available because of MOF chemistry, which has superior characteristics such as high stability, tuneable metrics, organic functionality and porosity [30].

Its exceptional porousness means that MOFs have potentially numerous applications; their demonstrated applications in gas storage, separations, catalysis, energy technology fuel cells, supercapacitors and catalytic conversions has made them objects of intensive study, industrial-scale production and application [36-39].

The unique characteristics of MOF-type substances that make them the focus of much worldwide research are their pore geometry and high porosity [40, 41], their central metals [42, 43], open metal sites [44, 45], functionalised linkers [46, 47] and their loading of active species [48, 49]. All these characteristics have been scientifically employed to successfully improve interactions between the sorbates and MOFs.

Specifically, these characteristics distinguish MOFs from other porous material in the field of adsorption processes for the effective removal of hazardous compounds [50]. Accordingly, MOFs are superior adsorbents because of their various host-guest interactions, acid-base [51, 52], π-complexation [53], H-bonding [54, 55] and coordination with open metal sites [44, 45, 50, 56, 57].

In the present study, Modified Zr-MOFs (UiO-66-Ca) of extremely high porosity and easy tunability of pore size and shape (from the microporous to the mesoporous scale) were used as sorbents to remove MB from an aqueous solution. UiO-66 was improved by changing the connectivity of the inorganic moiety and as a result of the nature of organic linkers [30, 50, 58]. MB was selected as a model pollutant to evaluate the capacity of Zr-MOFs to remove dyes from contaminated water. Calcium has chosen to modify Zr-MOF due to their atomic size in comparison to zirconium. A series of single metal and bimetal Zr-MOFs samples with various ratios of Ca/Zr were successfully and solvothermally obtained by direct synthesis, followed by activation processes with methanol with some modifications. The performance of UiO-66 was further enhanced for the removal of MB with improving its textural properties and open metal sites through the introduction of second metal such (Ca) into the framework in the synthesis process.

A kinetics study was conducted using pseudo first order and pseudo second order models as well as intraparticle diffusion. Further, an equilibrium study was undertaken using Langmuir and Freundlich isotherms.

4.3 Materials and methods

4.3.1 Synthesis and activation

All chemicals were supplied by Sigma-Aldrich (Australia) without further purifications.

Zr-MOF was synthesised successfully using a scaled-up procedure of a previously reported method [59] by modifying the $ZrCl_4$:BDC:DMF ratio: 2.27 mmol of $ZrCl_4$ and 2.27 mmol 1,4-benzenedicarboxylic acid (BDC) were added with continuous stirring to 405.38 mmol of N, N-dimethylformamide (DMF) in a solvothermal process in an autoclave at 393 K for 24 h. The produced Zr-MOF was immersed in chloroform

for 5 days as activation process. After the activation process, the solid was filtered and dried under vacuum at 463 K for 48 h.

UiO-66-10%Ca was synthesised by mixing $ZrCl_4$ (1.5 g) with terephthalic acid (1.1 g) in 73 mL of DMF. After mixing for 15 min, 0.15 g of Ca $(NO3)_2.4H_2O$ was added and followed by the addition of 2 mL of H_2O to the mixture. The solution was mixed for approximately 30 min; then transferred into a 125-mL Teflon-lined autoclave, which was tightly sealed and placed in a preheated oven at 132°C for 1 d.

UiO-66-30%Ca was synthesised by mixing $ZrCl_4$ (1.5 g, 6.44 mmol) with terephthalic acid (1.3 g, 7.82 mmol) in 70 mL of DMF. After mixing for 30 min, $Ca(NO_3)_2.4H_2O$ (0.45 g, 2.86 mmol, 99%; Sigma-Aldrich), followed by 5 mL of deionised water, was added into the mixture eventually, the mixture was transferred to a Teflon-lined autoclave that was tightly sealed and moved into a preheating oven at 430 K. The product was then filtered, dried and immersed in absolute methanol (100%, Sigma-Aldrich) for 5 d, after which it was filtered, dried and heated under vacuum at 473 K overnight before use as adsorbent.

4.3.2 Characterisation

The thermal stability of UiO-66, UiO66-10%Ca and UiO66-30%Ca was assessed by a thermogravimetric analysis (TGA) instrument (TGA/DSC1 STARe system; Mettler-Toledo). The samples were loaded into a pan and heated to 1173 K at a rate of 5 K/min. The air gas flow rate was maintained at 10 mL/min. FTIR spectra (Spectrum 100 FT-IR spectrometer, PerkinElmer, Waltham, USA) were obtained to assess the stability of the functional groups on the organic ligands. The spectra were scanned from 600 to 4000 cm^{-1} with a resolution of 4 cm^{-1} using an attenuated total reflectance technique. X-ray powder diffraction and patterns were obtained with an X-ray diffractometer (D8 Advance, Bruker AXS) using Cu Kα radiation (λ = 1.5406 Å) with accelerating voltage and current of 40 kV and 40 mA, respectively. N_2 adsorption/desorption (Autosorb-1, Quantachrome Instruments) was used to determine N_2 isotherms as well as the pore size and surface area of the MOFs. The samples were evacuated at 473 K for 24 h prior to adsorption measurements under high vacuum. The sample was then analysed to determine surface area, pore size and pore volume.

4.3.3 Adsorption process

An aqueous stock solution of MB (1000 ppm) was prepared by dissolving MB ($C_{16}H_{18}ClN_3S$, molecular weight 319.85 $g.mol^{-1}$; Sigma-Aldrich) in deionised water. Aqueous solutions with different concentrations of MB (5–100 ppm) were prepared by successive dilution of the stock solution with water. After obtaining the UV spectra of the solutions with a spectrophotometer (UV spectrophotometer), the MB concentrations were determined using absorbance at 668 nm wavelength of the solutions. A calibration curve was obtained from the spectra of the standard solutions (5–100 ppm).

Prior to adsorption, the adsorbents were dried overnight under vacuum at 373 K. Several glass containers were cleaned, dried and filled to 20 mL with MB of different concentrations ranging from 5 to 50 ppm. An exact amount of the MOF adsorbent (20 mg) was then put in each container.

The dye solutions containing the adsorbents were mixed well with a magnetic stirrer and maintained for 5 min to 24 h at 298 K. Samples for analysis were collected by a syringe filter at different sampling intervals. UV spectrometer was used to investigate the dye content in the supernatant. Adsorption mechanism and rate of diffusion were estimated using three kinetic models: pseudo first-order, pseudo second-order [60-62] and intraparticle diffusion model [63, 64]. The adsorbents' adsorption behaviours were simulated using the Freundlich and Langmuir adsorption isotherms [60-62, 65].

4.4 Results and discussion

4.4.1 Characterisation

Figure 4.3(a) compares the XRD pattern of UiO-66-Ca with that of UiO-66 before and after use in adsorption of MB. The results demonstrate that the integrity of the structure was maintained in all samples, which indicates that the synthesis and activation procedures succeeded reliably without suspected impurities of a metal oxide inside the pores.

Figure 4.3(b) shows that the spectra of all samples, including that of UiO-66 before and after use in adsorption of MB. They exhibit the same vibration bands with slight deviations in the position of some peaks with increases in the content of a second

metal. In addition, the peaks in the mixed-metal samples were broader than the peaks in the single-metal (Zr) sample, which indicates a difference in the dipole between ground state and excited state in the mixed-metal UiO-66 as a result of incorporating a second metal in the metal centre [66, 67]. The vibration band of 1615–1580 cm^{-1} was attributed to C=C-C stretching in the aromatic ring of terephthalate salts; however, this band extended from 1590 to 1525 cm^{-1} in the mixed-metal UiO-66 [68]. Further, the bands at 1500 and 1390 cm^{-1} were attributed to the stretching vibrations of symmetric COO^- and asymmetric COO^- in coordinated organic linkers, as shown in the spectrum of UiO-66.

Moreover, the weak bands at 881, 812 and 785 cm^{-1} were assigned to Zr-O whereas the peak at 730 cm^{-1} in the UiO-66 spectrum was assigned to the stretching vibration of C-H and out-of-plane bending of aromatic ring in the main skeleton of UiO-66; this peak was shifted to 744 cm^{-1} in the spectra of bimetal UiO-66 [67, 69]. In addition, the band at 1017 cm^{-1} belonged to C-H stretching in the MOF.

Table 4.1: Textural properties of the adsorbents based on N_2 adsorption/isotherm.

Adsorbents	Specific surface area (S_{BET}) (m^2g^{-1})	Pore volume (cc g^{-1})	Pore diameter (nm)
UiO-66	1585.5	0.82	1.04
UiO-66-10%Ca	918.115	1.10	2.39
UiO-66-30%Ca	557.681	0.25	0.91

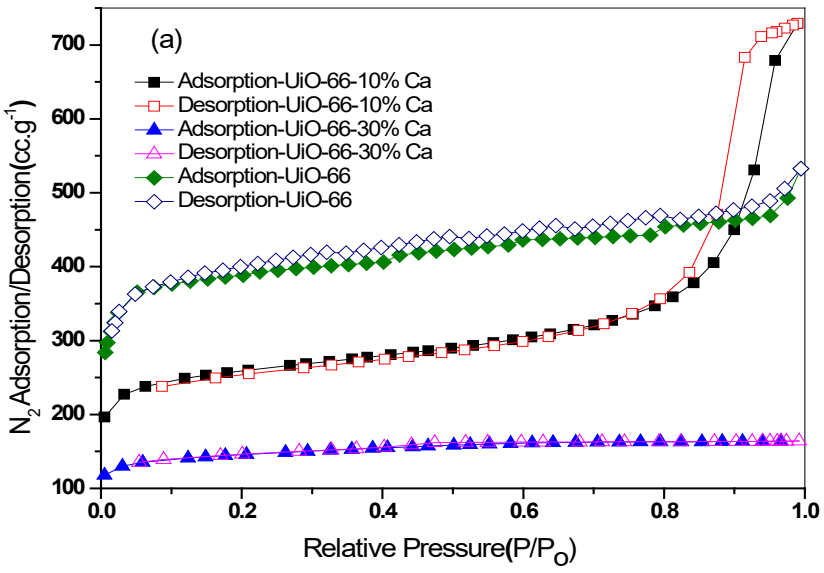

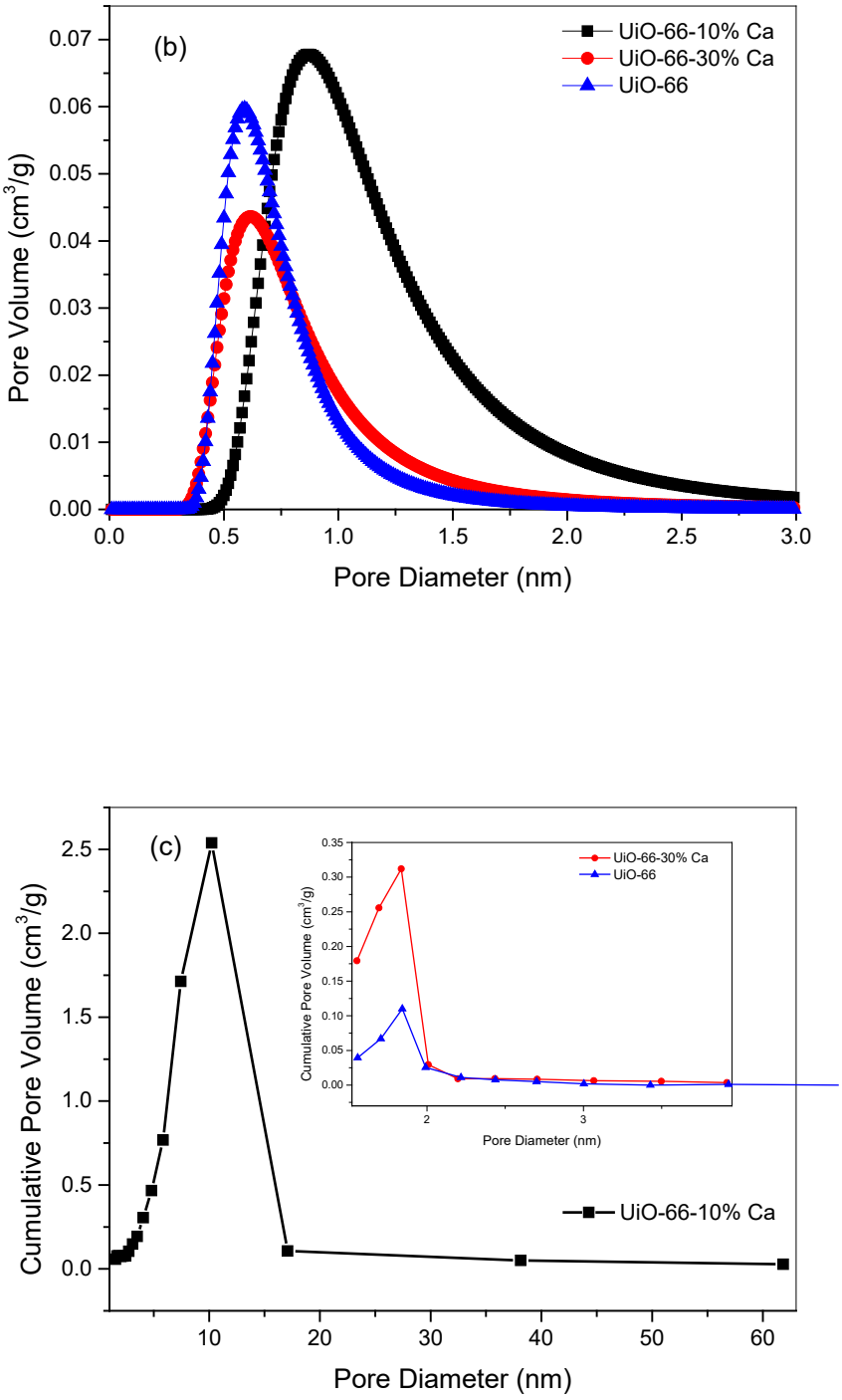

Figure 4.2: N_2 adsorption/desorption isotherm (a), micropore distribution (b) and mesopore distribution (c) of UiO-66, UiO-66-10% Ca and UiO-66-30% Ca.

Figure 4.2 (a) shows the N_2 adsorption/desorption isotherms for UiO-66-Ca and UiO-66. Hysteresis in the desorption isotherm is apparent and demonstrated by the Ca

content reducing with sharp increases in adsorption at relative pressures close to 0.999. This observation is strong evidence that the mesopore and macropore sizes were enhanced. Furthermore Figure 4.2 (b and c) illustrate micropore and mesopore distribution respectively.

In addition, Table 4.1 presents the textural properties of all adsorbents, according to the calculations of the N_2 adsorption isotherm. The specific surface area (S_{BET}) decreased with increasing content of a second metal. As shown in Table 4.1, the S_{BET} of parent UiO-66 was 1585.50 while with increasing the percentage of second metal (Ca), the S_{BET} of bimetal UiO-66 was impacted negatively to become 918.115 and 557.68 m^2g^{-1} for UiO-66-10%Ca and UiO-66-30%Ca, respectively.

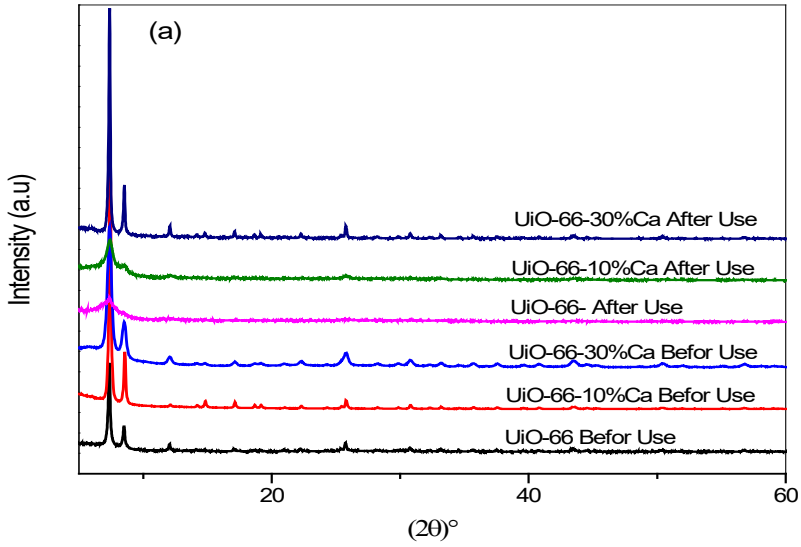

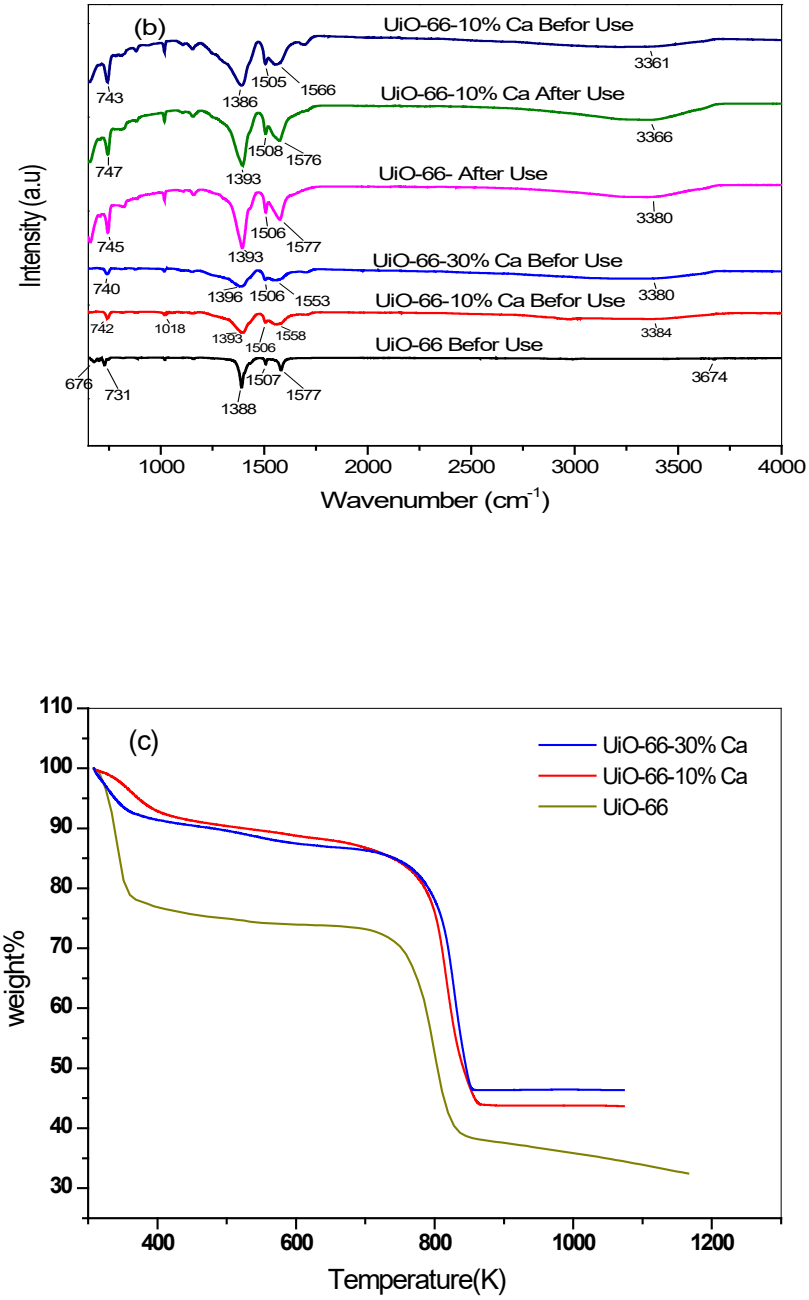

Figure 4.3: Characterisation of pristine and modified Zr-MOF samples. (a) PXRD patterns, (b) FTIR spectra and (c) TGA profiles.

However, the pore volume and average pore size were enhanced in the MOFs with the lowest content of the second metal. The highest pore volume and pore size were seen in UiO-66-10%Ca, which were 1.10 cc g^{-1} and 2.39 nm, respectively. The results indicate that the addition of low concentrations case of the second metal in the single-

pot synthesis enhance the pore volume and pore diameter. Also, the activation process using the solvent exchange method to replace the unreacted materials and by-product by methanol molecules which were discarded by the heating in the second stage of the activation process, further improve the textural properties.

Figure 4.3(c) presents the results of thermogravimetric analysis for all adsorbents in this study. All samples appear to have the same thermal stability, with structural stability at increasing temperatures up to 725 K.

4.4.2 Adsorption study

Adsorbed amounts of MB by the Zr-MOFs at each time interval of time, the equilibrium and percentage removal of MB were computed according to the

following equations:

$$q_t = (C_0 - C_t)\frac{V}{m} \tag{4.1}$$

$$q_e = (C_0 - C_e)\frac{V}{m} \tag{4.2}$$

$$R\% = \frac{(C_0 - C_t)}{C_0} X100, \tag{4.3}$$

Where:

q_t: the amount of MB adsorbed per unit weight of MOF at any time t (mg/g)

q_e: the amount of MB adsorbed per unit weight of MOF at equilibrium (mg/g)

C_0: the initial concentration of the MB solution at time zero (mg/L)

C_t: the concentration of the MB solution at time t (mg/L)

C_e: the concentration of the MB solution at equilibrium (mg/L)

V: volume of the MB solution in batch adsorption process (L)

R%: percentage removal of MB [8]

m: Zr-MOF mass used in adsorption batch process (g)[1, 8, 70].

Figure 4.4 below describes the adsorption kinetics of MB by single-metal Zr-MOF and bimetal Zr-MOF-Ca. The figure shows the amount of dye adsorbed (mg/g) given the contact time (min) at various initial concentrations of MB. The graphs in this figure demonstrate that for all MB concentrations, MB uptake at the commencement of the

adsorption process is very rapid; after an initial period of time, it proceeds at a slower rate until the end of reaction when saturation is attained [13, 71, 72].

This phenomenon can be explained thus: the first available MB (cationic dye) molecules are favourably adsorbed onto the most active sites (anionic sites and benzene ring) of the single-metal and bimetal Zr-MOF, and the high initial MB uptake is possible because of the accessibility of many active sites. A longer contact time between the MOFs and MB results in more removal of MB until equilibrium adsorption capacity is reached [72]. Another explanation is that higher initial concentrations of MB provides more MB molecules and greater driving force of the aqueous phase (MB) against the solid phase (MOFs) to overcome mass-transfer resistance. This fact gives rise to increased collisions between MB molecules and active sites on the adsorbent [73-76]. For instance, Figure 4.6a illustrates the adsorption capacity for MB onto UiO-66 at equilibrium which increased from 2.151 to 14.837 mg g^{-1} with increase in MB initial concentration from 5 to 50 mg L^{-1}.

Recent research has revealed that initial concentration of MB has a detrimental effect on adsorption process. Several factors, including initial concentration of MB, play a role in determining percentage removal of MB (R%) and equilibrium adsorption capacity (q_e); indeed, the initial concentration of MB has profound consequences for R% and q_e. The initial concentration of MB has been observed to have a positive relationship with q_e and a negative relationship with R%. It is now understood that initial concentrations of MB play an important role in the removal of dye [72, 77]. The observed decrease in MB removal (R% values of 43.03% to 29.67%) by UiO-66 was representative of the adsorption process in all systems, and confirmed the occupation of all accessible active sites on the UiO-66 above a certain concentration of MB. However, the increase in equilibrium adsorption capacity (q_e) from 2.15 to 14.83 mg/g can be attributed to the higher adsorption rate and the use of all available active sites on UiO-66 for sorption at higher concentrations of MB.

4.4.2.1 Effect of pH

It is crucial step to investigate the effects of pH and zeta potential of Zr-MOF on adsorption process to examine adsorption mechanism. The result of such study is very important to figure out the impact of the electrostatic interactions on adsorption. pH was selected in such a way to cover acidic and basic range between 3.75-10 and the

adsorption process carried out at condition of initial concentration of MB solutions at 50 ppm and using 0.1 M HCl and 0.1 M NaOH to adjust pH. As show in Figure 4.4 a that adsorption uptake increases with increasing of pH solution from 3.75 to 10, indicating the role of electrostatic attraction between negatively charged adsorbent and cationic dye (MB). At pH equal to 5.6 which pH of isoelectric point (pH_{iep}) Figure 4.4 (b) with no charge on adsorbent, the uptake still high signifying that other factors play roles in adsorption of adsorbate while if pH less than pH_{iep} the adsorption capacity decreases steeply due to repulsion between adsorbate and adsorbent. Consequently UiO-66 can be used over a wide range of pH for discolouration of wastewater at large scale. Figure 4.5 illustrates plausible mechanism was proposed based on pH effect and Zeta potential of UiO-66. It can be concluded from the results that the adsorption mechanism of MB onto Zr-MOF is mainly depended on the electrostatic interactions between the cationic dye of positive charge and UiO-66 of positive charge. In addition, π–π interactions between the benzene rings of UiO-66 and those of the dye could have contributed to the adsorption process.

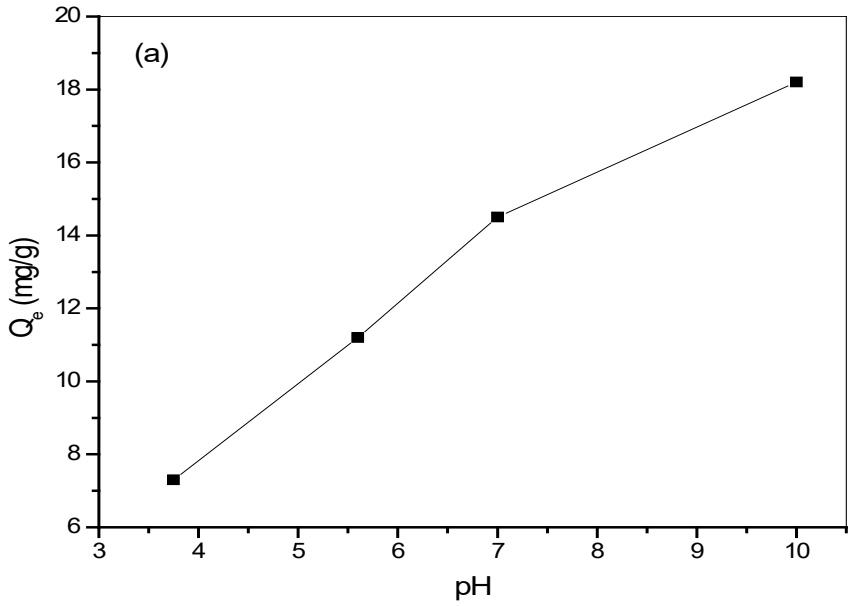

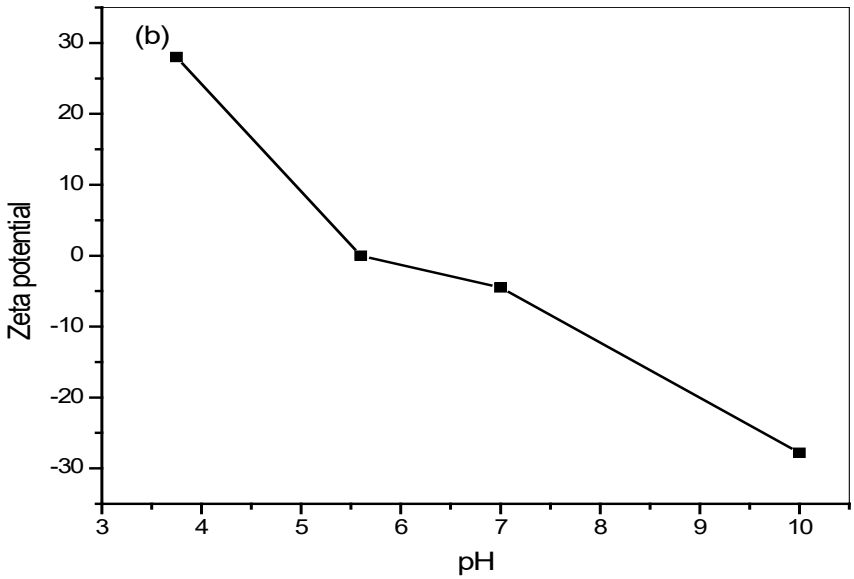

Figure 4.4: Effects of pH solution (a) and zeta potential of UiO-66 (b) on adsorption of MB onto UiO-66.

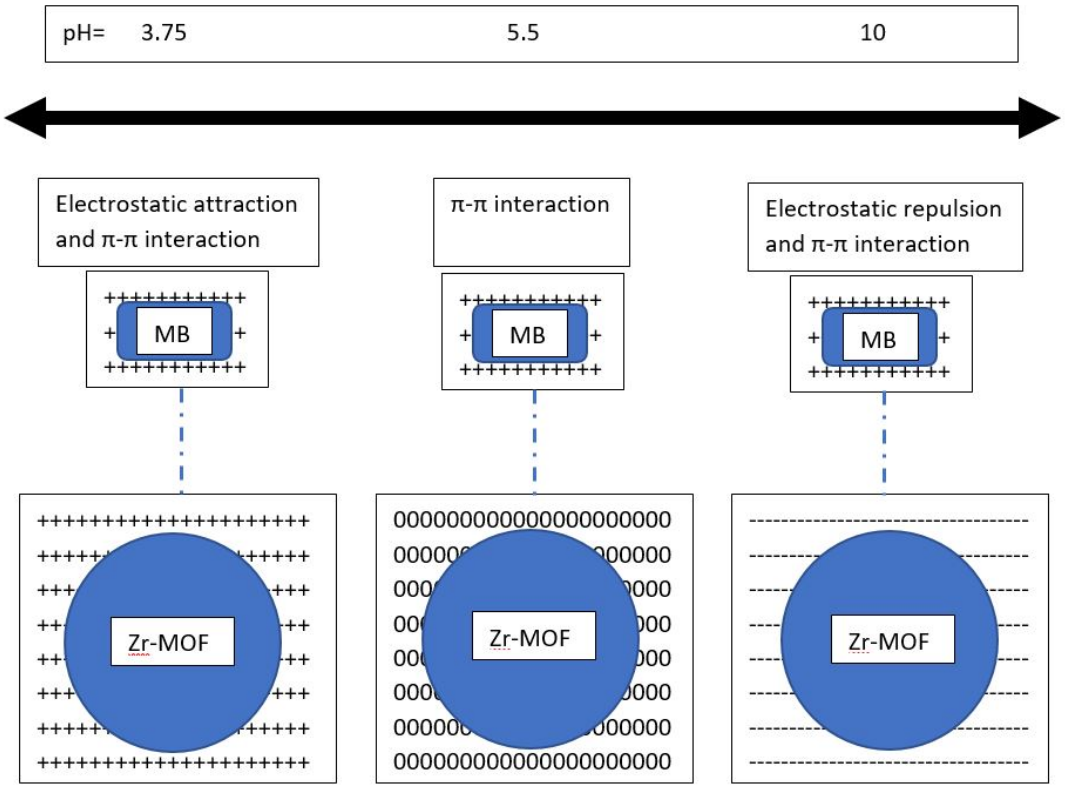

Figure 4.5: Plausible adsorption mechanism of MB onto Zr-MOF.

4.4.3 Kinetics study

The pseudo first-order and pseudo second-order model were employed for the adsorption of MB onto UiO-66, UiO-66-10%Ca and UiO-66-30%Ca. The linear

regression correlation, R^2, was calculated to identify the model of best fit; higher R^2 values means a better fit for the experimental data. The results of the correlational analysis of the amount of adsorbed dye (mg/g) against contact time, for the various initial concentrations of MB (5, 15, 30 and 50 ppm) are shown in Figure 4.6. The results indicate that the amount of dye loading (q_t [mg/g]) increases with contact time at each level of MB concentration. In addition, the amount of MB adsorbed increased with increases in initial MB concentration [70].

The kinetics of the adsorption process in the laboratory-based batch enables the prediction of the rate at which a pollutant is removed from bulk solutions, which informs the design of adsorption treatment plant columns [4]. However, the physical and chemical properties of the adsorbent significantly affect its adsorption kinetics, which in turn, affects the sorption mechanism [71]. Statistics from kinetics studies of pseudo first-order and pseudo second-order kinetics model equations have been investigated for fit with contact time data [71]. Tables 4.2 and 4.3 below present their main characteristics as calculated kinetic constants (k_1, k_2) and correlation coefficients (R^2) for C_i = 5, 15, 30 and 50 ppm. The nonlinear form of the Lagergren pseudo first-order kinetic equation can be written as follows [78, 79]:

$$\frac{dq}{dt} = k_1(q_e - q_t). \tag{4.4}$$

The linear form of the pseudo first-order kinetic equation can be expressed as follows:

$$l\,n(q_e - q_t) = l\,n(q_e) - k_1 t. \tag{4.5}$$

The nonlinear form of the pseudo second-order kinetic equation can be written as follows [80]:

$$\frac{dq}{dt} = k_2(q_e - q_t)^2. \tag{4.6}$$

The linear form of the pseudo second-order kinetic equation can be written as follows:

$$\frac{t}{q_t} = \frac{1}{k_2 \quad q_e^2} + \frac{1}{q_e}t, \tag{4.7}$$

Where:

q_e: the amount of MB adsorbed per unit weight of MOF at equilibrium (mg/g)

q_t: the amount of MB adsorbed per unit weight of MOF at any time t (mg/g)

k_1: pseudo first-order rate constant (min^{-1})

t: time (min)

k_2: pseudo second-order rate constant (g/mg min).

A linear plot of the pseudo first-order model ($\ln[q_e - q_t]$) against time provides the values for the kinetics sorption parameters, such as rate constant (k_1), equilibrium adsorption capacity (q_e) and the linear regression coefficient (R^2). Likewise, a linear plot of the pseudo second-order model (t/q_t) against time also provides the rate constant (k_2), equilibrium adsorption capacity (q_e) and the linear regression coefficient (R^2).

The values of these parameters for both plots are presented in Tables 4.2 and 4.3. According to the R^2 values obtained, they have been consistent and closer to unity for the pseudo second-order kinetic equation than for the pseudo first-order kinetic equation. Therefore, based on R^2 values, the sorption kinetics of MB removal using single-metal and bimetal Zr-MOF were well described by the pseudo second-order kinetic equation. Further, the calculated equilibrium adsorption capacity agreed with the experimental equilibrium adsorption capacity, further indicating that the sorption of aqueous MB onto single-metal and bimetal Zr-MOF perfectly obeyed pseudo second-order kinetics. Specifically, the sorption of MB by single and bimetal Zr-MOFs occurred through chemisorption (the exchange or sharing of electrons between the sorbate and sorbent via covalent forces and ion exchange)[80-82].

On the basis of the mechanism underlying pseudo second-order kinetics, the effects of the initial concentration on the adsorption kinetics of MB onto the three MOFs (i.e., all the sorbent systems) were similar over time. UiO-66-10% Ca was taken to be a representative adsorbent and was used to explain the effects of the initial concentration on the rate of adsorption. Table 4.2 shows that the adsorption rate constants (k_2) were 0.86348, 0.07616, 0.04628 and 0.02259 g mg^{-1} min^{-1} at initial MB concentrations of 5, 15, 30 and 50 mg L^{-1}, respectively, signifying a decrease in adsorption rate at higher initial concentrations of MB. Reductions in the amount adsorbed at higher initial concentrations may be due to MB molecules having to enter the pores through a longer diffusion path. On the other hand, with less amounts of MB adsorbed, MB molecules

tend to be rapidly adsorbed into the open pores of MOFs, which eventually increases the adsorption rate (k_2).

As shown in Table 4.2, the adsorption rate constants (k_2) for the initial MB concentration of 5 mg L^{-1} were computed as 0.86348, 0.01050 and 0.00498 g mg^{-1} min^{-1} for UiO-66-10% Ca, UiO-66 and UiO-66-30% Ca, respectively. These calculations take into account the pore diameter of the three sorbents (which from Table 4.1 are 2.39, 1.04 and 0.91 nm, respectively). The lower rate constant for MB adsorption onto the UiO-66-30% was tentatively ascribed to MB diffusion into the micropores of the MOF [83].

Table 4.2: Calculated kinetics constant (k_2) and correlation coefficient (R^2) for C_i = 5, 15, 30 and 50 ppm.

Adsorbent	Adsorbate	Pseudo second-order kinetics constant k_2 (g/(mg.min))							
		5 ppm		15 ppm		30 ppm		50 ppm	
		k_2	R^2	k_2	R^2	k_2	R^2	k_2	R^2
UiO-66	MB	0.01050	0.9989	0.00546	0.9992	0.00273	0.9992	0.00147	0.999
UiO-66-10% Ca	MB	0.86348	0.9999	0.07616	0.9963	0.04628	0.9999	0.02259	0.9998
UiO-66-30% Ca	MB	0.00498	0.9991	0.00212	0.9984	0.00167	0.9992	0.00217	0.9996

Table 4.3: Calculated kinetics constant (k_1) and correlation coefficient (R^2) for C_i = 5, 15, 30 and 50 ppm.

Adsorbent	Adsorbate	Pseudo first-order kinetics constant k_1 (min^{-1})							
		5 ppm		15 ppm		30 ppm		50 ppm	
		k_1	R^2	k_1	R^2	k_1	R^2	k_1	R^2
UiO-66	MB	0.0101	0.9888	0.0119	0.9920	0.0120	0.9925	0.0113	0.9813
UiO-66-10% Ca	MB	0.2669	0.9716	0.0913	0.9731	0.0395	0.9886	0.0370	0.9920
UiO-66-30% Ca	MB	0.0105	0.9930	0.0161	0.9636	0.0118	0.9927	0.0144	0.9960

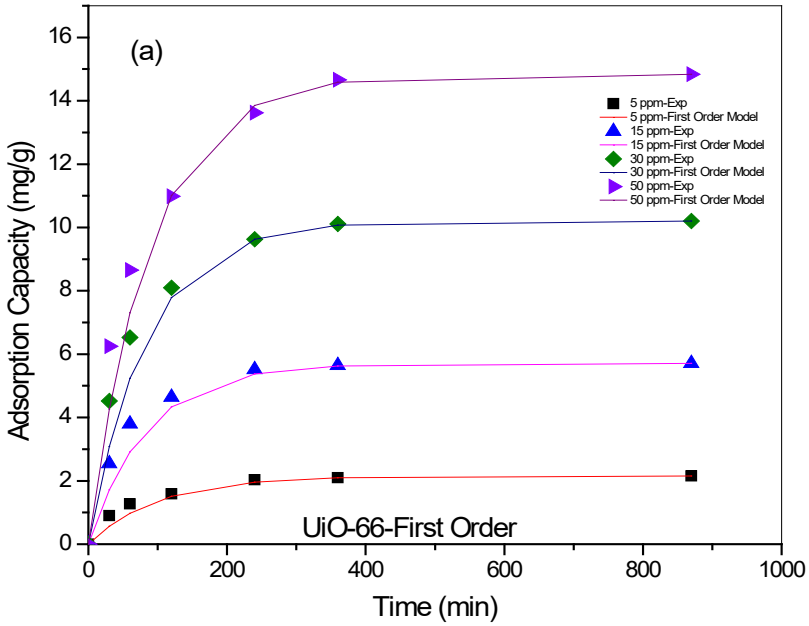
(a)
Adsorption Capacity (mg/g)
Time (min)
UiO-66-First Order
5 ppm-Exp
5 ppm-First Order Model
15 ppm-Exp
15 ppm-First Order Model
30 ppm-Exp
30 ppm-First Order Model
50 ppm-Exp
50 ppm-First Order Model

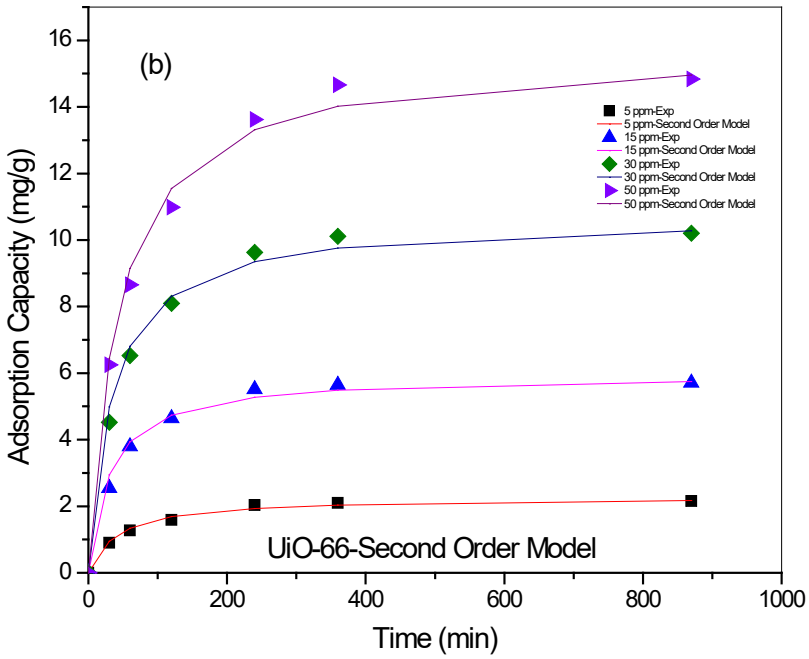
(b)
Adsorption Capacity (mg/g)
Time (min)
UiO-66-Second Order Model
5 ppm-Exp
5 ppm-Second Order Model
15 ppm-Exp
15 ppm-Second Order Model
30 ppm-Exp
30 ppm-Second Order Model
50 ppm-Exp
50 ppm-Second Order Model

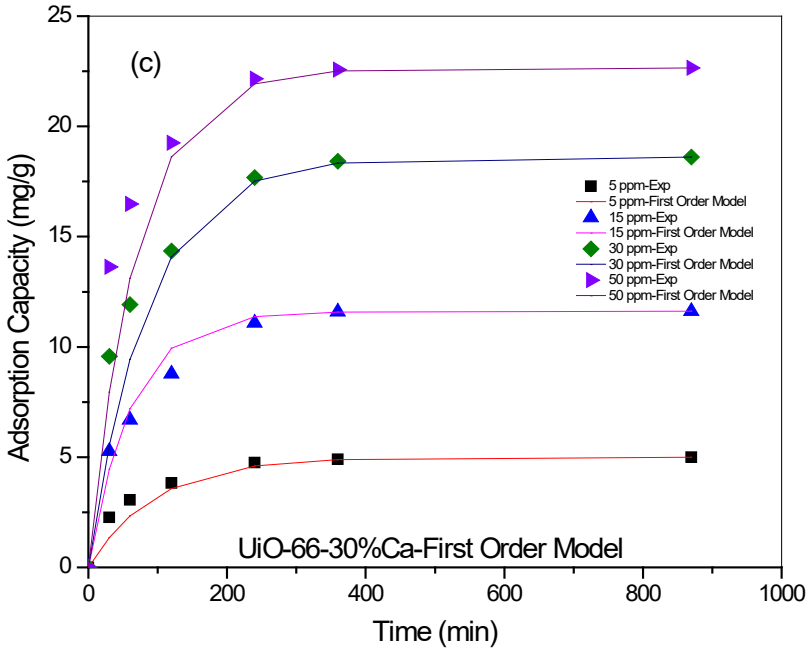
(c)
Adsorption Capacity (mg/g)
Time (min)
5 ppm-Exp
5 ppm-First Order Model
15 ppm-Exp
15 ppm-First Order Model
30 ppm-Exp
30 ppm-First Order Model
50 ppm-Exp
50 ppm-First Order Model
UiO-66-30%Ca-First Order Model

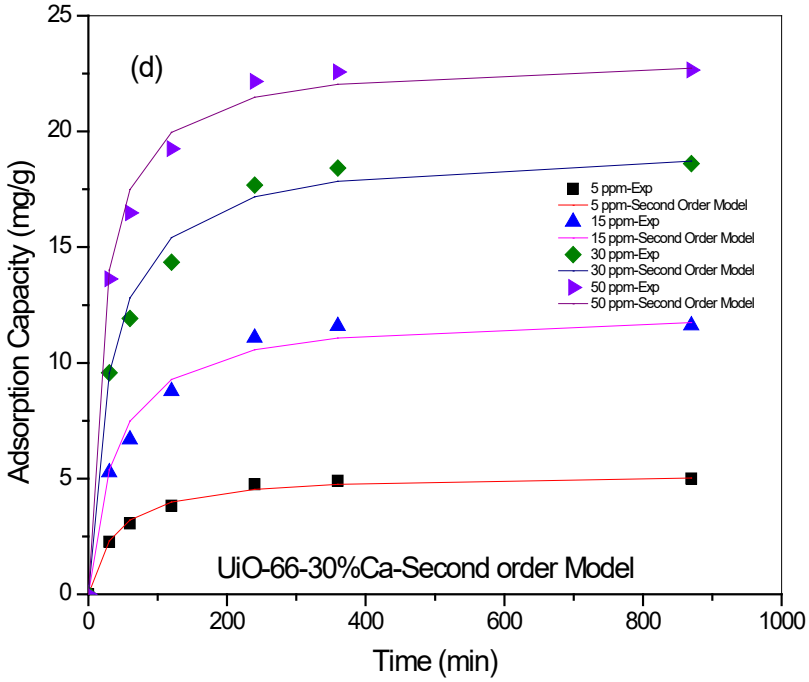
(d)
Adsorption Capacity (mg/g)
Time (min)
5 ppm-Exp
5 ppm-Second Order Model
15 ppm-Exp
15 ppm-Second Order Model
30 ppm-Exp
30 ppm-Second Order Model
50 ppm-Exp
50 ppm-Second Order Model
UiO-66-30%Ca-Second order Model

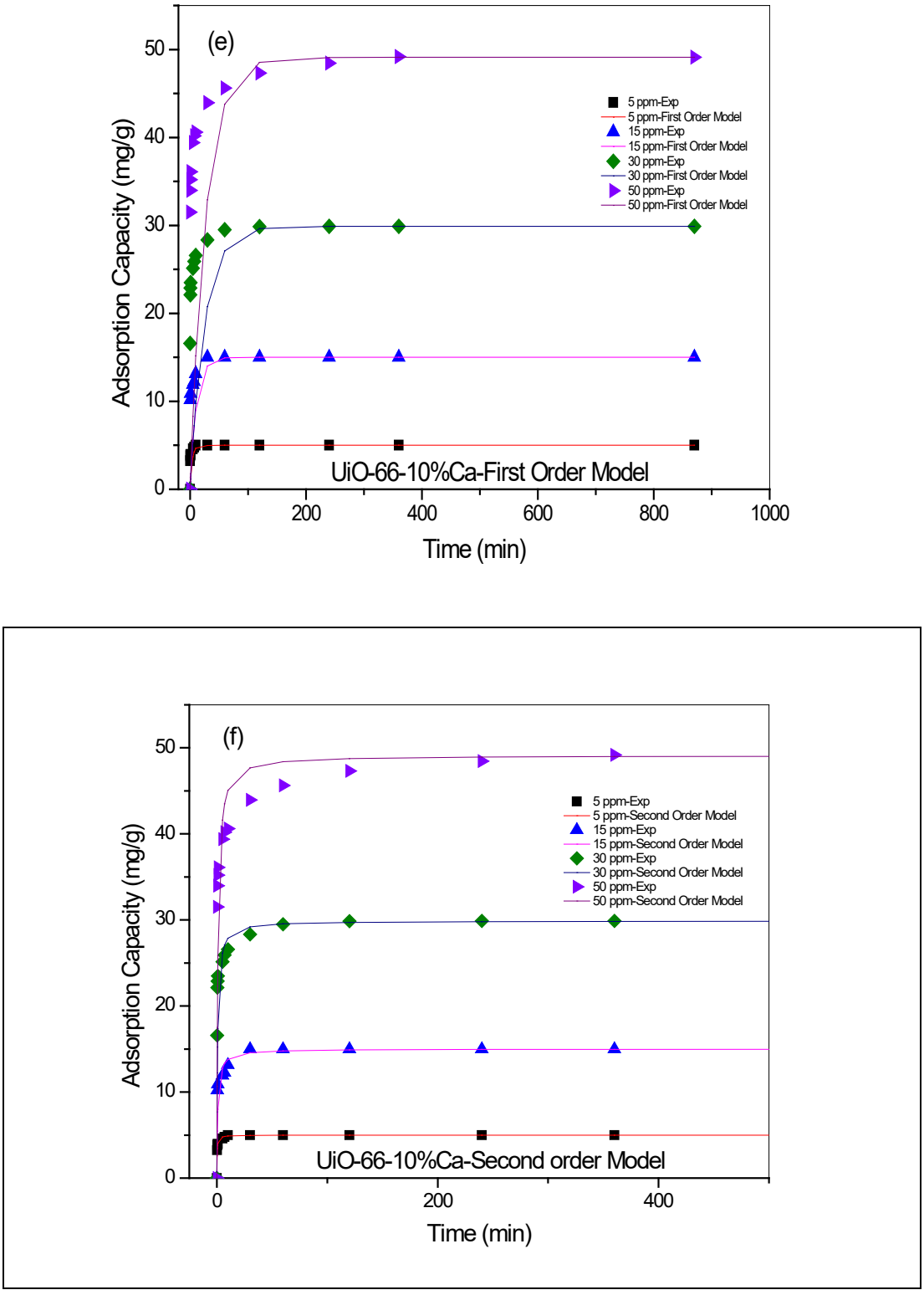

Figure 4.6 Fitting of experimental data by first-order and second-order kinetic models of MB adsorption onto UiO-66 (a, b), UiO-66-30%Ca (c, d) and UiO-66-10%Ca (e, f).

4.4.4 Equilibrium study

Equilibrium is crucial to understanding the adsorption process because it is a requirement in analysis and design of the adsorption column. Essential physiochemical data delivered by adsorption equilibria plays very important role in evaluating the applicability of the adsorption process as a unit [84]. Equilibrium isotherms were examined using the Langmuir and Freundlich isotherms.

The assumption of the Langmuir isotherm is monolayer coverage of sorbate over a sorbent with homogenous surface [8, 85, 86]. It assumes that the adsorption process occurs at specific homogenous sites over the adsorbent; that is, when an MB molecule occupies a specific site, additional sorption cannot happen again at the same site. Successful implantation of the Langmuir adsorption isotherm has been undertaken to explain the adsorption of basic dyes such as MB from aqueous solutions [8, 84, 87, 88].

The nonlinear form of the Langmuir isotherm can be expressed as:

$$q_e = \frac{q_m k_L C_e}{(1 + k_L C_e)}, \tag{4.8}$$

while the linear form can be written as [77]:

$$\frac{C_e}{q_e} = \frac{1}{q_m} C_e + \frac{1}{k_L q_m}, \tag{4.9}$$

Where:

q_m: Langmuir maximum loading capacity (mg/g)

k_L : the Langmuir constant related to the energy of adsorption and affinity of binding sites (L/mg)[89]

C_e: the equilibrium concentration of dye in solution (mg/L)

q_e: the amount of dye adsorbed at equilibrium per unit mass of sorbent (mg/g).

The equilibrium experimental data were fitted using the linear form of the Langmuir isotherm equation (Equation 4.9). Specifically, the Langmuir parameters q_m, K_L, and R^2 were obtained from the plot of (C_e/q_e) against C_e. Table 4.4 presents the results of the linear regression analysis.

The dimensionless constant separation factor, R_L, is vital to the Langmuir isotherm, and can be found in the following equation [86, 90-92]:

$$R_L = \frac{1}{(1 + k_L C_0)}, \tag{4.10}$$

Where C_0 is the initial concentration of adsorbate (mg/L) and K_L (L/mg) is the Langmuir constant.

The shape of the isotherm depends on R_L, because this factor indicates the adsorption process as:

- unfavourable ($R_L > 1$)
- linear ($R_L = 1$)
- favourable ($0 < R_L < 1$)
- irreversible ($R_L = 0$).

R_L must be between 0 and 1 to give rise to favourable adsorption. The calculated results for R_L are (0.89–0.44), (0.005–0.0005) and (0.28–0.03) for UiO-66, UiO-66-10%Ca and UiO-66-30%Ca, respectively. The separation factor (R_L) values for the sorption of MB onto single-metal and bimetal Zr-MOFs are in the range of $0 < R_L < 1$, indicating that the adsorption was favourable. Further, higher initial MB concentrations in the adsorption process can make it irreversible [93].

The Freundlich isotherm [8, 86, 94] is an empirical equation that assumes the adsorption process can occur over heterogeneous surfaces and adsorption capacity is associated with the concentration of MB dye at equilibrium. The nonlinear form of the Freundlich isotherm is written as:

$$q_e = k_F C_e^{1/n}, \tag{4.11}$$

whereas the linear form of the Freundlich isotherm equation can be written as [77, 84]:

$$\ln(q_e) = \ln(k_F) + \frac{1}{n}\ln(C_e), \tag{4.12}$$

Where K_F is the calculated Freundlich equilibrium constant ([mg/g] $[L/mg]^{1/n}$) and is an indicator of adsorption capacity, and n is a measure of the deviation from linearity of adsorption (g/L).

The favourability of adsorption can be estimated by the magnitude of the exponent (1/n), which predicts the feasibility of the adsorption process. The values of n must be greater than one for conditions to be favourable for an adsorption process [8, 95, 96]. The constant n values of UiO-66, UiO-66-10%Ca and UiO-66-30%Ca have been calculated to be 1.29, 5.01 and 3.09, respectively. These values confirm the favourability of adsorption of MB onto single-metal and bimetal Zr-MOF. The results of the correlational analysis for K_F, n and the linear regression coefficient (R^2) for the plot of the linear form of the Freundlich model are presented in Table 4.4.

Figure 4.7 below illustrates the experimental equilibrium data and the predicted theoretical isotherms for the adsorption of MB onto single-metal and bimetal Zr-MOFs. It is apparent, from Figure 4.7 and the R^2 values in Table 4.4, that there is closer fit between the experimental data and Freundlich isotherm compared to that with the Langmuir isotherm, particular at higher values of R^2.

Analyses and calculations of the Langmuir and Freundlich plots revealed that the values of the linear regression correlation coefficient (R^2) for the Langmuir model are 0.9889, 0.9951 and 0.9821, and for the Freundlich model 0.9979, 0.9973 and 0.9926, for UiO-66, UiO-66-10%Ca and UiO-66-30%Ca, respectively.

Further, Freundlich constants (K_F) related to the bonding energy of MB molecules with single-metal and bimetal Zr-MOFs were greater than Langmuir constants which were related to the affinity of MB molecules to single-metal and bimetal Zr-MOF in all cases. As a result, the adsorption of MB onto single-metal and bimetal Zr-MOF occurred as multilayer adsorption on a heterogeneous surface. The calculated maximum monolayer adsorption capacity (q_m) of Zr-MOF for MB is 50.25 mg/g for UiO-66-10%Ca, a relatively satisfactory adsorption capacity (see Table 4.4).

Table 4.5 lists the maximum adsorption capacity (q_m) of the Zr-MOF adsorbent for MB, relative to those reported in the literature for different adsorbents of MB. The performance of Zr-MOF in MB removal is relatively effective by comparison.

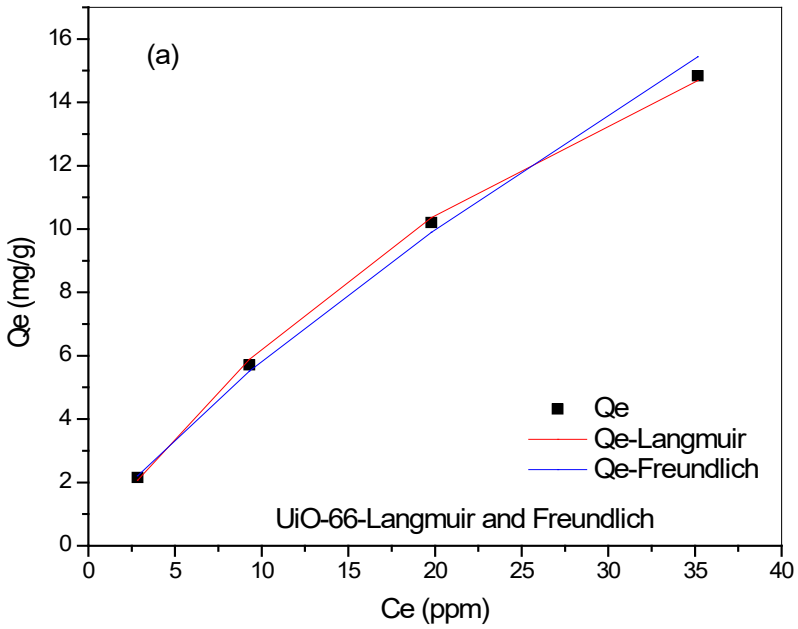
(a)
Qe (mg/g)
Ce (ppm)
Qe
Qe-Langmuir
Qe-Freundlich
UiO-66-Langmuir and Freundlich

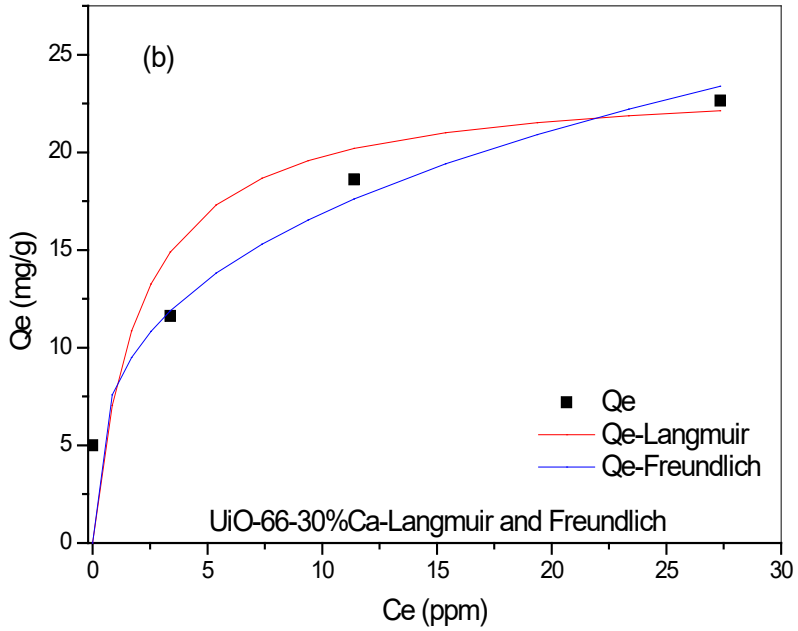
(b)
Qe (mg/g)
Ce (ppm)
Qe
Qe-Langmuir
Qe-Freundlich
UiO-66-30%Ca-Langmuir and Freundlich

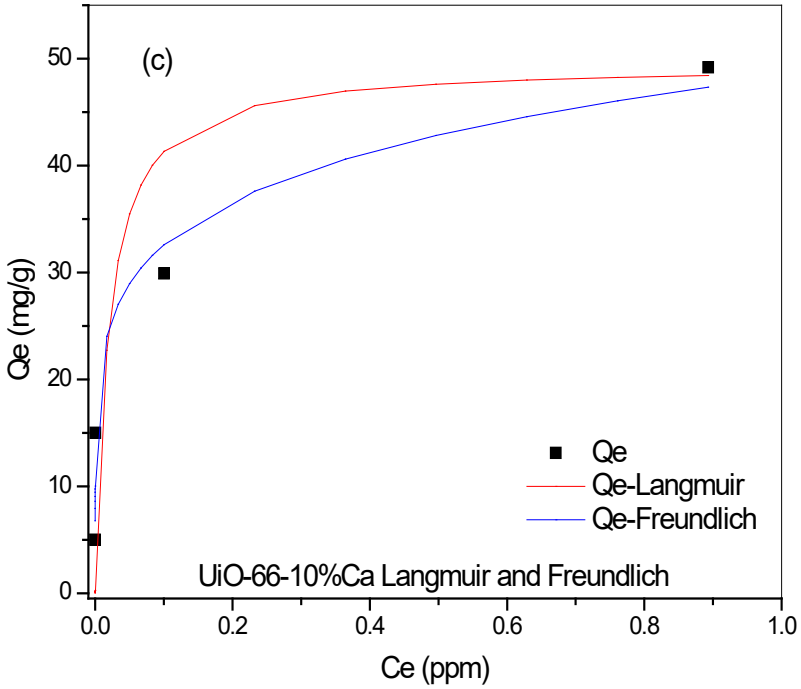

Figure 4.7. Fitting of experimental data using Langmuir and Freundlich models of MB adsorption onto UiO-66 (a), UiO-66-30%Ca (b) and UiO-66-10%Ca (c).

Table 4.4: Calculated equilibrium constants (k_L, k_F, q_m, n and correlation coefficient (R^2)) of MB adsorption onto UiO-66, UiO-66-30%Ca and UiO-66-10%Ca for C_i = 5, 15, 30 and 50 ppm.

Adsorbent	Adsorption isotherm model	Parameter	Value	R^2
UiO-66	Langmuir	q_m (mg/g)	31.74	0.9889
		K_L (L/mg)	0.02447	
	Freundlich	K_F ([mg/g] [L/mg]$^{1/n}$)	0.98157	0.9979
		n (g/L)	1.2918	
iO-66-10%Ca	Langmuir	q_m (mg/g)	50.2512	0.9951
		K_L (L/mg)	39.8	
	Freundlich	K_F ([mg/g] [L/mg]$^{1/n}$)	47.9855	0.9973
		n (g/L)	5.0150	
UiO-66-30%Ca	Langmuir	q_m (mg/g)	23.7529	0.9821
		K_L (L/mg)	0.4982	
	Freundlich	K_F ([mg/g] [L/mg]$^{1/n}$)	8.0164	0.9926
		n (g/L)	3.0911	

Table 4.5: Comparison of monolayer equilibrium capacity for methylene blue onto different adsorbents.

Adsorbent	Conditions	q_m (mg/g)	Reference
Untreated coffee husks	Normal	90.1	[97]
Sewage sludge from agrifood industry wastewater treatment plant	Normal	86.957	[98]
Raw date pits	Normal	80.29	[100]
Calcined pure clay	Normal	56.31	[101]
UiO-66-10%Ca	Normal	50.25	This study
UiO-66-30%Ca		23.75	This study
UiO-66		14.52	This study
Luffa cylindrica fibres	Normal	47	[102]
Carbon nanotubes	Normal	46.2	[103]
Rice husk	Normal	40.59	[9]
Garden grass	Normal	31.4	[104]
Raw clay	Normal	27.49	[101]
Jute processing waste	Normal	22.47	[105]
Fe (III)/Cr (III) hydroxide	Normal	22.8	[77]
Banana peel	Normal	20.8	[106]
Orange peel	Normal	18.6	[106]
Activated date pits (T = 900 °C)	Normal	17.27	[100]
Fly-ash	Normal	13.42	[29]
Calcined raw clay	Normal	13.44	[101]
Activated date pits (T = 500 °C)	Normal	12.94	[100]
Zeolite	Normal	12.7	[107]
Clay	Normal	6.3	[108]
Fly-ash	Normal	1.3	[107]

4.4.5 Intraparticle diffusion

As a result of the limitations of the pseudo first-order and pseudo second-order kinetic equations, the lack of an identified adsorption mechanism and the rate-limiting steps in the adsorption process, Weber and Morris established a new adsorption model [109]. In general, the migration of sorbate molecules in bulk to the surface of a solid sorbent by intraparticle diffusion process is what controls the rate of most liquid/solid sorption systems. The analysis using Weber and Morris's intraparticle diffusion model is as follows [63, 64]:

$$q_t = k_p t^{1/2} + C, \tag{4.13}$$

Where:

q_t: the amount of MB adsorbed per unit weight of MOF at any time t (mg/g)

k_p: intraparticle diffusion rate constant (mg/g $min^{0.5}$)

t: time (min)

C: intercept [102, 110, 111].

Typically, if the plot of the intraparticle diffusion model gives rise to two or more intercepting lines, the adsorption stages are independent of each other. Plots that display two intersecting lines with different slopes indicate that the sorption process is controlled by a multistep process, including external surface sorption and diffusion of MB into the internal pores of the MOF [2, 112].

Single-metal and bimetal Zr-MOFs (solid) and MB (liquid) system adsorption processes show that the transfer of MB takes place either by external diffusion or internal diffusion or both (film and intraparticle diffusion)[72]. From Figure 4.9, three sequential steps can be seen to govern any solid-liquid adsorption, including the adsorption of MB onto MOFs. A multistep adsorption process consists of the mass transfer of MB from the solution to the surface of single-metal and bimetal Zr-MOFs; this transfer determines the extent of reaction throughout the whole adsorption process [113]. Figures 4.8 and 4.9 show the classification of the adsorption process mechanism of MB onto MOFs into the following three stages:

1. film diffusion: the initial stage of rapid adsorption
2. successive intraparticle diffusion: the second stage of the process during which the adsorption rate slows
3. the final stage: the adsorption attains equilibrium and lasting constant [112].

Film diffusion is very fast because of the rapid sorption of MB to the surface of the MOF. This stage is featured by quick surface mass transfer caused by a large differential which acts as a driving force. This stage is when the most is adsorbed by adsorbents, according to Weng et al. [112]. Such a finding establishes MOF-MB systems as entailing a fast adsorption process. Consequently, these adsorbent systems are favourable alternatives for removing cationic dyes from wastewater effluent. The second stage, intraparticle diffusion, is slower because the occupation of MB molecules on many of the available external sites in the first step slows the diffusion of MB molecules into the pore spaces of the MOF [113].

The mechanism of MB sorption on the surface of MOF was investigated using contact time data. Specifically, experimental data were fitted to the intraparticle diffusion model (Equation 4.13) and the outcomes interpreted by plotting q_t versus $t^{1/2}$ in Figure 4.9. The most important aspects of the intraparticle diffusion plot are first, the linear

portion and the intercept of the plot (C), which indicates the effects of the boundary layer on the adsorption process.

The second linear portion of the plot can be used to interpret intraparticle diffusion. The plot can be used to derive values for parameters, such as k_p, C and R^2, as presented in Table 4.6. The second stage, the slowest rate-limiting stage of the adsorption process, does not pass through the origin (intercept C) because of the variance in rate of mass transfer in the first and last stages of adsorption. Subsequently, it can be concluded that the constant value (C) represents the boundary layer, the rate-controlling step during which the availability of adsorbed MB on MOF boundary layer can be measured.

In addition, k_p, the diffusion rate of the adsorption process, can be determined from the slope of the plot. The slope can be used to estimate the driving force of diffusion, which plays a critical role in the adsorption reaction. Experimental data analysis demonstrated that the k_p values increased from 0.0991 to 0.638 mg $g^{-1}min^{-(1/2)}$ with increases in the initial MB concentration from 5 to 50 mg L^{-1}. Therefore, higher initial concentrations of MB increase the driving force and subsequently increase the MB diffusion rate. Further, increasing initial MB concentrations over a similar range led to increases in the intercept value (C) from 0.5017 to 3.8144 mg g^{-1}, suggesting that an initial high concentration of basic dye is associated with a stronger boundary layer effect in the sorption process. In addition, increases in the intercept value (C) can indicate the availability of MB on the boundary layer of UiO-66.

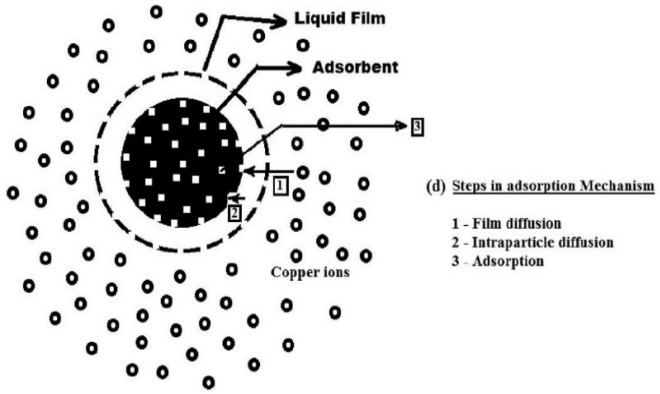

Figure 4.8. Steps of the adsorption mechanism.

Table 4.6: Calculated kinetics constant (k_p), C and correlation coefficient (R^2) for C_i = 5, 15, 30 and 50 ppm.

		Adsorption mechanism		
		Intraparticle diffusion model		
Adsorbent	**Initial concentration of MB solution (mg L^{-1})**	**k_p (mg $g^{-1}min^{-(1/2)}$)**	**C (mg g^{-1})**	**R^2**
UiO-66	5	0.0991	0.5017	0.9999
	15	0.22	2.1455	0.9918
	30	0.3955	3.5763	0.9884
	50	0.638	3.8144	0.9959
UiO-66-10%Ca	5	0.4851	3.4862	0.9981
	15	0.9352	9.927	0.9883
	30	0.7581	23.867	0.9655
	50	0.6585	39.364	0.9040
UiO-66-30%Ca	5	0.218	1.3901	0.9983
	15	0.5641	2.4216	0.9951
	30	0.7423	6.186	0.9999
	50	0.727	11.013	0.9928

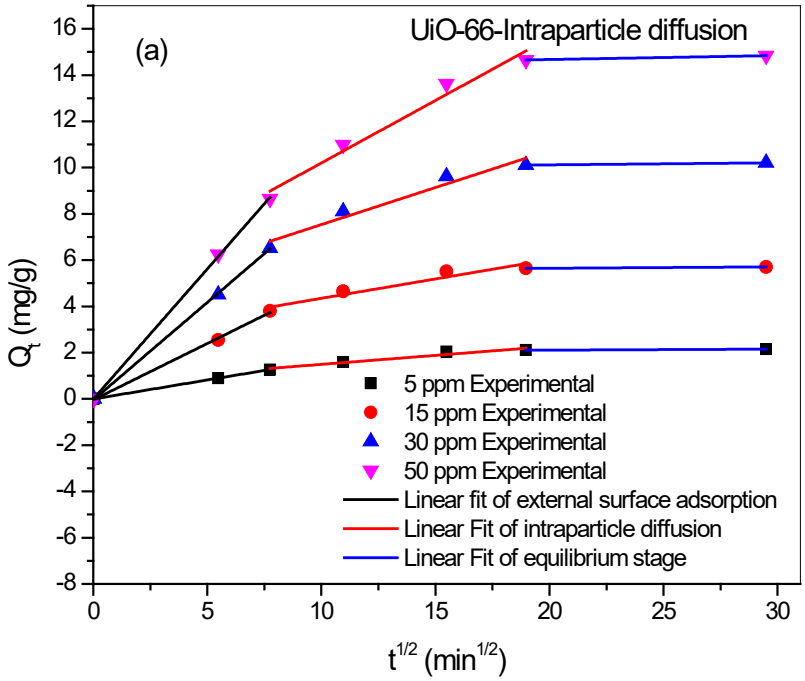

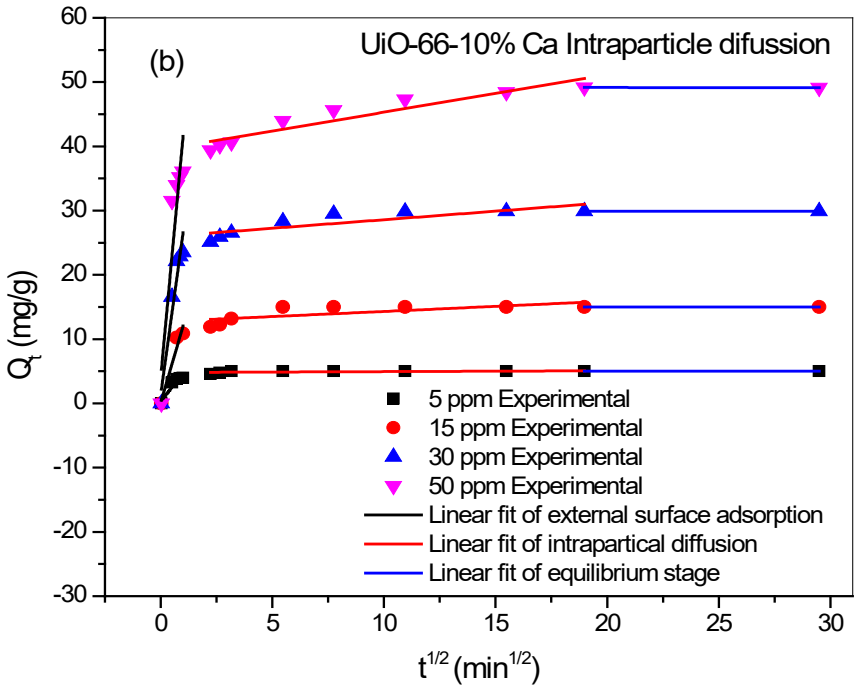

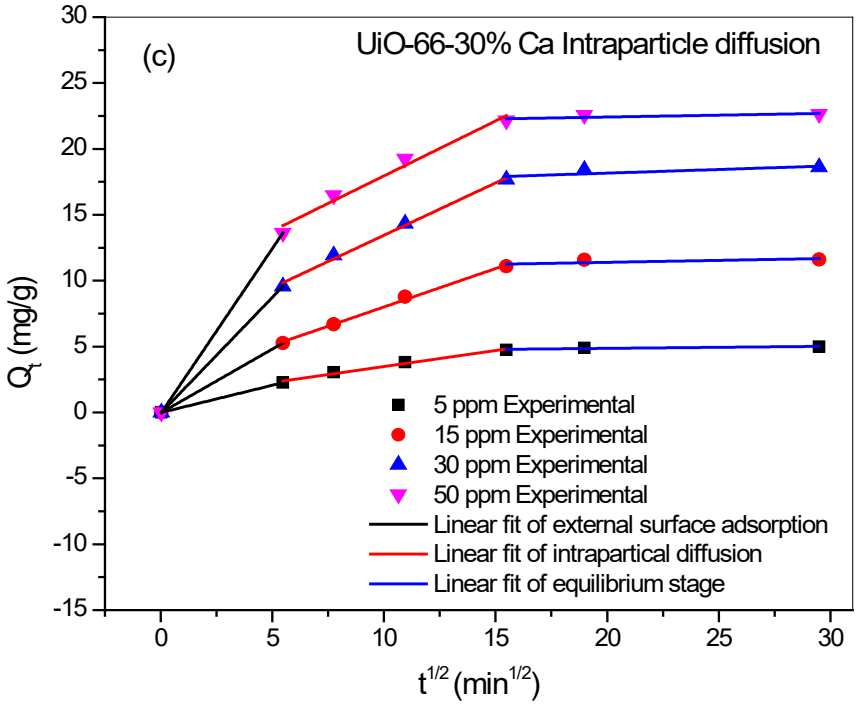

Figure 4.9. Fitting of experimental data using intraparticle diffusion models of MB adsorption onto UiO-66 (a), UiO-66-10%Ca (b) and UiO-66-30%Ca (c).

4.5 Conclusion

The main goal of the current study was to assess the adsorbent capacity of MOFs (UiO-66, UiO-66-10%Ca and UiO-66-30%Ca) and predict its loading of a cationic dye (MB). The MOFs were prepared according to a previously reported method with a modification using trace additives of a secondary chemical (Ca). Compared with the MOF without the modification, the textural properties of the modified MOFs were enriched and enhanced their performance in water and wastewater treatment applications.

Kinetic and equilibrium models were utilised to predict the adsorbed amount at any time (q_t), adsorption at equilibrium (q_e) and Langmuir maximum loading capacity (q_m) of basic dye. Based on its higher linear regression correlation coefficient (R^2), the pseudo second-order mechanism was used to obtain the rate of adsorption (k_2) and equilibrium capacity as a function of various initial concentrations of MB. Therefore, the kinetics of MB sorption onto MOFs (UiO-66, UiO-66-10%Ca and UiO-66-30%Ca) were examined using the pseudo second-order model. The results suggested that the chemical reaction was important in the rate-limiting step, and the pseudo second-order mechanism offered the best fit for the experimental data for all systems studied. However, the pseudo first-order model fit the experimental data well for a short time in the first stage of the adsorption process.

The equilibrium experimental data were fitted using linear forms of the Langmuir and Freundlich isotherms. Langmuir and Freundlich plot analyses and calculations revealed that the values of the linear regression correlation coefficient (R^2) for the Freundlich model were greater than those for the Langmuir model, for UiO-66, UiO-66-10%Ca and UiO-66-30%Ca.

Further, Freundlich constants related to the bonding energy of MB molecules with single-metal and bimetal Zr-MOF (K_F) were greater than the Langmuir constants related to the affinity of MB molecules to single-metal and bimetal Zr-MOF molecules, in all cases. As a result, the adsorption of MB onto single-metal and bimetal Zr-MOFs was considered to occur as multilayer adsorption on a heterogeneous surface. Specifically, the Langmuir maximum adsorption capacity of the most efficient adsorbent (UiO-66-10%Ca) was 50.25 mg/g.

In addition, the Langmuir maximum loading capacity (q_m) was compared with other reported adsorbents in previous studies. The values of the separation factor (R_L) for the sorption of MB onto single-metal and bimetal Zr-MOFs were in the range $0 < RL < 1$, indicating that the adsorption was a favourable process. Further, higher initial MB concentrations in the adsorption process can make it irreversible. Using the Freundlich linear model, constant n values for UiO-66, UiO-66-10%Ca, and UiO-66-30%Ca were found to be more than one (i.e., $n > 1$). These values confirm the favourability of MB adsorption onto single-metal and bimetal Zr-MOF.

The intraparticle diffusion adsorption model was used as an alternative model to overcome the limitations of the pseudo first-order and pseudo second-order kinetic models, the lack of an identified adsorption mechanism and to address the rate-limiting stage in the adsorption process. The mechanism of MB sorption onto the surface of MOFs was investigated using contact time data. Specifically, the fitting of experimental data to the intraparticle diffusion model identified three stages in the sorption process, and suggested that intraparticle diffusion is not the only rate-controlling stage.

References

1. Almeida, C.A.P., et al., *Removal of methylene blue from colored effluents by adsorption on montmorillonite clay.* Journal of Colloid and Interface Science, 2009. **332**(1): p. 46-53.
2. Bhattacharyya, K.G. and A. Sharma, *Kinetics and thermodynamics of methylene blue adsorption on neem (Azadirachta indica) leaf powder.* Dyes and pigments, 2005. **65**(1): p. 51-59.
3. Tunç, Ö., H. Tanacı, and Z. Aksu, *Potential use of cotton plant wastes for the removal of Remazol Black B reactive dye.* Journal of Hazardous Materials, 2009. **163**(1): p. 187-198.
4. Doğan, M., Y. Özdemir, and M. Alkan, *Adsorption kinetics and mechanism of cationic methyl violet and methylene blue dyes onto sepiolite.* Dyes and Pigments, 2007. **75**(3): p. 701-713.
5. Albert, M., M.S. Lessin, and B.F. Gilchrist, *Methylene blue: dangerous dye for neonates.* Journal of Pediatric Surgery, 2003. **38**(8): p. 1244-1245.
6. Gupta, V.K., et al., *Removal of Rhodamine B, Fast Green, and Methylene Blue from Wastewater Using Red Mud, an Aluminum Industry Waste.* Industrial & Engineering Chemistry Research, 2004. **43**(7): p. 1740-1747.
7. Salleh, M.A.M., et al., *Cationic and anionic dye adsorption by agricultural solid wastes: A comprehensive review.* Desalination, 2011. **280**(1): p. 1-13.
8. Hameed, B.H., *Spent tea leaves: A new non-conventional and low-cost adsorbent for removal of basic dye from aqueous solutions.* Journal of Hazardous Materials, 2009. **161**(2): p. 753-759.
9. Vadivelan, V. and K.V. Kumar, *Equilibrium, kinetics, mechanism, and process design for the sorption of methylene blue onto rice husk.* Journal of colloid and interface science, 2005. **286**(1): p. 90-100.
10. Bulut, Y. and H. Aydın, *A kinetics and thermodynamics study of methylene blue adsorption on wheat shells.* Desalination, 2006. **194**(1): p. 259-267.
11. Pathania, D., S. Sharma, and P. Singh, *Removal of methylene blue by adsorption onto activated carbon developed from Ficus carica bast.* Arabian Journal of Chemistry, 2017. **10**: p. S1445-S1451.
12. Auta, M. and B. Hameed, *Preparation of waste tea activated carbon using potassium acetate as an activating agent for adsorption of Acid Blue 25 dye.* Chemical Engineering Journal, 2011. **171**(2): p. 502-509.
13. Bulut, Y. and H. Aydın, *A kinetics and thermodynamics study of methylene blue adsorption on wheat shells.* Desalination, 2006. **194**(1-3): p. 259-267.
14. Tripathi, N., *Cationic and anionic dye adsorption by agricultural solid wastes: A comprehensive review.* Journal of Applied Chemistry, 2013. **5**: p. 91-108.
15. Rafatullah, M., et al., *Adsorption of methylene blue on low-cost adsorbents: A review.* Journal of Hazardous Materials, 2010. **177**(1): p. 70-80.

16. Arami, M., et al., *Removal of dyes from colored textile wastewater by orange peel adsorbent: Equilibrium and kinetic studies.* Journal of Colloid and Interface Science, 2005. **288**(2): p. 371-376.

17. Robinson, T., et al., *Remediation of dyes in textile effluent: a critical review on current treatment technologies with a proposed alternative.* Bioresource Technology, 2001. **77**(3): p. 247-255.

18. Wang, S. and Z. Zhu, *Characterisation and environmental application of an Australian natural zeolite for basic dye removal from aqueous solution.* Journal of hazardous materials, 2006. **136**(3): p. 946-952.

19. Meshko, V., et al., *Adsorption of basic dyes on granular acivated carbon and natural zeolite.* Water Research, 2001. **35**(14): p. 3357-3366.

20. Wang, S. and Z.H. Zhu, *Characterisation and environmental application of an Australian natural zeolite for basic dye removal from aqueous solution.* Journal of Hazardous Materials, 2006. **136**(3): p. 946-952.

21. Wang, S., et al., *Removal of dyes from aqueous solution using fly ash and red mud.* Water Research, 2005. **39**(1): p. 129-138.

22. Garg, V.K., et al., *Basic dye (methylene blue) removal from simulated wastewater by adsorption using Indian Rosewood sawdust: a timber industry waste.* Dyes and pigments, 2004. **63**(3): p. 243-250.

23. Qadeer, R., *Adsorption behavior of ruthenium ions on activated charcoal from nirtic acid medium.* Colloids and Surfaces A: Physicochemical and Engineering Aspects, 2007. **293**(1): p. 217-223.

24. Akbal, F., *Adsorption of basic dyes from aqueous solution onto pumice powder.* Journal of colloid and interface science, 2005. **286**(2): p. 455-458.

25. Gücek, A., et al., *Adsorption and kinetic studies of cationic and anionic dyes on pyrophyllite from aqueous solutions.* Journal of colloid and interface science, 2005. **286**(1): p. 53-60.

26. Doğan, M., et al., *Kinetics and mechanism of removal of methylene blue by adsorption onto perlite.* Journal of hazardous materials, 2004. **109**(1-3): p. 141-148.

27. Banerjee, S. and M. Dastidar, *Use of jute processing wastes for treatment of wastewater contaminated with dye and other organics.* Bioresource technology, 2005. **96**(17): p. 1919-1928.

28. Tsai, W., et al., *Characterization and adsorption properties of eggshells and eggshell membrane.* Bioresource technology, 2006. **97**(3): p. 488-493.

29. Wang, S., Y. Boyjoo, and A. Choueib, *A comparative study of dye removal using fly ash treated by different methods.* Chemosphere, 2005. **60**(10): p. 1401-1407.

30. Yaghi, O.M., et al., *Reticular synthesis and the design of new materials.* Nature, 2003. **423**(6941): p. 705.

31. Yaghi, O.M., et al., *Synthetic Strategies, Structure Patterns, and Emerging Properties in the Chemistry of Modular Porous Solids.* Accounts of Chemical Research, 1998. **31**(8): p. 474-484.

32. Batten, S.R. and R. Robson, *Interpenetrating nets: ordered, periodic entanglement.* Angewandte Chemie International Edition, 1998. **37**(11): p. 1460-1494.

33. Férey, G., *Building units design and scale chemistry.* Journal of Solid State Chemistry, 2000. **152**(1): p. 37-48.

34. Kitagawa, S. and M. Kondo, *Functional micropore chemistry of crystalline metal complex-assembled compounds.* Bulletin of the Chemical Society of Japan, 1998. **71**(8): p. 1739-1753.

35. Yaghi, O., M. O'Keeffe, and M. Kanatzidis, *Design of solids from molecular building blocks: golden opportunities for solid state chemistry.* Journal of Solid State Chemistry, 2000. **152**(1): p. 1-2.

36. Furukawa, H., et al., *The chemistry and applications of metal-organic frameworks.* Science, 2013. **341**(6149): p. 1230444.

37. Zhou, H.-C., J.R. Long, and O.M. Yaghi, *Introduction to metal–organic frameworks*. 2012, ACS Publications.

38. Mueller, U., et al., *Metal–organic frameworks—prospective industrial applications.* Journal of Materials Chemistry, 2006. **16**(7): p. 626-636.

39. Jacoby, M., *Heading to market with MOFs.* Chem. Eng. News, 2008. **86**(34): p. 13-16.

40. Furukawa, H., et al., *Ultrahigh porosity in metal-organic frameworks.* Science, 2010. **329**(5990): p. 424-428.

41. Millward, A.R. and O.M. Yaghi, *Metal− organic frameworks with exceptionally high capacity for storage of carbon dioxide at room temperature.* Journal of the American Chemical Society, 2005. **127**(51): p. 17998-17999.

42. Caskey, S.R., A.G. Wong-Foy, and A.J. Matzger, *Dramatic tuning of carbon dioxide uptake via metal substitution in a coordination polymer with cylindrical pores.* Journal of the American Chemical Society, 2008. **130**(33): p. 10870-10871.

43. Hamon, L., et al., *Comparative study of hydrogen sulfide adsorption in the MIL-53 (Al, Cr, Fe), MIL-47 (V), MIL-100 (Cr), and MIL-101 (Cr) metal− organic frameworks at room temperature.* Journal of the American Chemical Society, 2009. **131**(25): p. 8775-8777.

44. Karra, J.R. and K.S. Walton, *Effect of open metal sites on adsorption of polar and nonpolar molecules in metal− organic framework Cu-BTC.* Langmuir, 2008. **24**(16): p. 8620-8626.

45. Blanco-Brieva, G., et al., *Effectiveness of metal–organic frameworks for removal of refractory organo-sulfur compound present in liquid fuels.* Fuel, 2011. **90**(1): p. 190-197.

46. Arstad, B., et al., *Amine functionalised metal organic frameworks (MOFs) as adsorbents for carbon dioxide.* Adsorption, 2008. **14**(6): p. 755-762.

47. Haque, E., et al., *Adsorptive removal of methyl orange from aqueous solution with metal-organic frameworks, porous chromium-benzenedicarboxylates.* Journal of Hazardous Materials, 2010. **181**(1): p. 535-542.

48. Peterson, G.W., et al., *Ammonia vapor removal by Cu3 (BTC) 2 and its characterization by MAS NMR.* The Journal of Physical Chemistry C, 2009. **113**(31): p. 13906-13917.

49. Khan, N.A. and S.H. Jhung, *Adsorptive removal of benzothiophene using porous copper-benzenetricarboxylate loaded with phosphotungstic acid.* Fuel Processing Technology, 2012. **100**: p. 49-54.

50. Khan, N.A., Z. Hasan, and S.H. Jhung, *Adsorptive removal of hazardous materials using metal-organic frameworks (MOFs): A review.* Journal of Hazardous Materials, 2013. **244-245**: p. 444-456.

51. Khan, N.A., et al., *Remarkable adsorptive performance of a metal–organic framework, vanadium-benzenedicarboxylate (MIL-47), for benzothiophene.* Chemical Communications, 2011. **47**(4): p. 1306-1308.

52. Ahmed, I., et al., *Adsorptive denitrogenation of model fuels with porous metal-organic frameworks (MOFs): Effect of acidity and basicity of MOFs.* Applied Catalysis B: Environmental, 2013. **129**: p. 123-129.

53. Khan, N.A. and S.H. Jhung, *Low-temperature loading of Cu+ species over porous metal-organic frameworks (MOFs) and adsorptive desulfurization with Cu+-loaded MOFs.* Journal of Hazardous Materials, 2012. **237-238**: p. 180-185.

54. Britt, D., D. Tranchemontagne, and O.M. Yaghi, *Metal-organic frameworks with high capacity and selectivity for harmful gases.* Proceedings of the National Academy of Sciences, 2008. **105**(33): p. 11623-11627.

55. Hamon, L., et al., *Molecular insight into the adsorption of H2S in the flexible MIL-53 (Cr) and rigid MIL-47 (V) MOFs: infrared spectroscopy combined to molecular simulations.* The Journal of Physical Chemistry C, 2011. **115**(5): p. 2047-2056.

56. Glover, T.G., et al., *MOF-74 building unit has a direct impact on toxic gas adsorption.* Chemical Engineering Science, 2011. **66**(2): p. 163-170.

57. Huo, S.-H. and X.-P. Yan, *Metal–organic framework MIL-100 (Fe) for the adsorption of malachite green from aqueous solution.* Journal of Materials Chemistry, 2012. **22**(15): p. 7449-7455.

58. Kitagawa, S., R. Kitaura, and S.i. Noro, *Functional porous coordination polymers.* Angewandte Chemie International Edition, 2004. **43**(18): p. 2334-2375.

59. Cavka, J.H., et al., *A new zirconium inorganic building brick forming metal organic frameworks with exceptional stability.* Journal of the American Chemical Society, 2008. **130**(42): p. 13850-13851.

60. Hameed, B. and A. Rahman, *Removal of phenol from aqueous solutions by adsorption onto activated carbon prepared from biomass material.* Journal of Hazardous Materials, 2008. **160**(2): p. 576-581.

61. Ho, Y.-S. and G. McKay, *Pseudo-second order model for sorption processes.* Process biochemistry, 1999. **34**(5): p. 451-465.

62. Wang, S., H. Li, and L. Xu, *Application of zeolite MCM-22 for basic dye removal from wastewater.* Journal of colloid and interface science, 2006. **295**(1): p. 71-78.

63. Weber, W.J. and J.C. Morris, *Kinetics of adsorption on carbon from solution.* Journal of the Sanitary Engineering Division, 1963. **89**(2): p. 31-60.

64. Gupta, N., A.K. Kushwaha, and M.C. Chattopadhyaya, *Application of potato (Solanum tuberosum) plant wastes for the removal of methylene blue and malachite green dye from aqueous solution.* Arabian Journal of Chemistry, 2016. **9**: p. S707-S716.

65. Lin, S.-H. and R.-S. Juang, *Adsorption of phenol and its derivatives from water using synthetic resins and low-cost natural adsorbents: a review.* Journal of environmental management, 2009. **90**(3): p. 1336-1349.

66. Di Marino, A. and F. Mendicuti, *Thermodynamics of complexation of dimethyl esters of tere-, iso-, and phthalic acids with α-and β-cyclodextrins.* Applied spectroscopy, 2004. **58**(7): p. 823-830.

67. Dhumal, N.R., et al., *Molecular Interactions of a Cu-Based Metal–Organic Framework with a Confined Imidazolium-Based Ionic Liquid: A Combined Density Functional Theory and Experimental Vibrational Spectroscopy Study.* The Journal of Physical Chemistry C, 2016. **120**(6): p. 3295-3304.

68. Coates, J., *Interpretation of infrared spectra, a practical approach.* Encyclopedia of analytical chemistry, 2000. **12**: p. 10815-10837.

69. Aroke, U., A. Abdulkarim, and R. Ogubunka, *Fourier-transform infrared characterization of kaolin, granite, bentonite and barite.* ATBU Journal of Environmental Technology, 2013. **6**(1): p. 42-53.

70. Hameed, B.H. and A.A. Ahmad, *Batch adsorption of methylene blue from aqueous solution by garlic peel, an agricultural waste biomass.* Journal of Hazardous Materials, 2009. **164**(2): p. 870-875.

71. Ho, Y. and G. McKay, *The kinetics of sorption of basic dyes from aqueous solution by sphagnum moss peat.* The Canadian Journal of Chemical Engineering, 1998. **76**(4): p. 822-827.

72. Senthil Kumar, P., C. Senthamarai, and A. Durgadevi, *Adsorption kinetics, mechanism, isotherm, and thermodynamic analysis of copper ions onto the surface modified agricultural waste.* Environmental Progress & Sustainable Energy, 2014. **33**(1): p. 28-37.

73. Hameed, B.H., A.A. Ahmad, and N. Aziz, *Adsorption of reactive dye on palm-oil industry waste: Equilibrium, kinetic and thermodynamic studies.* Desalination, 2009. **247**(1): p. 551-560.

74. Ghaedi, M., A. Hassanzadeh, and S.N. Kokhdan, *Multiwalled Carbon Nanotubes as Adsorbents for the Kinetic and Equilibrium Study of the Removal of Alizarin Red S and Morin.* Journal of Chemical & Engineering Data, 2011. **56**(5): p. 2511-2520.

75. Ai, L. and J. Jiang, *Fast removal of organic dyes from aqueous solutions by AC/ferrospinel composite.* Desalination, 2010. **262**(1): p. 134-140.

76. Ai, L., C. Zhang, and Z. Chen, *Removal of methylene blue from aqueous solution by a solvothermal-synthesized graphene/magnetite composite.* Journal of Hazardous Materials, 2011. **192**(3): p. 1515-1524.

77. Namasivayam, C. and S. Sumithra, *Removal of direct red 12B and methylene blue from water by adsorption onto Fe (III)/Cr (III) hydroxide, an industrial solid waste.* Journal of environmental management, 2005. **74**(3): p. 207-215.

78. Uddin, M.T., et al., *Adsorptive removal of methylene blue by tea waste.* Journal of Hazardous Materials, 2009. **164**(1): p. 53-60.

79. Lagergren, S., *Zur theorie der sogenannten adsorption gel˙ster stoffe, Kungliga Svenska Vetenskapsakademiens. Handlingar. 24 (4), 1-39.* Microchemical Journal Environ. Sci. Technol. J. Colloid Interface Sci J. Colloid Interface Sci Environ. Sci. Technol. Rev. Soc. Quím. Perú, American Water Works Association Chem. Eng. J, 1898.

80. Ho, Y.S. and G. McKay, *Pseudo-second order model for sorption processes.* Process Biochemistry, 1999. **34**(5): p. 451-465.

81. Ho, Y.-S., *Review of second-order models for adsorption systems.* Journal of Hazardous Materials, 2006. **136**(3): p. 681-689.

82. Zaboon, S., et al., *Removal of monoethylene glycol from wastewater by using Zr-metal organic frameworks.* Journal of Colloid and Interface Science, 2018. **523**: p. 75-85.

83. Ji, B., et al., *Adsorption of methyl tert-butyl ether (MTBE) from aqueous solution by porous polymeric adsorbents.* Journal of Hazardous Materials, 2009. **161**(1): p. 81-87.

84. Kumar, K.V., V. Ramamurthi, and S. Sivanesan, *Modeling the mechanism involved during the sorption of methylene blue onto fly ash.* Journal of Colloid and Interface Science, 2005. **284**(1): p. 14-21.

85. Langmuir, I., *The adsorption of gases on plane surfaces of glass, mica and platinum.* Journal of the American Chemical society, 1918. **40**(9): p. 1361-1403.

86. Hameed, B.H., A.T.M. Din, and A.L. Ahmad, *Adsorption of methylene blue onto bamboo-based activated carbon: Kinetics and equilibrium studies.* Journal of Hazardous Materials, 2007. **141**(3): p. 819-825.

87. Hameed, B., A.M. Din, and A. Ahmad, *Adsorption of methylene blue onto bamboo-based activated carbon: kinetics and equilibrium studies.* Journal of hazardous materials, 2007. **141**(3): p. 819-825.

88. Hameed, B., A. Ahmad, and K. Latiff, *Adsorption of basic dye (methylene blue) onto activated carbon prepared from rattan sawdust.* Dyes and pigments, 2007. **75**(1): p. 143-149.

89. Gupta, G., et al., *Removal of chrome dye from aqueous solutions by fly ash.* Water, Air, and Soil Pollution, 1988. **37**(1-2): p. 13-24.

90. Hameed, B.H., A.L. Ahmad, and K.N.A. Latiff, *Adsorption of basic dye (methylene blue) onto activated carbon prepared from rattan sawdust.* Dyes and Pigments, 2007. **75**(1): p. 143-149.

91. Hall, K.R., et al., *Pore-and solid-diffusion kinetics in fixed-bed adsorption under constant-pattern conditions.* Industrial & Engineering Chemistry Fundamentals, 1966. **5**(2): p. 212-223.

92. Gupta, G.S., et al., *Removal of chrome dye from aqueous solutions by fly ash.* Water, Air, and Soil Pollution, 1988. **37**(1): p. 13-24.

93. Ponnusami, V., S. Vikram, and S.N. Srivastava, *Guava (Psidium guajava) leaf powder: Novel adsorbent for removal of methylene blue from aqueous solutions.* Journal of Hazardous Materials, 2008. **152**(1): p. 276-286.

94. Freundlich, H., *Uber die adsorption in losungen [Adsorption in solution]" Zeitschrift für Physikalische Chemie, 57.* 1906.

95. Treybal, R.E., *Mass transfer operations.* New York, 1980.

96. Ho, Y.-S. and G. McKay, *Sorption of dye from aqueous solution by peat.* Chemical engineering journal, 1998. **70**(2): p. 115-124.

97. Oliveira, L.S., et al., *Evaluation of untreated coffee husks as potential biosorbents for treatment of dye contaminated waters.* Journal of Hazardous Materials, 2008. **155**(3): p. 507-512.

98. Otero, M., et al., *Kinetic and equilibrium modelling of the methylene blue removal from solution by adsorbent materials produced from sewage sludges.* Biochemical Engineering Journal, 2003. **15**(1): p. 59-68.

99. Han, R., et al., *Biosorption of methylene blue from aqueous solution by fallen phoenix tree's leaves.* Journal of Hazardous Materials, 2007. **141**(1): p. 156-162.

100. Banat, F., S. Al-Asheh, and L. Al-Makhadmeh, *Evaluation of the use of raw and activated date pits as potential adsorbents for dye containing waters.* Process Biochemistry, 2003. **39**(2): p. 193-202.

101. Ghosh, D. and K. Bhattacharyya, *Removing colour from aqueous medium by sorption on natural clay: a study with methylene blue.* INDIAN JOURNAL OF ENVIRONMENTAL PROTECTION, 2001. **21**(10): p. 903-910.

102. Demir, H., et al., *Dye adsorption behavior of Luffa cylindrica fibers.* Journal of Hazardous Materials, 2008. **153**(1-2): p. 389-394.

103. Yao, Y., et al., *Adsorption behavior of methylene blue on carbon nanotubes.* Bioresource Technology, 2010. **101**(9): p. 3040-3046.

104. Kumar, K.V. and K. Porkodi, *Mass transfer, kinetics and equilibrium studies for the biosorption of methylene blue using Paspalum notatum.* Journal of Hazardous Materials, 2007. **146**(1): p. 214-226.

105. Banerjee, S. and M.G. Dastidar, *Use of jute processing wastes for treatment of wastewater contaminated with dye and other organics.* Bioresource Technology, 2005. **96**(17): p. 1919-1928.

106. Annadurai, G., R.-S. Juang, and D.-J. Lee, *Use of cellulose-based wastes for adsorption of dyes from aqueous solutions.* Journal of Hazardous Materials, 2002. **92**(3): p. 263-274.

107. Woolard, C.D., J. Strong, and C.R. Erasmus, *Evaluation of the use of modified coal ash as a potential sorbent for organic waste streams.* Applied Geochemistry, 2002. **17**(8): p. 1159-1164.

108. Gürses, A., et al., *Determination of adsorptive properties of clay/water system: methylene blue sorption.* Journal of Colloid and Interface Science, 2004. **269**(2): p. 310-314.

109. Hameed, B.H., *Spent tea leaves: a new non-conventional and low-cost adsorbent for removal of basic dye from aqueous solutions.* Journal of hazardous materials, 2009. **161**(2-3): p. 753-759.

110. Rattanaphani, S., et al., *An adsorption and thermodynamic study of lac dyeing on cotton pretreated with chitosan.* Dyes and pigments, 2007. **72**(1): p. 88-96.

111. Moussavi, G. and R. Khosravi, *The removal of cationic dyes from aqueous solutions by adsorption onto pistachio hull waste.* Chemical Engineering Research and Design, 2011. **89**(10): p. 2182-2189.

112. Weng, C.-H., Y.-T. Lin, and T.-W. Tzeng, *Removal of methylene blue from aqueous solution by adsorption onto pineapple leaf powder.* Journal of Hazardous Materials, 2009. **170**(1): p. 417-424.

113. Gupta, N., A.K. Kushwaha, and M. Chattopadhyaya, *Adsorption studies of cationic dyes onto Ashoka (Saraca asoca) leaf powder.* Journal of the Taiwan Institute of Chemical Engineers, 2012. **43**(4): p. 604-613.

Chapter 5

Lifting removal of cationic dye (methylene blue) from wastewater by improving Zr-MOFs via second metal Al coordination

5

Chapter 5: Lifting removal of cationic dye (methylene blue) from wastewater by improving Zr-MOFs via second metal Al coordination

5.1 Abstract

Metal organic frameworks (MOFs) are frequently used as adsorbents in adsorption processes to remove dyes from effluent produced by the textile industry. Today, dye contaminants have become an important environmental problem. One of these dyes is methylene blue (MB) and its removal from wastewater is a priority because it is persistent and nondegradable. MB is used in many industries although it has potential harmful effects on human and aquatic life and can be considered a hazardous chemical when in wastewater. The present study shows the potential applications for enhanced forms of UiO-66 MOFs, such as UiO-66, UiO-66-10%Al and UiO-66-30%Al. These forms were prepared to remove MB from wastewater using batch experiments. Characterisation of adsorbents were accomplished successfully using Fourier transform infrared, X-ray powder diffraction, Brunauer–Emmett–Teller surface area and thermogravimetric analysis techniques. To investigate equilibrium adsorptive behaviour, Langmuir and Freundlich isotherm models were tested against the experimental data. Based on linear regression correlation coefficient (R^2), the Freundlich model described the equilibrium isotherm of MOF/MB better than the Langmuir model. Of all forms of UiO-66 MOF, UiO-66-10%Al had the maximum Langmuir adsorption capacity at 49.26 mg/g. A kinetics study examined pseudo first-order, pseudo second order and Elovich models to determine which could explain the sorption mechanism. While the pseudo second order and Elovich models showed a good fit with the experimental data, the correlation coefficient of the pseudo second-order model was the highest. These results indicate that adsorption of MB is controlled by a chemisorption mechanism. Further, intraparticle diffusion was utilised to describe the adsorption mechanism and determine the rate-limiting steps in the adsorption process.

5.2 Introduction

Despite government regulations, ensuring environmental compliance with established terms of wastewater release and chemical handling is difficult [1]. Today, dye contaminants have become one of the most important environmental problems in the world. Effluent with organic dyes discarded into natural watercourses endanger living creatures and the environment because of their toxicity and carcinogenic effects [2]. In addition, dye content in water prevents sunlight penetration which decreases plant photosynthesis [1].

Significant amounts of dyes are employed in a wide range of industries involved in producing paper, textile, leather, pharmaceutics, food, cosmetics, print products, iron-steel products, coke, petroleum, pesticides, paints, solvents, wood-preserving chemicals. Further, their manufacturing plants consume large volumes of water that in turn generate large volumes of wastewater [3]. Almost 100,000 dyes and pigments have been tabulated to exist, consisting of 7000 kinds of chemical structures, that are used to produce 7×10^5 tonnes per year worldwide [4-8]. The majority of these dyes are resistant to biodegradation and oxidation processes [9]. About 10–15% of the dyes is discharged into the effluent during the dyeing process [10, 11]. Recently, studies have reported that around 12% of synthetic dyes are wasted through colouring processes and operations [12]; 20% of lost dyes enter industrial wastewaters [13, 14].

Dyes can be divided into two main groups, anionic (acidic) and cationic (basic) colour dyes. Methylene blue (MB) is a basic dye that is a focus of this study. Although MB is used in some medical applications, it is also widely used in colouring paper, dyed cottons, wools, coating for paper stocks, etc. Though MB is not strongly hazardous, it has some harmful effects. Acute exposure to MB will cause increased heart rate, vomiting, shock, Heinz body formation, cyanosis, jaundice, quadriplegia and tissue necrosis in humans [15].

Environmentally, it is essential to remove dyes from industrial wastewater because of their toxicity and high visibility [7, 16-18]. Consequently, there is a continuous urgent need to ensure the removal these pollutants from industrial effluent and to comply with government legislation [19]. Many techniques have been attempted to discolour industrial discharge that involve chemical, biological and physical removal methods; however, most are unsuccessful because of their limitations and disadvantages [20].

Adsorption is a well-known and favourite technique because of its feasibility, simplicity and efficiency in the removal of such contaminants [21]. Many adsorbents have been employed to treat industrial wastewater containing dye. They include activated carbon derived from different sources of raw materials [22-33], agricultural solid waste [34-47], biosorbents [17, 18, 48-60], zeolites [61-66], industrial solid wastes [15, 67-74], natural clay minerals [75-83], resins [84-87], metal oxides [88, 89], metal organic frameworks (MOFs)[2, 90-93].

Activated carbon from various sources has been the most investigated adsorbent in laboratories and most used by industries to remove basic dyes from their wastewaters [87, 94-97]. However, its cost has limited its commercial use as a sorbent. As a result, many studies have been undertaken in the last decade to identify a cost-effective sorbent [98].

MOF [99-106], or hybrid inorganic and organic framework [107], is a 21st century material with tuneable options, organic functionality, open metal sites in its skeleton, large-sized pores, high surface areas (1000 to 10,000 m^2/g) as well as high thermal, water, chemical, architectural and mechanical stability [2, 108]. It is a class of ultra-high porous material constructed with secondary building units (SBUs)[109] and synthesised by reticular chemistry [110, 111] that connect the inorganic part with the metal ion to the organic part with polytopic carboxylate group to form vertices and linkers with strong bonds [112]. The variety of geometry, size and functionality of the constituents of MOFs has enabled scientists around the world to synthesise more than 84,185 MOF structures [102]. Their variety and multiplicity, as well as permanent porosity, make them favourable materials in many applications, such as CO_2 capture, hydrogen and methane storage, sensors, photocatalysis, drug delivery, catalysis applications and the adsorptive removal of contaminants from aqueous solutions [90, 112-117].

The objective of the present study is to describe the synthesis and characterisation of single-metal Zr-MOF (UiO-66) and bimetal Zr-MOFs (UiO-66-10%Al and UiO-66-30%Al), and examine their potential as sorbents to remove MB, a cationic basic dye, in wastewater. The kinetics and equilibrium of the adsorption process were fitted to kinetics models and equilibrium theoretical models. Further, the mechanism that limits

the rate of sorption reaction was investigated using an intraparticle diffusion method to improve understanding of the dynamics in the adsorption process.

5.3 Materials and methods

5.3.1 Synthesis and activation

All chemicals were supplied by Sigma-Aldrich (Australia) without further purifications.

A scaled-up procedure of a previously reported method [59] of synthesising Zr-MOF was successfully undertaken, using a modified ratio of $ZrCl_4$:BDC:DMF (2.27 mmol $ZrCl_4$, 2.27 mmol 1,4-benzenedicarboxylic acid [BDC]). The abovementioned chemicals were mixed with continuous agitation with 405.38 mmol N, N-dimethylformamide (DMF) solvothermally. The resulting mixture was placed in an autoclave at 393 K for 1 d. The product Zr-MOF was filtered, dried and immersed in chloroform for 5 d. After activation by chloroform was completed, the solid was filtered and dried using vacuum and heated at 463 K for 48 h.

The following method was used to synthesise UiO-66-10%Al. Terephthalic acid (1.1 g, 98%; Sigma-Aldrich) and DMF (73 mL, 99%; Sigma-Aldrich) were mixed together and stirred until the acid dissolved. Within 10 min of the clear solution forming, ZrCl4 (1.5 g; Sigma-Aldrich, 99%) was added to the solution with continued stirring for another 5 min. Al $(NO_3)_3.9H_2O$ (0.15 g) was then added, along with 2 mL of H_2O, to the mixture and stirred for another 15 min. The solution was transferred to a 125-mL Teflon-lined autoclave, which was tightly sealed and then placed in a preheated oven at 132 °C for 24h. The white powder product of UiO-66-10% Al was collected using a centrifuge machine and washed in DMF three times. The resultant product was dried in an oven and activated by immersing it in absolute methanol (100%; Sigma-Aldrich) for 5 d. Before using the MOF as an adsorbent, it was filtered, dried and heated in vacuum at 473K overnight.

To synthesise UiO-66-30%Al, $ZrCl_4$ (1.5 g) was mixed with terephthalic acid (1.3 g) in DMF (60.2 mL). After mixing for 15 min, Al $(NO_3)_3.9H_2O$ (0.45 g) was added and then 5 mL of H_2O was added to the mixture. The solution was mixed for approximately 30 min. It was then moved to a 125-mL Teflon-lined autoclave, which was tightly

sealed and then placed in a preheated oven at 157°C for 1d. The white powder product of UiO-66-10% Al was collected using a centrifuge machine and washed in DMF three times. The resultant product was dried in an oven and activated by immersing in absolute methanol (100%; Sigma-Aldrich) for 5d. Before using the MOF as an adsorbent, it was filtered, dried and heated in a vacuum at 473K overnight.

5.3.2 Characterisation

Thermogravimetric analysis (TGA) of the single-metal and bimetal Zr-MOFs was done using a TGA instrument (TGA/DSC1 STARe system; Mettler-Toledo). All MOF samples were placed in crucibles and transferred to the machine and heated at a rate of 5K/min until 1173K when the air gas flow rate was maintained at 10 mL/min.

The stability of the functional groups on the organic linkers were assessed using Fourier transform infrared spectroscopy (FTIR; Spectrum 100 FT-IR spectrometer, PerkinElmer). A scanning process was undertaken by an attenuated total reflectance technique to obtain the FTIR spectra range 600 to 4000 cm^{-1} with a resolution of 4 cm^{-1}.

To check the integrity of the MOF structure, X-ray powder diffraction patterns were obtained using an X-ray diffractometer (D8 Advance, Bruker AXS) with Cu Kα radiation (λ = 1.5406 Å), accelerating voltage 40 kV and current 40 mA.

N_2 adsorption/desorption isotherms were performed using a Quantachrome instrument (Autosorb-1), and textural properties of the Zr-MOFs were determined, such as pore size, pore volume and surface area. All MOFs were prepared by heat and vacuum for 1 d before loading to the machine to determine their adsorption properties.

5.3.3 Adsorption process

An aqueous stock solution of MO (1000 ppm) was prepared by dissolving MB ($C_{16}H_{18}ClN_3S$, molecular weight 319.85 $g.mol^{-1}$; Sigma-Aldrich) in deionised water. Aqueous solutions with different concentrations of MB (5–100 ppm) were prepared by successive dilution of the stock solution with water, and MB concentrations were determined using absorbance at 668 nm wavelength of the solution after obtaining the UV spectra of the solution with a spectrophotometer (UV spectrophotometer). A

calibration curve was obtained from spectra of the standard solutions (5–100 ppm). Prior to adsorption, the adsorbents were dried overnight in a vacuum at 373 K. Several glass containers were cleaned, dried and filled to 20 mL with MB of different concentrations ranging from 5 to 50 ppm. Following this, an exact amount of an MOF adsorbent (20 mg) was put in each glass container.

The dye solutions containing the adsorbents were mixed well by a magnetic stirrer and maintained for 5 min to 24h at 298K. The samples for analysis were collected by syringe filter at different sampling intervals. A UV spectrometer was used to investigate the dye content in the supernatant.

5.3.4 Adsorption study

The adsorption mechanism and rate of diffusion were estimated using three kinetic models: are pseudo second-order [119], pseudo first-order [120] and intraparticle diffusion models [121]. Adsorption behaviours were simulated using the Langmuir [122] and Freundlich [123] adsorption isotherms.

5.3.4.1 Kinetics study

Batch adsorption laboratory techniques were used to design the experiments. All practical kinetics experiments were conducted by preparing the specified initial concentrations (5–50 mg/L) and adding a predetermined dose of the adsorbent into a definite volume of MB solution at room temperature. Agitation was performed with a magnetic stirrer machine at 200 rpm to optimise mass transfer and contact with the interfacial area for a predetermined time interval. MB concentration was measured using the supernatant at each predetermined time interval using a UV spectroscopy machine.

The amount of MB adsorbed onto UiO-66, UiO-66-10%Al and UiO-66-30%Al MOFs at any time was calculated using Equation 5.1 [124]. However, the percentage removal of MB was computed by Equation 5.2 [125].

$$q_t = (C_0 - C_t)\frac{V}{m} \tag{5.1}$$

$$R\% = \frac{(C_0 - C_t)}{C_0} X100 \tag{5.2}$$

Where:

q_t: the amount of MB adsorbed per unit weight of MOF at any time t (mg/g)

C_0: initial concentration of the MB solution at time zero (mg/L)

C_t: the concentration of MB solution at time t (mg/L)

V: volume of the MB solution in the batch adsorption process (L)

R%: percentage removal of MB

m: MOF mass used in the adsorption batch process (g).

5.3.4.1.1 Pseudo first-order model

The MOF removal of MB from simulated wastewater can be represented by a linear pseudo first-order model of adsorption [120, 126] expressed below:

$$l\,n(q_e - q_t) = l\,n(q_e) - k_1 t, \tag{5.3}$$

Where:

q_e: the amount of MB adsorbed per unit weight of MOF at equilibrium (mg/g)

q_t: the amount of MB adsorbed per unit weight of MOF at any time t (mg/g)

k_1: pseudo first-order rate constant (min^{-1})

t: time (min).

The linear relationship between values of $\ln(q_e - q_t)$ and t can be plotted as a straight line, from which q_e and k_1 can be found easily from the intercept and slope, respectively.

5.3.4.1.2 Pseudo second-order model

The sorption kinetics of the MOF/MB system may also be described by a linearised form of the pseudo second-order model [119], based on adsorption equilibrium capacity expressed in the following form:

$$\frac{t}{q_t} = \frac{1}{k_2 \quad q_e^2} + \frac{1}{q_e} t, \tag{5.4}$$

Where:

q_e: the amount of MB adsorbed per unit weight of MOF at equilibrium (mg/g)

q_t: the amount of MB adsorbed per unit weight of MOF at any time t (mg/g)

t: time (min)

k_2: pseudo second-order rate constant (g/mg min).

The values of (t/q_t) are linearly correlated with t, and the plot of (t/q_t) against t should be a straight line. The determination of q_e and k_2 can be done from the slope and intercept, respectively.

5.3.4.1.3 Elovich kinetic model

The Elovich equation is generally used for chemisorption applications and can be written as follows:

$$\left(\frac{dq_t}{dt}\right) = \alpha\, Exp(-\beta q_t), \tag{5.5}$$

Where:

q_t: the amount of MB adsorbed per unit weight of MOF at any time t (mg/g)

α: a constant representing the initial rate of adsorption

β: constant during any one experiment

t: time (min).

It appears that the initial adsorption rate at the beginning of contact time is not controlled by exponential law because when q_t approaches zero, dq_t/d_t equals α [127]. Integrating Equation 5.5 by assuming $q_t = 0$ at $t = 0$, the result will be:

$$q_t = \left(\frac{1}{\beta}\right)\ln(1 + \alpha.\beta t). \tag{5.6}$$

If αβt > 1, the simple form of Equation 5.6 can be expressed as follows:

$$q_t = \left(\frac{1}{\beta}\right)\ln(\alpha.\beta) + \left(\frac{1}{\beta}\right)\ln(t). \tag{5.7}$$

In a plot of the straight-line equation of q_t as a function of ln(t), the slope and intercept will be (1/β) and (1/β) ln(αβ), respectively.

Equation 5.7 can facilitate the determination of the applicability of the Elovich kinetic equation on MOF/MB systems [128].

5.3.4.1.4 Intraparticle diffusion model

The intraparticle diffusion–based model is commonly used to test the mechanism of adsorption of pollutants onto a sorbent. This model is employed to identify the adsorption mechanism of MB onto MOF, and can be written as follows:

$$q_t = k_p t^{1/2} + C, \quad (5.8)$$

Where:

q_t: the amount of MB adsorbed per unit weight of MOF at any time t (mg/g)

k_p: intraparticle diffusion rate constant (mg/ g $min^{0.5}$)

t: time (min)

C: intercept.

Based on this model, which is a linear relationship, the loading capacity is proportional to $t^{1/2}$ as well as the intraparticle diffusion rate constant (k_p); k_p and C can be determined from the slope and intercept of the intraparticle diffusion equation plot, respectively.

5.3.4.2 Equilibrium studies

Equilibrium studies were also performed in the same experiments carried out for kinetics studies. Agitation was done using a magnetic stirrer machine at 200 rpm until the process reached equilibrium.

The amount of MB adsorbed onto UiO-66, UiO-66-10%Al and UiO-66-30%Al MOFs at equilibrium can be expressed by Equation (2)[129]:

$$q_e = (C_0 - C_e)\frac{V}{m}, \quad (5.9)$$

Where:

q_e: the amount of MB adsorbed per unit weight of MOF at equilibrium (mg/g)

C_0: initial concentration of MB solution at time zero (mg/L)

C_e: concentration of MB solution at equilibrium (mg/L)

V: volume of MB solution in batch adsorption process (L)

m: MOF mass used in the adsorption batch process (g).

5.3.4.2.1 Isotherm models

Identifying an adsorption isotherm is essential for describing the interaction of the pollutant (MB) with the adsorbent (MOF), so that the adsorbent can be optimised [130]. The two common isotherms are the Langmuir [131] and the Freundlich [123] isotherms.

5.3.4.2.1.1 The Langmuir model

A nonlinear form of the Langmuir isotherm model can be expressed as:

$$q_e = \frac{q_m k_L C_e}{(1 + k_L C_e)}. \quad (5.10)$$

It is possible to linearise the Langmuir isotherm equation to give the following:

$$\frac{C_e}{q_e} = \frac{1}{q_m} C_e + \frac{1}{k_L q_m}, \quad (5.11)$$

Where:

q_m: Langmuir maximum loading capacity (mg/g)

K_L: Langmuir constant related to the energy of adsorption and affinity of binding sites (L/mg)

C_e: the equilibrium concentration of adsorbate (mg/L)

q_e: adsorption capacity at equilibrium (mg/g).

A plot of C_e/q_e versus Ce should obtain a linear relationship. Therefore, q_m and K_L can be determined from the slope and intercept of the plot.

The dimensionless constant separation factor R_L is an important characteristic of the Langmuir isotherm that can be represented by the following equation [96, 132-134]:

$$R_L = \frac{1}{(1 + k_L C_0)}, \quad (5.12)$$

Where:

C_0: initial concentration of MB (mg/L)

K_L: Langmuir constant (L/mg).

The value of R_L plays a very important role in the shape of the isotherm because it indicates the adsorption process is:

- unfavourable (RL > 1)
- linear (RL = 1)
- favourable (0 < RL < 1)
- irreversible (RL = 0).

5.3.4.2.1.2 The Freundlich model

The nonlinear model of the Freundlich isotherm [123] can be expressed as:

$$q_e = k_F C_e^{1/n}. \tag{5.13}$$

The linear equation of the Freundlich isotherm can be expressed as [15, 135]:

$$\ln(q_e) = \ln(k_F) + \frac{1}{n}\ln(C_e), \tag{5.14}$$

Where:

K_F: the calculated Freundlich equilibrium constant ([mg/g] $[L/mg]^{1/n}$) as an indicator of adsorption capacity

n: a measure of the deviation from linearity of adsorption (g/L).

A plot of $\ln(q_e)$ versus ln(Ce) should obtain a linear relationship; therefore, n and K_F can be determined from the slope and intercept of the plot.

If the value of n > 1, it is good indication that the adsorption process is favourable.

5.4 Results and discussion

5.4.1 Characterisation

As shown in Figure 5.1(a), the XRD pattern for the modified bimetal Zr-MOF (UiO-66-10%Al and UiO-66-30%Al), in contrast to the parent single-metal Zr-MOF (UiO-66) before and after use, verify the phase purity and structural integrity of the MOF samples. Therefore, they are good signs of successful synthesis and activation of MOFs with pores free of oxide contaminants. Furthermore, Figure 5.1(a) show also the XRD patterns of the same above-mentioned MOFs after use in adsorption process.

Figure 5.1(b) illustrates FTIR spectra of parent (UiO-66) and modified bimetal Zr-MOF (UiO-66-10%Al and UiO-66-30%Al) before and after use. According to FTIR spectra of the three Zr-MOFs (single-metal and bimetal samples) shown in Figure 5.1(b), the application of the same vibration bands resulted in a slight deviation in the position of some peaks for the bimetal samples, with broader peaks verifying a difference in the dipole between ground state and excited state of bimetal Zr- MOFs due to incorporation of the second metal centre [136, 137]. The extension of the vibration bands of bimetal MOFs was 1590 to 1525 cm^{-1}; it was originally in the range 1615 to 1580 cm^{-1} because of C=C-C stretching in the aromatic ring of terephthalate salts [138]. In addition, the FTIR spectrum shows the stretching vibration of symmetric COO^- and asymmetric COO^- in organic linkers at bands 1500 and 1390 cm^{-1}. However, bands at 881, 812 and 785 cm^{-1} were assigned to Zr-O stretching. In addition, stretching vibration of C-H at 730 cm^{-1} was attributed to the out-of-plane bending of aromatic ring of UiO-66, in comparison with that at 744 cm^{-1} attributed to the spectrum of bimetal Zr-MOF [137, 139] and the stretching vibration of C-H at 1017 cm^{-1} to Zr-MOF.

Thermal stability of UiO-66, UiO66-10%Al and UiO66-30%Al were investigated using a TGA machine (TGA/DSC1 STARe system; Mettler-Toledo). The results of thermogravimetric analysis of all Zr-MOFs (single-metal and bimetal) are shown in Figure 5.1(c). They validate the thermal stability and structural robustness up to 725 K with a continuous mass loss of 15% and 25% for bimetal and single-metal MOFs, respectively. However, the variation in the weight loss of the samples is due to pre-treatment (dehydrated and hydrated) and solvent molecules in the pore interior of the material [140].

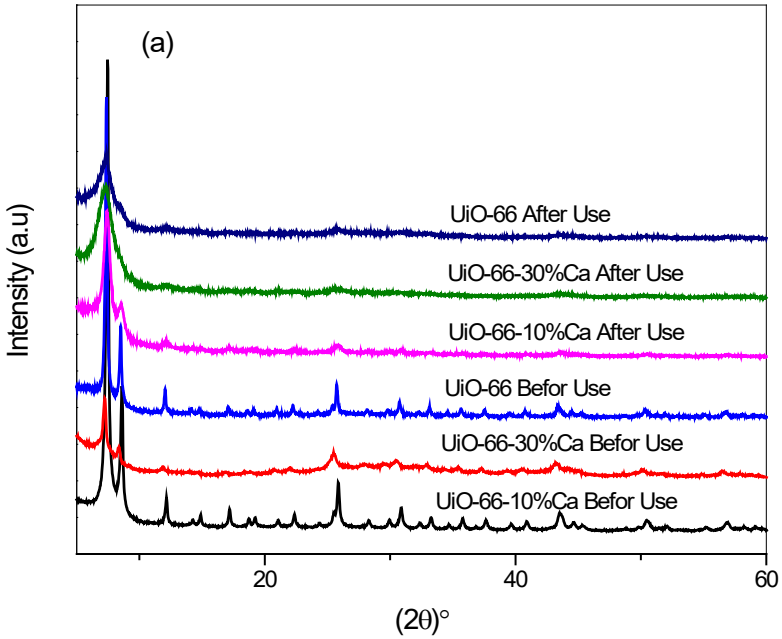
(a)
UiO-66 After Use
UiO-66-30%Ca After Use
UiO-66-10%Ca After Use
UiO-66 Befor Use
UiO-66-30%Ca Befor Use
UiO-66-10%Ca Befor Use
Intensity (a.u)
20
40
60
(2θ)°

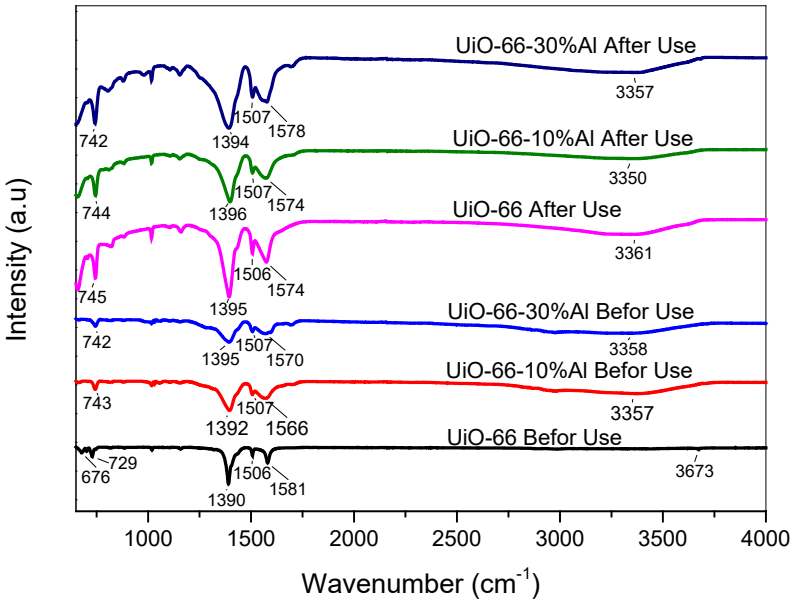
UiO-66-30%Al After Use
3357
742
1394
1507
1578
UiO-66-10%Al After Use
3350
744
1396
1507
1574
UiO-66 After Use
3361
745
1395
1506
1574
UiO-66-30%Al Befor Use
3358
742
1395
1507
1570
UiO-66-10%Al Befor Use
3357
743
1392
1507
1566
UiO-66 Befor Use
3673
676
729
1390
1506
1581
Intensity (a.u)
1000
1500
2000
2500
3000
3500
4000
Wavenumber (cm-1)

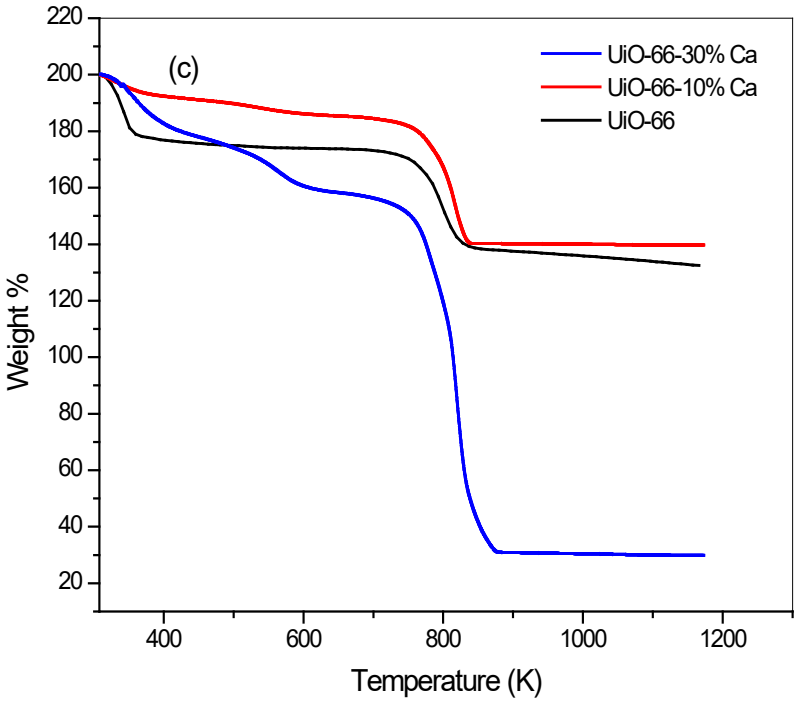

Figure 5.1: Characterisation of metal organic framework samples: (a) PXRD patterns, (b) FTIR spectra and (c) TGA profiles of pristine and modified UiO-66 samples.

Measurements of N_2 adsorption/desorption isotherms, pore size and surface area of Zr-MOFs (single-metal and bimetal) were obtained (Autosorb-1, Quantachrome Instruments). The isotherms of UiO-66-Al and UiO-66 are illustrated in Figure 5.2(a) and (b). According to Figure 5.2(a), the parent UiO-66 MOF exhibits the analogous of type IV adsorption–desorption isotherm, which is proof of a typical mesoporous network. Moreover, hysteresis from 0.1–1.0 relative pressure indicates a homogeneous pore size distribution [2].

On the other hand, Figure 5.2(b) shows hysteresis in the desorption isotherm of UiO-66-10%Al and rapid increase in adsorption at approximate relative pressure equal to 0.999, indicating improving mesopore and macropore size. Based on the N_2 adsorption–desorption isotherms, the values for the surface area, pore volume and pore size (textural properties) of Zr-MOF were calculated and listed in Table 5.1. These values indicate decreases in the specific surface area (S_{BET}) with increases in the percentage of the second metal. That is, the S_{BET} gradually decreased from

1585.5 m^2g^{-1} in UiO-66 to become 1145.953 m^2g^{-1} in UiO-66-10%Al, and reached 769.011 m^2g^{-1} in UiO-66-30%Al.

In contrast, the pore volume and diameter were enlarged in UiO-66-10%Al, at 1.34 cc g^{-1} and 2.33 nm, respectively. The reason for such augmentation is attributable to the replacement of methanol molecules by the second metal in the first activation process involving solvent exchange and discarding it in the second activation process by heating and vacuum.

Table 5.1: Textural properties of adsorbents based on N_2 adsorption/isotherms.

Adsorbents	Specific surface area (S_{BET}) (m^2g^{-1})	Pore volume (cc g^{-1})	Pore diameter (nm)
UiO-66	1585.5	0.82	1.04
UiO-66-10% Al	1145.953	1.34	2.33
UiO-66-30% Al	769.011	0.39	1.01

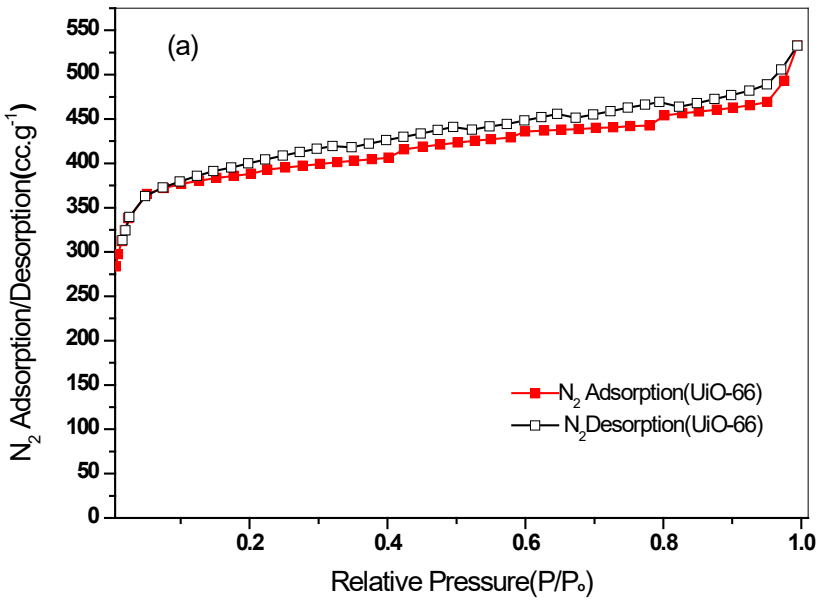

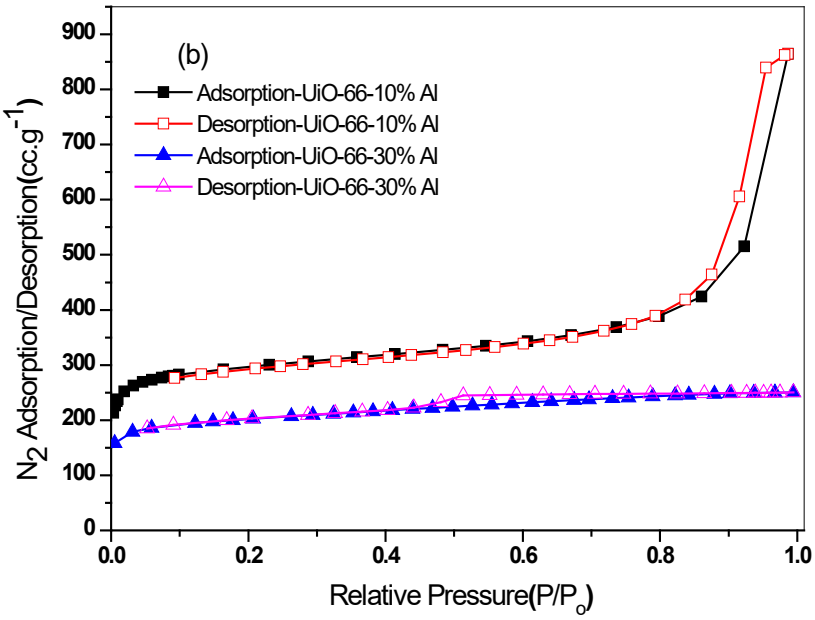
(b)
Adsorption-UiO-66-10% Al
Desorption-UiO-66-10% Al
Adsorption-UiO-66-30% Al
Desorption-UiO-66-30% Al
N2 Adsorption/Desorption(cc.g-1)
Relative Pressure(P/Po)
0
100
200
300
400
500
600
700
800
900
0.0
0.2
0.4
0.6
0.8
1.0

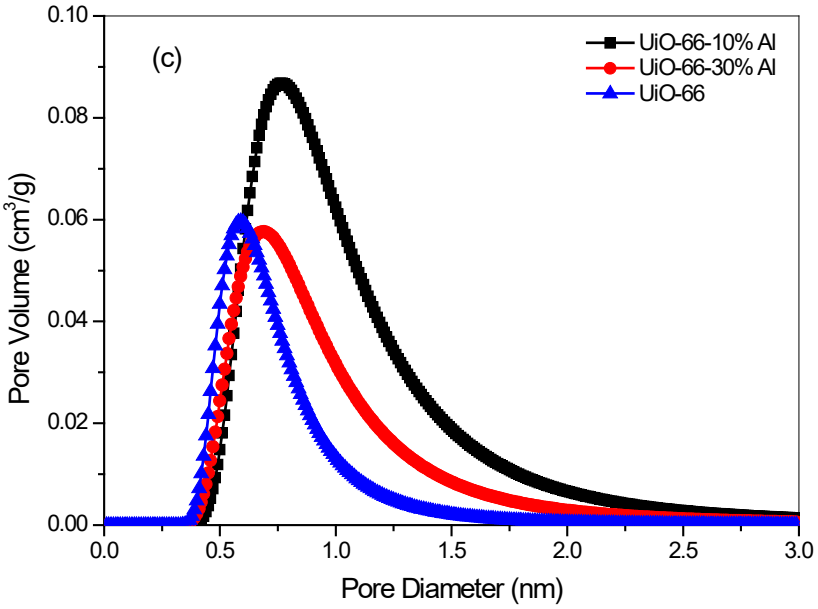
(c)
UiO-66-10% Al
UiO-66-30% Al
UiO-66
Pore Volume (cm3/g)
Pore Diameter (nm)
0.00
0.02
0.04
0.06
0.08
0.10
0.0
0.5
1.0
1.5
2.0
2.5
3.0

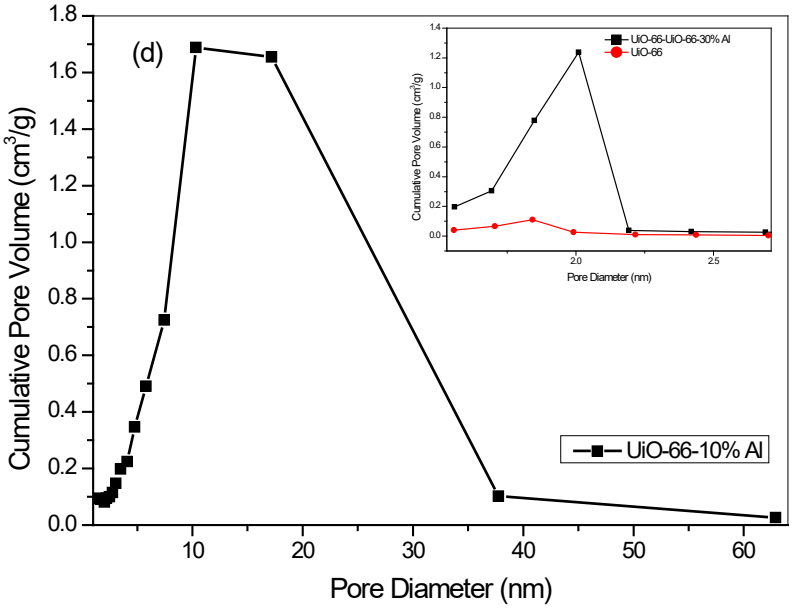

Figure 5.2: N_2 adsorption/desorption isotherm of UiO-66 (a), N_2 adsorption/desorption isotherms of UiO-66-Al samples (b), micropore distribution (b)and mesopore distribution (c) of. UiO-66, UiO-66-10% Al and UiO-66-30% Al.

5.4.2 Kinetics studies

Studies of kinetics are an essential part of a sorption process to enable the researchers to determine the rate and mechanism of adsorption [141]. To investigate the adsorption mechanism, including the mass transfer and chemical reaction [2], experimental data were examined using pseudo first-order, pseudo second-order and Elovich models. All the information and parameters relating to mechanism of adsorption can be obtained via adsorption kinetics, which are vital in treatment of aqueous effluent [142].

The adsorption process of the three solid /liquid (MOF/MB) systems were examined using pseudo first-order, pseudo second-order [143-145] and Elovich models [128, 141, 146]. The key feature of these equations is the ease with which adsorption properties (e.g., adsorption capacity, rate constant) can be assigned, and the initial adsorption rate can be easily found from the linear equations of these models without previous knowledge of any parameter.

As adsorption processes involve chemisorption, they can be described by pseudo second-order rate expression [143-145] and Elovich model [128, 141, 146]. Moreover,

the pseudo second-order model showed the highest linear correlation coefficient (R^2) and therefore, the highest agreement with the kinetics experimental data than did the Elovich model, for all MB/Zr-MOF systems.

The pseudo first-order equation did not fit well for the entire range of reactions in all MOF/MB systems. In general, the equation was only applicable to the first 20 or 30 min of the adsorption interaction process this is consistent with the reported literature [147-160]. Consequently, the MOF/MB systems did not fit the pseudo first-order equation for the whole range of contact time.

Kinetics adsorption studies are crucial indicators of a criteria of adsorbent efficiency (i.e., the rate of adsorption) and provide a clear picture of the mechanism of adsorption.

Figure 5.3 below explains the variation in the amount of adsorbate on adsorbent (q_t) as a function of contact time. The rate of MB adsorption was high at the beginning of the sorption process before slowing as the reaction progressed until reaching an equilibrium saturation. That the rate of adsorption was faster at the start may be due to the accessibility of adsorptive sites of the MOFs [161, 162]. The adsorption of MB by UiO-66-10%Al took less time than by the other two MOFs, which indicate that the rate of dye sorption by UiO-66-10%Al was the quickest among the three MOFs examined.

Figure 5.3 also illustrates the dependency of MB uptake on contact time given different initial concentrations of MB. It confirms that higher initial concentrations of MB lead to increases in adsorption capacity for MB dye. Consequently, MB uptake per unit mass of MOF, or adsorption density, also increases. Specifically, higher initial concentrations of MB may reduce accessibility of adsorption sites, which can increase the amount of adsorbate on adsorbent [163]. The increase in adsorption density or capacity with higher initial concentrations of MB is generally due to the availability of unsaturated adsorption sites on the surface of MOFs during the sorption batch process [164, 165].

To analyse the adsorption kinetics of the dye/MOF system, pseudo first-order [120], pseudo second-order [166] and Elovich equations [127] were examined. Tables 5.2 and 5.3 present the resultant values of the parameters fitted to the pseudo second order and Elovich models, respectively.

There pseudo first-order equation was not a good fit for the entire range of reactions in all MOF/MB systems; however, it can be generally applied to the first 20 or 30 min of the adsorption interaction process. This is consistent with the reported literature [147]. Consequently, the MOF/MB systems did not obey the equation during the whole of the contact time through the equation was mostly valid for the initial stage of the sorption process. In addition, the experimental q_e values, which can be obtained from the intercept of the linear relationship between $\ln(q_e - q_t)$ and time, did not agree with the computed values. These results are proof that the adsorption of MB onto Zr-MOFs (single-metal and bimetal) is not based on first-order kinetics [94].

The obtained experimental data were further fitted to the pseudo second-order equation. The values for q_e and k_2 were obtained from the slope and intercept of the linear plots of (t/q_t) versus t, respectively, and listed in Table 5.2. Figure 5.3(b), (d) and (f) show that MB uptake by Zr-MOF increased with increases in contact time for each of the different initial MB concentrations, as well as at higher initial MB concentrations. The correlation coefficients of the plots showed that the pseudo second-order equation had the best fit with the experimental data, with the range of R^2 values (0.9953–0.9999) listed in Table 5.2. These results verify the agreement of this kinetic model and the second-order behaviour of the adsorption process of MB by Zr-MOFs. Based on the linear regression correlation coefficient values (R^2), the nature of the sorption process over the whole range of contact time for all solid/liquid systems in this study can be considered a chemisorption mechanism, as the rate-controlling step related to valence forces of sharing or exchanging electrons between Zr-MOFs and MB.

The results of the correlational analysis of the amount of dye adsorbed (mg/g) against contact time for four initial MB concentrations (5, 15, 30 and 50 ppm) are shown in Figure 5.3. The results indicate that the amount of dye loading, q_t (mg/g), increased with contact time for each concentration separately.

The Elovich model can be applied to the chemisorption reaction; it is a model reasonably employed in chemisorption processes and to a wide range of slow adsorption processes. Specifically, this model may facilitate those systems for which the adsorption surface is heterogeneous.

Experimental data of MOF/MB batch adsorption systems were incorrectly described using the pseudo first-order model. Further, these systems can be represented by a combination of two or three sequential and instantaneous pseudo first-order reactions. The basic form of the Elovich equation described the experimental data well; however, the Elovich equation can be easily fitted to the experimental data using one straight line to describe the whole progress of contact time [128].

The experimental data were also examined with respect to the Elovich model, with the values of all parameters derived and the slope and intercept of the linear relationship indicating the constants α and β, respectively. In addition, these constants can be comparison parameters of reaction rates of MB adsorption in the various kinds of Zr-MOF; the values of α and β, derived from the linear plots of q_t versus ln(t), are listed in Table 5.3. According to the Elovich model, the increase in α and/or the decrease in β should increase the adsorption rate, which in turn increases MB uptake. Therefore, the relative loading of the three Zr-MOFs are UiO-66-10%Al > UiO-66-30%Al > UiO-66 [128].

Figure 5.3(a), (c) and (e) illustrate the changes in Zr-MOFs capacities at different initial MB concentrations with time. Loading capacities are increased with increasing contact time at each initial concentration, and with higher initial MB concentrations. Based on the values of the correlation coefficient (R^2) and the fact that higher R^2 values reflect better bit with the adsorption kinetics model, the best fit for the experimental data was exhibited by the Elovich equation model for all MB/MOF systems (single-metal and bimetal). The range of R^2 values (0.9242–0.9986) is listed in Table 5.3. These results indicate and emphasise that all the investigated sorption systems obey chemisorption kinetics.

Table 5.2: Calculated kinetics constant (k_2) and correlation coefficient (R^2) of the pseudo second-order model for C_i = 5, 15, 30 and 50 mg/L.

Adsorbent	Adsorbate	Pseudo second-order kinetics constant k_2 (g/[mg.min])							
		5 ppm		15 ppm		30 ppm		50 ppm	
		k_2	R^2	k_2	R^2	k_2	R^2	k_2	R^2
UiO-66	MB	0.01050	0.9989	0.00546	0.9992	0.00273	0.9992	0.00147	0.9990
UiO-66-10% Al	MB	1.34913	0.9999	0.01560	0.9997	0.00653	0.9995	0.00158	0.9953
UiO-66-30% Al	MB	0.00520	0.9977	0.00212	0.9984	0.00060	0.9975	0.00074	0.9990

Table 5.3: Calculated kinetics constants (α and β) and correlation coefficient (R^2) of Elovich model for C_i = 5, 15, 30 and 50 mg/L.

Adsorbent	Adsorbate	Pseudo first-order kinetics constant k_1 (min^{-1})											
		5 ppm			15 ppm			30 ppm			50 ppm		
		α	β	R^2	α	β	R^2	α	β	R^2	α	β	R^2
UiO-66	MB	0.102294	1.9857	0.9903	0.372103	0.7922	0.9738	0.619666	0.4416	0.9925	0.708909	0.2908	0.9986
UiO-66-10% Al	MB	19160.34	2.5654	0.9242	2375.29	0.9349	0.9752	166.6202	0.3296	0.9843	198.8533	0.2332	0.9367
UiO-66-30% Al	MB	0.275313	0.8190	0.9839	1.53989	0.4659	0.9626	1.530019	0.3055	0.9861	3.477099	0.2610	0.9884

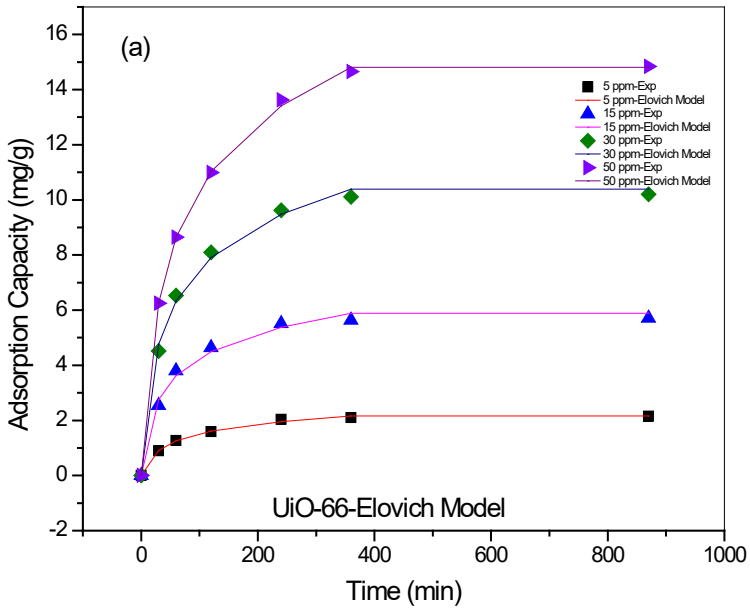
(a)
5 ppm-Exp
5 ppm-Elovich Model
15 ppm-Exp
15 ppm-Elovich Model
30 ppm-Exp
30 ppm-Elovich Model
50 ppm-Exp
50 ppm-Elovich Model
UiO-66-Elovich Model
Adsorption Capacity (mg/g)
Time (min)

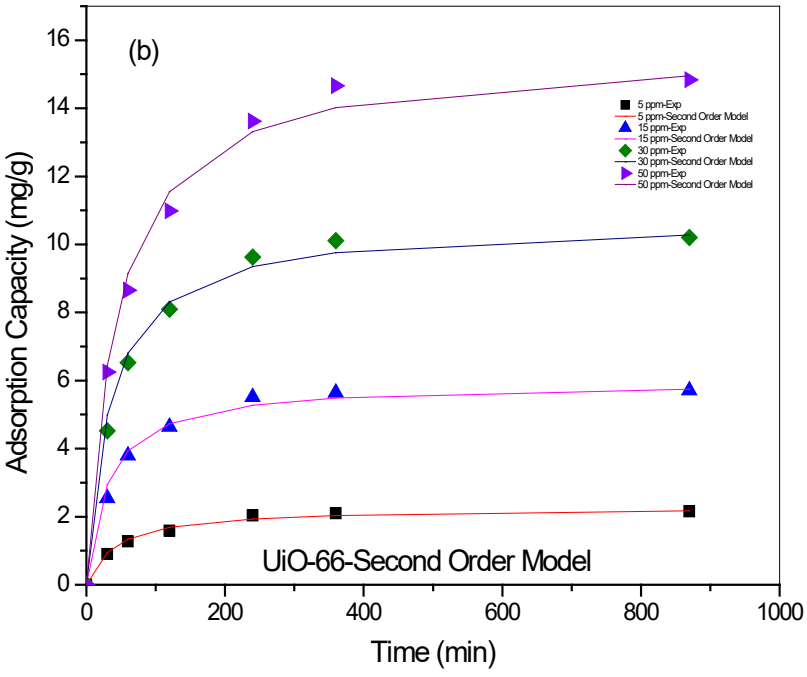
(b)
5 ppm-Exp
5 ppm-Second Order Model
15 ppm-Exp
15 ppm-Second Order Model
30 ppm-Exp
30 ppm-Second Order Model
50 ppm-Exp
50 ppm-Second Order Model
UiO-66-Second Order Model
Adsorption Capacity (mg/g)
Time (min)

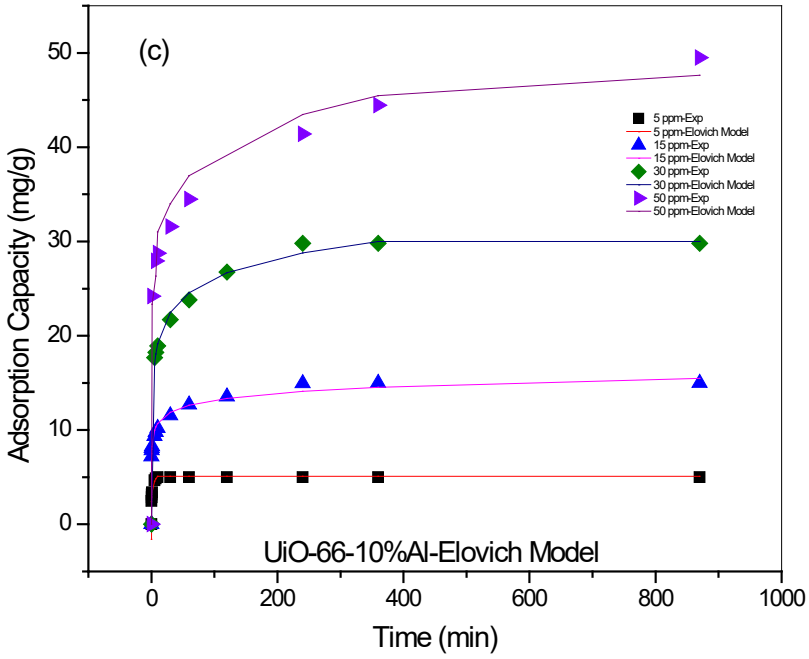
(c)
Adsorption Capacity (mg/g)
Time (min)
UiO-66-10%Al-Elovich Model
5 ppm-Exp
5 ppm-Elovich Model
15 ppm-Exp
15 ppm-Elovich Model
30 ppm-Exp
30 ppm-Elovich Model
50 ppm-Exp
50 ppm-Elovich Model

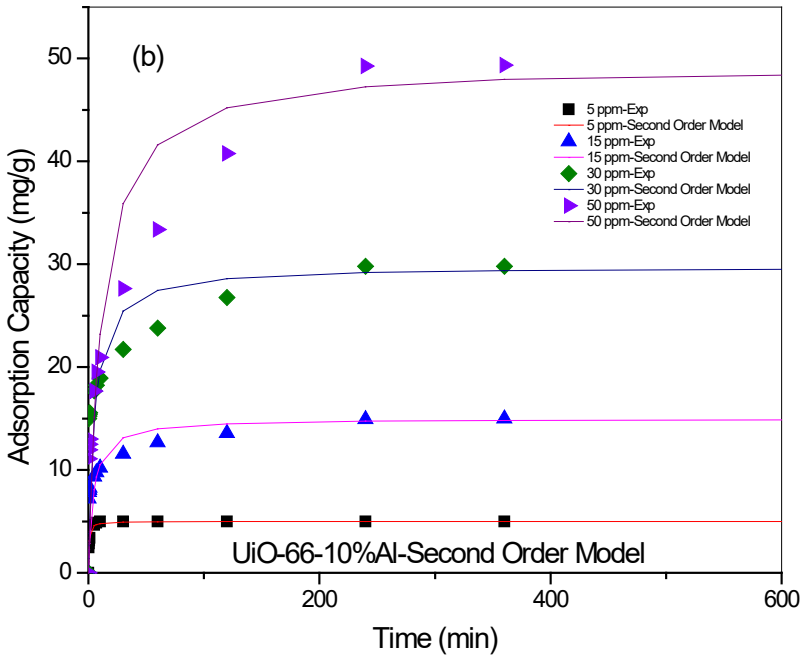
(b)
Adsorption Capacity (mg/g)
Time (min)
UiO-66-10%Al-Second Order Model
5 ppm-Exp
5 ppm-Second Order Model
15 ppm-Exp
15 ppm-Second Order Model
30 ppm-Exp
30 ppm-Second Order Model
50 ppm-Exp
50 ppm-Second Order Model

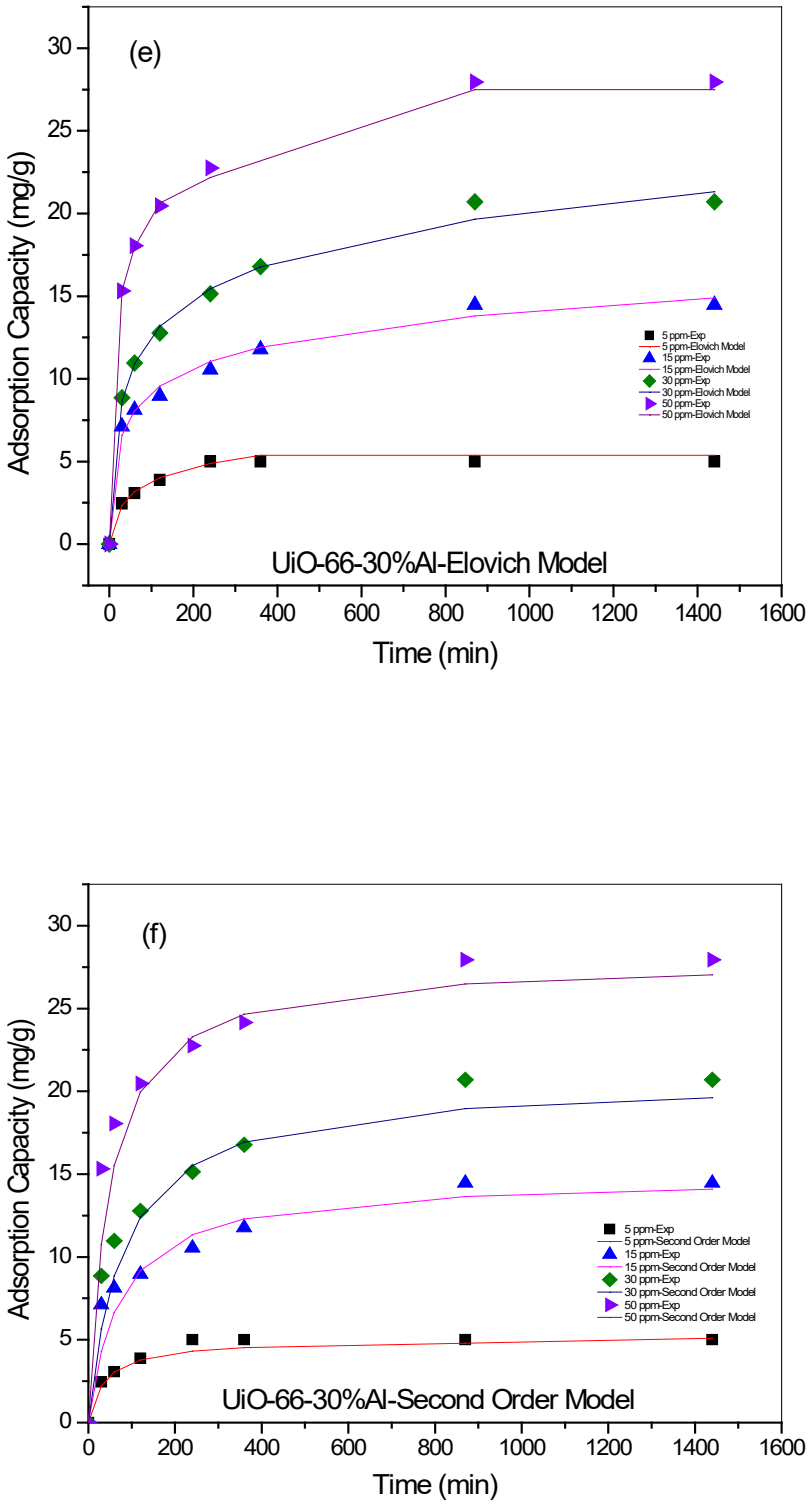

Figure 5.3: Fitting of experimental data using Elovich and second-order kinetics models of MB adsorption MB onto UiO-66 (a, b), UiO-66-10%Al (c, d) and UiO-66-30%Al (e, f).

5.4.3 Intraparticle diffusion studies

In addition, the intraparticle diffusion model suggested by Weber and Morris [121] was utilise to recognise the diffusion mechanism. Based on this model, the loading q_t against the square root of the contact time varies almost proportionally. Further, intraparticle diffusion models are vital to identifying the steps involved in the adsorption process to facilitate understanding of the adsorption mechanism [167].

The lack of descriptions of the adsorption mechanism and rate-controlling step of the adsorption process are some of the limitations of the pseudo first-order, pseudo second order and Elovich kinetic models. In response to these limitations, Weber and Morris created the intraparticle diffusion model [168]. The migration of the pollutant (MB) from bulk phase to the surface of the sorbent (Zr-MOFs) can be either by film or external diffusion, pore diffusion, surface diffusion and adsorption on the pore surface, or a combination of more than one of these steps [169].

Figure 5.4 plots the q_t against $t^{1/2}$ rather than t, for the various initial MB concentrations. Linear variations in uptake with $t^{1/2}$ is gained for a certain initial fraction of the reaction. The straight-line plot of qt versus $t^{1/2}$ may provide the values of the intraparticle diffusion rate constant k_p; k_p and C can be found from the slope and intercept of the model, respectively. Table 5.4 lists these values as well as the correlation coefficients (R^2) for the initial MB concentrations 5, 15, 30 and 50 mg/L. The focus of the intraparticle diffusion model is on the second linear portion of the plot, in which the slope characterises the rate constant (k_p) while the intercept (C) is related to the thickness of the boundary layer [15].

Figure 5.4 illustrates the three stages of the adsorption mechanism, which are represented by the three linear relationships. The first part of the plot is inclined sharply, indicating rapid sorption or external surface adsorption. The second part represents the rate-controlling step which is intraparticle diffusion, the slowest stage of adsorption [170]. The last part is the equilibrium where the processes of adsorption of MB onto Zr-MOFs reach a plateau because either the active adsorptive sites on MOFs have been occupied or the concentration of MB in the solution is extremely low [95]. Specifically, Figure 5.4 shows that the second straight line does not pass through the origin or initial point of adsorption because of variations in mass-transfer rate between the saturation and equilibrium steps of sorption [171-174]. In addition, this

kind of deviation from the origin is proof that pore diffusion is not the only rate-limiting factor [175].

Table 5.4: Calculated kinetics constant (k_p), C and correlation coefficient (R^2) for C_i = 5, 15, 30 and 50 ppm.

Adsorption mechanism				
Intraparticle diffusion model				
Adsorbent	**Initial concentration of MB solution (mg L^{-1})**	**k_p (mg $g^{-1}min^{-(1/2)}$)**	**C (mg g^{-1})**	**R^2**
UiO-66	5	0.0991	0.5017	0.9999
	15	0.22	2.1455	0.9918
	30	0.3955	3.5763	0.9884
	50	0.638	3.8144	0.9959
UiO-66-10%Al	5	0.4314	3.8489	0.9850
	15	0.5717	7.9333	0.9552
	30	1.011	15.226	0.9797
	50	1.1428	24.123	0.9720
UiO-66-30%Al	5	0.2536	1.0889	0.9994
	15	0.2958	5.8863	0.9947
	30	0.4446	7.9245	0.9901
	50	0.4402	15.395	0.9775

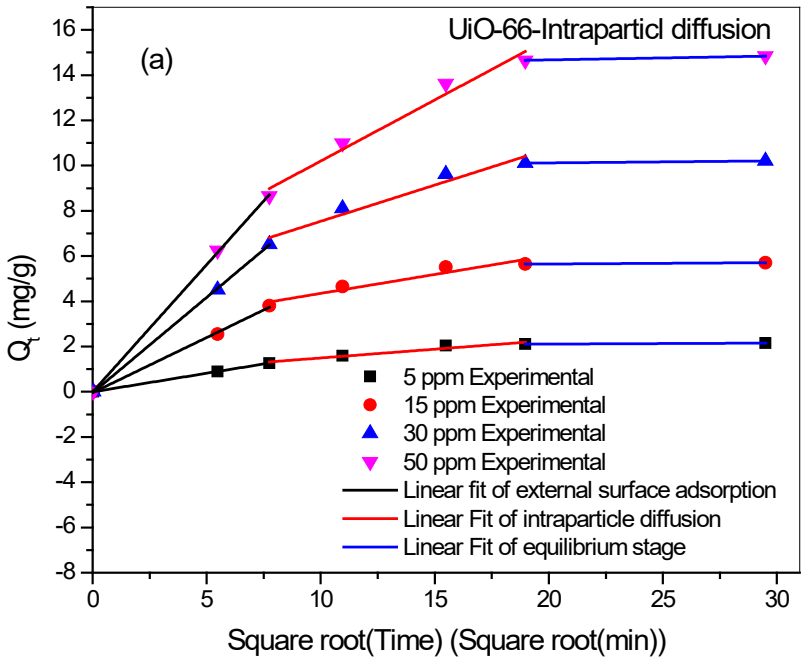

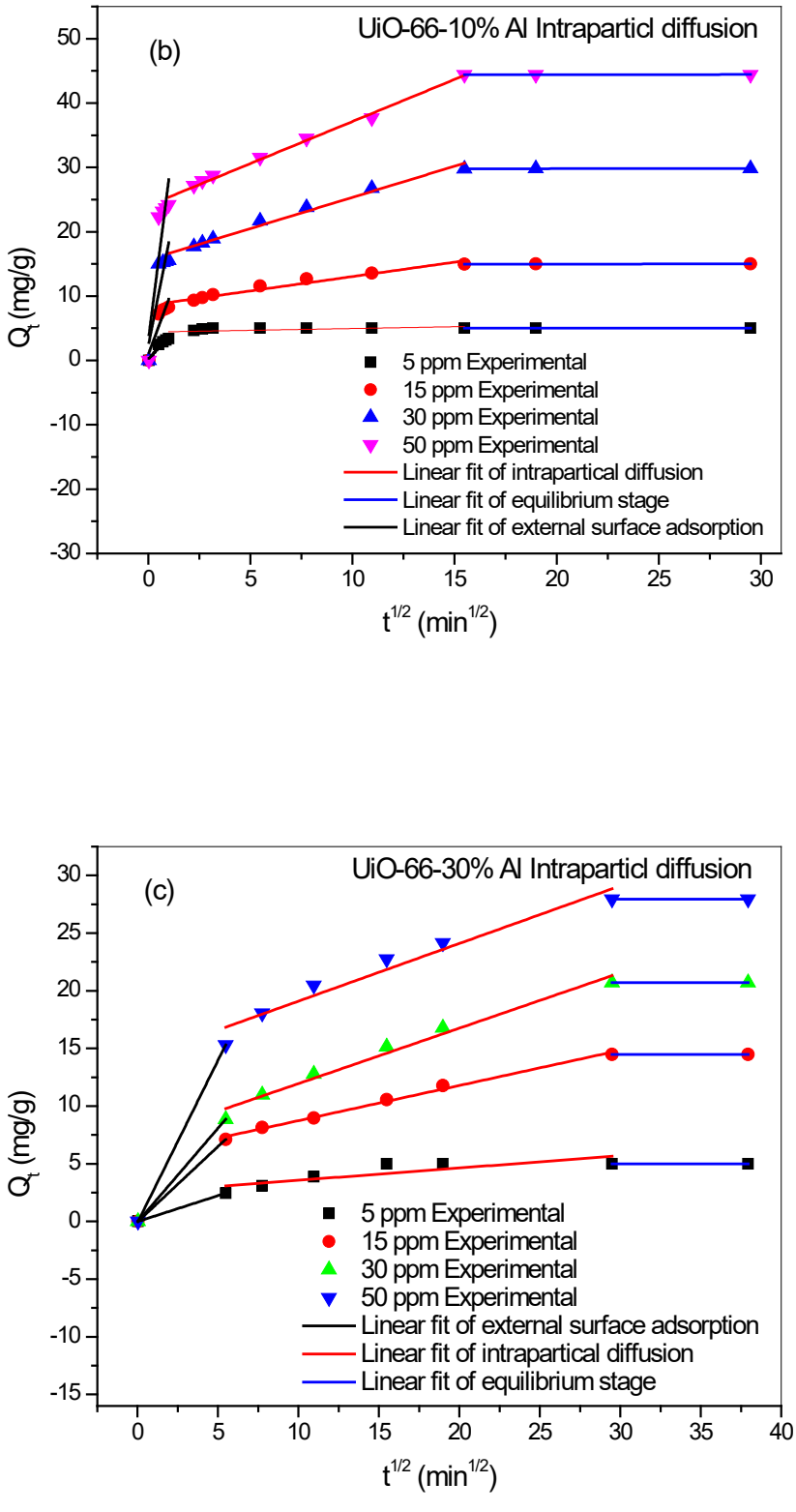

Figure 5.4: Fitting of experimental data using intraparticle diffusion models of MB adsorption onto UiO-66 (a), UiO-66-10%Al (b) and UiO-66-30%Al (c).

5.4.4 Equilibrium studies

A set of batch experiments was conducted with various initial MB concentrations: 5, 15, 30 and 50 mg/L. The one factor allowed us to vary concentrations of MB while maintaining other process factors like MOF dose, stirrer speed, volume of the solution and temperature unchanged. Data from the equilibrium experiments were investigated using Langmuir [131] and Freundlich [123] isotherms.

The assumption of the Langmuir isotherm theory is described as monolayer coverage of adsorbate (MB) onto a homogenous adsorbent (Zr-MOFs) surface [131]. Hence, its basic assumption is that sorption takes place at specific homogeneous sites on the adsorbent. As soon as an adsorbent site is occupied by an MB molecule, no additional adsorption can occur at that site again.

The equilibrium data were examined using a Langmuir model. The values of the parameters and constants, together with the R^2 values, were obtained from the slope and intercept of the linear plot and listed in Table 5.5. Figure 5.5(a), (b) and (c) illustrate the experimental equilibrium data and the predicted theoretical Langmuir isotherm for the adsorption process of MB onto Zr-MOF (single-metal and bimetal).

The fundamental characteristics of the Langmuir model can be expressed in terms of a dimensionless constant separation factor, R_L, or Equation 5.12 [133]. The value of R_L is an indication of the shape of the isotherm. Basically, the R_L value determines the favourability of the adsorption process, which can be either unfavourable ($RL > 1$), linear ($RL = 1$), favourable ($0 < RL < 1$) or irreversible ($RL = 0$). The equilibrium analysis revealed that the R_L values were between 0 and 1, indicating a favourable adsorption process for all MB/ Zr-MOF (single-metal and bimetal) systems.

The Freundlich model [123] is an empirical equation that assumes the adsorption process can occur on heterogeneous surfaces and that the adsorption capacity depends on the concentration of MB. According to Equation 5.13, equilibrium adsorption properties such as k_F and (1/n) are rough indicators of the adsorption capacity and the adsorption intensity, respectively. The favourability of the adsorption process can be determined from the magnitude of the exponent (1/n); the criterion for a favourable adsorption is that the values of n must be greater than one [176].

The equilibrium data were further tested by the Freundlich isotherm model. Freundlich isotherm constants and correlation coefficient (R^2) values are tabulated in Table 5.5. As shown in Table 5.5, the correlation coefficient of the Freundlich isotherm for all MB/MOF systems were higher than those based on the Langmuir model, proving strong linearity. The analysis verified that the values of n for all systems were greater than one, as tabulated in Table 5.5. Such a result is solid confirmation of favourable adsorption and easy loading of MB onto Zr-MOFs from aqueous solutions [177].

The maximum Langmuir adsorption capacity was exhibited by UiO-66-10%Al, with q_m of 49.26 mg/g. Furthermore, the comparative adsorption capacity of Zr-MOFs for MB in this study, relative to that of other adsorbents reported in the literature, is provided in Table 5.6.

Table 5.5: Calculated equilibrium constants (k_L, k_F, q_m, n and correlation coefficient (R^2)) of MB adsorption onto UiO-66, UiO-66-10%Al and UiO-66-30%Al for C_i = 5, 15, 30 and 50 mg/L.

Adsorbent	Adsorption isotherm model	Parameter	Value	R^2
UiO-66	Langmuir	q_m (mg/g)	14.52	0.9889
		K_L (L/mg)	0.02447	
	Freundlich	K_F ([mg/g] [L/mg]$^{1/n}$)	0.98157	0.9979
		n (g/L)	1.2918	
UiO-66-10%Al	Langmuir	q_m (mg/g)	49.26	0.9396
		K_L (L/mg)	29	
	Freundlich	K_F ([mg/g] [L/mg]$^{1/n}$)	53.53	0.9711
		n (g/L)	4.05	
UiO-66-30%Al	Langmuir	q_m (mg/g)	27.85	0.9777
		K_L (L/mg)	1.10	
	Freundlich	K_F ([mg/g] [L/mg]$^{1/n}$)	16.71	0.9888
		n (g/L)	7.52	

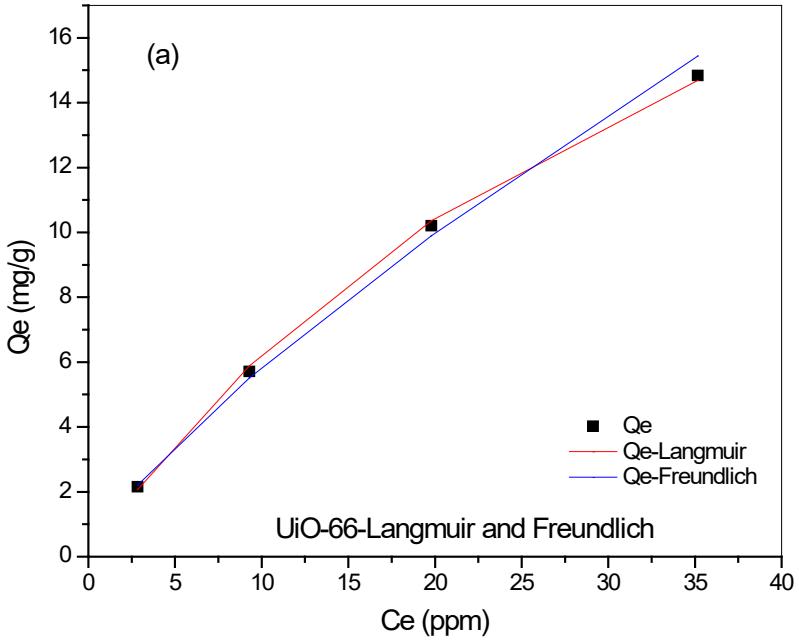
(a)
Qe (mg/g)
Ce (ppm)
Qe
Qe-Langmuir
Qe-Freundlich
UiO-66-Langmuir and Freundlich

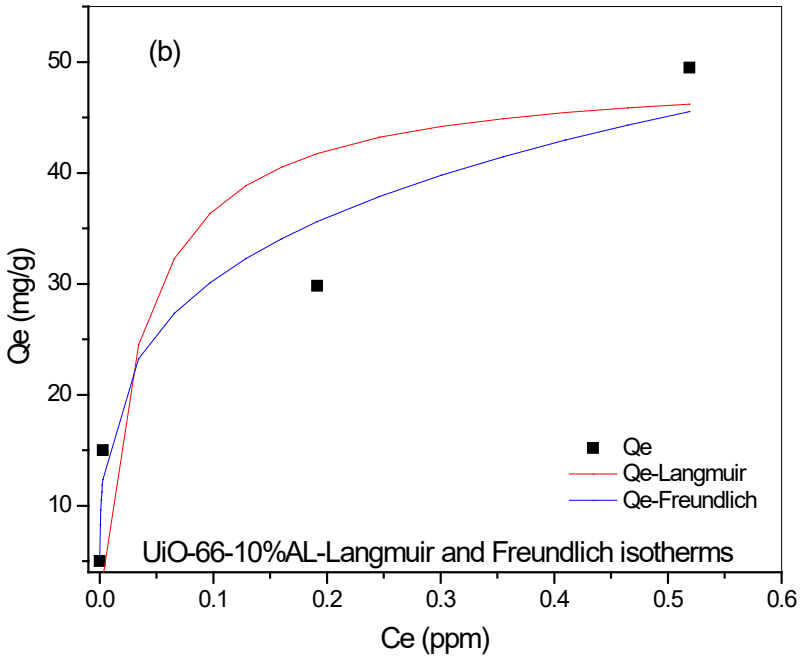
(b)
Qe (mg/g)
Ce (ppm)
Qe
Qe-Langmuir
Qe-Freundlich
UiO-66-10%AL-Langmuir and Freundlich isotherms

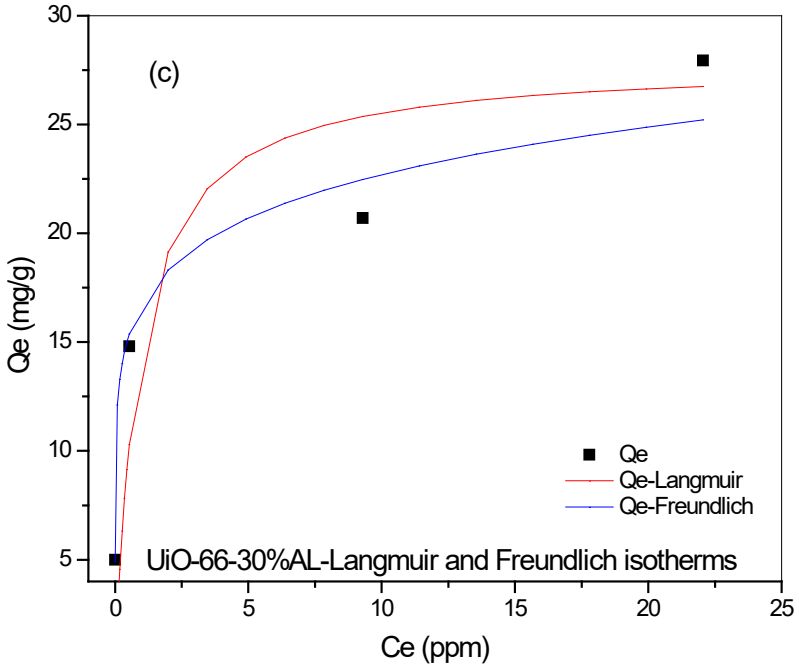

Figure 5.5: Fitting of experimental data using Langmuir and Freundlich models of MB adsorption onto UiO-66 (a), UiO-66-10%Al (b) and UiO-66-30%Al (c).

Table 5.6: Comparison of monolayer equilibrium capacity for methylene blue onto different sorbents.

Adsorbent	Condition	q_m (mg/g)	Reference
UiO-66-10%Al	Normal	49.26	This study
UiO-66-30%Al		27.85	This study
UiO-66		14.52	This study
Tobacco stem ash	Normal	35.70	[185]
Oak sawdust	Normal	29.94	[187]
$ZnCl_2$ activated POME sludge	Normal	22.40	[189]
Salvadora persica stem ash	Normal	22.78	[190]
Activated fly-ash	Normal	14.28	[192]
Fly-ash A	Normal	6.0	[72]
Coir pith carbon	Normal	5.87	[194]
Neem sawdust	Normal	3.62	[195]

5.5 Effect of pH

It is crucial step to investigate the effects of pH and zeta potential of Zr-MOF on adsorption process to examine adsorption mechanism. The result of such study is very important to figure out the impact of the electrostatic interactions on adsorption. pH

was selected in such a way to cover acidic and basic range between 3.75-10 and the adsorption process carried out at condition of initial concentration of MB solutions at 50 ppm and using 0.1 M HCl and 0.1 M NaOH to adjust pH. As show in Figure 5.6 (a) that adsorption uptake increases with increasing of pH solution from 3.75 to 10, indicating the role of electrostatic attraction between negatively charged adsorbent and cationic dye (MB). At pH equal to 5.6 which pH of isoelectric point (pH_{iep}) Figure 5.6 (b) with no charge on adsorbent, the uptake still high signifying that other factors play roles in adsorption of adsorbate while if pH less than pH_{iep} the adsorption capacity decreases steeply due to repulsion between adsorbate and adsorbent. Consequently UiO-66 can be used over a wide range of pH for discolouration of wastewater at large scale. Figure 5.7 illustrates plausible mechanism was proposed based on pH effect and Zeta potential of UiO-66. It can be concluded from the results that the adsorption mechanism of MB onto Zr-MOF is mainly depended on the electrostatic interactions between the cationic dye of positive charge and UiO-66 of positive charge. In addition, π–π interactions between the benzene rings of UiO-66 and those of the dye could have contributed to the adsorption process.

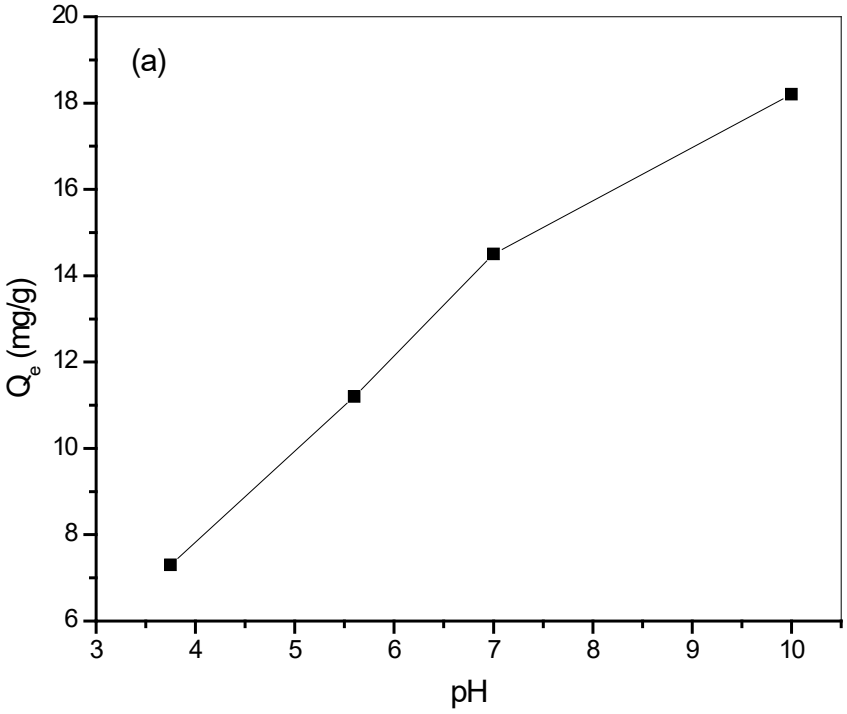

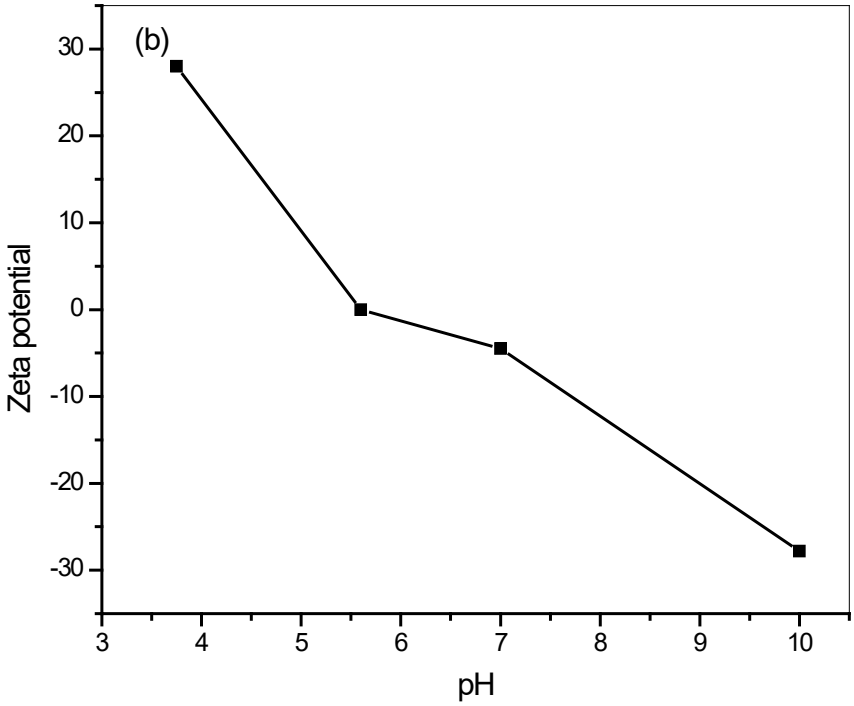

Figure 5.6. Effects of pH solution (a) and zeta potential of UiO-66 (b) on adsorption of MB onto UiO-66.

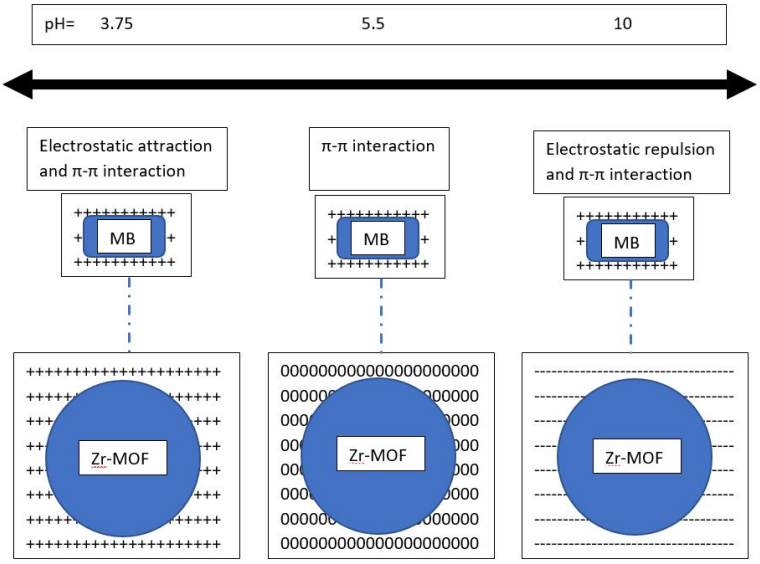

Figure 5.7. Plausible adsorption mechanism of MB onto Zr-MOF.

5.6 Conclusion

The results of the present examination of the three Zr-MOFs (single-metal and bimetal) show that these MOFs are favourable adsorbents of the basic (cationic) dye MB from aqueous solutions at a wide range of MB concentrations. The characterisation of Zr-MOFs reflected the integrity of their structures, the stability of the functional groups on the organic linkers, the suitability of their textural properties and thermal stability. Such characterisation was performed using XRD patterns, FTIR spectrum, N_2 adsorption/desorption isotherm and TGA profiles of the UiO-66 samples.

The most efficient adsorbent among the three Ze-MOFs was UiO-66-10%Al, with the largest pore volume (1.34 cc. g^{-1}) and pore diameter (2.33 nm), verifying that the addition of up to 10% Al enhanced the textural properties of the prototype Zr-MOF. For all MB/MOF systems, high initial concentrations of MB were found to facilitate adsorption capacity.

It can be concluded that the pseudo first-order model does not fit the experimental data well. While it can be generally applied to the initial period of the first step of the adsorption—consistent with reports of most sorption studies in the literature—the applicability of pseudo first-order mechanisms are restricted to a limited fraction of the beginning of the contact time [147]. The Elovich and pseudo second-order models showed the highest correlation in all MOF/MB systems studied over a longer period of adsorption. Besides, adsorption kinetics obeyed the pseudo second order kinetics model nicely, based on the fact that the highest correlation coefficients (R^2) were achieved with this model.

Equilibrium data were tested using the Langmuir and Freundlich models, and were found to be best defined by the Freundlich isotherm. The maximum adsorption capacity of the most efficient adsorbent was 49.26 mg/g for UiO-66-10%Al. This performance was compared with that of other porous adsorbents in previous studies.

The gained parameters from this study support the design and lay the foundations for establishing a continuous treatment process that removes MB from wastewater.

References

1. Wang, S., et al., *Removal of dyes from aqueous solution using fly ash and red mud.* Water Research, 2005. **39**(1): p. 129-138.
2. Lin, S., et al., *Adsorption behavior of metal–organic frameworks for methylene blue from aqueous solution.* Microporous and Mesoporous Materials, 2014. **193**: p. 27-34.
3. Aksu, Z., *Application of biosorption for the removal of organic pollutants: a review.* Process Biochemistry, 2005. **40**(3): p. 997-1026.
4. Garg, V., R. Kumar, and R. Gupta, *Removal of malachite green dye from aqueous solution by adsorption using agro-industry waste: a case study of Prosopis cineraria.* Dyes and Pigments, 2004. **62**(1): p. 1-10.
5. Chakrabarti, T., P. Subrahmanyam, and B. Sundaresan, *Biodegradation of recalcitrant industrial wastes.* 1988.
6. Clarke, E. and R. Anliker, *Handbook of environmental chemistry.* Organic Dyes and Pigments, Springer-Verlag, Heidelberg, 1980: p. 181-215.
7. Clarke, E. and R. Anliker, *Organic dyes and pigments*, in *Anthropogenic compounds*. 1980, Springer. p. 181-215.
8. Struve, W.S. and A.D. Reidinger, *Azo dyes and pigments*. 1957, Google Patents.
9. Pitter, P. and J. Chudoba, *Biodegradability of organic substance in the aquatic environment*. 1990.
10. Young, L. and J. Yu, *Ligninase-catalysed decolorization of synthetic dyes.* Water Research, 1997. **31**(5): p. 1187-1193.
11. Lian, L., L. Guo, and C. Guo, *Adsorption of Congo red from aqueous solutions onto Ca-bentonite.* Journal of Hazardous Materials, 2009. **161**(1): p. 126-131.
12. Hessel, C., et al., *Guidelines and legislation for dye house effluents.* Journal of Environmental Management, 2007. **83**(2): p. 171-180.
13. Hema, M. and S. Arivoli, *Comparative study on the adsorption kinetics and thermodynamics of dyes onto acid activated low cost carbon.* International Journal of Physical Sciences, 2007. **2**(1): p. 10-17.
14. Essawy, A.A., A.E.-H. Ali, and M.S.A. Abdel-Mottaleb, *Application of novel copolymer-TiO2 membranes for some textile dyes adsorptive removal from aqueous solution and photocatalytic decolorization.* Journal of Hazardous Materials, 2008. **157**(2): p. 547-552.
15. Kumar, K.V., V. Ramamurthi, and S. Sivanesan, *Modeling the mechanism involved during the sorption of methylene blue onto fly ash.* Journal of Colloid and Interface Science, 2005. **284**(1): p. 14-21.

16. Chiou, M.-S., P.-Y. Ho, and H.-Y. Li, *Adsorption of anionic dyes in acid solutions using chemically cross-linked chitosan beads.* Dyes and pigments, 2004. **60**(1): p. 69-84.

17. Fu, Y. and T. Viraraghavan, *Fungal decolorization of dye wastewaters: a review.* Bioresource technology, 2001. **79**(3): p. 251-262.

18. Banat, I.M., et al., *Microbial decolorization of textile-dyecontaining effluents: a review.* Bioresource technology, 1996. **58**(3): p. 217-227.

19. Lee, J.-W., et al., *Evaluation of the performance of adsorption and coagulation processes for the maximum removal of reactive dyes.* Dyes and pigments, 2006. **69**(3): p. 196-203.

20. Sulak, M., E. Demirbas, and M. Kobya, *Removal of Astrazon Yellow 7GL from aqueous solutions by adsorption onto wheat bran.* Bioresource technology, 2007. **98**(13): p. 2590-2598.

21. Qadeer, R., *Adsorption behavior of ruthenium ions on activated charcoal from nirtic acid medium.* Colloids and Surfaces A: Physicochemical and Engineering Aspects, 2007. **293**(1-3): p. 217-223.

22. Pollard, S., et al., *Low-cost adsorbents for waste and wastewater treatment: a review.* Science of the Total Environment, 1992. **116**(1-2): p. 31-52.

23. Valix, M., W. Cheung, and G. Mckay, *Preparation of activated carbon using low temperature carbonisation and physical activation of high ash raw bagasse for acid dye adsorption.* Chemosphere, 2004. **56**(5): p. 493-501.

24. Namasivayam, C. and D. Kavitha, *Removal of Congo Red from water by adsorption onto activated carbon prepared from coir pith, an agricultural solid waste.* Dyes and pigments, 2002. **54**(1): p. 47-58.

25. Namasivayam, C., D. Prabha, and M. Kumutha, *Removal of direct red and acid brilliant blue by adsorption on to banana pith.* Bioresource Technology, 1998. **64**(1): p. 77-79.

26. Valix, M., W.H. Cheung, and G. McKay, *Preparation of activated carbon using low temperature carbonisation and physical activation of high ash raw bagasse for acid dye adsorption.* Chemosphere, 2004. **56**(5): p. 493-501.

27. Tan, I.A.W., A.L. Ahmad, and B.H. Hameed, *Preparation of activated carbon from coconut husk: Optimization study on removal of 2,4,6-trichlorophenol using response surface methodology.* Journal of Hazardous Materials, 2008. **153**(1): p. 709-717.

28. Juang, R.-S., F.-C. Wu, and R.-L. Tseng, *Characterization and use of activated carbons prepared from bagasses for liquid-phase adsorption.* Colloids and Surfaces A: Physicochemical and Engineering Aspects, 2002. **201**(1): p. 191-199.

29. Pollard, S.J.T., et al., *Low-cost adsorbents for waste and wastewater treatment: a review.* Science of The Total Environment, 1992. **116**(1): p. 31-52.

30. Mohamed, M.M., *Acid dye removal: comparison of surfactant-modified mesoporous FSM-16 with activated carbon derived from rice husk.* Journal of Colloid and Interface Science, 2004. **272**(1): p. 28-34.

31. Aygün, A., S. Yenisoy-Karakaş, and I. Duman, *Production of granular activated carbon from fruit stones and nutshells and evaluation of their physical, chemical and adsorption properties.* Microporous and Mesoporous Materials, 2003. **66**(2): p. 189-195.

32. Tseng, R.-L., F.-C. Wu, and R.-S. Juang, *Liquid-phase adsorption of dyes and phenols using pinewood-based activated carbons.* Carbon, 2003. **41**(3): p. 487-495.

33. Malik, P.K., *Use of activated carbons prepared from sawdust and rice-husk for adsorption of acid dyes: a case study of Acid Yellow 36.* Dyes and Pigments, 2003. **56**(3): p. 239-249.

34. Weng, C.-H., Y.-T. Lin, and T.-W. Tzeng, *Removal of methylene blue from aqueous solution by adsorption onto pineapple leaf powder.* Journal of hazardous materials, 2009. **170**(1): p. 417-424.

35. El-Halwany, M.M., *Study of adsorption isotherms and kinetic models for Methylene Blue adsorption on activated carbon developed from Egyptian rice hull (Part II).* Desalination, 2010. **250**(1): p. 208-213.

36. Leechart, P., W. Nakbanpote, and P. Thiravetyan, *Application of 'waste'wood-shaving bottom ash for adsorption of azo reactive dye.* Journal of environmental management, 2009. **90**(2): p. 912-920.

37. McKay, G., J. Porter, and G. Prasad, *The removal of dye colours from aqueous solutions by adsorption on low-cost materials.* Water, Air, and Soil Pollution, 1999. **114**(3-4): p. 423-438.

38. Hameed, B., *Grass waste: A novel sorbent for the removal of basic dye from aqueous solution.* Journal of Hazardous Materials, 2009. **166**(1): p. 233-238.

39. Hameed, B.H., *Evaluation of papaya seeds as a novel non-conventional low-cost adsorbent for removal of methylene blue.* Journal of Hazardous Materials, 2009. **162**(2): p. 939-944.

40. Hameed, B., D. Mahmoud, and A. Ahmad, *Sorption of basic dye from aqueous solution by pomelo (Citrus grandis) peel in a batch system.* Colloids and Surfaces A: Physicochemical and Engineering Aspects, 2008. **316**(1-3): p. 78-84.

41. Ponnusami, V., S. Vikram, and S. Srivastava, *Guava (Psidium guajava) leaf powder: novel adsorbent for removal of methylene blue from aqueous solutions.* Journal of hazardous materials, 2008. **152**(1): p. 276-286.

42. Hameed, B., *Removal of cationic dye from aqueous solution using jackfruit peel as non-conventional low-cost adsorbent.* Journal of hazardous materials, 2009. **162**(1): p. 344-350.

43. Hameed, B., D. Mahmoud, and A. Ahmad, *Sorption equilibrium and kinetics of basic dye from aqueous solution using banana stalk waste.* Journal of Hazardous Materials, 2008. **158**(2-3): p. 499-506.

44. Ofomaja, A.E., *Sorption dynamics and isotherm studies of methylene blue uptake on to palm kernel fibre.* Chemical Engineering Journal, 2007. **126**(1): p. 35-43.

45. Gong, R., et al., *Removal of basic dyes from aqueous solution by sorption on phosphoric acid modified rice straw.* Dyes and Pigments, 2007. **73**(3): p. 332-337.

46. Hameed, B. and M. El-Khaiary, *Sorption kinetics and isotherm studies of a cationic dye using agricultural waste: broad bean peels.* Journal of Hazardous Materials, 2008. **154**(1-3): p. 639-648.

47. Ponnusami, V., V. Gunasekar, and S. Srivastava, *Kinetics of methylene blue removal from aqueous solution using gulmohar (Delonix regia) plant leaf powder: multivariate regression analysis.* Journal of Hazardous Materials, 2009. **169**(1-3): p. 119-127.

48. Aksu, Z. and S. Tezer, *Equilibrium and kinetic modelling of biosorption of Remazol Black B by Rhizopus arrhizus in a batch system: effect of temperature.* Process Biochemistry, 2000. **36**(5): p. 431-439.

49. Chu, H.C. and K.M. Chen, *Reuse of activated sludge biomass: I. Removal of basic dyes from wastewater by biomass.* Process Biochemistry, 2002. **37**(6): p. 595-600.

50. Fu, Y. and T. Viraraghavan, *Removal of Congo Red from an aqueous solution by fungus Aspergillus niger.* Advances in Environmental Research, 2002. **7**(1): p. 239-247.

51. Aksu, Z. and J. Yener, *A comparative adsorption/biosorption study of mono-chlorinated phenols onto various sorbents.* Waste Management, 2001. **21**(8): p. 695-702.

52. Mou, D.-G., K.K. Lim, and H.P. Shen, *Microbial agents for decolorization of dye wastewater.* Biotechnology Advances, 1991. **9**(4): p. 613-622.

53. Hu, T.-L., *Removal of reactive dyes from aqueous solution by different bacterial genera.* Water Science and Technology, 1996. **34**(10): p. 89-95.

54. Fu, Y. and T. Viraraghavan, *Dye biosorption sites in Aspergillus niger.* Bioresource Technology, 2002. **82**(2): p. 139-145.

55. Basibuyuk, M. and C.F. Forster, *An examination of the adsorption characteristics of a basic dye (Maxilon Red BL-N) on to live activated sludge system.* Process Biochemistry, 2003. **38**(9): p. 1311-1316.

56. Jacobsen, B.N., E. Arvin, and M. Reinders, *Factors affecting sorption of pentachlorophenol to suspended microbial biomass.* Water Research, 1996. **30**(1): p. 13-20.

57. Benoit, P., E. Barriuso, and R. Calvet, *Biosorption characterization of herbicides, 2,4-D and atrazine, and two chlorophenols on fungal mycelium.* Chemosphere, 1998. **37**(7): p. 1271-1282.

58. Aksu, Z. and D. Akpınar, *Modelling of simultaneous biosorption of phenol and nickel(II) onto dried aerobic activated sludge.* Separation and Purification Technology, 2000. **21**(1): p. 87-99.

59. Aksu, Z. and F. Gönen, *Biosorption of phenol by immobilized activated sludge in a continuous packed bed: prediction of breakthrough curves.* Process Biochemistry, 2004. **39**(5): p. 599-613.

60. Lièvremont, D., F. Seigle-murandi, and J.-l. Benoit-guyod, *Removal of PCNB from aqueous solution by a fungal adsorption process.* Water Research, 1998. **32**(12): p. 3601-3606.

61. Alpat, S.K., et al., *The adsorption kinetics and removal of cationic dye, Toluidine Blue O, from aqueous solution with Turkish zeolite.* Journal of Hazardous Materials, 2008. **151**(1): p. 213-220.

62. Han, R., et al., *Comparison of linear and nonlinear analysis in estimating the Thomas model parameters for methylene blue adsorption onto natural zeolite in fixed-bed column.* Journal of Hazardous Materials, 2007. **145**(1): p. 331-335.

63. Wang, S. and Z.H. Zhu, *Characterisation and environmental application of an Australian natural zeolite for basic dye removal from aqueous solution.* Journal of Hazardous Materials, 2006. **136**(3): p. 946-952.

64. Wang, S., H. Li, and L. Xu, *Application of zeolite MCM-22 for basic dye removal from wastewater.* Journal of Colloid and Interface Science, 2006. **295**(1): p. 71-78.

65. Li, C., et al., *Removal of basic dye (methylene blue) from aqueous solution using zeolite synthesized from electrolytic manganese residue.* Journal of Industrial and Engineering Chemistry, 2015. **23**: p. 344-352.

66. Sun, Z., C. Li, and D. Wu, *Removal of methylene blue from aqueous solution by adsorption onto zeolite synthesized from coal fly ash and its thermal regeneration.* Journal of Chemical Technology & Biotechnology, 2010. **85**(6): p. 845-850.

67. Gulnaz, O., et al., *Sorption of basic dyes from aqueous solution by activated sludge.* Journal of Hazardous Materials, 2004. **108**(3): p. 183-188.

68. Gupta, V.K., et al., *Removal of Rhodamine B, Fast Green, and Methylene Blue from Wastewater Using Red Mud, an Aluminum Industry Waste.* Industrial & Engineering Chemistry Research, 2004. **43**(7): p. 1740-1747.

69. Otero, M., et al., *Kinetic and equilibrium modelling of the methylene blue removal from solution by adsorbent materials produced from sewage sludges.* Biochemical Engineering Journal, 2003. **15**(1): p. 59-68.

70. Wang, S., Y. Boyjoo, and A. Choueib, *A comparative study of dye removal using fly ash treated by different methods.* Chemosphere, 2005. **60**(10): p. 1401-1407.

71. Wang, S., Q. Ma, and Z.H. Zhu, *Characteristics of coal fly ash and adsorption application.* Fuel, 2008. **87**(15): p. 3469-3473.

72. Janoš, P., H. Buchtová, and M. Rýznarová, *Sorption of dyes from aqueous solutions onto fly ash.* Water Research, 2003. **37**(20): p. 4938-4944.

73. Lin, J.X., et al., *Adsorption of basic dye from aqueous solution onto fly ash.* Journal of Environmental Management, 2008. **87**(1): p. 193-200.

74. Sun, D., et al., *Adsorption of anionic dyes from aqueous solution on fly ash.* Journal of Hazardous Materials, 2010. **181**(1): p. 335-342.

75. Ghosh, D. and K.G. Bhattacharyya, *Adsorption of methylene blue on kaolinite.* Applied Clay Science, 2002. **20**(6): p. 295-300.

76. Atun, G., et al., *Adsorptive removal of methylene blue from colored effluents on fuller's earth.* Journal of Colloid and Interface Science, 2003. **261**(1): p. 32-39.

77. Hong, S., et al., *Adsorption thermodynamics of Methylene Blue onto bentonite.* Journal of Hazardous Materials, 2009. **167**(1): p. 630-633.

78. Gürses, A., et al., *Determination of adsorptive properties of clay/water system: methylene blue sorption.* Journal of Colloid and Interface Science, 2004. **269**(2): p. 310-314.

79. Shawabkeh, R.A. and M.F. Tutunji, *Experimental study and modeling of basic dye sorption by diatomaceous clay.* Applied Clay Science, 2003. **24**(1): p. 111-120.

80. Hajjaji, M., A. Alami, and A.E. Bouadili, *Removal of methylene blue from aqueous solution by fibrous clay minerals.* Journal of Hazardous Materials, 2006. **135**(1): p. 188-192.

81. Al-Futaisi, A., A. Jamrah, and R. Al-Hanai, *Aspects of cationic dye molecule adsorption to palygorskite.* Desalination, 2007. **214**(1): p. 327-342.

82. Al-Ghouti, M.A., et al., *The removal of dyes from textile wastewater: a study of the physical characteristics and adsorption mechanisms of diatomaceous earth.* Journal of Environmental Management, 2003. **69**(3): p. 229-238.

83. Weng, C.-H. and Y.-F. Pan, *Adsorption of a cationic dye (methylene blue) onto spent activated clay.* Journal of Hazardous Materials, 2007. **144**(1): p. 355-362.

84. Senkal, B.F. and E. Yavuz, *Preparation of poly (vinyl pyrrolidone) grafted sulfonamide based polystyrene resin and its use for the removal of dye from water.* Polymers for advanced technologies, 2006. **17**(11-12): p. 928-931.

85. Senkal, B.F., et al., *Preparation of poly (glycidyl methacrylate) grafted sulfonamide based polystyrene resin with tertiary amine for the removal of dye from water.* Reactive and Functional Polymers, 2007. **67**(12): p. 1471-1477.

86. Yu, Y., et al., *Adsorption of water-soluble dyes onto modified resin.* Chemosphere, 2004. **54**(3): p. 425-430.

87. Wawrzkiewicz, M., *Removal of CI Basic Blue 3 dye by sorption onto cation exchange resin, functionalized and non-functionalized polymeric sorbents*

from aqueous solutions and wastewaters. Chemical Engineering Journal, 2013. **217**: p. 414-425.

88. Kumar, K.Y., et al., *Low-cost synthesis of metal oxide nanoparticles and their application in adsorption of commercial dye and heavy metal ion in aqueous solution.* Powder technology, 2013. **246**: p. 125-136.

89. Afkhami, A. and R. Moosavi, *Adsorptive removal of Congo red, a carcinogenic textile dye, from aqueous solutions by maghemite nanoparticles.* Journal of Hazardous Materials, 2010. **174**(1): p. 398-403.

90. Haque, E., J.W. Jun, and S.H. Jhung, *Adsorptive removal of methyl orange and methylene blue from aqueous solution with a metal-organic framework material, iron terephthalate (MOF-235).* Journal of Hazardous materials, 2011. **185**(1): p. 507-511.

91. Hasan, Z. and S.H. Jhung, *Removal of hazardous organics from water using metal-organic frameworks (MOFs): plausible mechanisms for selective adsorptions.* Journal of Hazardous Materials, 2015. **283**: p. 329-339.

92. Haque, E., et al., *Adsorptive removal of methyl orange from aqueous solution with metal-organic frameworks, porous chromium-benzenedicarboxylates.* Journal of hazardous materials, 2010. **181**(1-3): p. 535-542.

93. Du, J.-J., et al., *New photocatalysts based on MIL-53 metal–organic frameworks for the decolorization of methylene blue dye.* Journal of hazardous materials, 2011. **190**(1-3): p. 945-951.

94. Hameed, B., A.M. Din, and A. Ahmad, *Adsorption of methylene blue onto bamboo-based activated carbon: kinetics and equilibrium studies.* Journal of hazardous materials, 2007. **141**(3): p. 819-825.

95. Tan, I., B. Hameed, and A. Ahmad, *Equilibrium and kinetic studies on basic dye adsorption by oil palm fibre activated carbon.* Chemical Engineering Journal, 2007. **127**(1-3): p. 111-119.

96. Hameed, B.H., A.L. Ahmad, and K.N.A. Latiff, *Adsorption of basic dye (methylene blue) onto activated carbon prepared from rattan sawdust.* Dyes and Pigments, 2007. **75**(1): p. 143-149.

97. Tan, I., A. Ahmad, and B. Hameed, *Optimization of preparation conditions for activated carbons from coconut husk using response surface methodology.* Chemical Engineering Journal, 2008. **137**(3): p. 462-470.

98. Hameed, B.H. and M.I. El-Khaiary, *Sorption kinetics and isotherm studies of a cationic dye using agricultural waste: Broad bean peels.* Journal of Hazardous Materials, 2008. **154**(1): p. 639-648.

99. Li, H., et al., *Design and synthesis of an exceptionally stable and highly porous metal-organic framework.* nature, 1999. **402**(6759): p. 276.

100. Férey, G., *Hybrid porous solids: past, present, future.* Chemical Society Reviews, 2008. **37**(1): p. 191-214.

101. Horike, S., S. Shimomura, and S. Kitagawa, *Soft porous crystals.* Nature chemistry, 2009. **1**(9): p. 695.

102. Moghadam, P.Z., et al., *Development of a Cambridge Structural Database subset: a collection of metal–organic frameworks for past, present, and future.* Chemistry of Materials, 2017. **29**(7): p. 2618-2625.

103. Kuppler, R.J., et al., *Potential applications of metal-organic frameworks.* Coordination Chemistry Reviews, 2009. **253**(23-24): p. 3042-3066.

104. Li, H., et al., *Establishing microporosity in open metal− organic frameworks: gas sorption isotherms for Zn (BDC)(BDC= 1, 4-benzenedicarboxylate).* Journal of the American Chemical Society, 1998. **120**(33): p. 8571-8572.

105. Li, J.R., J. Sculley, and H.C. Zhou, *Metal–Organic Frameworks for Separations.* Chem. Rev., 2012. **112**: p. 869.

106. Llewellyn, P.L., et al., *High Uptakes of CO2 and CH4 in Mesoporous Metal–Organic Frameworks MIL-100 and MIL-101.* Langmuir, 2008. **24**: p. 7245.

107. Biradha, K., A. Ramanan, and J.J. Vittal, *Coordination polymers versus metal− organic frameworks.* Crystal Growth and Design, 2009. **9**(7): p. 2969-2970.

108. Conference, C.a.B.D.S.a.T.C.S.T. *Keynote Speaker: Dr. Omar Yaghi*. 2015 [cited 2018 10/11/2018]; Available from: https://www.youtube.com/watch?v=m6sRQjKFssk.

109. Yaghi, O.M., et al., *Reticular synthesis and the design of new materials.* Nature, 2003. **423**(6941): p. 705.

110. O'Keeffe, M., et al., *The reticular chemistry structure resource (RCSR) database of, and symbols for, crystal nets.* Accounts of chemical research, 2008. **41**(12): p. 1782-1789.

111. Ockwig, N.W., et al., *Reticular chemistry: occurrence and taxonomy of nets and grammar for the design of frameworks.* Accounts of chemical research, 2005. **38**(3): p. 176-182.

112. Furukawa, H., et al., *The Chemistry and Applications of Metal-Organic Frameworks.* Science, 2013. **341**(6149): p. 1230444.

113. Yaghi, O.M., et al., *Reticular synthesis and the design of new materials.* Nature, 2003. **423**: p. 705.

114. Eddaoudi, M., et al., *Systematic Design of Pore Size and Functionality in Isoreticular MOFs and Their Application in Methane Storage.* Science, 2002. **295**(5554): p. 469.

115. Ke, F., et al., *Facile fabrication of magnetic metal–organic framework nanocomposites for potential targeted drug delivery.* Journal of Materials Chemistry, 2011. **21**(11): p. 3843-3848.

116. Dai, W., et al., *Adsorptive separation of thiophene derivatives via metal organic framework material MOF-5.* Journal of Fuel Chemistry and Technology, 2010. **38**(5): p. 626-630.

117. Chen, C., et al., *Kinetic and thermodynamic studies on the adsorption of xylenol orange onto MIL-101(Cr).* Chemical Engineering Journal, 2012. **183**: p. 60-67.

118. Haque, E., et al., *Adsorptive removal of methyl orange from aqueous solution with metal-organic frameworks, porous chromium-benzenedicarboxylates.* Journal of Hazardous Materials, 2010. **181**(1): p. 535-542.

119. Ho, Y.-S. and G. McKay, *Pseudo-second order model for sorption processes.* Process biochemistry, 1999. **34**(5): p. 451-465.

120. Lagergren, S., *About the theory of so-called adsorption of soluble substances.* Sven. Vetenskapsakad. Handingarl, 1898. **24**: p. 1-39.

121. Weber, W.J. and J.C. Morris, *Kinetics of adsorption on carbon from solution.* Journal of the Sanitary Engineering Division, 1963. **89**(2): p. 31-60.

122. Langmuir, I., *The constitution and fundamental properties of solids and liquids. II. Liquids.* Journal of the American Chemical Society, 1917. **39**(9): p. 1848-1906.

123. Freundlich, H., *Über die adsorption in lösungen.* Zeitschrift für physikalische Chemie, 1907. **57**(1): p. 385-470.

124. Hameed, B.H. and A.A. Rahman, *Removal of phenol from aqueous solutions by adsorption onto activated carbon prepared from biomass material.* Journal of Hazardous Materials, 2008. **160**(2): p. 576-581.

125. Hameed, B.H., *Spent tea leaves: A new non-conventional and low-cost adsorbent for removal of basic dye from aqueous solutions.* Journal of Hazardous Materials, 2009. **161**(2): p. 753-759.

126. Lagergren, S., *Zur theorie der sogenannten adsorption gelöster stoffe, 1898.* Availableat: http://books. google. com. eg/books/about/Zur_Theorie_der_sogenannten_Adsorption_g. html.

127. Low, M., *Kinetics of chemisorption of gases on solids.* Chemical Reviews, 1960. **60**(3): p. 267-312.

128. Chien, S. and W. Clayton, *Application of Elovich equation to the kinetics of phosphate release and sorption in soils 1.* Soil Science Society of America Journal, 1980. **44**(2): p. 265-268.

129. Kushwaha, J.P., V.C. Srivastava, and I.D. Mall, *Treatment of dairy wastewater by commercial activated carbon and bagasse fly ash: Parametric, kinetic and equilibrium modelling, disposal studies.* Bioresource Technology, 2010. **101**(10): p. 3474-3483.

130. Hameed, B., *Evaluation of papaya seeds as a novel non-conventional low-cost adsorbent for removal of methylene blue.* Journal of Hazardous materials, 2009. **162**(2-3): p. 939-944.

131. Langmuir, I., *The constitution and fundamental properties of solids and liquids. Part I. Solids.* Journal of the American chemical society, 1916. **38**(11): p. 2221-2295.

132. Hameed, B.H., A.T.M. Din, and A.L. Ahmad, *Adsorption of methylene blue onto bamboo-based activated carbon: Kinetics and equilibrium studies.* Journal of Hazardous Materials, 2007. **141**(3): p. 819-825.

133. Hall, K.R., et al., *Pore-and solid-diffusion kinetics in fixed-bed adsorption under constant-pattern conditions.* Industrial & Engineering Chemistry Fundamentals, 1966. **5**(2): p. 212-223.

134. Gupta, G.S., et al., *Removal of chrome dye from aqueous solutions by fly ash.* Water, Air, and Soil Pollution, 1988. **37**(1): p. 13-24.

135. Namasivayam, C. and S. Sumithra, *Removal of direct red 12B and methylene blue from water by adsorption onto Fe (III)/Cr (III) hydroxide, an industrial solid waste.* Journal of Environmental Management, 2005. **74**(3): p. 207-215.

136. Di Marino, A. and F. Mendicuti, *Thermodynamics of complexation of dimethyl esters of tere-, iso-, and phthalic acids with α-and β-cyclodextrins.* Applied spectroscopy, 2004. **58**(7): p. 823-830.

137. Dhumal, N.R., et al., *Molecular Interactions of a Cu-Based Metal–Organic Framework with a Confined Imidazolium-Based Ionic Liquid: A Combined Density Functional Theory and Experimental Vibrational Spectroscopy Study.* The Journal of Physical Chemistry C, 2016. **120**(6): p. 3295-3304.

138. Coates, J., *Interpretation of infrared spectra, a practical approach.* Encyclopedia of analytical chemistry, 2000. **12**: p. 10815-10837.

139. Aroke, U., A. Abdulkarim, and R. Ogubunka, *Fourier-transform infrared characterization of kaolin, granite, bentonite and barite.* ATBU Journal of Environmental Technology, 2013. **6**(1): p. 42-53.

140. Schlichte, K., T. Kratzke, and S. Kaskel, *Improved synthesis, thermal stability and catalytic properties of the metal-organic framework compound Cu3(BTC)2.* Microporous and Mesoporous Materials, 2004. **73**(1): p. 81-88.

141. Aljeboree, A.M., A.N. Alshirifi, and A.F. Alkaim, *Kinetics and equilibrium study for the adsorption of textile dyes on coconut shell activated carbon.* Arabian journal of chemistry, 2017. **10**: p. S3381-S3393.

142. de Menezes, E.W., et al., *Ionic silica based hybrid material containing the pyridinium group used as an adsorbent for textile dye.* Journal of Colloid and Interface Science, 2012. **378**(1): p. 10-20.

143. Ho, Y.-S., *Second-order kinetic model for the sorption of cadmium onto tree fern: A comparison of linear and non-linear methods.* Water Research, 2006. **40**(1): p. 119-125.

144. Ho, Y.-S., *Adsorption of heavy metals from waste streams by peat.* Ph. D. Thesis, The University of Brimingham, 1995.

145. Ho, Y.S. and G. McKay, *A kinetic study of dye sorption by biosorbent waste product pith.* Resources, Conservation and Recycling, 1999. **25**(3): p. 171-193.

146. Badmus, M., T. Audu, and B. Anyata, *Removal of lead ion from industrial wastewaters by activated carbon prepared from periwinkle shells (Typanotonus fuscatus).* Turkish journal of engineering and environmental sciences, 2007. **31**(4): p. 251-263.

147. Ho, Y.S. and G. McKay, *A Comparison of Chemisorption Kinetic Models Applied to Pollutant Removal on Various Sorbents.* Process Safety and Environmental Protection, 1998. **76**(4): p. 332-340.

148. Namasivayam, C. and N. Kanchana, *Waste banana pith as adsorbent for color removal from wastewaters.* Chemosphere, 1992. **25**(11): p. 1691-1705.

149. Namasivayam, C. and R. Yamuna, *Removal of congo red from aqueous solutions by biogas waste slurry.* Journal of Chemical Technology & Biotechnology, 1992. **53**(2): p. 153-157.

150. Namasivayam, C. and R. Yamuna, *Removal of Rhodamine-B by biogas waste slurry from aqueous solution.* Water, Air, and Soil Pollution, 1992. **65**(1-2): p. 101-109.

151. Yamuna, R. and C. Namasivayam, *Color removal from aqueous solution by biogas residual slurry.* Toxicological & Environmental Chemistry, 1993. **38**(3-4): p. 131-143.

152. Namasivayam, C. and K. Periasamy, *Bicarbonate-treated peanut hull carbon for mercury (II) removal from aqueous solution.* Water Research, 1993. **27**(11): p. 1663-1668.

153. Namasivayam, C. and K. Ranganathan, *Waste Fe (III)/Cr (III) hydroxide as adsorbent for the removal of Cr (VI) from aqueous solution and chromium plating industry wastewater.* Environmental Pollution, 1993. **82**(3): p. 255-261.

154. Namasivayam, C., K. Thamaraiselvi, and R.T. Yamuna, *Removal of paraquat by adsorption on 'waste'Fe (III)/Cr (III) hydroxide: adsorption rates and equilibrium studies.* Pesticide science, 1994. **41**(1): p. 7-12.

155. Singh, B.K. and N.S. Rawat, *Comparative sorption kinetic studies of phenolic compounds on fly ash and impregnated fly ash.* Journal of Chemical Technology & Biotechnology: International Research in Process, Environmental AND Clean Technology, 1994. **61**(1): p. 57-65.

156. Lee, C., K. Low, and S. Chow, *Chrome sludge as an adsorbent for colour removal.* Environmental technology, 1996. **17**(9): p. 1023-1028.

157. Lee, C., K. Low, and K. Kek, *Removal of chromium from aqueous solution.* Bioresource Technology, 1995. **54**(2): p. 183-189.

158. Low, K., C. Lee, and K. Tan, *Biosorption of basic dyes by water hyacinth roots.* Bioresource technology, 1995. **52**(1): p. 79-83.

159. Mittal, A.K. and S. Gupta, *Biosorption of cationic dyes by dead macro fungus Fomitopsis carnea: batch studies.* Water science and technology, 1996. **34**(10): p. 81-87.

160. Namasivayam, C., et al., *Removal of dyes from aqueous solutions by cellulosic waste orange peel.* Bioresource Technology, 1996. **57**(1): p. 37-43.

161. Kilic, M., E. Apaydin-Varol, and A.E. Pütün, *Adsorptive removal of phenol from aqueous solutions on activated carbon prepared from tobacco residues:*

equilibrium, kinetics and thermodynamics. Journal of Hazardous Materials, 2011. **189**(1-2): p. 397-403.

162. Shi, Y., et al., *Adsorption of soy isoflavones by activated carbon: Kinetics, thermodynamics and influence of soy oligosaccharides.* Chemical engineering journal, 2013. **215**: p. 113-121.

163. Shahul Hameed, K., P. Muthirulan, and M. Meenakshi Sundaram, *Adsorption of chromotrope dye onto activated carbons obtained from the seeds of various plants: Equilibrium and kinetics studies.* Arabian Journal of Chemistry, 2017. **10**: p. S2225-S2233.

164. Malik, R., D.S. Ramteke, and S.R. Wate, *Adsorption of malachite green on groundnut shell waste based powdered activated carbon.* Waste Management, 2007. **27**(9): p. 1129-1138.

165. Yener, J., et al., *Adsorption of Basic Yellow 28 from aqueous solutions with clinoptilolite and amberlite.* Journal of Colloid and Interface Science, 2006. **294**(2): p. 255-264.

166. Ho, Y.S. and G. McKay, *Pseudo-second order model for sorption processes.* Process Biochemistry, 1999. **34**(5): p. 451-465.

167. Ponnusami, V., S. Vikram, and S.N. Srivastava, *Guava (Psidium guajava) leaf powder: Novel adsorbent for removal of methylene blue from aqueous solutions.* Journal of Hazardous Materials, 2008. **152**(1): p. 276-286.

168. Hameed, B.H., *Spent tea leaves: a new non-conventional and low-cost adsorbent for removal of basic dye from aqueous solutions.* Journal of hazardous materials, 2009. **161**(2-3): p. 753-759.

169. Hameed, B. and F. Daud, *Adsorption studies of basic dye on activated carbon derived from agricultural waste: Hevea brasiliensis seed coat.* Chemical Engineering Journal, 2008. **139**(1): p. 48-55.

170. Allen, S., G. Mckay, and K. Khader, *Intraparticle diffusion of a basic dye during adsorption onto sphagnum peat.* Environmental Pollution, 1989. **56**(1): p. 39-50.

171. Mohanty, K., D. Das, and M. Biswas, *Adsorption of phenol from aqueous solutions using activated carbons prepared from Tectona grandis sawdust by ZnCl2 activation.* Chemical Engineering Journal, 2005. **115**(1-2): p. 121-131.

172. Mohanty, K., et al., *Preparation and characterization of activated carbons from Terminalia arjuna nut with zinc chloride activation for the removal of phenol from wastewater.* Industrial & engineering chemistry research, 2005. **44**(11): p. 4128-4138.

173. Panday, K., G. Prasad, and V. Singh, *Mixed adsorbents for Cu (II) removal from aqueous solutions.* Environmental Technology, 1986. **7**(1-12): p. 547-554.

174. Mohanty, K., et al., *Removal of chromium (VI) from dilute aqueous solutions by activated carbon developed from Terminalia arjuna nuts activated with zinc chloride.* Chemical Engineering Science, 2005. **60**(11): p. 3049-3059.

175. Poots, V., G. McKay, and J. Healy, *Removal of basic dye from effluent using wood as an adsorbent.* Journal (Water Pollution Control Federation), 1978: p. 926-935.

176. Marrakchi, F., et al., *High-surface-area and nitrogen-rich mesoporous carbon material from fishery waste for effective adsorption of methylene blue.* Powder Technology, 2017. **321**: p. 428-434.

177. Islam, M.A., et al., *Mesoporous activated coconut shell-derived hydrochar prepared via hydrothermal carbonization-NaOH activation for methylene blue adsorption.* Journal of Environmental Management, 2017. **203**: p. 237-244.

178. Oliveira, L.S., et al., *Evaluation of untreated coffee husks as potential biosorbents for treatment of dye contaminated waters.* Journal of Hazardous Materials, 2008. **155**(3): p. 507-512.

179. Han, R., et al., *Biosorption of methylene blue from aqueous solution by fallen phoenix tree's leaves.* Journal of Hazardous Materials, 2007. **141**(1): p. 156-162.

180. Banat, F., S. Al-Asheh, and L. Al-Makhadmeh, *Evaluation of the use of raw and activated date pits as potential adsorbents for dye containing waters.* Process Biochemistry, 2003. **39**(2): p. 193-202.

181. Ghosh, D. and K. Bhattacharyya, *Removing colour from aqueous medium by sorption on natural clay: a study with methylene blue.* INDIAN JOURNAL OF ENVIRONMENTAL PROTECTION, 2001. **21**(10): p. 903-910.

182. Demir, H., et al., *Dye adsorption behavior of Luffa cylindrica fibers.* Journal of Hazardous Materials, 2008. **153**(1-2): p. 389-394.

183. Yao, Y., et al., *Adsorption behavior of methylene blue on carbon nanotubes.* Bioresource Technology, 2010. **101**(9): p. 3040-3046.

184. Vadivelan, V. and K.V. Kumar, *Equilibrium, kinetics, mechanism, and process design for the sorption of methylene blue onto rice husk.* Journal of Colloid and Interface Science, 2005. **286**(1): p. 90-100.

185. Ghosh, R.K. and D.D. Reddy, *Tobacco stem ash as an adsorbent for removal of methylene blue from aqueous solution: equilibrium, kinetics, and mechanism of adsorption.* Water, Air, & Soil Pollution, 2013. **224**(6): p. 1582.

186. Kumar, K.V. and K. Porkodi, *Mass transfer, kinetics and equilibrium studies for the biosorption of methylene blue using Paspalum notatum.* Journal of Hazardous Materials, 2007. **146**(1): p. 214-226.

187. Ferrero, F., *Dye removal by low cost adsorbents: Hazelnut shells in comparison with wood sawdust.* Journal of Hazardous Materials, 2007. **142**(1-2): p. 144-152.

188. Banerjee, S. and M.G. Dastidar, *Use of jute processing wastes for treatment of wastewater contaminated with dye and other organics.* Bioresource Technology, 2005. **96**(17): p. 1919-1928.

189. Sapawe, N., et al., *Cost-effective microwave rapid synthesis of zeolite NaA for removal of methylene blue.* Chemical Engineering Journal, 2013. **229**: p. 388-398.

190. Bazrafshan, E., F.K. Mostafapour, and M.A. Zazouli, *Methylene blue (cationic dye) adsorption into Salvadora persica stems ash.* African Journal of Biotechnology, 2012. **11**(101): p. 16661-16668.

191. Annadurai, G., R.-S. Juang, and D.-J. Lee, *Use of cellulose-based wastes for adsorption of dyes from aqueous solutions.* Journal of Hazardous Materials, 2002. **92**(3): p. 263-274.

192. Banerjee, S., et al., *Kinetic and equilibrium modeling for the adsorptive removal of methylene blue from aqueous solutions on of activated fly ash (AFSH).* Journal of Environmental Chemical Engineering, 2014. **2**(3): p. 1870-1880.

193. Woolard, C.D., J. Strong, and C.R. Erasmus, *Evaluation of the use of modified coal ash as a potential sorbent for organic waste streams.* Applied Geochemistry, 2002. **17**(8): p. 1159-1164.

194. Kavitha, D. and C. Namasivayam, *Experimental and kinetic studies on methylene blue adsorption by coir pith carbon.* Bioresource Technology, 2007. **98**(1): p. 14-21.

195. Khattri, S. and M. Singh, *Colour removal from synthetic dye wastewater using a bioadsorbent.* Water, Air, and Soil Pollution, 2000. **120**(3-4): p. 283-294.

Chapter 6

Boosting adsorption of methylene blue onto Zr-MOF in aqueous solution by second metal Co coordination

6

Chapter 6: Boosting adsorption of methylene blue onto Zr-MOF in aqueous solution by second metal Co coordination

6.1 Abstract

The present study employed three kinds of water and structurally stable metal organic frameworks (MOFs) (Zr-MOFs) to adsorb nonbiodegradable cationic dye (methylene blue [MB]). Their chemical properties, textural tuneability, high surface area as well as their ability to remove MB dyes MB were stimulated. Three modified materials of UiO-66 MOFs (UiO-66, UiO-66-10%Co and UiO-66-30%Co) were produced solvothermally and reported in this study. The adsorbents were characterised with a Fourier transform infrared spectrophotometer (FTIR), X-ray powder diffractometer (XRD), a Brunauer–Emmett–Teller (BET) surface area measurement machine and thermogravimetric analysis instrument (TGA). Batch sorption processes were conducted to explore the effects of contact time and initial concentration, ranging from 5–50 mg $L^{-1,}$ on the removal of MB. Higher initial MB concentrations and longer contact times led to increases in adsorption capacity. Pseudo first-order, pseudo second order, Elovich and intraparticle diffusion kinetics models were employed to investigate the experimental data and comparatively assess the chemical and diffusion adsorption processes. The pseudo second-order model displayed the best fit to the data among the kinetic models, indicating that the sorption batches of MOF/MB are generally controlled by the chemisorption process. In addition, the intraparticle diffusion study found that the overall rate of MB sorption by Zr-MOFs was controlled by more than one step. Results from the kinetics study verified effectiveness of MOFs to remove methylene blue from aqueous solutions. Experimental equilibrium data were fitted to the Langmuir and the Freundlich isotherms. While the data agreed well with the Freundlich equilibrium model, the UiO-66-10%Co was identified in the Langmuir model as achieving the maximum adsorption uptake at 51.02 mgg^{-1}.

6.2 Introduction

Advances in the modern industrial revolution in all fields have led to the production of huge amounts of effluent consisting of biodegradable, volatile and recalcitrant organic compounds, toxic metals, suspended solids, plant nutrients, dyes, microbial

pathogens and parasites [1-3]. Rapid industrialisation has severely affected the environment and especially natural water bodies to the extent that environmentalists have issued a warning to threaten the flora and fauna as well as aquatic aesthetics as a very little quantity of dyes is highly visible in water and reduce the growth of bacteria which degrade the impurities of water [4-6]. Organic pollutants, particularly dyes, are considered a serious environmental problem when released from plants and factories as wastewater into natural receiving waters, as they adversely affect the quality of treated water for public consumption. As these contaminants pose a hazard to human life, their removal is necessary [7, 8]. It is reported that there are approximately 100,000 known commercial dyes, with annual production at 700,000 tonnes for consumption by the textile industry, which discharges approximately 10,000 tons per year into waste streams. Approximately 1000 tons per year are discharged by industries involved in printing, dyeing, textile, food, cosmetics, colouring, papermaking, leather and paper [9-20].

Methylene blue (MB), a basic cationic dyestuff commonly used in cotton, wood and silk industries [21-23], has a toxic and carcinogenesis effect [24]. It also causes numerous symptoms such as breathing difficulty, nausea and vomiting [25, 26]. Moreover, direct contact with MB can cause cancer, mutation, dermatological diseases [27] and can weaken photosynthetic processes of aquatic plants [28, 29]. Specifically, its chemical stability and the resistance of its aromatic structure to biodegradation have presented the challenge of identifying an adsorbent that can efficiently remove MB to ensure the environmental health of waterways [30-34].

Various treatments utilised to remove dyes in wastewater have included chemical, physical and biological techniques [35-45]. Among these treatments, adsorption is the most popular because of its simplicity, feasibility and efficiency [31, 46-49].

The most commonly used sorbent to treat polluted industrial effluent worldwide is activated carbon (AC), which has been widely consumed in large quantities around the world [50-52]. Despite the effectiveness of AC in removing pollutants in wastewater, its high cost has inspired researchers to seek alternative sorbents to remove contaminants from aqueous solutions, such as chitosan bead [53], diatomite [54], dolomite [55], fuller's earth [56], bentonite [57], zeolite [58], peat [59], lignite [60], kudzu [61] as well as other adsorbents, such as oil palm trunk fibre [62], fly-ash [63],

dried biomass of baker's yeast [64], durian peel [65], guava leaf powder [66][19], almond shell [67], pomelo peel [68], treated parthenium biomass [69], orange peel [70], banana and orange peel [71], kohlrabi peel [72], Citrus limetta peel and broad bean peel [73, 74].

Metal organic frameworks (MOFs) are a class of materials of highly porous crystalline extended structures consisting of clusters of cations (vertices) linked to multitopic organic strut ions or molecules. The diversity of inorganic metal ions, organic linkers and structural motifs leads to countless numbers of possible combinations; post-synthesis modifications of MOFs further enhances their variety [75, 76]. In addition, the level of tunability, structural variety and diversity of chemical and physical properties of MOFs have made them unmatched among the classes of highly porous materials.

MOFs are comparators for zeolites, based on their surface area, porosity and high degree of crystallinity, which make them useful in applications like gas storage and separation, biomedicine and drug delivery, adsorption of organic molecules, heterogeneous catalysis and removal of dyes [77-84].

The present study investigated three versions of modified Zr-MOFs (UiO-66, UiO-66-10%Co and UiO-66-30%Co) synthesised successfully with high pore volume, nanosized crystal, as well as high water and thermal stability. Cobalt has chosen to modify Zr-MOF due to their atomic size in comparison to zirconium. A series of single metal and bimetal Zr-MOFs samples with different ratios of Co/Zr were successfully obtained by direct synthesis, followed by activation processes with methanol with some modifications. The performance of UiO-66 was further enhanced for the removal of MB with improving its textural properties and open metal sites through the introduction of second metal such (Co) into the framework in the synthesis process.

These MOFs were assessed for their capacity to remove basic dye MB from wastewater, using batch adsorption with respect to initial MB concentration and contact time. Sorption capacities were determined for various initial MB concentrations in the effluent. In addition, sorption kinetics and equilibrium analyses were performed.

6.3 Materials and methods

6.3.1 Synthesis and activation

The chemicals used in this study were provided by Sigma-Aldrich (Australia) without further purifications.

Under autogenous pressure with some modifications, UiO-66 was successfully synthesised based on the method described in the literature [85, 86]. A modified ratio of $ZrCl_4$: BDC: DMF was prepared. $ZrCl_4$, (2.27 mmol) and 1,4-benzenedicarboxylic acid (BDC 2.27 mmol) were added to a mixing container containing 405.38 mmol of N, N-dimethylformamide (DMF) with continuous stirring. The reactants were then transferred to an autoclave at 393 K for 24 h for a solvothermal process. The resultant solid product was extracted by filtration followed a drying process. For activation, the dried Zr-MOF was immersed in chloroform for 5d followed by filtration and drying under vacuum at 463K for 48h.

The first step of UiO-66-10%Co synthesis involved mixing 1.1 g terephthalic acid (98%; Sigma-Aldrich) with 1.5 g $ZrCl_4$ in 73 mL DMF (99%; Sigma-Aldrich), using a magnet stirrer for 15 min. The second step consisted of adding 0.15 g Co $(NO_3)_2.6H_2O$ (99%; Sigma-Aldrich) followed by 2 mL H_2O to the solution with continuous stirring for another 15 min. The mixture was then poured into a 125-mL Teflon-lined autoclave that was tightly sealed and then placed in a preheated oven at 132°C for 1d. The suspension of UiO-66-10%Co white powder was separated from the solution using centrifuge and washed three times in DMF. The powder was then dried completely to immerse for 5d in absolute methanol (100%; Sigma-Aldrich). When the activation process with methanol was completed, the powder was filtered, dried and heated under vacuum at 473K overnight before use as adsorbent.

The same procedure was used to synthesise UiO-66-30%Co, by mixing 1.5 g $ZrCl_4$ with 1.3 g terephthalic acid in 70 mL DMF. After mixing for 15 min, 0.45 g Co $(NO_3)_2.6H_2O$ was added, followed by 5 mL H_2O, into the mixture with continuous stirring for approximately 30 min. The solution was transferred to a 125-mL Teflon lined autoclave which was tightly sealed and then placed in a preheated oven at 157°C for 24h. The suspension of UiO-66-30%Co white powder was separated from the solution using centrifuge and washed three times in DMF. The powder was then dried completely and immersed for 5 d in absolute methanol (100%; Sigma-Aldrich). When

the activation process with methanol had completed, the power was filtered, dried and heated under vacuum at 473K overnight before use as adsorbent.

6.3.2 Characterisation

A thermogravimetric analysis (TGA) instrument (TGA/DSC1 STARe system; Mettler-Toledo) was used to test the thermal stability of UiO-66, UiO66-10%Co and UiO66-30%Co. The pan of the instrument was loaded with Zr-MOF samples and heated to 1173K at a rate of 5K/min with air gas flow rate of 10 mL/min.

The stability of the functional groups on the organic linkers was checked by obtaining FTIR spectra (Spectrum 100, FT-IR spectrometer; PerkinElmer). The spectra were scanned from 600 to 4000 cm^{-1} with a resolution of 4 cm^{-1} using an attenuated total reflectance technique.

The crystallinity of the samples was checked by X-ray powder diffraction patterns obtained with an X-ray diffractometer (D8 Advance; Bruker AXS) using Cu Kα radiation (λ = 1.5406 Å) while maintaining the accelerating voltage and current at 40 kV and 40 mA, respectively.

N_2 adsorption/desorption isotherms, pore size and surface area of Zr-MOF samples were determined using Autosorb-1 (Quantachrome Instruments). The samples were activated under heat and vacuum at 473K for 1d before performing the adsorption/desorption measurements. By this technique, N_2 adsorption/desorption isotherms for the sample were obtained as well as surface area, pore size and pore volume.

6.3.3 Adsorption process

A 1000 mg/L stock solution of cationic MB dye was prepared using MB powder ($C_{16}H_{18}ClN_3S$, molecular weight 319.85 $g.mol^{-1}$; Sigma-Aldrich) with ultra-pure water. Standards (5–100 ppm) and various initial concentrations of MB (5,15, 30 and 50) were prepared from stock solution by dilution. A calibration curve was determined using the standards with known concentration at a set absorbance of 668 nm in the UV spectrophotometer. In addition, the unknown concentration of MB in the supernatant after the adsorption process can be found from absorbance in the UV machine and

calibration curve. For the adsorption process, 20 mL MB of various initial concentrations (between 5–50 mg/L) were each mixed with 20 mg and stirred well using a magnetic stirrer for a period ranging 5 min to 24 h at room temperature. The supernatant of each sample was collected using syringe filter and analysed by a UV machine.

The sorption capacity of the MOFs at any time can be determined from Equation 6.1, while the sorption capacity of the MOFs at equilibrium may be found from Equation 6.2. Further, percentage removal of MB can be computed by Equation 6.3 [53, 87-90].

$$q_t = (C_0 - C_t)\frac{V}{m} \tag{6.1}$$

$$q_e = (C_0 - C_e)\frac{V}{m} \tag{6.2}$$

$$R\% = \frac{(C_0 - C_t)}{C_0} X100 \tag{6.3}$$

Where:

q_t: the amount of MB adsorbed per unit weight of MOF at any time t (mg/g)

q_e: the amount of MB adsorbed per unit weight of MOF at equilibrium (mg/g)

C_0: initial concentration of MB solution at time zero (mg/L)

C_t: concentration of MB solution at time t (mg/L)

C_e: concentration of MB solution at equilibrium (mg/L)

V: volume of MB solution in the batch adsorption process (L)

R%: percentage removal of MB

m: Zr-MOF mass used in the adsorption batch process (g).

A kinetics study was performed using pseudo first-order Equation 6.4 [91], pseudo second-order Equation 6.5 [92], Elovich Equation 6.6 [93, 94] and the intraparticle diffusion model expressed by Equation 6.7 [95]. Further, an equilibrium study of the adsorption process was undertaken using the Langmuir and Freundlich adsorption isotherms, expressed by Equation 6.8 [96] and Equation 6.9 [97], respectively.

$$l\,n(q_e - q_t) = l\,n(q_e) - k_1 t, \tag{6.4}$$

Where:

q_e: the amount of MB adsorbed per unit weight of MOF at equilibrium (mg/g)

q_t: the amount of MB adsorbed per unit weight of MOF at any time t (mg/g)

k_1: pseudo first-order rate constant (min^{-1})

t: time (min).

If the MOF/MB system adsorption agrees with the pseudo first-order model according to the values of a linear regression correlation coefficient (R^2), a plot of $\ln(q_e - q_t)$ versus t will yield a linear relationship with slope ($-k_1$) and intercept $\ln(q_e)$. The pseudo first-order constant k_1 and q_e can be computed from the slope and intercept of such a plot.

$$\frac{t}{q_t} = \frac{1}{k_2 \quad q_e^2} + \frac{1}{q_e} t, \tag{6.5}$$

Where:

q_e: the amount of MB adsorbed per unit weight of MOF at equilibrium (mg/g)

q_t: the amount of MB adsorbed per unit weight of MOF at any time t (mg/g)

t: time (min)

k_2: pseudo second-order rate constant (g/mg min).

If the MOF/MB system adsorption agrees with the pseudo second-order model according to the values of a linear regression correlation coefficient (R^2), a plot of (t/q_t) versus t will yield a linear relationship with slope $(1/q_e)$ and intercept $(1/k_2[q_e]^2)$. The pseudo second-order constant q_e and k_2 can be computed from the slope and intercept of such a plot.

$$q_t = \left(\frac{1}{\beta}\right) \ln(\alpha.\beta) + \left(\frac{1}{\beta}\right) \ln(t), \tag{6.6}$$

Where:

q_t: the amount of MB adsorbed per unit weight of MOF at any time t (mg/g)

α: a constant representing the initial rate of adsorption

β: constant during any one experiment

t: time (min).

If the MOF/MB system adsorption agrees with the Elovich model according to the values of a linear regression correlation coefficient (R^2), a plot of q_t versus ln(t) will

yield a linear relationship with slope (1/β) and intercept ((1/β) ln(αβ)). The Elovich constants β and α can be computed from the slope and intercept of such a plot.

$$q_t = k_p t^{1/2} + C, \tag{6.7}$$

Where:

qt: the amount of MB adsorbed per unit weight of MOF at any time t (mg/g)

k_p: intraparticle diffusion rate constant (mg/ g $min^{0.5}$)

t: time (min)

C: intercept.

If the MOF/MB system adsorption agrees with the intraparticle diffusion model according to the values of a linear regression correlation coefficient (R^2), a plot of q_t versus $t^{1/2}$ will yield a linear relationship with slope k_p and intercept C. The parameters k_p and C in the intraparticle diffusion model can be computed from the slope and intercept of such plot.

$$\frac{C_e}{q_e} = \frac{1}{q_m} C_e + \frac{1}{k_L q_m}, \tag{6.8}$$

Where:

q_m: Langmuir maximum loading capacity (mg/g)

k_L: Langmuir constant related to the energy of adsorption and affinity of binding sites (L/mg)

C_e: the equilibrium concentration of dye in solution (mg/L)

q_e: amount of dye adsorbed at equilibrium per unit mass of sorbent (mg/g).

If the MOF/MB system adsorption agrees with the Langmuir isotherm model according to the values of the linear regression correlation coefficient (R^2), a plot of (C_e/q_e) versus C_e will yield a linear relationship with slope ($1/q_m$) and intercept ($1/k_L q_e$). The parameters q_m and k_L in the Langmuir isotherm model can be computed from the slope and intercept of such plot.

$$\ln(q_e) = \ln(k_F) + \frac{1}{n} \ln(C_e), \tag{6.9}$$

Where:

K_F: the calculated Freundlich equilibrium constant ([mg/g] $[L/mg]^{1/n}$), which is an indicator of the adsorption capacity

C_e: the equilibrium concentration of dye in solution (mg/L)

q_e: amount of dye adsorbed at equilibrium per unit mass of sorbent (mg/g)

n: a measure of the deviation from linearity of adsorption (g/L).

If the MOF/MB system adsorption agrees with the Freundlich isotherm model according to the values of linear regression correlation coefficient (R^2), a plot of $\ln(q_e)$ versus $\ln(C_e)$ will yield a linear relationship of slope (1/n) and intercept $\ln(k_F)$. The parameters n and k_F in the Freundlich isotherm model can be computed from the slope and intercept of such a plot.

6.4 Results and discussion

6.4.1 Characterisation

From Figure 6.2(a), the XRD patterns for UiO-66, UiO-66-10%Co and UiO-66-30%Co before and after use in adsorption of MB confirm that Zr-MOF structures were maintained, indicating that synthesis and activation procedures had succeeded and the pores of all samples were free of metal oxides impurities.

Spectra from the FTIR machine in Figure 6.2(b) illustrate that the single-metal and bimetal Zr-MOFs before and after use showed the same vibration bands. However, a higher percentage of the second metal shifted some peaks from its original position compared with those of the parent single-metal Zr-MOF. Further, the bimetal Zr-MOF had broader peaks than the single-metal Zr-MOF, reflecting the variance of the dipole between ground state and excited state of the bimetal Zr-MOF came from including the second metal in the vertices of the MOF [98, 99]. Figure 3(b) demonstrates that C=C-C stretching in the aromatic ring of terephthalate salts of the single-metal MOF was in the vibration band range 1615–1580 cm^{-1} while it was extended from 1590 to 1525 cm^{-1} in the case of bimetal MOFs [100]. In addition, Zr-MOF spectra indicate that the vibration band at 1500 and 1390 cm^{-1} could be assigned to stretching of symmetric COO^- and asymmetric COO^- in the coordinated organic strut. However, the vibration bands at 881, 812 and 785 cm^{-1} were assigned to Zr-O. Specifically, the

peak of stretching vibration of C-H and out-of-plane bending of the aromatic ring in the main skeleton of UiO-66 appeared at 730 cm^{-1}, whereas the same peak is displaced to 744 cm^{-1} in the spectra of bimetal Zr-MOFs [99, 101]. Moreover, the peak at 1017 cm^{-1} represents the stretching vibration of C-H.

Isotherms of N_2 adsorption/desorption of the powder samples of single and bimetal Zr-MOFs are shown in Figure 6.1. It is clear from Figure 6.1that bimetal MOF with 10% Co had hysteresis in the desorption isotherm with sudden jump in the value of sorption near the relative pressure of 0.999. This result can confirmation that the mesopore and macropore sizes and isotherm of Uio-66-10%Co are consistent with type IV adsorption isotherm with hysteresis H3. In terms of the shape for adsorption isotherms, classification by IUPAC can be divided into five kinds: type I, II, III, IV and V. However, hysteresis H3 is a good indication of the occurrence of capillary condensation inside the pores of Zr-MOF [102].

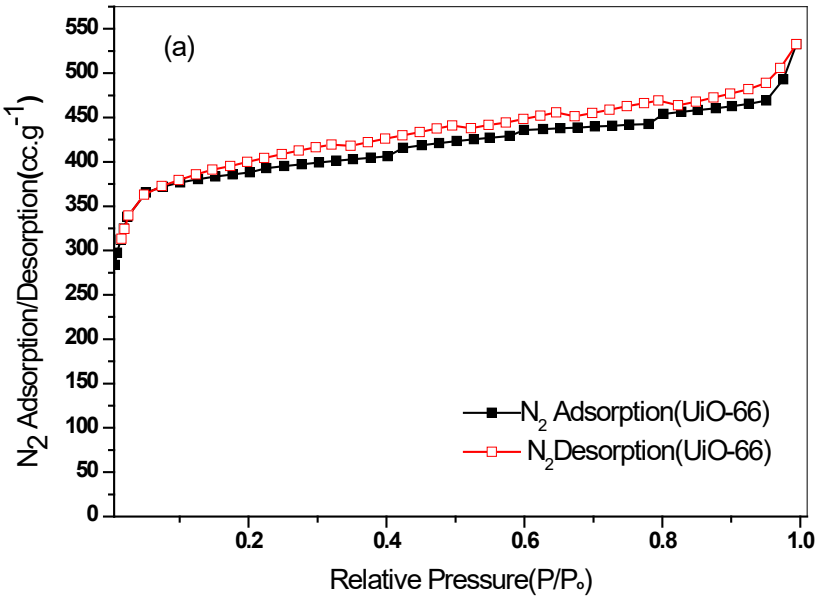

Table 6.1 lists the calculations for the textural properties of the Zr-MOF samples, based on adsorption isotherms. Notably, the values of the specific surface area (S_{BET}) decreased the higher the percentage of cobalt. Specifically, the S_{BET} of UiO-66 was 1585.50 $m^2g^{-}1$; with higher percentage content of the second metal, the S_{BET} became 978.863 and 592.378 m^2g^{-1} for UiO-66-10%Co and UiO-66-30%Co, respectively.

Table 6.1 also shows that the average pore volume and pore size of UiO-66-10%Co was the highest of the three Zr-MOFs, at 1.07 cc g^{-1} and 2.18 nm, respectively. Further, with the cobalt percentage at 30%, the values of pore volume and average pore size became less than the pore volume and average pore size of UiO-66. The first stage of the activation process by methanol, which was followed by heating activation, played a very important role in enhancing pore volume and average pore size of UiO-66-10%Co by replacing cobalt with methanol molecules, which were then evaporated in the heat activation.

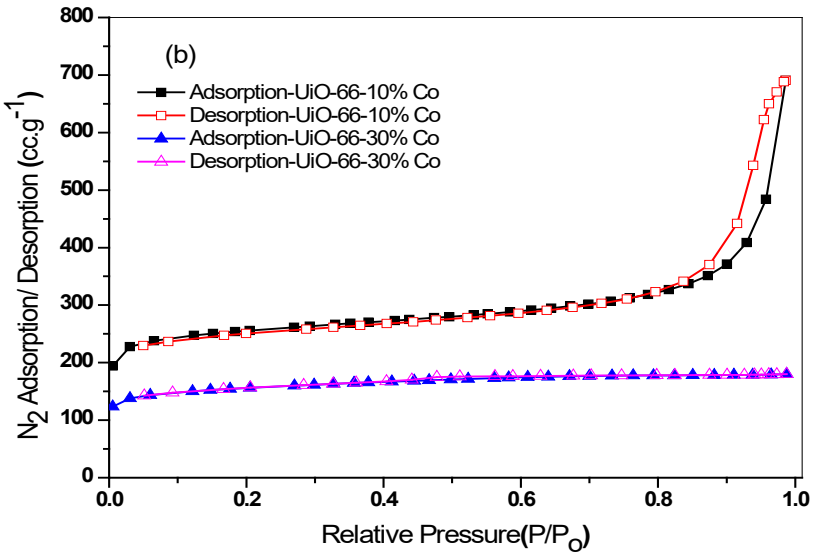

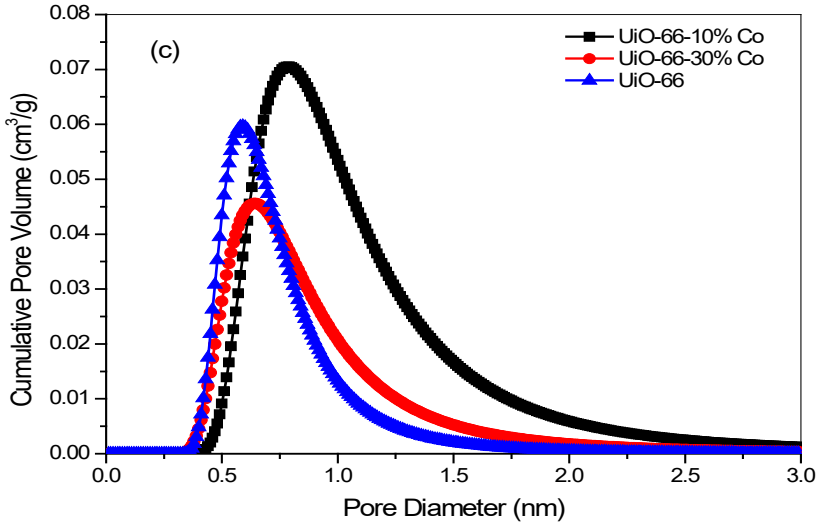

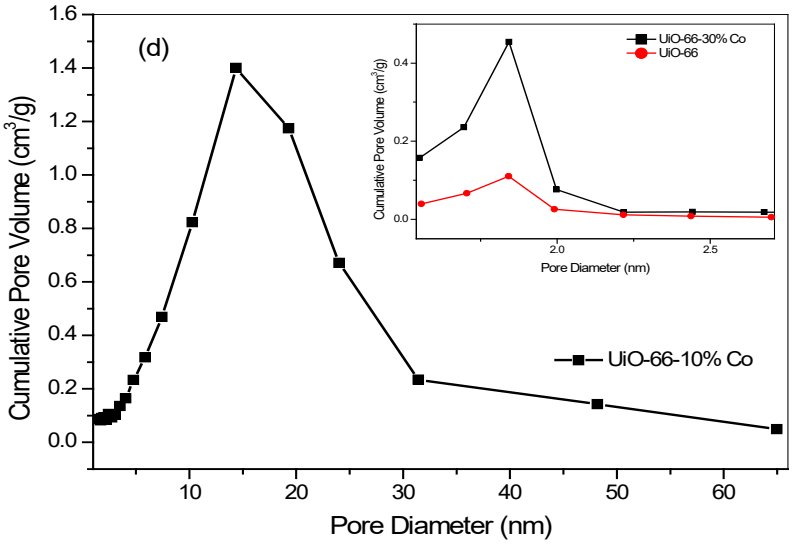

Figure 6.1: N_2 adsorption/desorption isotherm of UiO-66 (a), N_2 adsorption/desorption isotherm of UiO-66-Co samples (b), and micropore distribution (b)and mesopore distribution (c) of. UiO-66, UiO-66-10% Co and UiO-66-30% Co.

Table 6.1: Textural properties of the adsorbents based on N_2 adsorption/desorption isotherms.

Adsorbent	Specific surface area (S_{BET}) (m^2g)	Pore volume (cc g^{-1})	Pore diameter (nm)
UiO-66	1585.5	0.82	1.04
UiO-66-10% Co	978.863	1.07	2.18
UiO-66-30% Co	592.378	0.28	0.94

The TGA profiles for the single-metal and bimetal UiO-66 samples are illustrated in Figure 6.2(c). It is apparent from Figure 6.2(c) that all adsorbent samples possess similar thermal and structural stability at temperatures up to 725K.

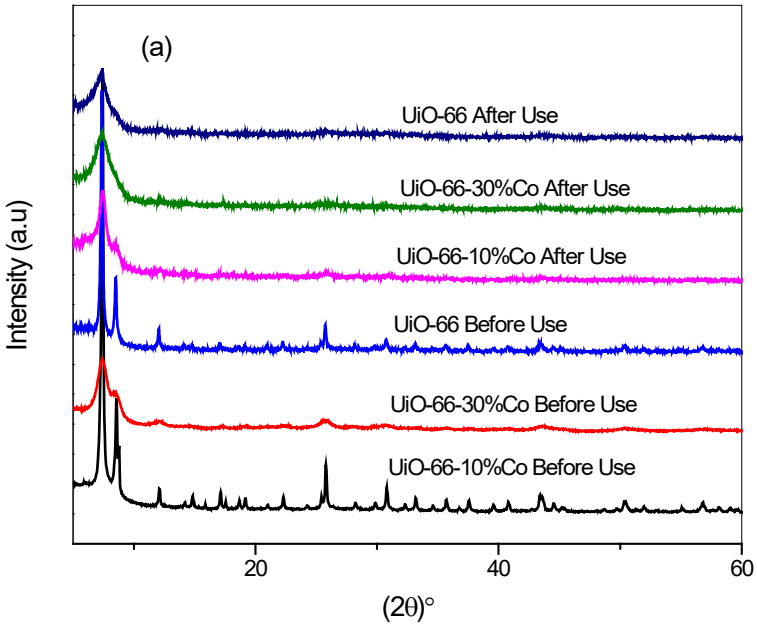
(a)
UiO-66 After Use
UiO-66-30%Co After Use
UiO-66-10%Co After Use
UiO-66 Before Use
UiO-66-30%Co Before Use
UiO-66-10%Co Before Use
Intensity (a.u)
20
40
60
(2θ)°

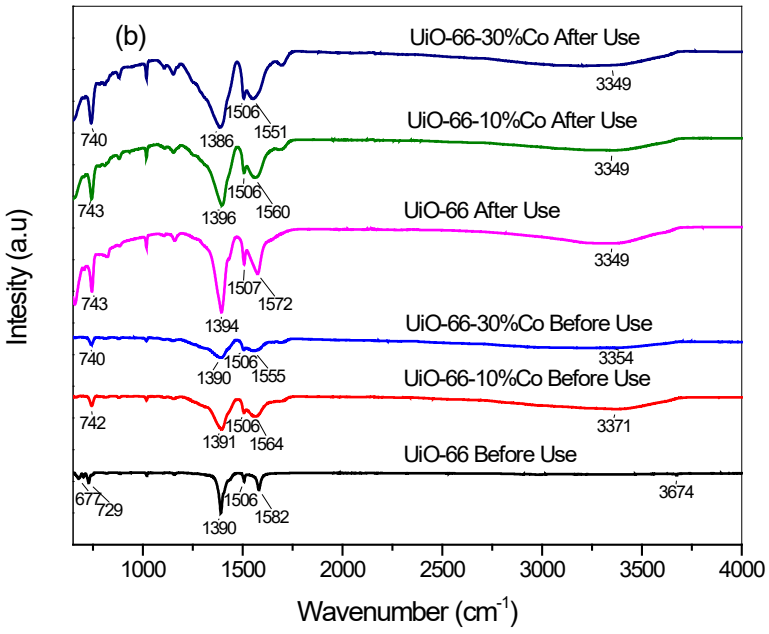
(b)
UiO-66-30%Co After Use
3349
740
1386
1506
1551
UiO-66-10%Co After Use
3349
743
1396
1506
1560
UiO-66 After Use
3349
743
1394
1507
1572
UiO-66-30%Co Before Use
3354
740
1390
1506
1555
UiO-66-10%Co Before Use
3371
742
1391
1506
1564
UiO-66 Before Use
3674
677
729
1390
1506
1582
Intesity (a.u)
1000
1500
2000
2500
3000
3500
4000
Wavenumber (cm-1)

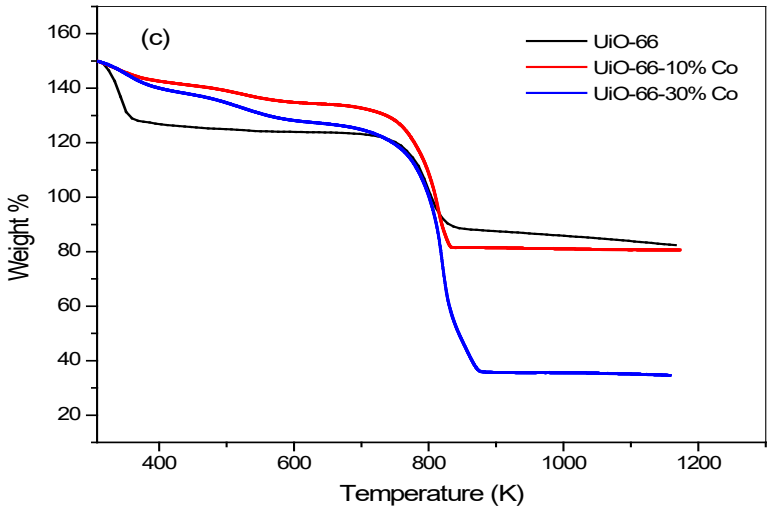

Figure 6.2: Characterisation of adsorbents. (a) PXRD patterns, (b) FTIR spectra and (c) TGA profiles of UiO-66, UiO-66-10% Co. and UiO-66-30% Co samples.

6.4.2 Adsorption study

Figure 6.3 clearly demonstrates that MB uptake by Zr-MOFs varies with the duration of the adsorption process, from 0 to time at equilibrium. The graphs are given as loading capacity (mg. g^{-1}) of MB onto MOFs with contact time. If we examine the trend over time, we can see that there is a noticeable steep upward relationship between loading of MB onto Zr-MOFs at the beginning period; as the contact time increases, this loading gradually slows as a plateau is reached. Therefore, the graphs in Figure 6.3 illustrate the rapid uptake of basic dye onto the external surface of Zr-MOFs initially, followed by intraparticle diffusion into the interior of the adsorbents until reaching adsorption and desorption equilibrium [103]. Abundant and active Zr-MOF sites were available at the primary stage of the interaction between the dye and adsorbents. Subsequently, as the contact time lengthened, MB uptake decreased drastically as the active sites are occupied by MB molecules. Likewise, higher initial concentrations of basic dye led to increased loading rate of MB onto adsorbents. This behaviour reflects the growth of driving force of mass transfer of dye towards unfilled Zr-MOF sites [104]. In contrast, the percentage removal of MB was reduced with higher initial MB concentration. This phenomenon was attributed to the large amounts of MB molecules in the bulk solution and the inadequate number of vacant active sites on Zr-MOFs. Further, lower initial concentration of the dye gave rise to a large number

of active vacant sites relative to the limited number of MB molecules, so dynamic equilibrium was more rapidly reached [105].

6.4.3 Kinetics study

Despite improvements to industrial applications using adsorption processes, most applications rely on the cost and efficiency of the adsorbent. The kinetics and mechanism of the sorption process are important because they enable the calculation of the designed absorbent [106]. In another words, a kinetics study examines the time taken by the adsorbent to reach saturation or equilibrium to facilitate the design of wastewater treatment processes. In addition, adsorption kinetics study is very important to assessing the efficiency of a sorbent [107].

Figure 6.3 shows how the quantity of adsorbate varies with contact time. It is apparent from the graphs that UiO-66-10%Co has a higher adsorption capacity than the other MOFs because of its higher specific surface areas and pore volumes relative to the other MOFs. Specifically, adsorption process depends on pore size since a higher adsorption uptake results from wider pores and larger surface area [108]. These conclusions prove that the textural properties of any adsorbent have a significant effect on the adsorption capacity of adsorbate.

To evaluate the effectiveness of the single-metal and bimetal Zr-MOFs, as well as to study the mechanism of rate-limiting steps, three kinetics models were employed to examine the experimental data and determine the mechanism of mass transfer and/or chemical reaction of the adsorption process of Zr-MOFs/MB systems. The three kinetics models used were pseudo first-order [91], pseudo second-order [92] and Elovich [93, 94] models.

Graphs of q_t against t at different initial MB concentrations were plotted for the adsorbents of interest in the present study. The application of pseudo first-order equation for all Zr-MOF/dye systems revealed that the model does not have a good fit with the experimental data for the whole period of the adsorption. It was only applicable to the beginning period of the adsorption process [109], consistent with reported findings in the literature [110-119].

The same experimental data were examined using the linear form of the pseudo second-order model. Table 6.2 lists the value of the parameters obtained from these

plots, including the kinetic constants (k_2) and correlation coefficients (R^2) for the different initial MB concentrations (5, 15, 30 and 50 ppm).

Based on the correlation coefficient (R^2), the pseudo second-order equation produced the highest correlation coefficient (> 0.99) for all Zr-MOF/MB systems as well as all initial MB concentrations. Therefore, the pseudo second-order model deserves significant consideration in this discussion, because its agreement with the experimental data was much higher than that achieved by the other two models. Specifically, the pseudo second-order equation can validate the behaviour of adsorbate/adsorbent interactions over the entire duration of the adsorption process, and prove that the rate-controlling step is chemisorption.

Further, the experimental data were investigated using the linear form of the Elovich equation; the constants from these plots are listed in Table 6.3, including the kinetic constants α, β and correlation coefficients (R^2) for initial MB concentrations (5, 15, 30 and 50 ppm). These correlation coefficients were close to those obtained for the pseudo second-order model ($0.946 \leq R^2 \leq 0.990$), highlighting that the mechanism of basic dye adsorption onto adsorbents may be chemically rate-controlling.

It can be seen from Table 6.2 that the pseudo second-order rate constant (k_2) decreases with higher initial concentrations of MB. For instance, the values of the rate constant k_2 of UiO-66-10%Co was 0.73164, 0.05289, 0.02747 and 0.00519 g mg^{-1} min^{-1} for basic dye at initial concentrations of 5, 15, 30 and 50 mg L^{-1}, respectively, indicating that higher initial MB concentrations would lead to a decrease in the adsorption rate of MB due to the long path of MB diffusion through the pores of Zr-MOFs. However, lower initial dye concentrations would give rise to higher rates of adsorption on the surface and through the open pores of MOFs.

Table 6.2 also provides the adsorption rate constants (k_2) of UiO-66-10%Co, UiO-66 and UiO-66-30%Co for initial MB concentration of 5 mg L^{-1}, calculated as 0.73164, 0.01050 and 0.00487 g mg^{-1} min^{-1}, respectively. These results verify the effect of pore diameter and volume of the sorbents, which were 2.18, 1.04 and 0.94 nm and 1.07, 0.82 and 0.28 for UiO-66-10%Co, UiO-66 and UiO-66-30%Co, respectively. It appears that the low rate constant (k_2) for MB adsorption onto the UiO-66-30%Co is attributable to the slower diffusion of dye molecules through the adsorbent's micropores.

Table 6.2: Calculated kinetics constant (k_2) and correlation coefficients (R^2) for C_i = 5, 15, 30 and 50 ppm.

Adsorbent	Adsorbate	Pseudo second-order kinetics constant k_2 (g/[mg.min])							
		5 ppm		15 ppm		30 ppm		50 ppm	
		k_2	R^2	k_2	R^2	k_2	R^2	k_2	R^2
UiO-66	MB	0.01050	0.9989	0.00546	0.9992	0.00273	0.9992	0.00147	0.999
UiO-66-10% Co	MB	0.73164	0.9970	0.05289	0.9999	0.02747	0.9999	0.00519	0.9998
UiO-66-30% Co	MB	0.00487	0.9976	0.00188	0.9985	0.00107	0.9983	0.00092	0.9933

Table 6.3: Calculated kinetic constants (α and β) and correlation coefficient (R^2) for Elovich model C_i = 5, 15, 30 and 50 mg/L.

Adsorbent	Adsorbate	Pseudo first-order kinetics constant k_1 (min^{-1})											
		5 ppm			15 ppm			30 ppm			50 ppm		
		α	β	R^2	α	β	R^2	α	β	R^2	α	β	R^2
UiO-66	MB	0.102294	1.9857	0.9903	0.372103	0.7922	0.9738	0.619666	0.4416	0.9925	0.708909	0.2908	0.9986
UiO-66-10% Co	MB	2974.821	2.2836	0.9812	3741.221	0.8586	0.9757	150558.1	0.5534	0.9694	39262.68	0.3364	0.9462
UiO-66-30% Co	MB	12.59526	2.0669	0.9868	16.72872	0.7945	0.9703	12.73342	0.4756	0.9802	13.77527	0.4279	0.9735

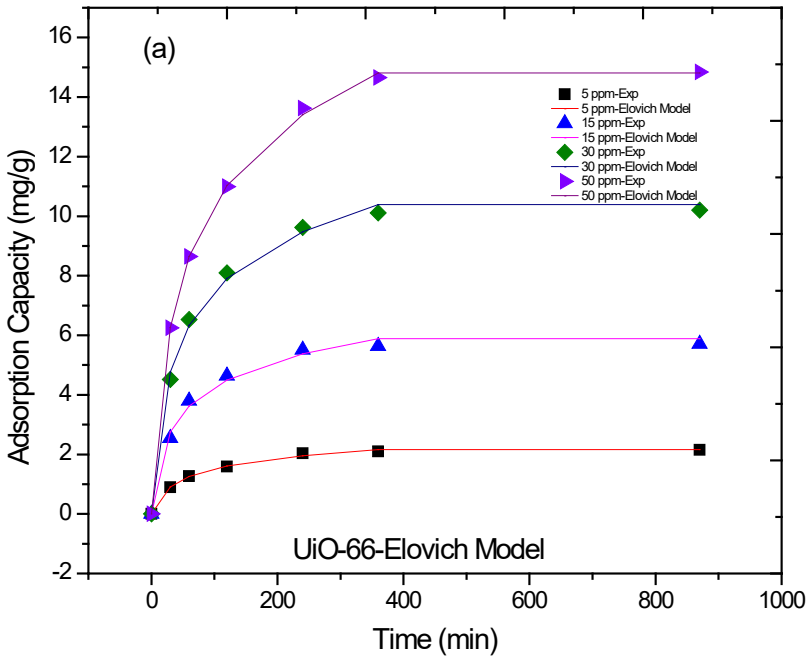
(a)
5 ppm-Exp
5 ppm-Elovich Model
15 ppm-Exp
15 ppm-Elovich Model
30 ppm-Exp
30 ppm-Elovich Model
50 ppm-Exp
50 ppm-Elovich Model
UiO-66-Elovich Model
Adsorption Capacity (mg/g)
Time (min)

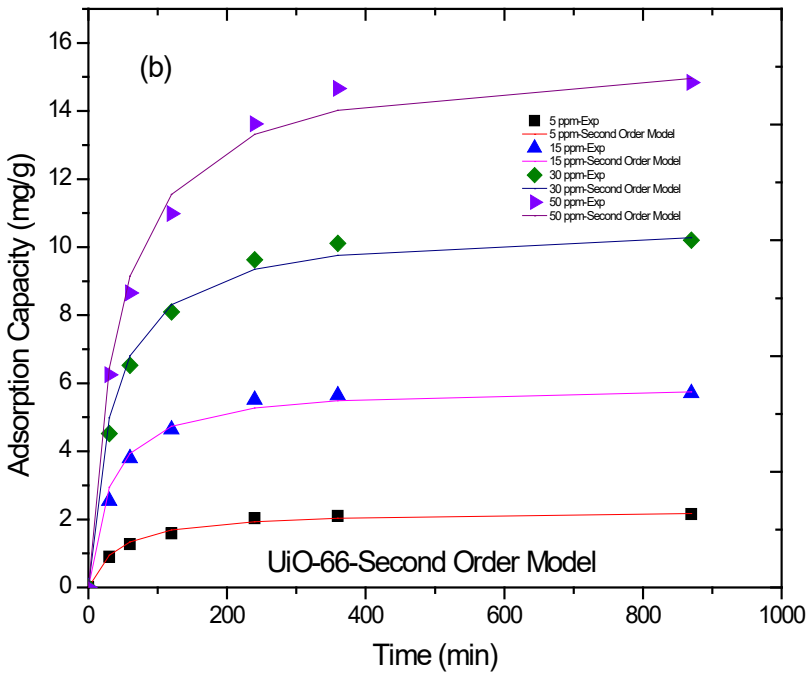
(b)
5 ppm-Exp
5 ppm-Second Order Model
15 ppm-Exp
15 ppm-Second Order Model
30 ppm-Exp
30 ppm-Second Order Model
50 ppm-Exp
50 ppm-Second Order Model
UiO-66-Second Order Model
Adsorption Capacity (mg/g)
Time (min)

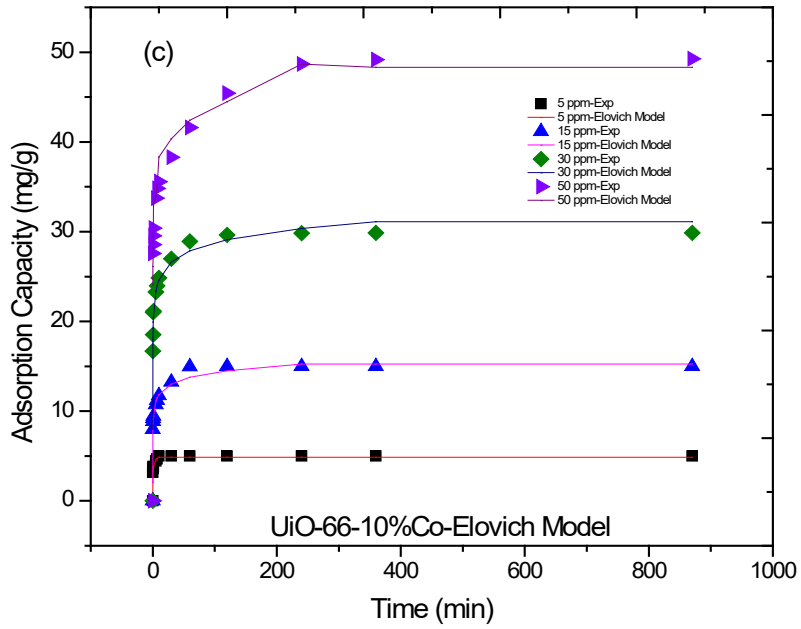
(c)
5 ppm-Exp
5 ppm-Elovich Model
15 ppm-Exp
15 ppm-Elovich Model
30 ppm-Exp
30 ppm-Elovich Model
50 ppm-Exp
50 ppm-Elovich Model
Adsorption Capacity (mg/g)
Time (min)
UiO-66-10%Co-Elovich Model

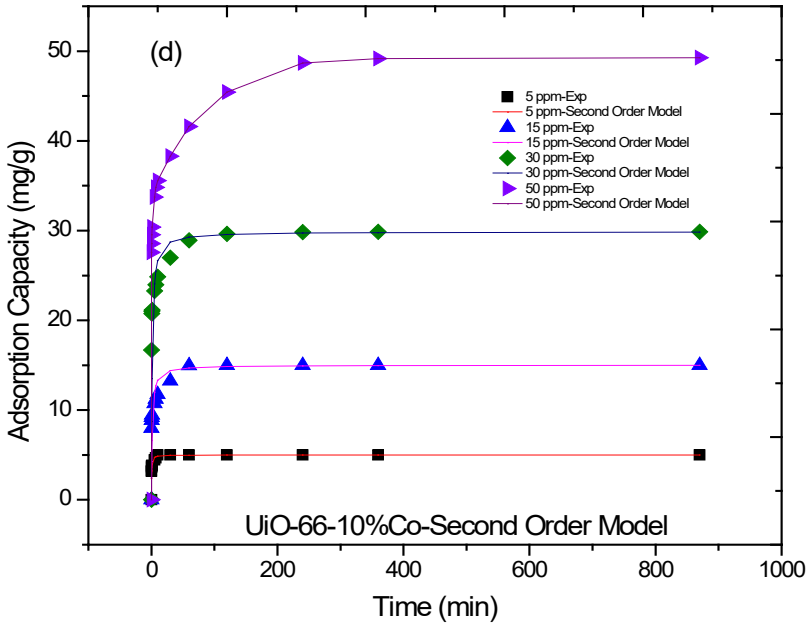
(d)
5 ppm-Exp
5 ppm-Second Order Model
15 ppm-Exp
15 ppm-Second Order Model
30 ppm-Exp
30 ppm-Second Order Model
50 ppm-Exp
50 ppm-Second Order Model
Adsorption Capacity (mg/g)
Time (min)
UiO-66-10%Co-Second Order Model

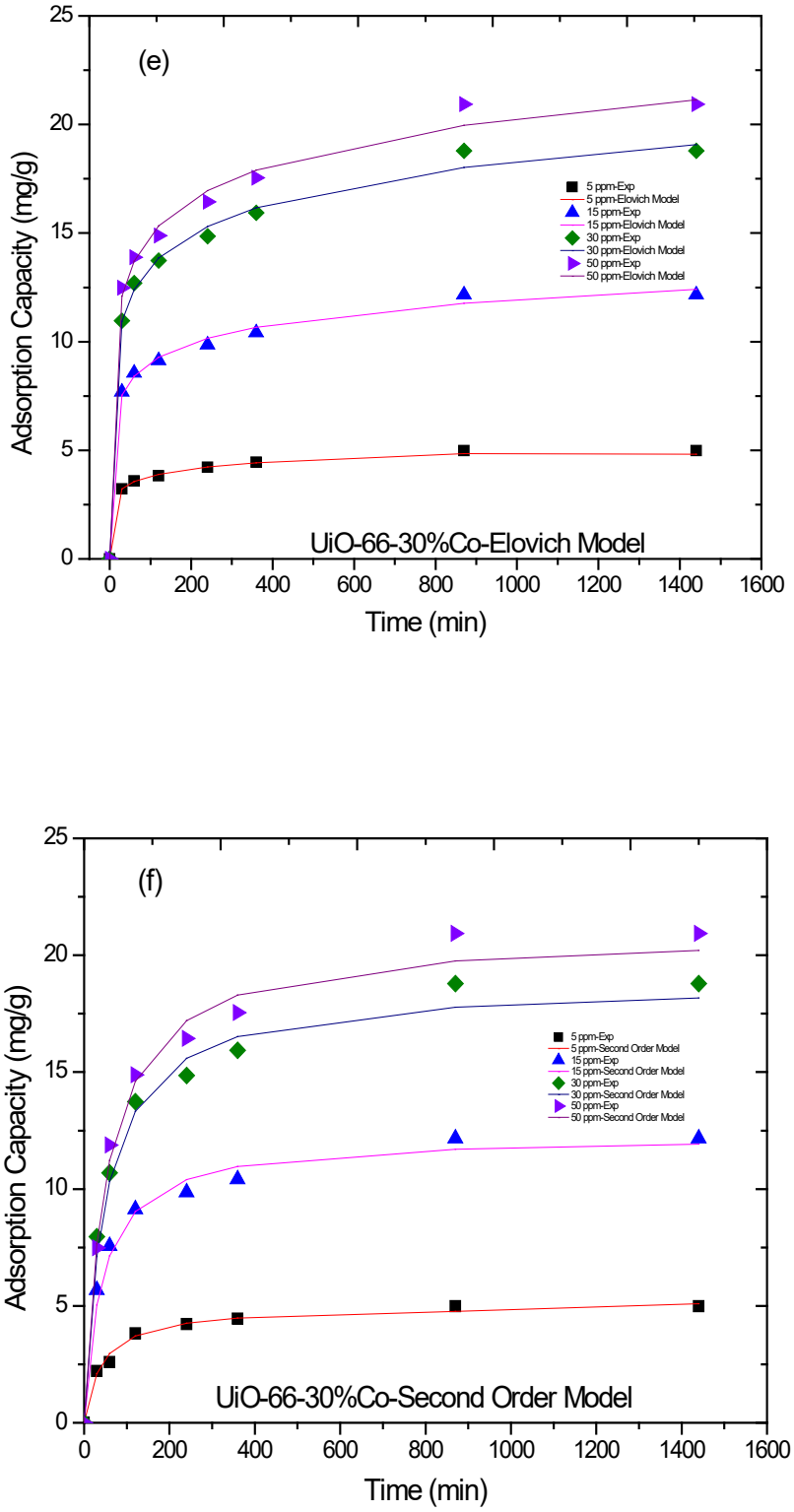

Figure 6.3: Fitting of experimental data using Elovich and second-order kinetics models of MB adsorption onto UiO-66 (a, b), UiO-66-10%Co (c, d) and UiO-66-30%Co (e, f).

6.4.4 Equilibrium study

The distribution of MB between the solution and Zr-MOF at equilibrium can be evaluated according to the various adsorption isotherms, including Langmuir and Freundlich models [120]. A prerequisite step of any column design is to fit the experimental data to these isotherms to determine the most appropriate model [121]. Coverage of the adsorbent's homogeneous surface with a monolayer of MB molecules should be tested by the Langmuir isotherm. However, the Freundlich isotherm assumes multilayered adsorption of heterogenous surface at various energy of adsorptive sites [105]. Figures 6.4(a), (b) and (c) illustrate the Langmuir and Freundlich isotherm profiles; the obtained parameters are listed in Table 6.4.

Based on the evaluation of the experimental data on adsorption processes of MB/Zr-MOF systems using the Freundlich isotherm, the sorption processes can be described as multilayer adsorption of heterogenous surfaces. The obtained higher correlation coefficient (R^2) for Zr-MOF-30%Co suggests it follows the Langmuir isotherm with low affinity between the dye and adsorbent [65], as evident in Table 6.4. This behaviour is due to the fact that this MOF has the lowest specific surface area (592.378 m^2g^{-1}), pore volume (0.28 cc g^{-1}) and pore diameter (0.94 nm) compared to UiO-66-Co10% and UiO-66, as shown in Table 6.1.

Modified Zr-MOF-10%Co exhibited enhanced internal volume, demonstrated by the fact that it had the highest pore volume (1.07 cc g^{-1}) and pore diameter (2.18 nm). Consequently, enhanced textural properties of UiO-66-10%Co may be the reason for its capacity to adsorb more dye molecules (51.02 mg g^{-1}) at higher initial MB concentration.

Increased MB uptake can also be described in terms of the Co enhancing the negative charge of the Zr-MOF surface. Moreover, increasing the electrostatic attraction between the positively charged MB molecules and MOF particles would increase the loading capacity of the adsorbent. Table 6.5 provides the maximum sorption loading capacity for MB that was found in the present study, relative to that found for other adsorbents in other studies.

Equation 6.10 identifies the essential characteristics of the Langmuir isotherm, expressed below in terms of a dimensionless constant separation factor R_L [122].

$$R_L = \frac{1}{(1 + k_L C_0)}, \quad (6.10)$$

Where C_0 is the initial concentration of adsorbate (mg/L) and K_L (L/mg) is the Langmuir constant.

The numeric value of R_L indicates the type of isotherm to be either:

- unfavourable ($R_L > 1$)
- linear ($R_L = 1$)
- favourable ($0 < R_L < 1$)
- irreversible ($R_L = 0$).

An examination of experimental data showed that all values of R_L ranged from 0 to 1, verifying that the adsorption of basic dye was favourable for all single-metal and bimetal Zr-MOF adsorbents, and at high initial concentrations of MB the adsorption tends to be nearly irreversible [123].

In general, the Freundlich model parameters K_F, n and 1/n for all adsorbents in this study exhibited favourable adsorption processes ($n > 1$)[124], with ample opportunity to form multilayer sorption of MB on the active sites of heterogeneous surfaces ($0 < 1/n < 1$). This behaviour is attributable to irregular pore shape, pore size, surface functional groups and impurities [125], as 1/n is the adsorption intensity and K_F is a rough indicator of adsorption capacity. Specifically, as the value of K_F increases, Zr-MOFs' adsorption capacity for MB increases. Further, the adsorption intensity or surface heterogeneity (1/n) fluctuates between 0 to 1, which can be closer to heterogeneity when the value approaches to zero [126]. Moreover, a value of 1/n that is less than 1 indicates a normal Freundlich isotherm whereas a value greater than 1 is a sign of cooperative adsorption [127].

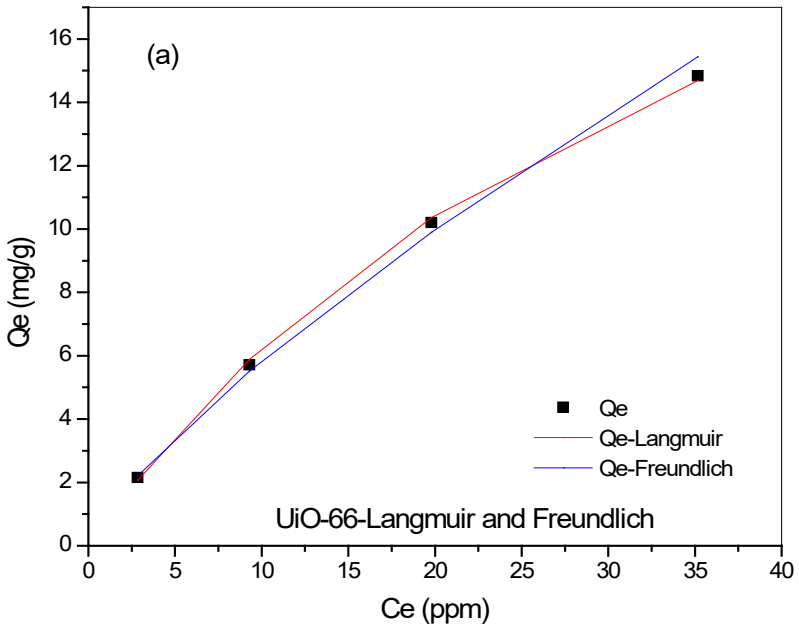
(a)
Qe (mg/g)
Ce (ppm)
Qe
Qe-Langmuir
Qe-Freundlich
UiO-66-Langmuir and Freundlich

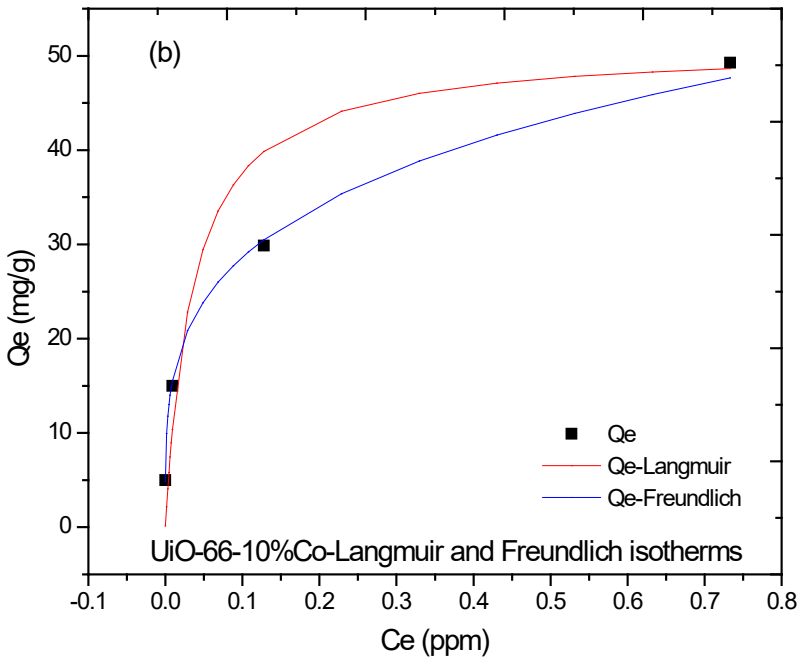
(b)
Qe (mg/g)
Ce (ppm)
Qe
Qe-Langmuir
Qe-Freundlich
UiO-66-10%Co-Langmuir and Freundlich isotherms

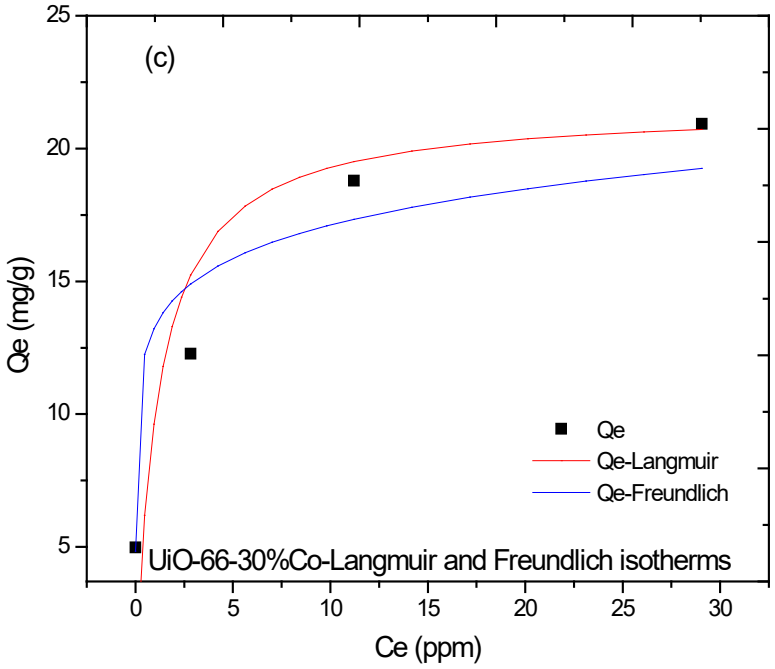

Figure 6.4: Fitting of experimental data using Langmuir and Freundlich models of MB adsorption onto UiO-66 (a), UiO-66-10%Co (b) and UiO-66-30%Co (c).

Table 6.4: Calculated equilibrium constants (k_L, k_F, q_m, n and correlation coefficient (R^2)) of MB adsorption onto UiO-66, UiO-66-30%Co and UiO-66-10%Co for C_i = 5, 15, 30 and 50 ppm.

Adsorbent	Adsorption isotherm model	Parameter	Value	R^2
UiO-66	Langmuir	q_m (mg/g)	14.52	0.989
		K_L (L/mg)	0.024	
	Freundlich	K_F ([mg/g] [L/mg]$^{1/n}$)	0.981	0.9979
		n (g/L)	1.291	
		1/n (L/g)	0.775	
UiO-66-10%Co	Langmuir	q_m (mg/g)	51.02	0.9879
		K_L (L/mg)	28.00	
	Freundlich	K_F ([mg/g] [L/mg]$^{1/n}$)	51.57	0.9989
		n (g/L)	3.912	
		1/n (L/g)	0.256	
UiO-66-30%Co	Langmuir	q_m (mg/g)	21.55	0.9949
		K_L (L/mg)	0.852	
	Freundlich	K_F ([mg/g] [L/mg]$^{1/n}$)	13.29	0.9593
		n (g/L)	9.107	
		1/n (L/g)	0.109	

Table 6.5: Comparison of monolayer equilibrium capacity for methylene blue onto different sorbents.

Adsorbent	Condition	q_m (mg/g)	Reference
Garlic peel	Normal	82.64	[128]
Charcoal	Normal	62.7	[129]
Heated montmorillonite	Normal	62	[130]
Natural clay	Normal	58.20	[106]
Raw KT3B kaolin	Normal	52.76	[131]
UiO-66-10%Co	Normal	51.02	This study
UiO-66-30%Co		21.55	This study
UiO-66		14.52	This study
Zirconium-pillared clay	Normal	27	[132]
Aluminium-pillared clay	Normal	21	[132]
Alkaline-treated clinoptilolite	Normal	47.3	[133]
Sulfuric acid–treated parthenium	Normal	39.68	[134]
Raw ball clay	Normal	34.65	[135]
Pure kaolin	Normal	15.55	[136]
Raw kaolin	Normal	13.99	[136]
Activated rice husks	Normal	0.21	[137]
Chitosan/organic rectorite composite	Normal	24.69	[138]
NaOH-treated pure koalin	Normal	20.49	[136]
NaOH-treated raw koalin	Normal	16.34	[136]
Beech sawdust pretreated with $CaCl_2$	Normal	13.02	[139]
Clay biochar	Normal	11.94	[140]
Modified chitosan	Normal	10.91	[141]
Hazelnut shell–activated carbon	Normal	8.82	[142]
Apricot stone–activated carbon	Normal	4.11	[142]
Walnut shell–activated carbon	Normal	3.53	[142]
Almond shell–activated carbon	Normal	1.33	[142]
Chrome sludge	Normal	0.51	[143]

6.4.5 Intraparticle diffusion study

A lack of description of an adsorption mechanism as well as of the rate-controlling step of the adsorption reaction, in addition to the limitations in the pseudo first-order and pseudo second-order kinetics models, prompted Weber and Morris to derive the intraparticle diffusion model to explain adsorption kinetics of adsorption (Equation 6.7).

Intraparticle diffusion consists of three sequential steps. Its stages are as follows [144]:

1. Rapid mass transfer of adsorbate from bulk solution to external surface of the adsorbent through external molecular diffusion or film diffusion.
2. Slow mass transfer of adsorbate from the surface of adsorbent into interior sites.

3. Adsorption of the adsorbate molecules onto the surface of the pores until equilibrium is reached.

The slow or rate-controlling step(s) of the adsorption process plays a very important role in controlling the overall rate of the sorption process. The determination of the nature of this step in any batch adsorption process depends on the properties of both the adsorbate and adsorbent [3].

In this study, the intraparticle diffusion–based mechanism of dye adsorption onto Zr-MOFs was investigated, as is common to identify the stages of the sorption process. The empirical equation for intraparticle diffusion was fitted to the obtained experimental data, which found that the loading of MB varies proportionally with $t^{1/2}$. All obtained values for the parameters are listed in Table 6.6.

When intraparticle diffusion takes place, the relationship between q_t and $t^{1/2}$ must be linear. In addition, the rate-controlling step of the adsorption process is only attributable to the intraparticle diffusion when the straight line of the plot passes through the origin. If the plot passes through the origin, then the rate-limiting step is only attributable to intraparticle diffusion. If the plot does not pass through the origin, additional mechanisms along with intraparticle diffusion are involved [145].

Figures 6.5(a), (b) and (c) show that each sorption process can be plotted with more than one intercepting line with various slopes, proving that the stages of adsorption are independent of each other. Therefore, it is evident that the adsorption process of the Zr-MOFs/MB systems occurs in multiple stages, including surface adsorption and pore diffusion of dye onto Zr-MOFs. The graphs in Figure 6.5 were also nonlinear over the entire duration of contact, suggesting that the adsorption process was influenced by more than one step. This observed phenomenon is consistent with that reported in the literature [146].

All graphs in Figure 6.5 demonstrate two behaviours: the initial portion of the plot which represents the effects of boundary layer diffusion, and the final segment which signifies the effects of intraparticle diffusion. Intercept C of the final part of with the y axis is related to the thickness of the boundary layer [147].

external molecular diffusion or film diffusion is very fast process causing rapid adsorption of dye onto Zr-MOFs surfaces. A characteristic of this step is the large

difference in driving force, which quickens MB transport and leads to the adsorption of the most quantity of dye in this step [148]. This finding enables the classification of Zr-MOFs/MB systems as involving a rapid sorption process. Accordingly, the present systems in this study can be considered important alternatives for removing basic dyes in wastewater. However, the slow stage of intraparticle diffusion can be interpreted as the occupation of adsorbent surface sites by dye molecules in film diffusion and the slow diffusion of dye molecules into adsorbent pores, leading to a slower adsorption rate [149].

Fitting the experimental data showed that for all adsorption systems, higher initial concentrations of MB resulted in higher k_p values. For example, comparing the initial MB concentration of 5 mg L^{-1} versus 50 mg L^{-1} for the UiO-66-10%Co/MB system, the value of intraparticle diffusion rate constant (k_p) jumped from 0.5277 to 1.2837 mg $g^{-1}min^{-(1/2)}$, respectively. Hence, the driving force increases with higher initial MB concentration, which in turn increases the rate of MB diffusion.

In addition, higher initial MB concentrations cause the intercept value (C) to increase. For instance, for initial MB concentrations of 5 mg L^{-1} versus 50 mg L^{-1} with the same UiO-66-10%Co/MB, the intercept value (C) increased from 3.2949 to 30.483 mg g^{-1}, respectively. Therefore, higher initial dye concentrations enhance the effects of the boundary layer in the adsorption process.

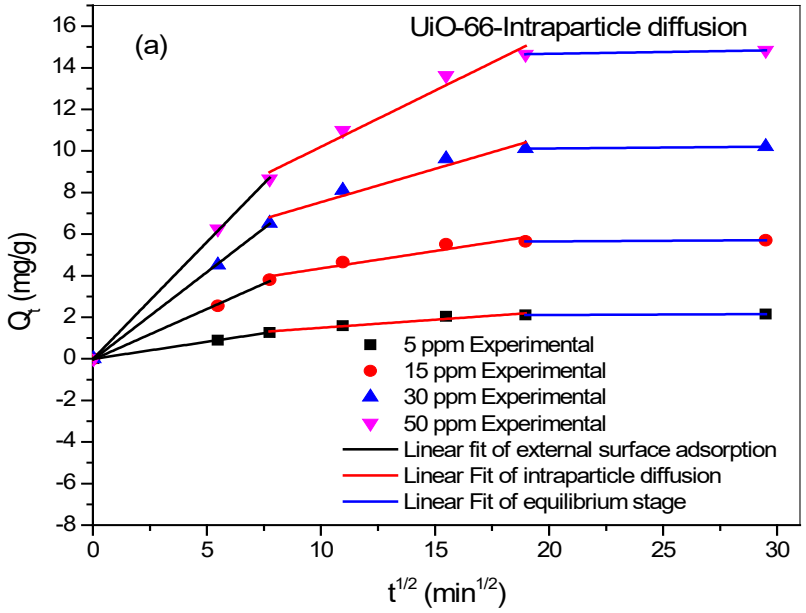

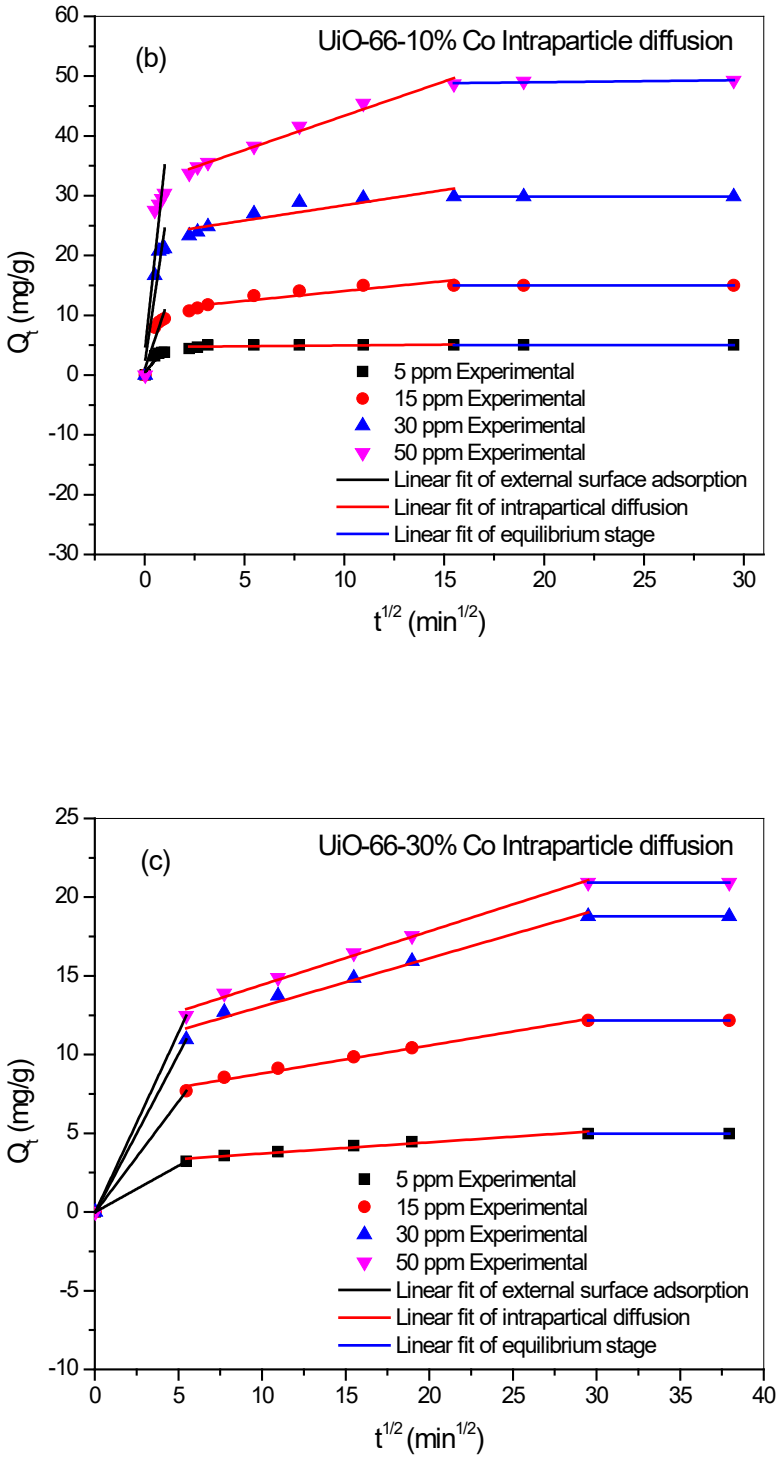

Figure 6.5: Fitting of experimental data using intraparticle diffusion models of MB adsorption onto UiO-66 (a), UiO-66-10%Co (b) and UiO-66-30%Co (c).

Table 6.6: Calculated kinetics constant (k_p), C and correlation coefficient (R^2) for C_i = 5, 15, 30 and 50 ppm.

		Adsorption mechanism		
		Intraparticle diffusion model		
Adsorbent	**Initial concentration of MB solution (mg L^{-1})**	**k_p (mg $g^{-1}min^{-(1/2)}$)**	**C (mg g^{-1})**	**R^2**
UiO-66	5	0.0991	0.5017	0.9999
	15	0.22	2.1455	0.9918
	30	0.3955	3.5763	0.9884
	50	0.638	3.8144	0.9959
UiO-66-10%Co	5	0.5277	3.2949	0.9968
	15	0.8475	8.6541	0.9816
	30	1.1482	20.512	0.9706
	50	1.2837	30.483	0.9602
UiO-66-30%Co	5	0.0712	3.0025	0.9649
	15	0.1775	7.0291	0.9865
	30	0.3061	9.9984	0.9772
	50	0.3407	11.022	0.9938

6.5 Effect of pH

It is crucial step to investigate the effects of pH and zeta potential of Zr-MOF on adsorption process to examine adsorption mechanism. The result of such study is very important to figure out the impact of the electrostatic interactions on adsorption. pH was selected in such a way to cover acidic and basic range between 3.75-10 and the adsorption process carried out at condition of initial concentration of MB solutions at 50 ppm and using 0.1 M HCl and 0.1 M NaOH to adjust pH. As show in Figure 6.6 (a) that adsorption uptake increases with increasing of pH solution from 3.75 to 10, indicating the role of electrostatic attraction between negatively charged adsorbent and cationic dye (MB). At pH equal to 5.6 which pH of isoelectric point (pH_{iep}) Figure 6.6 (b) with no charge on adsorbent, the uptake still high signifying that other factors play roles in adsorption of adsorbate while if pH less than pH_{iep} the adsorption capacity decreases steeply due to repulsion between adsorbate and adsorbent. Consequently UiO-66 can be used over a wide range of pH for discolouration of wastewater at large scale. Figure 6.7 illustrates plausible mechanism was proposed based on pH effect and Zeta potential of UiO-66. It can be concluded from the results that the adsorption mechanism of MB onto Zr-MOF is mainly depended on the electrostatic interactions

between the cationic dye of positive charge and UiO-66 of positive charge. In addition, π–π interactions between the benzene rings of UiO-66 and those of the dye could have contributed to the adsorption process.

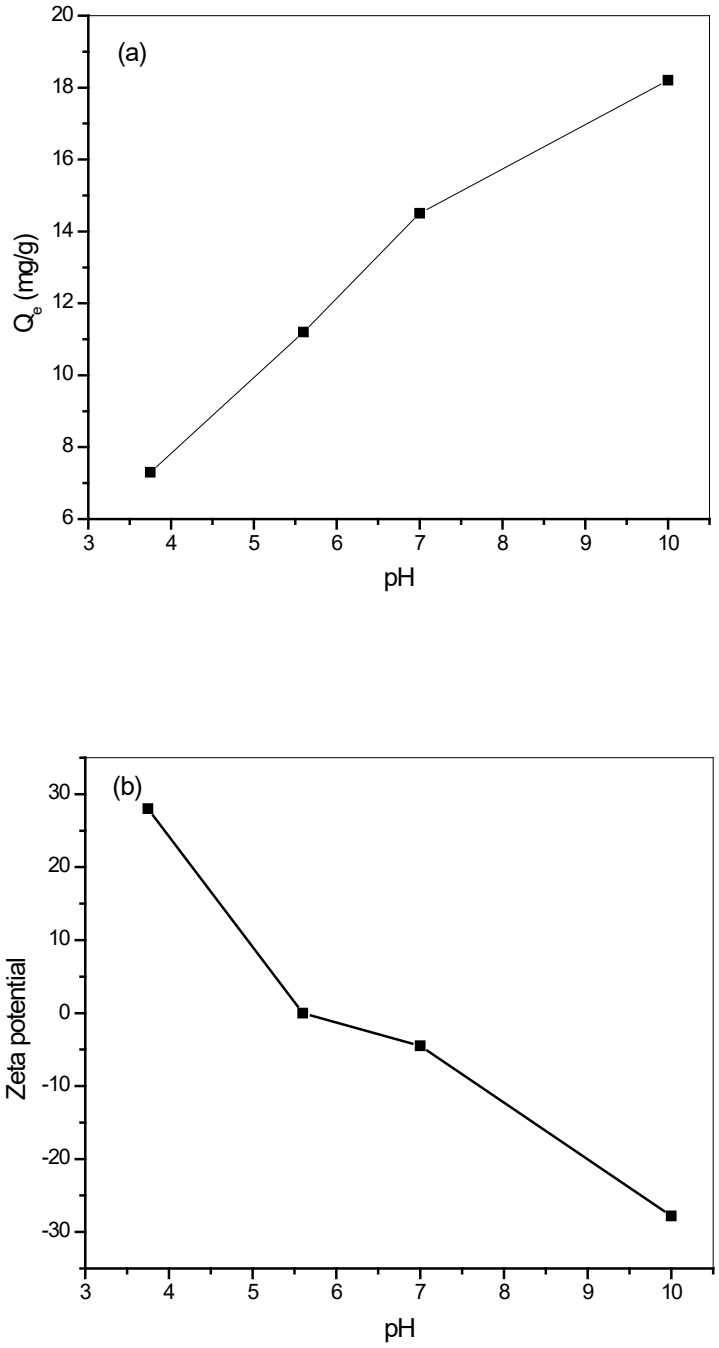

Figure 6.6. Effects of pH solution (a) and zeta potential of UiO-66 (b) on adsorption of MB onto UiO-66.

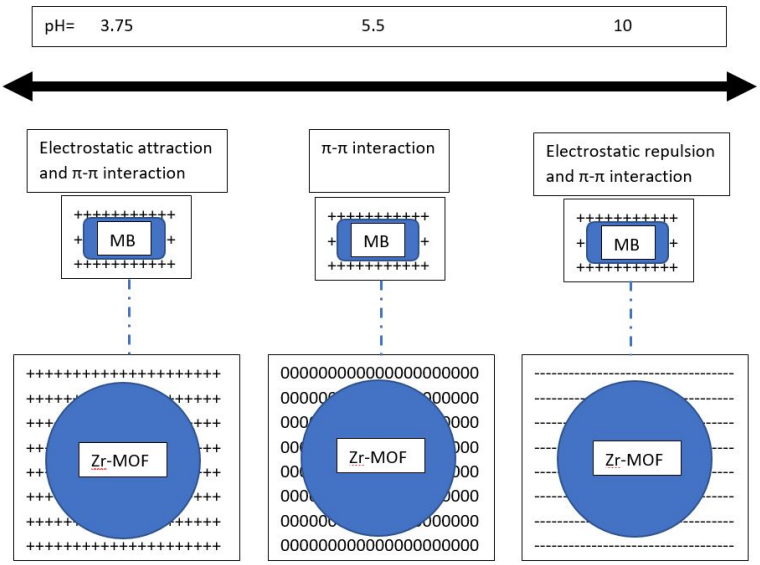

Figure 6.7. Plausible adsorption mechanism of MB onto Zr-MOF.

6.6 Conclusion

Three versions Zr-MOFs were prepared successfully and used as adsorbents for the removal of MB from aqueous solutions of four different initial MB concentrations. Modification of UiO-66 with 10% Co was found to enhance its adsorption capacity for basic dye and made it an excellent alternative adsorbent in industrial wastewater treatment, whereas increasing the percentage metal to 30% Co led to reduction in MB uptake. Experimental data were fitted to Langmuir and Freundlich equilibrium isotherms. Based on the coefficients of determination (R^2), the data had good agreement with the Freundlich isotherm, indicating that the adsorption process involved multilayer adsorption of heterogenous surface with maximum Langmuir monolayer adsorption capacity of 51.02 mg g^{-1}—comparable with the reported values for other adsorbents in earlier studies. The kinetic rate of adsorption was found to obey the pseudo second-order model with a high correlation coefficient ($R^2 \geq 0.99$). The results prove that Zr-MOFs are favourable substitutes for the removal of MB from industrial wastewater. The outcomes of fitting the experimental data to the intraparticle

diffusion equation suggested that intraparticle diffusion was not the only rate-limiting step in the adsorption process.

References

1. Bitton, G., *Wastewater microbiology*. 2005: John Wiley & Sons.
2. Sidat, M., H. Kasan, and F. Bux, *Laboratory-scale investigation of biological phosphate removal from municipal wastewater.* WATER SA, 1999. **25**(4): p. 459-462.
3. Gürses, A., et al., *The adsorption kinetics of the cationic dye, methylene blue, onto clay.* Journal of Hazardous Materials, 2006. **131**(1): p. 217-228.
4. Marungrueng, K. and P. Pavasant, *Removal of basic dye (Astrazon Blue FGRL) using macroalga Caulerpa lentillifera.* Journal of Environmental Management, 2006. **78**(3): p. 268-274.
5. Wang, C.-C., et al., *Adsorption of basic dyes onto montmorillonite.* Journal of Colloid and Interface Science, 2004. **273**(1): p. 80-86.
6. Hameed, B.H., D.K. Mahmoud, and A.L. Ahmad, *Sorption of basic dye from aqueous solution by pomelo (Citrus grandis) peel in a batch system.* Colloids and Surfaces A: Physicochemical and Engineering Aspects, 2008. **316**(1): p. 78-84.
7. Poots, V., G. Mckay, and J. Healy, *The removal of acid dye from effluent using natural adsorbents—I peat.* Water research, 1976. **10**(12): p. 1061-1066.
8. Doğan, M., M. Alkan, and Y. Onganer, *Adsorption of methylene blue from aqueous solution onto perlite.* Water, Air, and Soil Pollution, 2000. **120**(3-4): p. 229-248.
9. Inthorn, D., et al., *Decolorization of basic, direct and reactive dyes by pre-treated narrow-leaved cattail (Typha angustifolia Linn.).* Bioresource technology, 2004. **94**(3): p. 299-306.
10. Choy, K.K., G. McKay, and J.F. Porter, *Sorption of acid dyes from effluents using activated carbon.* Resources, Conservation and Recycling, 1999. **27**(1-2): p. 57-71.
11. Hameed, B.H., A.A. Ahmad, and N. Aziz, *Isotherms, kinetics and thermodynamics of acid dye adsorption on activated palm ash.* Chemical Engineering Journal, 2007. **133**(1): p. 195-203.
12. Bulut, Y. and H. Karaer, *Adsorption of methylene blue from aqueous solution by crosslinked chitosan/bentonite composite.* Journal of Dispersion Science and Technology, 2015. **36**(1): p. 61-67.
13. Bhattacharyya, R. and S.K. Ray, *Removal of congo red and methyl violet from water using nano clay filled composite hydrogels of poly acrylic acid and polyethylene glycol.* Chemical Engineering Journal, 2015. **260**: p. 269-283.
14. Roosta, M., et al., *Optimization of the combined ultrasonic assisted/adsorption method for the removal of malachite green by gold nanoparticles loaded on activated carbon: experimental design.*

Spectrochimica Acta Part A: Molecular and Biomolecular Spectroscopy, 2014. **118**: p. 55-65.

15. Pelekani, C. and V.L. Snoeyink, *A kinetic and equilibrium study of competitive adsorption between atrazine and Congo red dye on activated carbon: the importance of pore size distribution.* Carbon, 2001. **39**(1): p. 25-37.

16. Liu, Y., et al., *Attapulgite/bentonite interactions for methylene blue adsorption characteristics from aqueous solution.* Chemical Engineering Journal, 2014. **237**: p. 403-410.

17. Suchithra, P., et al., *Mesoporous organic–inorganic hybrid aerogels through ultrasonic assisted sol–gel intercalation of silica–PEG in bentonite for effective removal of dyes, volatile organic pollutants and petroleum products from aqueous solution.* Chemical engineering journal, 2012. **200**: p. 589-600.

18. Hareesh, P., K. Babitha, and S. Shukla, *Processing fly ash stabilized hydrogen titanate nano-sheets for industrial dye-removal application.* Journal of hazardous materials, 2012. **229**: p. 177-182.

19. Robati, D., et al., *Removal of hazardous dyes-BR 12 and methyl orange using graphene oxide as an adsorbent from aqueous phase.* Chemical Engineering Journal, 2016. **284**: p. 687-697.

20. Angın, D., T.E. Köse, and U. Selengil, *Production and characterization of activated carbon prepared from safflower seed cake biochar and its ability to absorb reactive dyestuff.* Applied Surface Science, 2013. **280**: p. 705-710.

21. Kuan, W.-H. and Y.-C. Chan, *pH-dependent mechanisms of methylene blue reacting with tunneled manganese oxide pyrolusite.* Journal of hazardous materials, 2012. **239**: p. 152-159.

22. Nuñez, S.C., et al., *Urea enhances the photodynamic efficiency of methylene blue.* Journal of Photochemistry and Photobiology B: Biology, 2015. **150**: p. 31-37.

23. Núñez, S.C., et al., *Effects of ionic strength on the antimicrobial photodynamic efficiency of methylene blue.* Photochemical & Photobiological Sciences, 2014. **13**(3): p. 595-602.

24. Senthilkumaar, S., et al., *Adsorption of methylene blue onto jute fiber carbon: kinetics and equilibrium studies.* Journal of colloid and interface science, 2005. **284**(1): p. 78-82.

25. Junqueira, H.C., et al., *Modulation of methylene blue photochemical properties based on adsorption at aqueous micelle interfaces.* Physical Chemistry Chemical Physics, 2002. **4**(11): p. 2320-2328.

26. Severino, D., et al., *Influence of Negatively Charged Interfaces on the Ground and Excited State Properties of Methylene Blue*¶. Photochemistry and photobiology, 2003. **77**(5): p. 459-468.

27. Kumar, P.S., S. Ramalingam, and K. Sathishkumar, *Removal of methylene blue dye from aqueous solution by activated carbon prepared from cashew*

nut shell as a new low-cost adsorbent. Korean Journal of Chemical Engineering, 2011. **28**(1): p. 149-155.

28. Stawiński, W., et al., *Acid-base treated vermiculite as high performance adsorbent: insights into the mechanism of cationic dyes adsorption, regeneration, recyclability and stability studies.* Chemosphere, 2017. **173**: p. 107-115.

29. Xu, J., et al., *Magnetic properties and methylene blue adsorptive performance of CoFe2O4/activated carbon nanocomposites.* Materials Chemistry and Physics, 2014. **147**(3): p. 915-919.

30. Paz, A., et al., *Biological treatment of model dyes and textile wastewaters.* Chemosphere, 2017. **181**: p. 168-177.

31. Ayati, A., et al., *Emerging adsorptive removal of azo dye by metal–organic frameworks.* Chemosphere, 2016. **160**: p. 30-44.

32. Stawiński, W., et al., *The influence of acid treatments over vermiculite based material as adsorbent for cationic textile dyestuffs.* Chemosphere, 2016. **153**: p. 115-129.

33. Zhu, S., et al., *High adsorption capacity for dye removal by CuZn hydroxyl double salts.* Environmental Science: Nano, 2014. **1**(2): p. 172-180.

34. Xiao, Z., et al., *The enhancing effect of weak magnetic field on degradation of Orange II by zero-valent iron.* Desalination and Water Treatment, 2016. **57**(4): p. 1659-1670.

35. Behnajady, M., N. Modirshahla, and F. Ghanbary, *A kinetic model for the decolorization of CI Acid Yellow 23 by Fenton process.* Journal of Hazardous Materials, 2007. **148**(1-2): p. 98-102.

36. Huang, Y.-H., et al., *Degradation of commercial azo dye reactive Black B in photo/ferrioxalate system.* Journal of hazardous materials, 2007. **140**(1-2): p. 382-388.

37. Neelavannan, M., M. Revathi, and C.A. Basha, *Photocatalytic and electrochemical combined treatment of textile wash water.* Journal of Hazardous Materials, 2007. **149**(2): p. 371-378.

38. Sohrabi, M.R. and M. Ghavami, *Photocatalytic degradation of Direct Red 23 dye using UV/TiO2: Effect of operational parameters.* Journal of Hazardous Materials, 2008. **153**(3): p. 1235-1239.

39. Abbasi, M. and N.R. Asl, *Sonochemical degradation of Basic Blue 41 dye assisted by nanoTiO2 and H2O2.* Journal of hazardous materials, 2008. **153**(3): p. 942-947.

40. Lodha, B. and S. Chaudhari, *Optimization of Fenton-biological treatment scheme for the treatment of aqueous dye solutions.* Journal of Hazardous Materials, 2007. **148**(1-2): p. 459-466.

41. Daneshvar, N., et al., *Biodegradation of dye solution containing Malachite Green: Optimization of effective parameters using Taguchi method.* Journal of Hazardous Materials, 2007. **143**(1-2): p. 214-219.

42. Garcia-Montano, J., et al., *Environmental assessment of different photo-Fenton approaches for commercial reactive dye removal.* Journal of hazardous materials, 2006. **138**(2): p. 218-225.

43. Sudarjanto, G., B. Keller-Lehmann, and J. Keller, *Optimization of integrated chemical–biological degradation of a reactive azo dye using response surface methodology.* Journal of hazardous materials, 2006. **138**(1): p. 160-168.

44. Fan, L., et al., *Electrochemical degradation of aqueous solution of Amaranth azo dye on ACF under potentiostatic model.* Dyes and Pigments, 2008. **76**(2): p. 440-446.

45. Islam, M.A., et al., *Methylene blue adsorption on factory-rejected tea activated carbon prepared by conjunction of hydrothermal carbonization and sodium hydroxide activation processes.* Journal of the Taiwan Institute of Chemical Engineers, 2015. **52**: p. 57-64.

46. Labanda, J., J. Sabaté, and J. Llorens, *Experimental and modeling study of the adsorption of single and binary dye solutions with an ion-exchange membrane adsorber.* Chemical engineering journal, 2011. **166**(2): p. 536-543.

47. Reddy, D.H.K. and Y.-S. Yun, *Spinel ferrite magnetic adsorbents: alternative future materials for water purification?* Coordination Chemistry Reviews, 2016. **315**: p. 90-111.

48. Rafatullah, M., et al., *Adsorption of methylene blue on low-cost adsorbents: a review.* Journal of hazardous materials, 2010. **177**(1-3): p. 70-80.

49. Chen, R., et al., *Rapid hydrothermal synthesis of magnetic CoxNi1− xFe2O4 nanoparticles and their application on removal of Congo red.* Chemical Engineering Journal, 2014. **242**: p. 226-233.

50. Heidari, A., et al., *Adsorptive removal of CO2 on highly microporous activated carbons prepared from Eucalyptus camaldulensis wood: Effect of chemical activation.* Journal of the Taiwan Institute of Chemical Engineers, 2014. **45**(2): p. 579-588.

51. Cheremisinoff, P.N. and F. Ellerbusch, *Carbon adsorption handbook*. 1978: Ann Arbor Science Publishers.

52. Roman, S., et al., *Production of low-cost adsorbents with tunable surface chemistry by conjunction of hydrothermal carbonization and activation processes.* Microporous and Mesoporous Materials, 2013. **165**: p. 127-133.

53. Kyzas, G.Z., et al., *Synthesis and adsorption application of succinyl-grafted chitosan for the simultaneous removal of zinc and cationic dye from binary hazardous mixtures.* Chemical Engineering Journal, 2015. **259**: p. 438-448.

54. Aguedal, H., et al., *Effect of thermal regeneration of diatomite adsorbent on its efficacy for removal of dye from water.* International Journal of Environmental Science and Technology, 2018: p. 1-12.

55. Ziane, S. and A. Khelifa. *Kinetics and Isotherms Adsorption of Reactive Dye by Thermally Treated Dolomite*. in *International Symposium on Materials and Sustainable Development*. 2017. Springer.

56. Shah, J., et al., *Kinetic and equilibrium profile of the adsorptive removal of Acid Red 17 dye by surfactant-modified fuller's earth.* Water Science and Technology, 2017. **75**(6): p. 1410-1420.

57. Anirudhan, T. and M. Ramachandran, *Adsorptive removal of basic dyes from aqueous solutions by surfactant modified bentonite clay (organoclay): kinetic and competitive adsorption isotherm.* Process Safety and Environmental Protection, 2015. **95**: p. 215-225.

58. Li, C., et al., *Removal of basic dye (methylene blue) from aqueous solution using zeolite synthesized from electrolytic manganese residue.* Journal of Industrial and Engineering Chemistry, 2015. **23**: p. 344-352.

59. Chieng, H.I., L.B. Lim, and N. Priyantha, *Sorption characteristics of peat from Brunei Darussalam for the removal of rhodamine B dye from aqueous solution: adsorption isotherms, thermodynamics, kinetics and regeneration studies.* Desalination and Water Treatment, 2015. **55**(3): p. 664-677.

60. Xu, H., et al., *Removal of quinoline from aqueous solutions by lignite, coking coal and anthracite. Adsorption kinetics.* Physicochemical Problems of Mineral Processing, 2016. **52**.

61. Allen, S.J., et al., *Comparison of optimised isotherm models for basic dye adsorption by kudzu.* Bioresource Technology, 2003. **88**(2): p. 143-152.

62. Hameed, B. and M. El-Khaiary, *Batch removal of malachite green from aqueous solutions by adsorption on oil palm trunk fibre: equilibrium isotherms and kinetic studies.* Journal of hazardous materials, 2008. **154**(1-3): p. 237-244.

63. El-Bindary, A., et al., *Removal of reactive blue 19 from aqueous solution using rice straw fly ash.* Journal of Materials and Environmental Sciences, 2016. **7**(3): p. 1023-1036.

64. Farah, J.Y., N.S. El-Gendy, and L.A. Farahat, *Biosorption of Astrazone Blue basic dye from an aqueous solution using dried biomass of Baker's yeast.* Journal of hazardous materials, 2007. **148**(1-2): p. 402-408.

65. Hameed, B. and H. Hakimi, *Utilization of durian (Durio zibethinus Murray) peel as low cost sorbent for the removal of acid dye from aqueous solutions.* Biochemical Engineering Journal, 2008. **39**(2): p. 338-343.

66. Ponnusami, V., S. Vikram, and S. Srivastava, *Guava (Psidium guajava) leaf powder: novel adsorbent for removal of methylene blue from aqueous solutions.* Journal of hazardous materials, 2008. **152**(1): p. 276-286.

67. Ardejani, F.D., et al., *Adsorption of Direct Red 80 dye from aqueous solution onto almond shells: Effect of pH, initial concentration and shell type.* Journal of hazardous materials, 2008. **151**(2-3): p. 730-737.

68. Hameed, B., D. Mahmoud, and A. Ahmad, *Sorption of basic dye from aqueous solution by pomelo (Citrus grandis) peel in a batch system.* Colloids and Surfaces A: Physicochemical and Engineering Aspects, 2008. **316**(1-3): p. 78-84.

69. Lata, H., et al., *Removal of a dye from simulated wastewater by adsorption using treated parthenium biomass.* Journal of Hazardous Materials, 2008. **153**(1-2): p. 213-220.

70. Sivaraj, R., C. Namasivayam, and K. Kadirvelu, *Orange peel as an adsorbent in the removal of Acid violet 17 (acid dye) from aqueous solutions.* Waste Management, 2001. **21**(1): p. 105-110.

71. Annadurai, G., R.-S. Juang, and D.-J. Lee, *Use of cellulose-based wastes for adsorption of dyes from aqueous solutions.* Journal of Hazardous Materials, 2002. **92**(3): p. 263-274.

72. Gong, R., et al., *Uptake of cationic dyes from aqueous solution by biosorption onto granular kohlrabi peel.* Bioresource Technology, 2007. **98**(6): p. 1319-1323.

73. Shakoor, S. and A. Nasar, *Removal of methylene blue dye from artificially contaminated water using citrus limetta peel waste as a very low cost adsorbent.* Journal of the Taiwan Institute of Chemical Engineers, 2016. **66**: p. 154-163.

74. Hameed, B. and M. El-Khaiary, *Sorption kinetics and isotherm studies of a cationic dye using agricultural waste: broad bean peels.* Journal of Hazardous Materials, 2008. **154**(1-3): p. 639-648.

75. Tranchemontagne, D.J., et al., *Secondary building units, nets and bonding in the chemistry of metal–organic frameworks.* Chemical Society Reviews, 2009. **38**(5): p. 1257-1283.

76. Wang, Z. and S.M. Cohen, *Postsynthetic modification of metal–organic frameworks.* Chemical Society Reviews, 2009. **38**(5): p. 1315-1329.

77. Kreno, L.E., et al., *Metal–Organic Framework Materials as Chemical Sensors.* Chemical Reviews, 2012. **112**(2): p. 1105-1125.

78. Collins, D.J. and H.-C. Zhou, *Hydrogen storage in metal–organic frameworks.* Journal of Materials Chemistry, 2007. **17**(30): p. 3154-3160.

79. Li, J.-R., et al., *Carbon dioxide capture-related gas adsorption and separation in metal-organic frameworks.* Coordination Chemistry Reviews, 2011. **255**(15): p. 1791-1823.

80. Li, J.-R., R.J. Kuppler, and H.-C. Zhou, *Selective gas adsorption and separation in metal–organic frameworks.* Chemical Society Reviews, 2009. **38**(5): p. 1477-1504.

81. Lee, J., et al., *Metal–organic framework materials as catalysts.* Chemical Society Reviews, 2009. **38**(5): p. 1450-1459.

82. Horcajada, P., et al., *Metal–Organic Frameworks in Biomedicine.* Chemical Reviews, 2012. **112**(2): p. 1232-1268.

83. Chen, B., et al., *A Microporous Metal–Organic Framework for Gas-Chromatographic Separation of Alkanes.* Angewandte Chemie International Edition, 2006. **45**(9): p. 1390-1393.

84. Adeyemo, A.A., I.O. Adeoye, and O.S. Bello, *Metal organic frameworks as adsorbents for dye adsorption: overview, prospects and future challenges.* Toxicological & Environmental Chemistry, 2012. **94**(10): p. 1846-1863.

85. Haque, E., et al., *Adsorptive removal of methyl orange from aqueous solution with metal-organic frameworks, porous chromium-benzenedicarboxylates.* Journal of Hazardous Materials, 2010. **181**(1): p. 535-542.

86. Haque, E., J.W. Jun, and S.H. Jhung, *Adsorptive removal of methyl orange and methylene blue from aqueous solution with a metal-organic framework material, iron terephthalate (MOF-235).* Journal of Hazardous materials, 2011. **185**(1): p. 507-511.

87. Zhu, H.-Y., et al., *Novel multifunctional NiFe2O4/ZnO hybrids for dye removal by adsorption, photocatalysis and magnetic separation.* Applied Surface Science, 2016. **369**: p. 1-10.

88. Liu, L., et al., *Adsorption Removal of Dyes from Single and Binary Solutions Using a Cellulose-based Bioadsorbent.* ACS Sustainable Chemistry & Engineering, 2015. **3**(3): p. 432-442.

89. Banerjee, S. and M.C. Chattopadhyaya, *Adsorption characteristics for the removal of a toxic dye, tartrazine from aqueous solutions by a low cost agricultural by-product.* Arabian Journal of Chemistry, 2017. **10**: p. S1629-S1638.

90. Muthukumaran, C., V.M. Sivakumar, and M. Thirumarimurugan, *Adsorption isotherms and kinetic studies of crystal violet dye removal from aqueous solution using surfactant modified magnetic nanoadsorbent.* Journal of the Taiwan Institute of Chemical Engineers, 2016. **63**: p. 354-362.

91. Lagergren, S., *About the theory of so-called adsorption of soluble substances.* Sven. Vetenskapsakad. Handingarl, 1898. **24**: p. 1-39.

92. Ho, Y.-S. and G. McKay, *Pseudo-second order model for sorption processes.* Process biochemistry, 1999. **34**(5): p. 451-465.

93. Ho, Y.-S., *Review of second-order models for adsorption systems.* Journal of Hazardous Materials, 2006. **136**(3): p. 681-689.

94. Zeldowitsch, J., *Über den mechanismus der katalytischen oxydation von CO an MnO2.* Acta Physicochim. URSS, 1934. **1**: p. 364-449.

95. Weber, W.J. and J.C. Morris, *Kinetics of adsorption on carbon from solution.* Journal of the Sanitary Engineering Division, 1963. **89**(2): p. 31-60.

96. Langmuir, I., *The constitution and fundamental properties of solids and liquids. II. Liquids.* Journal of the American Chemical Society, 1917. **39**(9): p. 1848-1906.

97. Freundlich, H., *Über die adsorption in lösungen.* Zeitschrift für physikalische Chemie, 1907. **57**(1): p. 385-470.

98. Di Marino, A. and F. Mendicuti, *Thermodynamics of complexation of dimethyl esters of tere-, iso-, and phthalic acids with α-and β-cyclodextrins.* Applied spectroscopy, 2004. **58**(7): p. 823-830.

99. Dhumal, N.R., et al., *Molecular Interactions of a Cu-Based Metal–Organic Framework with a Confined Imidazolium-Based Ionic Liquid: A Combined Density Functional Theory and Experimental Vibrational Spectroscopy Study.* The Journal of Physical Chemistry C, 2016. **120**(6): p. 3295-3304.

100. Coates, J., *Interpretation of infrared spectra, a practical approach.* Encyclopedia of analytical chemistry, 2000. **12**: p. 10815-10837.

101. Aroke, U., A. Abdulkarim, and R. Ogubunka, *Fourier-transform infrared characterization of kaolin, granite, bentonite and barite.* ATBU Journal of Environmental Technology, 2013. **6**(1): p. 42-53.

102. Marrakchi, F., M. Bouaziz, and B. Hameed, *Adsorption of acid blue 29 and methylene blue on mesoporous K2CO3-activated olive pomace boiler ash.* Colloids and Surfaces A: Physicochemical and Engineering Aspects, 2017. **535**: p. 157-165.

103. Yagub, M.T., T.K. Sen, and H. Ang, *Equilibrium, kinetics, and thermodynamics of methylene blue adsorption by pine tree leaves.* Water, Air, & Soil Pollution, 2012. **223**(8): p. 5267-5282.

104. Tan, I., A. Ahmad, and B. Hameed, *Adsorption of basic dye using activated carbon prepared from oil palm shell: batch and fixed bed studies.* Desalination, 2008. **225**(1-3): p. 13-28.

105. Auta, M. and B.H. Hameed, *Modified mesoporous clay adsorbent for adsorption isotherm and kinetics of methylene blue.* Chemical Engineering Journal, 2012. **198-199**: p. 219-227.

106. Gürses, A., et al., *The adsorption kinetics of the cationic dye, methylene blue, onto clay.* Journal of Hazardous Materials, 2006. **131**(1-3): p. 217-228.

107. Gil, A., et al., *Removal of dyes from wastewaters by adsorption on pillared clays.* Chemical Engineering Journal, 2011. **168**(3): p. 1032-1040.

108. Valix, M., W. Cheung, and G. McKay, *Roles of the textural and surface chemical properties of activated carbon in the adsorption of acid blue dye.* Langmuir, 2006. **22**(10): p. 4574-4582.

109. Sarkar, D. and D. Chattoraj, *Activation parameters for kinetics of protein adsorption at silica-water interface.* Journal of colloid and interface science, 1993. **157**(1): p. 219-226.

110. Bhargava, D. and S. Sheldarkar, *Use of TNSAC in phosphate adsorption studies and relationships. Effects of adsorption operating variables and related relationships.* Water Research, 1993. **27**(2): p. 313-324.

111. Kaur, A., et al., *Removal of copper and lead from wastewater by adsorption on bottom ash.* Indian J Environ Prot, 1991. **11**: p. 433-5.

112. Panday, K., G. Prasad, and V. Singh, *Removal of Cr (V1) from aqueous solutions by adsorption on fly ash-wollastonite.* Journal of Chemical Technology and Biotechnology. Chemical Technology, 1984. **34**(7): p. 367-374.

113. Panday, K.K., G. Prasad, and V.N. Singh, *Copper(II) removal from aqueous solutions by fly ash.* Water Research, 1985. **19**(7): p. 869-873.

114. Khare, S.K., et al., *Removal of victoria blue from aqueous solution by fly ash.* Journal of Chemical Technology & Biotechnology, 1987. **38**(2): p. 99-104.

115. Singh, D., et al., *As (III) removal from aqueous solution by adsorption.* Water, Air, and Soil Pollution, 1988. **42**(3-4): p. 373-386.

116. Sharma, Y., et al., *Use of wollastonite in the removal of Ni (II) from aqueous solutions.* Water, Air, and Soil Pollution, 1990. **49**(1-2): p. 69-79.

117. Sharma, Y., G. Prasad, and D. Rupainwar, *Removal of Ni (II) from aqueous solutions by sorption.* International journal of environmental studies, 1991. **37**(3): p. 183-191.

118. Gupta, G., G. Prasad, and V. Singh, *Removal of chrome dye from aqueous solutions by mixed adsorbents: fly ash and coal.* Water Research, 1990. **24**(1): p. 45-50.

119. Chaturvedi, A., et al., *Defluoridation of water by adsorption on fly ash.* Water, Air, and Soil Pollution, 1990. **49**(1-2): p. 51-61.

120. Hameed, B.H., A.T.M. Din, and A.L. Ahmad, *Adsorption of methylene blue onto bamboo-based activated carbon: Kinetics and equilibrium studies.* Journal of Hazardous Materials, 2007. **141**(3): p. 819-825.

121. El-Geundi, M.S., *Homogeneous surface diffusion model for the adsorption of basic dyestuffs onto natural clay in batch adsorbers.* Adsorption Science & Technology, 1991. **8**(4): p. 217-225.

122. Hall, K.R., et al., *Pore-and solid-diffusion kinetics in fixed-bed adsorption under constant-pattern conditions.* Industrial & Engineering Chemistry Fundamentals, 1966. **5**(2): p. 212-223.

123. Hameed, B.H. and M.I. El-Khaiary, *Malachite green adsorption by rattan sawdust: Isotherm, kinetic and mechanism modeling.* Journal of Hazardous Materials, 2008. **159**(2): p. 574-579.

124. Ho, Y.-S. and G. McKay, *Sorption of dye from aqueous solution by peat.* Chemical engineering journal, 1998. **70**(2): p. 115-124.

125. Balathanigaimani, M., et al., *Effects of structural and surface energetic heterogeneity properties of novel corn grain-based activated carbons on dye adsorption.* Microporous and Mesoporous Materials, 2009. **118**(1-3): p. 232-238.

126. Haghseresht, F. and G. Lu, *Adsorption characteristics of phenolic compounds onto coal-reject-derived adsorbents.* Energy & Fuels, 1998. **12**(6): p. 1100-1107.

127. Fytianos, K., E. Voudrias, and E. Kokkalis, *Sorption–desorption behaviour of 2, 4-dichlorophenol by marine sediments.* Chemosphere, 2000. **40**(1): p. 3-6.

128. Hameed, B.H. and A.A. Ahmad, *Batch adsorption of methylene blue from aqueous solution by garlic peel, an agricultural waste biomass.* Journal of Hazardous Materials, 2009. **164**(2): p. 870-875.

129. Banat, F., et al., *Bench-scale and packed bed sorption of methylene blue using treated olive pomace and charcoal.* Bioresource technology, 2007. **98**(16): p. 3017-3025.

130. Nogueira, F.G., et al., *Reactive adsorption of methylene blue on montmorillonite via an ESI-MS study.* Applied Clay Science, 2009. **43**(2): p. 190-195.

131. Mouni, L., et al., *Removal of Methylene Blue from aqueous solutions by adsorption on Kaolin: Kinetic and equilibrium studies.* Applied Clay Science, 2018. **153**: p. 38-45.

132. Gil, A., et al., *Removal of dyes from wastewaters by adsorption on pillared clays.* Chemical Engineering Journal, 2011. **168**(3): p. 1032-1040.

133. Akgül, M. and A. Karabakan, *Promoted dye adsorption performance over desilicated natural zeolite.* Microporous and Mesoporous Materials, 2011. **145**(1-3): p. 157-164.

134. Lata, H., V. Garg, and R. Gupta, *Removal of a basic dye from aqueous solution by adsorption using Parthenium hysterophorus: an agricultural waste.* Dyes and pigments, 2007. **74**(3): p. 653-658.

135. Auta, M. and B. Hameed, *Modified mesoporous clay adsorbent for adsorption isotherm and kinetics of methylene blue.* Chemical Engineering Journal, 2012. **198**: p. 219-227.

136. Ghosh, D. and K.G. Bhattacharyya, *Adsorption of methylene blue on kaolinite.* Applied clay science, 2002. **20**(6): p. 295-300.

137. Gupta, V.K., et al., *Adsorption of Safranin-T from wastewater using waste materials—activated carbon and activated rice husks.* Journal of Colloid and Interface Science, 2006. **303**(1): p. 80-86.

138. Zeng, L., et al., *Chitosan/organic rectorite composite for the magnetic uptake of methylene blue and methyl orange.* Carbohydrate polymers, 2015. **123**: p. 89-98.

139. Batzias, F. and D. Sidiras, *Dye adsorption by calcium chloride treated beech sawdust in batch and fixed-bed systems.* Journal of hazardous materials, 2004. **114**(1-3): p. 167-174.

140. Yao, Y., et al., *Characterization and environmental applications of clay–biochar composites.* Chemical Engineering Journal, 2014. **242**: p. 136-143.

141. Karaer, H. and İ. Uzun, *Adsorption of basic dyestuffs from aqueous solution by modified chitosan.* Desalination and Water Treatment, 2013. **51**(10-12): p. 2294-2305.

142. Aygün, A., S. Yenisoy-Karakaş, and I. Duman, *Production of granular activated carbon from fruit stones and nutshells and evaluation of their physical, chemical and adsorption properties.* Microporous and mesoporous materials, 2003. **66**(2-3): p. 189-195.

143. Lee, C., K. Low, and S. Chow, *Chrome sludge as an adsorbent for colour removal.* Environmental technology, 1996. **17**(9): p. 1023-1028.

144. Ugurlu, M., et al., *Removal of phenolic and lignin compounds from bleached kraft mill effluent by fly ash and sepiolite.* Adsorption, 2005. **11**(1): p. 87-97.

145. Cheung, W., Y. Szeto, and G. McKay, *Intraparticle diffusion processes during acid dye adsorption onto chitosan.* Bioresource technology, 2007. **98**(15): p. 2897-2904.

146. Wu, C.-H., *Adsorption of reactive dye onto carbon nanotubes: equilibrium, kinetics and thermodynamics.* Journal of hazardous materials, 2007. **144**(1-2): p. 93-100.

147. Markovska, L., et al., *Solid diffusion control of the adsorption of basic dyes onto granular activated carbon and natural zeolite in fixed bed.* J. Serb. Chem. Soc, 2001. **66**(7): p. 463-475.

148. Weng, C.-H., Y.-T. Lin, and T.-W. Tzeng, *Removal of methylene blue from aqueous solution by adsorption onto pineapple leaf powder.* Journal of Hazardous Materials, 2009. **170**(1): p. 417-424.

149. Gupta, N., A.K. Kushwaha, and M. Chattopadhyaya, *Adsorption studies of cationic dyes onto Ashoka (Saraca asoca) leaf powder.* Journal of the Taiwan Institute of Chemical Engineers, 2012. **43**(4): p. 604-613.

Chapter 7

Conclusions and recommendations for future work

7

Chapter 7: Conclusions and recommendations for future work

7.1 Conclusion

Metal organic frameworks (MOFs) are a class of highly porous materials whose inorganic and organic units can be linked together by strong bonds (reticular synthesis). According to the Cambridge Crystallographic Data Centre, there are 84,185 different types of MOF structures as at 7 June 2018. In addition, many thousands of publications on their synthesis, structure and applications are issued every year. The amount of exploration and production in this field is possible because of the secondary building unit (SBU) method of synthesis as well as the diversity and flexibility of MOF constituents, such as its geometry, size and functionality.

The origin of reticular chemistry comes from Latin word 'reticulum' which has the meaning of having the form of a net or being netlike. The SBU method can be considered pivotal to the discovery of permanently porous MOFs and to the foundation of a new field of chemistry, called reticular chemistry. Thus, reticular chemistry is chemistry which deals with binding molecular building blocks (molecules and clusters) to obtained crystalline extended structures by making strong bonds.

The impetus for synthesising MOFs lies in coordination networks that have single-metal nodes in their vertices. These vertices consist of single-metal ion node bonded weakly to a neutral organic donor linker such as the Cu-N (pyridine, nitrile)-type bond (e.g., adiponitrile = $NC[CH_2]_4CN$).

The SBU approach uses molecular chemistry laws (organic and inorganic) to obtain extended solid-state structures. Therefore, the carboxylate functional group is used to link metal ions and latch them together to form rigid and directional metal–oxygen–carbon clusters, which have points of extension like the C atoms of carboxylates that define geometrical shapes referred to as SBUs. This innovation has made the SBU an important concept in the design and development of MOFs, and has widened the field of possibilities for controlling the constituents of the material at the molecular level to make 'materials on demand', such as zero-dimensional (0D), one-dimensional (1D),

two-dimensional (2D) and three-dimensional (3D) crystalline porous extended materials.

Linking metal-containing units (inorganic) with ditopic or polytopic carboxylates units (organic) using reticular synthesis produces architecturally robust crystalline MOF structures with typical porosity exceeding 50% of the MOF crystal volume. Using reticular synthesis, it is also possible to synthesise and modify MOFs of comparable framework topology (isoreticular framework) along with different pore size and functional groups of the organic linkers. The typical MOF surface areas reported range between 1000 to 10,000 m^2/g—larger than those materials well known for its porosity, such as zeolites and carbons. Its extensive variety and multiplicity, along with its everlasting porosity, make MOFs ideal for a wide range of applications, such as carbon dioxide capture, catalysis, gas/vapour separation, luminescence, drug delivery, storage of fuels like hydrogen and methane and as adsorbents to remove pollutants from wastewater.

MOFs exhibit high thermal stability (250–500 °C) due to the strong bonds which they are entirely composed (e.g., C-C, C-H, C-O and Metal-O). Water stability is an essential indication of MOFs that successfully used in water treatment. As a result of their chemical properties, some MOFs (e.g., MOF-5 or its isoreticulars) are sensitive to water content and are gradually affected by moisture in the atmosphere.

The requirement to comply with environmental standards has pushed many industries to utilise a range of techniques—chemical, biological and physical—to remove contaminants from effluent, but these treatments are not sufficiently efficient because of restrictions and limitations.

One physical treatment is adsorption, considered the best technique for removing pollutants in wastewater as it uses low-cost materials. In this vein, materials such as activated carbons, zeolites, biological materials, polymer resins and oxides have generated increasing excitement. The simplicity, feasibility and reliability of the adsorption method makes it the first choice in wastewater treatment.

Based on the objectives of this thesis, a series of Zr-MOFs were synthesised and activated along with its modifications. These include UiO-66, UiO-66-Ce, UiO-66-NH_4, UiO-66-10%Ca, UiO-66-30%Ca, UiO-66-45%Ca, UiO-66-10%Al, UiO-66-30%Al, UiO-66-10%Co and UiO-66-30%Co. These MOFs were studied for their

adsorption capacity to remove dye pollutants such as methyl orange (MO) and methylene blue (MB), as well as to determine the MOF with the highest uptake. The following conclusions can be made in light of the results obtained.

Three adsorbents (UiO-66, UiO-66-Ca and UiO-66-NH_4) were used to remove acidic dye methyl orange (MO). They were synthesised using different methods with trace additives of a secondary chemical. Their textural properties were enhanced for the purpose of water treatment applications. The characterisation of single-metal and bimetal Zr-MOFs reveals that they have water and thermal stability, with robust structure and robust textural properties and functional groups. Experimental data were fitted to adsorption kinetics and adsorption equilibrium models. It was apparent that adsorption by MO/Zr-MOFs systems depended on the initial concentration of dye, with uptake by MOFs increasing with higher initial concentrations of MO.

The best correlation coefficient identified among all MO/Zr-MOF adsorption systems demonstrated compliance with pseudo second-order kinetics, and indicated that the overall rate of MO uptake in Zr-MOFs processes appeared to be controlled by chemisorption processes, including valence forces in the sharing or exchange of electrons.

However, all MO/Zr-MOF systems obeyed the Langmuir isotherm model, verifying that the adsorption of dye molecules occurred through a monolayer on a structurally homogeneous adsorbent with adsorptive sites of identical energy. Moreover, UiO-66-Ce was the best adsorbent for MO removal, exhibiting maximum adsorption capacity at 71.5 mg g^{-1}. The performances of these modified versions of UiO-66 make them feasible candidates for industrial applications to remove other contaminants from wastewater.

Examination of the three Zr-MOFs (single-metal and bimetal: UiO-66, UiO-66-10%Al and UiO-66-30%Al) showed that they are favourable adsorbents of basic (cationic) dye such as MB from aqueous solutions over a wide range of concentrations. The characterisation of Zr-MOFs by XRD patterns, FTIR spectra, N_2 adsorption/desorption isotherms and TGA profiles demonstrated the integrity of their structures, the stability of the functional groups on the organic linkers, textural properties and thermal stability, respectively. The best adsorbent among the three Zr-MOFs was UiO-66-10%Al, with the largest pore size (1.34 cc. g^{-1}) and pore diameter (2.33 nm), verifying

that adding between 0.1–10% Al improved the textural properties of prototype Zr-MOF. For all MB/MOF systems, MB was found to have a good adsorption capacity.

It can be concluded that the pseudo first-order model is not a good fit for the experimental data. However, it is generally applicable to the initial period of the first step of the reaction in the adsorption interaction—consistent with the reported findings of most sorption studies in the literature that have considered pseudo first-order mechanisms. These studies have found that this model is restricted to a limited fraction of the beginning of contact time. The Elovich and pseudo second-order models showed the highest correlation for all MOF/MB systems studied over longer adsorption contact times. Based on the obtained correlation coefficients (R^2), the adsorption kinetics in the data neatly followed the pseudo second-order kinetic model.

Equilibrium data were tested using the Langmuir and Freundlich models; based on their relative R^2, the experimental data were best defined by the Freundlich isotherm. The maximum loading capacity (q_m) of the most efficient MOF adsorbent studied (UiO-66-10%Al) was 49.26 mg/g. In addition, the obtained q_m was compared with that of other porous adsorbents reported in previous studies.

The parameters identified in this study can support the design and lay the foundations of a continuous treatment process to remove MB from water and wastewater.

The main goal of the study on adsorption of a cationic dye (MB) onto Zr-MOFs (UiO-66, UiO-66-10%Ca and UiO-66-30%Ca) was to assess the capacity of MOFs as dye adsorbents and to assess their dye loading. They were prepared according to a previously reported method with a modification in trace additives of the secondary chemical Ca. The textural properties were enhanced for the purposes of water and wastewater treatment applications. Kinetics and equilibrium models were utilised so that the adsorbed amount at any time (q_t), sorption at equilibrium (q_e) and Langmuir maximum loading capacity (q_m) of basic dye could be predicted.

Of the models, the pseudo second-order model produced the highest R^2 with the experimental data. This model enabled rate of adsorption (k_2) and equilibrium capacity to be obtained as a function of various initial concentrations of MB. Therefore, the kinetics of MB sorption onto MOFs (UiO-66, UiO-66-10%Ca and UiO-66-30%Ca) were examined based on the pseudo second-order rate model. The results indicate that the chemical reaction may be important in the rate-limiting step and the pseudo

second-order mechanism offer the best fit for the experimental data for all systems studied.

However, the pseudo first-order model fit the experimental data well for an initial short period of the first step of the adsorption process. The equilibrium experimental data were fitted using the linear forms of the Langmuir and Freundlich isotherms. Langmuir and Freundlich plot analyses and calculations revealed that the R^2 for the Freundlich model was greater than that for the Langmuir model, for UiO-66/MB, UiO-66-10%Ca/MB and UiO-66-30%Ca/MB adsorption systems.

Further, Freundlich constants related to the bonding energy of MB molecules with single-metal and bimetal Zr-MOFs (K_F) were larger than the Langmuir constants related to the affinity of MB molecules to single-metal and bimetal Zr-MOFs in all cases. As a result, the adsorption of MB onto single-metal and bimetal Zr-MOFs was considered a multilayer adsorption on a heterogeneous surface. Specifically, the Langmuir maximum adsorption capacity of the most efficient adsorbent (UiO-66-10%Ca) was 50.25 mg/g.

In addition, the obtained q_m was compared with that of other reported adsorbents in previous studies. The values of the separation factor (R_L) of MB sorption by single-metal and bimetal Zr-MOFs were in the range $0 < R_L < 1$, indicating that the adsorption was a favourable process. Further, higher initial MB concentrations in the adsorption process tend to make the process irreversible. From the linear form of the Freundlich model, the calculated constant n values of UiO-66, UiO-66-10%Ca and UiO-66-30%Ca were more than 1 (i.e., $n > 1$). These values confirmed the favourability of adsorption of MB onto single-metal and bimetal Zr-MOFs.

The intraparticle diffusion adsorption model was employed to overcome the limitations of the pseudo first-order and pseudo second-order kinetic equations, a lack of described adsorption mechanism and the rate-limiting steps in the adsorption process. Mechanism of MB sorption on the surface of MOFs was investigated using contact time data. Specifically, experimental data were fitted to the intraparticle diffusion model and the results indicated that the sorption mechanism consists of three steps and that the intraparticle diffusion was not the only rate-controlling step.

Three versions Zr-MOFs (UiO-66, UiO-66-10%Co and UiO-66-30%Co) were prepared successfully and used as adsorbents to remove MB from aqueous solutions

of four different initial MB concentrations. Characterisation of the Zr-MOFs established that modification of UiO-66 with 10% Co enhanced its adsorption capacity for basic dye and made it an excellent alternative adsorbent for industrial wastewater treatment, whereas increasing the percentage to 30% Co led to reductions in MB uptake.

Experimental data were fitted to Langmuir and Freundlich equilibrium isotherms. Based on the coefficients of determination (R2), the data was shown to have good agreement with the Freundlich isotherm, indicating that the adsorption process can be described as multilayer adsorption on a heterogenous surface with maximum Langmuir monolayer adsorption capacity of 51.02 mg g^{-1}—comparable with the reported values of other adsorbents in earlier studies. The kinetic rate of adsorption was found to obey the pseudo second-order model, with a high correlation coefficient ($R2 \geq 0.99$). The results prove that Zr-MOFs are potentially favourable alternatives for removing MB from industrial wastewater. The outcomes of the intraparticle diffusion equation suggested that intraparticle diffusion was not the only rate-limiting step.

The outcomes of these investigations show that the experimental equilibrium data agreed well with the Langmuir model for Zr-MOF/MO systems, while the data was a good fit with the Freundlich equilibrium model for Zr-MOF/MB systems. However, based on the Langmuir model, the maximum adsorption capacity of Zr-MOF/MO systems and Zr-MOF/MB systems was exhibited by UiO-66-Ce (71.5 mgg^{-1}) and UiO-66-10%Co (51.02 mgg^{-1}), respectively. Further, the maximum monolayer adsorption capacity of several adsorbents for uptake of MO and MB and it appears that the maximum adsorption capacity of Zr-MOFs for MO and MB in this study is comparable with those previously reported elsewhere. The results presented here may facilitate further improvements to Zr-MOFs and to the synthesis of bimetal MOFs in future research.

It is clear from the result of this study that pristine and modified Zr-MOFs were used to remove pollutants from aqueous solution of anionic and cationic dyes, including MO and MB. The removal efficiencies of these dyes by parent and modified Zr-MOFs were much better than by conventional adsorbents such as activated carbon. It can be concluded Zr-MOFs can be attractive adsorbents of some harmful chemicals, like dyes in wastewater. The adsorption mechanism was attributed to the presence of

electrostatic interactions between the dye and the adsorbent. Specifically, those MOFs can have positive (framework) and negative charges (charge-balancing anion), respectively; therefore, it can capture anionic and cationic dyes. This finding agreed with Haque et al. (2011) who claimed that an Fe-BDC MOF (MOF-235) was used to clarify the aqueous solution of anionic and cationic dyes, including MO and MB.

The results presented in this study especially that of modified Zr-MOFs with a low second metal content which were boosted the adsorption capacity of UiO-66 remarkably, may facilitate and enhance further improvements to UiO-66 for the purpose of synthesising bimetal MOFs in future research and applications. Furthermore, these updated UiO-66 samples can be selected as potential candidates for industrial application for removal dyes and other contaminants from wastewater.

7.2 Recommendations for future work

1. Further to the reported literature, the flexibility of varying the metrics and nature of MOF structures keeping original topology will lead to the iso-reticular principle and for designing and synthesis of MOFs for specific application, including the largest pore aperture (98 Å) and lowest density (0.13 g/cm^3). This will enable scientists to selectively accommodate for large molecules, such as vitamin B_{12} and green fluorescent protein, and exploit pores as reaction vessels.

2. The construction of tables and charts that list the sizes of molecules to be accommodated into MOFs and MOF metrics (pore aperture, surface area, etc.) will be helpful for researchers choosing the appropriate MOF given the molecule to be adsorbed.

3. Further, the thermal and chemical stability of many MOFs make them amenable to post-synthetic covalent organic linkers and metal-complex functionalisation of vertices. These features hold considerable opportunities to advance their use in gas storage and will give rise to their extensive study in the catalysis of organic reactions, activation of small molecules (hydrogen, methane and water), gas separation, biomedical imaging, as well as proton, electron and ion conduction.

4. The SBU approach represented by reticular synthesis can be a potential solution to the longstanding challenge of designing and constructing new crystalline solid materials from molecular building blocks. Designing the net structure with

enhanced control over chemical functionalisation and tuning of its metric dimensions presents exciting opportunities. This conceptual approach is in the beginning stage and needs to be encouraged and explored to open a substantial assembly of ordered frameworks with predetermined structures, compositions and properties. New products are predicted to have diverse systematic pore metrics and functionalities, including ultra-high porosity and an exceptionally large surface area for applications in emerging technologies.

5. Future challenges exist in designing building blocks that carry structural and functional information of a specific targeted material. Such designs and materials will have countless advantages for various emerging technologies, such as molecular electronics, miniature fuel cells, chiral catalysis and materials with hybrid properties.

6. Achieving accurate control over the design and assembly of MOFs is expected to boost this area of research further into new fields of synthetic chemistry. Such an advance will increase the accessibility of desirable materials, or 'materials on demand', with the following properties:

    - compartments joined to each other to operate separately yet function synergistically
    - intelligence to perform parallel operations
    - capacity to count, sort and code information
    - dynamic abilities with high reliability.

    The direction of much research thus far has been consistent with the above recommendations; however, further research is required into a large number of various functional groups within the pores of MOFs. By varying the arranged functionalities, resultant MOFs will be multivariate and lead to porous extended solids with a combination of synergistic properties. Future work should focus on the design and synthesis of structures using numerous kinds of building units that have structures with specifically arranged constituents, by dictating functional groups and heterogeneity.

7. In this thesis, one or two metal ions as well as one ditopic linker in a terephthalic acid (BDC) were used to design and synthesise single-metal and bimetal Zr-MOFs. However, it would be interesting to examine a range of other possibilities by using a different second ion with the primary ion (Zr^{+4}), or using endless options of organic linkers ranging between 2 to 11 or more straight or branched phenalene groups, or using more than two metal ions along with more than one linkers to prepare Zr-MOFs. The resultant MOFs can be tested against acidic and basic dyes, other pollutants in wastewater or for other potential applications.

8. The possibilities for synthesising bimetal Zr-MOFs are exciting. Beginning with 1–99% second metal ion and applying this basic step to Zr-MOFs with more than two metal ions, a systematic library can be created to record and itemise the hundreds or thousands of Zr-MOFs and their designed purpose, whether it be for the removal of dyes and other contaminants from aqueous solutions or other applications.

9. Water stability in all modified Zr-MOFs can be employed to investigate the effect of water content on their behaviour or capacities as adsorbents. These capacities can be further designed and modified for new applications such as water harvesting from air by adsorbing moisture at night and releasing during day at higher temperatures, as reported by some researchers using other types of MOFs. However, this area requires further research and development before it can be reliable and feasible.

10. In this thesis, one factor was studied at a time, such as the initial concentration of dye and the adsorption response by single-metal and bimetal Zr-MOFs. However, it is possible to examine more than one factor simultaneously, including initial concentration, contact time, percentage of the second ion, adsorbent dose, pH and so on, by employing a sequence of designed experiments (response surface methodology [RSM]) to determine the optimum conditions for the highest MOF uptake by 3D and contour plots, as well as ANOVA analysis.

11. It is worthwhile using a software to design and analyse response-surface experiments based on more than one factor at a time, including the amount of inorganic substance, amount of organic compound, amount of solvent, percentage of the second metal etc., to identify the optimum Zr-MOF with the most suitable

textural properties and highest capacity for adsorption, based on characterisation analysis.

12. It will be challenging to study thermal, chemical and water stability of all known MOFs and search for new methods of strengthening their properties, by returning to fundamental basics and building a strong foundation for the design and synthesis of MOFs, analogous to the SBU approach, to overcome the many obstacles and restrictions that exist with current methods of designing and synthesising MOFs for their various applications.

13. Based on the reported reticular table containing information on the shape of both molecular building blocks (organic and inorganic), one can imagine and predict the obtainable structure of MOF. However, some structures are very difficult to imagine while others have yet to be reported. It will be beneficial for researchers to construct a computer-aided software that matches the building blocks and provides a prediction of the range of structures that are likely to be produced.

14. The impetus for the synthesis of MOFs came from the discovery of the structure of coordination polymers, which are constructed from metal vertices linked to organic ligands. It may be useful to review all coordination polymers since the mid–20th century and replace the metals by clusters containing metals, characterise them and examine their use in various applications.

15. The activation process of MOF is done by removing solvent and unreacted substances trapped in the pores by several methods like simple heating under vacuum and exchange the solvent with another one has lower boiling point before heating under vacuum. Each of these common strategies suffer from defects. Simple heating under vacuum way result in structure collapse and/or lesser because of high surface tension and capillary forces during phase transition process of the trapped solvent. Exchange the solvent prier heating strategy also is difficult as MOFs necessitate soaking for a very long time to confirm that the new solvent permeates. Despite of activation by supercritical CO2 and freeze-drying activation techniques at which surface tension and capillary forces are eliminated still there is more research to be done to find easier activation technique to be applicable in laboratory and industry.

16. Modern life and the growing demands for energy leads to more serious environmental issues resulting from using fossil fuel as a main source of energy. pollution motivated many researchers around the world to find clean source of energy such as solar and wind energy to produce electricity. The huge demand on renewable energy storage in the transportation market open the doors for reliable energy storage technologies electrical energy storage (EES) devices, supercapacitors (SCs) lithium-ion batteries LIBs. large research efforts need to be devoted to the development of next generation batteries and SCs. In addition, more investigations on the applications of MOFs and their derivatives in EES systems as well as the important applications of MOFs in electrochemistry such as the development of MOFs for clean energy applications, including hydrogen production and storage, fuel cells, lithium-ion batteries LIBs, SCs and solar cells.

17. The big demand of MOFs and their commercialization by companies working with MOFs in production, have push the production of metal organic frameworks (MOFs) at a large scale. To address the promising opportunity, many approaches of synthesis of MOFs especially with the potential of production with large scale such as electrochemical, microwave, mechanochemical, spray drying and flow chemistry and design of chemical engineering need further study to develop the main process (reactor) of synthesis and the downstream unit operations (activation and washing units, dryer, Shaping) to be suitable for high commercial production rates.

18. The optimum adsorbents for removal of MB among the three Zr-MOFs (UiO-66-Ca,UiO-66-Al and UiO-66-Co) were the ones with 10% second metal coordination (Ca, Al and Co) due to improvement in pore size and pore diameter, verifying that adding between 0–10% Al improved the textural properties of prototype Zr-MOF. For all MB/MOF systems, bimetal MOFs were found to have a good adsorption capacity .The results presented in this study especially that of modified Zr-MOFs with a low second metal content which were boosted the adsorption capacity of UiO-66 significantly, may facilitate and enhance further improvements to UiO-66 for the purpose of synthesising bimetal MOFs in future research and applications. Furthermore, these updated UiO-66 samples can be selected as potential candidates for industrial application for removal dyes and other contaminants from wastewater. We recommend synthesizing more bimetal MOFs (Zr-MOF, MIL, etc) with second

metal of percentage of 0.1-10 to find the optimum texture properties and adsorption capacity. In addition, we encourage further research to prepare MOFs (Zr-MOF, MIL, etc) with second coordinated metal (Ca, Al, Co, etc) of percentage between 10.1-30 to investigate the percentage in which no enhancement or weakening in the texture properties.

19. Based on this study and other studies of adsorbents, it can be concluded that:

    - some adsorbents operate rapidly (the adsorbent process is very fast, completing in less than 1 h)
    - others operate moderately quickly (the speed of the adsorbent process is moderate, between 1 to 24 h)
    - while others operate slowly (the speed of the adsorbent process is very slow (more than 24 h).

    The idea is that there is a lack of studies on the potential to convert moderate and slow adsorbents, through physical and/or chemical treatments, to become fast adsorbents.

Appendix 1

Attribution Agreements

1

Appendix 1: Attribution Agreements

Paper "Facile directions for synthesis, modification and activation of MOFs #1. Journal of Materials Today Chemistry, 2020. 17: p. 100343."

	Conception and Design	Acquisition of data & method	Data condition & manipulation	Analyses & statistical method	Interpretation & discussion	Final approval
Dr Hussein Rasool Abid						[redacted]
I acknowledge that these represent my contribution to the above research output Signed:						
Dr Saad Al-Saadi						X
I acknowledge that these represent my contribution to the above research output Signed: [redacted]						
Dr Shaobin Wang				✓	✓	[redacted]
I acknowledge that these represent my contribution to the above research output Signed:						
Dr Shaomin Liu				✓	✓	[redacted]
I acknowledge that these represent my contribution to the above research output Signed:						

Paper "Enhancing Acidic Dye Adsorption by Updated Version of UiO-66 #2. Journal of Applied Materials and Technology, 2020. 1(2): p. 54-62."

	Conception and Design	Acquisition of data & method	Data condition & manipulation	Analyses & statistical method	Interpretation & discussion	Final approval
Dr Hussein Rasool Abid						
I acknowledge that these represent my contribution to the above research output Signed:						
Dr Shaobin Wang						
I acknowledge that these represent my contribution to the above research output Signed:						
Dr Shaomin Liu						
I acknowledge that these represent my contribution to the above research output Signed:						

Paper "Removal of methylene blue (MB) by bimetallic-Metal Organic Framework#3. Journal of Applied Materials and Technology, 2020, In Press."

	Conception and Design	Acquisition of data & method	Data condition & manipulation	Analyses & statistical method	Interpretation & discussion	Final approval
Dr Hussein Rasool Abid						
I acknowledge that these represent my contribution to the above research output Signed:						
Dr Shaobin Wang						
I acknowledge that these represent my contribution to the above research output Signed:						
Dr Shaomin Liu						
I acknowledge that these represent my contribution to the above research output Signed:						